

Turbulence as Clebsch Confinement

Alexander Migdal^{a,b}

^a*SPD, Abu Dhabi Investment Authority, 211 Corniche Street, Abu Dhabi, 3600, Abu Dhabi, United Arab Emirates*

^b*Department of Physics, New York University Abu Dhabi, Saadiyat Island, Abu Dhabi, PO Box 129188, Abu Dhabi, United Arab Emirates*

Abstract

We argue that in the strong turbulence phase, as opposed to the weak one, the Clebsch variables compactify to the sphere S_2 and are not observable as wave excitations. Various topologically nontrivial configurations of this confined Clebsch field are responsible for vortex sheets.

Stability equations (CVS) for closed vortex surfaces (bubbles of Clebsch field) are derived and investigated. The exact non-compact solution for the stable vortex sheet family is presented. Compact solutions are proven not to exist by De Lellis and Brué.

Asymptotic conservation of anomalous dissipation on stable vortex surfaces in the turbulent limit is discovered. We derive an exact formula for this anomalous dissipation as a surface integral of the square of velocity gap times the square root of minus local normal strain.

Topologically stable time-dependent solutions, which we call Kelvinons, are introduced. They have a conserved velocity circulation around **stationary** loop; this makes them responsible for asymptotic PDF tails of velocity circulation, **perfectly matching numerical simulations**.

The loop equation for circulation PDF as functional of the loop shape is derived and studied. This equation is **exactly** equivalent to the Schrödinger equation in loop space, with viscosity ν playing the role of Planck's constant. This equivalence opens the way for direct numerical simulation of turbulence on quantum computers.

Kelvinons are fixed points of the loop equation at WKB limit $\nu \rightarrow 0$.

Area law and the asymptotic scaling law for mean circulation at a large area are derived. The representation of the solution of the loop equation in terms of a singular stochastic equation for momentum loop trajectory is presented.

Contents

1	Historical Notes. Field-String Duality	7
2	Introduction	9
2.1	The statement of the problem and basic results	9
2.2	Stable vortex sheets and irreversibility of turbulence	12
3	Hamiltonian Dynamics of Vortex Sheets	14
3.1	Kelvin-Helmholtz instability	15
3.2	The Burgers-Townsend vortex sheet	17
3.3	Clebsch variables	18
3.4	Gauge invariance	19
3.5	Spherical parametrization of Clebsch field	21
3.6	Euler flow as Clebsch flow in product space	23
3.7	Topological Invariants for closed surface	24
3.8	The vortex sheet dynamics and parametric invariance	28
3.9	Multivalued Action	30
3.10	Steady State as a Minimum of the Hamiltonian	32
3.11	Does Steady Surface mean Steady Flow?	35
4	Clebsch Bubbles	37
4.1	New Steady Solutions of the Navier-Stokes equations	37
4.2	The CVS as a linear boundary problem	38
4.3	Numerical Simulations and stability properties	41
4.4	Topological stability of CVS and the Euler limit of NS	42
4.5	Velocity gap on a curved surface	43
4.6	Invariant form of CVS constraints	44
4.7	The CVS Equations in depth	45
4.8	Anomalous dissipation	48
4.9	The Surface enstrophy conservation	50
4.10	Mathematical Studies of CVS	52
5	CVS Equation for Cylindrical Geometry	53
5.1	Spontaneous breaking of time-reversal symmetry and Normal strain	56
5.2	Complex Curves	58

5.3	Parabolic curves	59
5.4	Hyperbolic curves	66
5.5	Clipping the Cusps	75
5.6	Velocity Gap and Circulation	82
5.7	Minimizing Euler Energy	82
5.8	The induced background strain	84
5.9	Energy dissipation and its distribution	88
6	Energy pumping	91
6.1	Kolmogorov Anomaly	91
6.2	Alternative energy pumping	93
7	Kelvinon as Clebsch domain wall	96
7.1	Initial data for the Kelvinon	97
7.2	Discontinuity surface vs. minimal surface	101
7.3	Topology of the Kelvinon	105
7.4	Kelvinon equation and WKB approximation for the Hopf equation	110
7.5	Stability of Kelvinon and the first De Lellis-Brué theorem .	114
7.6	Estimates of parameters	115
7.7	PDF for the velocity circulation	116
7.8	Discussion. Comparing with Numerical Simulations	117
8	The Loop equation and its turbulent limit	123
8.1	Introduction	123
8.2	The Loop Calculus	125
8.3	Loop Equation	135
8.4	External forces and Dissipation	136
8.5	Loop Equation for the Circulation PDF	140
8.6	How could classical statistics be exactly equivalent to quan- tum mechanics?	141
8.7	The loop equation in the WKB limit and weak Euler solutions	143
8.8	Kelvinon vs instanton	144
8.9	Tensor Area law	145
8.10	Scalar Area law	148
8.11	Discussion	151
8.12	Loop Expansion	152
8.13	Matrix Model	157

8.14	The Reduced Dynamics	159
8.15	Initial Data	161
8.16	Possible Numerical Implementation	166
8.17	Uniqueness of the tensor area law	167
8.18	Minimal surfaces	169
8.19	Kolmogorov triple correlation and time reversal	174
9	Exact Scaling Index	175
9.1	Introduction	175
9.2	Equation for Scaling Index	182
9.3	Higher Correlations	184
9.4	Discussion	187
10	Area Law	192
10.1	Introduction	192
10.2	Stokes Condition and Mean Curvature	196
10.3	Loop Equation Beyond Logarithmic Approximation	197
10.4	Exact Solution for Flat Loop	198
10.5	Loop Equation in Quadratic approximation	200
10.6	Minimal Area In Conformal Metric Field	201
10.7	Vorticity Correlations and Equation for Scaling Index	204
10.8	Conclusion	205
11	Recent progress of the Kelvinon Solution and Circulation PDF	205
11.1	Time evolution of the Kelvinon	205
11.2	Kelvinon loop functionals and Gaussian forces	208
11.3	Kelvinon and the Minimal Surface	210
11.4	The algebraic solution for the loop functional	210
11.5	PDF tails and time symmetry breaking	212
11.6	Matching the Kelvinon solution to the DNS	213
11.7	The circulation moments in Kelvinon solution	216
11.8	Sum over topologies and quantum equivalence	218
12	Conclusions and discussion	220
12.1	Clebsch confinement and compactification phase transition	220
12.2	Matching the DNS	222
12.3	Extreme intermittency and its microscopic mechanism	222
12.4	Kelvinon as the substitute of Gibbs distribution	223

12.5	Duality	225
12.6	The local velocity and strain statistics	227
12.7	Heuristic model for the multi-fractal laws	228
12.8	More predictions	230
Appendix A	The Cylindrical CVS equations	241
Appendix B	Symmetric Traceless Random Matrices	242
Appendix C	Spherical Gauge	243
Appendix D	Geometric structure of constrained vortex surfaces (by Camillo De Lellis, Elia Brué)	247
Appendix D.1	CVS conditions: geometric interpretation and instability in the compact case	248
Appendix D.2	Rigidity of the CVS condition for closed surfaces	251
Appendix D.3	Proof of Theorem Appendix D.6	253
Appendix D.4	Proof of Theorem Appendix D.7	253
Appendix D.4.1	Proof of Lemma Appendix D.11	254
Appendix D.5	Proof of Theorem Appendix D.10	255
Appendix D.6	Solutions with cylindrical symmetry	259
Appendix E	Topological defects in Turbulent flows, (by Grig- ory Volovik)	263
Appendix E.1	Classical vs quantum turbulence	264
Appendix E.2	Clebsch hydrodynamics vs Heisenberg ferro- magnets	264
Appendix E.3	Topological objects: hedgehog, instanton, do- main wall, quantum of circulation	265
Appendix E.4	Dynamic invariants in hydrodynamics (circu- lation and helicity) and their quantization in superfluids . .	266
Appendix E.5	Hydrodynamics in terms of tetrads	267
Appendix E.6	Dirac monopole with observable Dirac strings	268
Appendix E.7	Dirac monopole with one Dirac string	268
Appendix E.8	Dirac monopole with two Dirac strings	269
Appendix E.9	General case with two Dirac strings and monopole with charge N	269
Appendix E.10	Monopole in spherical layer	269

Appendix E.11	From monopole to pancake vortex sheet	271
Appendix E.12	Wall bounded by string	273
Appendix E.13	$SO(3)$ hydrodynamics of incompressible liquid	274
Appendix E.14	Spin connection and torsion	275
Appendix E.15	Conclusion	276

1. Historical Notes. Field-String Duality

The potential role of vortex sheets as dominant structures in fully developed turbulence was first suggested by Burgers in 1948¹ with his famous planar vortex sheet. This solution was then extended by Townsend,² but nothing much was done with this solution until recently.

In the late '80s, we found that the vortex sheet dynamics represent a gauge-invariant 2D Hamiltonian system with multivalued Action.³ The steady-state corresponded to the minimum of the Hamiltonian of this system.

This correspondence was the first manifestation of Duality between the fluctuating vector field and fluctuating geometry. The ADS/CFT Duality in quantum field theory discovered by Juan Maldacena in 1999 became one of the most important developments in modern theoretical physics.

The velocity-vortex sheet duality is still developing, with some important advances in recent years.

We proposed in⁴ a discrete version of the system with a triangulated surface with conserved variables Γ at vertices.

There were multiple works by applied mathematicians studying this time evolution numerically (Kaneda⁵ and some others). The consensus was that this evolution suffered from the Kelvin-Helmholtz instability, leading to the loss of smooth shape and possibly a finite time roll-up singularity.

Recently we made some more progress in vortex sheet theory as Lagrangian dynamics and studied solutions with various topologies.

Various fascinating regimes preceded the fully developed isotropic turbulence, such as shear flows.⁶ There are complex patterns of periodic motions in these intermediate regimes, suggesting even more complex patterns in extreme turbulence.

We suggested^{7,8,9} that turbulence is a 2D statistical field theory of random vortex sheets, using some elements of the string theory. The problem with that approach is that random surfaces are unstable as a statistical field theory in 3 dimensions.

The vortex surfaces are also unstable due to Kelvin-Helmholtz, so this idea is questionable.

The Navier-Stokes Hopf equation for statistical distribution was reduced to the loop equation in.⁷ Mathematically, this reduced dynamical variables from vector field $\vec{v}(\vec{r})$ in three dimensions to the loop field $\vec{C}(\theta)$

in one dimension.

We have found some asymptotic relations from this equation, including Area law.

This loop equation is equivalent to a Schrödinger equation in loop space with complex Hamiltonian and viscosity in place of Planck's constant.

This analogy with quantum mechanics is not a poetic metaphor nor some model approximation: this is an **exact** mathematical equivalence. There are observable "quantum" effects in classical turbulence rooted in this amazing analogy.

The Area law was derived from the loop equation and later confirmed in remarkable DNS by Sreenivasan with collaborators.^{10,11}

This inspired the further development of the geometric theory of turbulence.^{12,13,14,15,16,8,17,18,19,9,20,21}

In particular, recently, it was discovered^{19,22} that there are new generic solutions of the Navier-Stokes equations with arbitrary constant background strain near the planar vortex sheet. The stable vortex sheets satisfy the local nonlinear equation $\hat{S}(\vec{r}) \cdot \Delta \vec{v}(\vec{r}) = 0$ where \hat{S} is a strain at every point \vec{r} of the vortex sheet.

These equations restrict the shape of the vortex sheet, and we have solved them exactly for cylindrical geometry. This solution represents a stable fixed point of the Euler dynamics.

Unfortunately, compact CVS surfaces were proven not to exist by De Lellis and Rué (see Appendix D.6). Our solution (5.64) was non-compact, which made it less relevant for the turbulence problem.

Recently we found relevant compact solutions of Euler dynamics, with conserved velocity circulation around a static loop due to the nontrivial topology of the Clebsch field. Similar topological defects (KLS domain walls bounded by Alice strings) were observed in real experiments in the superfluid helium.^{23,24}

These solutions (Kelvinons) are responsible for the PDF tails of velocity circulation $\Gamma = \oint_C v_\alpha dr_\alpha$ in the extreme turbulent limit $|\Gamma| \gg \nu$.

We initially thought these solutions were instantons (classical trajectories in imaginary time for a quantum system). However, at a closer look, Kelvinons turned out to be something else. They are not stationary in real-time nor minimize any known Action in imaginary time.

These are time-dependent Euler-Clebsch flows, conserving the velocity circulation for a fixed loop in space R_3 . This conservation occurs because the flow is stagnant at this particular loop.

To be more precise, the loop becomes a closed trajectory of this flow so that the points at the loop move around but never leave it, making it a stationary geometric object. Then, according to the Kelvin theorem, the circulation is conserved because the loop does not move.

The most striking feature of these solutions is the hidden compact motion of Clebsch field in the target space S_2 , accompanied by time-dependent diffeomorphisms (gauge transformation). The Euler Clebsch flow is a direct sum of the incompressible flow in R_3 and the incompressible flow in the target space S_2 .

In other words, the Clebsch field is subject to time-dependent gauge transformations. The Clebsch confinement due to unbroken gauge invariance makes the vorticity distribution invariant.

Compact motion is associated with quantized winding numbers, which label Kelvinons. The PDF of velocity circulation represents the sum of exponential terms with quantized slopes, like the black body radiation.

In the case of radiation, the energy quantization follows from the compactness of motions of electrons in atoms. In our case, quantization of the winding numbers, which define the decrements of exponential PDF decay, is a consequence of the compactness of the target space S_2 for Clebsch variables.

This quantization is one of the quantum effects that all follow from the loop equation's equivalence to quantum mechanics in loop space.

As we recently found, Kelvinon also explains and correctly describes the asymmetry of the circulation PDF (i.e., time-reversal breaking).

The perfect fit of the observed circulation PDF¹⁰ by the Kelvinon prediction confirms the Duality of the turbulence theory and the Kelvinon mechanism of the intermittency of velocity circulation.

On a deeper level, it provides a strong argument in favor of the quantum mechanical description of the classical turbulence by the loop equation.

2. Introduction

2.1. *The statement of the problem and basic results*

The ultimate goal of turbulence studies is to solve the Navier-Stokes equations and determine why and how the solution covers some manifold rather than staying unique given initial data and boundary conditions.

We also need to understand why it is irreversible even at zero viscosity when the Navier-Stokes equations formally become the Euler equation corresponding to the reversible Hamiltonian system with conserved energy.

Once we know why and how the solution covers some manifold – a degenerate fixed point of the Navier-Stokes equations – we would like to know the parameters and the invariant measure on this manifold.

The first obstacle to overcome on this path is understanding the irreversibility of the Navier-Stokes dynamics in a limit when the viscosity goes to zero at fixed energy dissipation.

We know (or at least assume) that the vortex structures in this extreme turbulent flow collapse into thin clusters in physical space. Snapshots of vorticity in numerical simulations^{25,26} show a collection of tube-like structures relatively sparsely distributed in space.

The large vorticity domains and the large strain domain lead to anomalous dissipation: the enstrophy integral is dominated by these domains so that the viscosity factor in front of this integral is compensated, leading to a finite dissipation rate. It was observed years ago and studied in the DNS.²⁷

There was an excellent recent DNS^{10,11} studying statistics of vorticity structures in isotropic turbulence with a high Reynolds number. Their distribution of velocity circulation appeared compatible with 2D vortex structures (which we now call Kelvinons) suggested in¹⁵ following our early suggestions about area law for the velocity circulation.⁷

They confirmed the area law and compared it with the tensor area law, which would correspond to a constant uniform vortex, irrelevant to the turbulence. These two laws are indistinguishable for simple loops like a square, and they both are solutions to the loop equation but are very different for twisted or non-planar loops.

Their data supported the area law, which inspired our search for the relevant vorticity structures behind that law.

Some recent works also modeled sparse vortex structures in classical²⁸ and quantum²⁹ turbulence.

We know such 2D structures in the Euler dynamics: these are vortex surfaces. Vorticity collapses into a thin boundary layer around the surface, moving in a self-generated velocity field. Such motion is known to be unstable against the Kelvin-Helmholtz instabilities, which undermines the whole idea of random vortex surfaces.

However, the exact solutions of the Navier-Stokes equations discovered

in the previous century by Burgers and Townsend^{1,2} show stable planar sheets with Gaussian profile of the vorticity in the normal direction, peaked at the plane.

Thus, the viscosity effects in certain cases suppress the Kelvin-Helmholtz instabilities leading to stable, steady vortex structures.

This stable Gaussian solution is not the most general one; it takes some tuning of parameters in the background flow. We found this tuning to reduce to a simple local equation for the arithmetic mean of strain tensors on two sides of the surface (this tensor annihilates the velocity gap vector).

Let us define the conditions and assumptions we take.

We adopt Einstein's implied summation over repeated Greek indexes $\alpha, \beta, \gamma, \dots$. We also use the conventional vector notation for coordinates \vec{r} , velocity \vec{v} , and vorticity $\vec{\omega} = \vec{\nabla} \times \vec{v}$. The Greek indexes α, β, \dots run from 1 to 3 and correspond to physical space R_3 , and the lower case Latin indexes a, b, \dots take values 1, 2 and correspond to the internal parameters on the surface. We shall also use the Kronecker delta $\delta_{\alpha\beta}, \delta_{ab}$ in three and two dimensions as well as the antisymmetric tensors $e_{\alpha\beta\gamma}, e_{ab}$.

1. We address the turbulence problem from the first principle, the Navier-Stokes equation, forced at the volume boundary.
2. We study an infinite isotropic flow in the extreme turbulent limit (viscosity going to zero at a fixed dissipation rate).
3. We start with steady solutions (fixed points of Euler equations) and investigate the stability of these fixed points, leading to new boundary conditions (CVS) of the Euler equations on vortex surfaces.
4. New mathematical theorems eliminate stable, compact vortex sheets, leaving only unbounded surfaces. We find exact analytical solutions for the family of such surfaces and related flow.
5. We assume potential random forcing at the boundary of the turbulent volume. We argue that such forcing is sufficient to create energy flux from the boundary, dissipating later on the dense vorticity structures at small scales.
6. We compute the dissipation on stable vortex sheets in the extreme turbulent limit as a surface integral and prove that it is conserved as a consequence of CVS.
7. We also compute the PDF tails for the velocity circulations, dominated, as we argue, by a Kelvinon: nontrivial topological defect of the

Clebsch field with two winding numbers and conserved circulation around a static (not moving) loop.

8. This PDF perfectly matches the exponential laws observed in DNS. The time-odd topological winding number explains the time-reversal breaking in the DNS.
9. We derive and systematically investigate the loop equations for the circulation PDF and express the turbulent limit as the WKB limit.
10. We elaborate a mystifying mathematical equivalence of the loop equation to the Schrödinger equation in loop space with complex Hamiltonian, leading to quantization of classical circulation on the topological solutions.
11. Another surprising consequence of this equivalence is the superposition principle. The general solution for circulation PDF involves a sum over topological classes of Kelvinons.
12. We do not take any model simplifications in our theory, but certain parameters remain phenomenological constants, which we cannot yet compute.

2.2. Stable vortex sheets and irreversibility of turbulence

The recent research^{19,22} revealed that the Burgers-Townsend regime required certain restrictions on the eigenvalues and eigenvectors of the background strain¹ for the planar vortex sheet solution.

This research is summarized and reviewed in our paper.²⁰ The reader can find the exact solutions and the plots illustrating the vorticity leaks in the case of the non-degenerate background strain.

Abstracting from these observations, we conjectured in that paper that the local stability condition of the vortex surface with the local normal vector $\vec{\sigma}$ and local mean boundary value of the strain tensor \hat{S} reduces to three equations (with \vec{v}_{\pm} being the boundary values of velocity on each side)

$$\vec{v}_{\pm} \cdot \vec{\sigma} = 0; \quad (2.1)$$

$$\hat{S} \cdot (\vec{v}_{+} - \vec{v}_{-}) = 0; \quad (2.2)$$

$$\hat{S}_{nn} = \vec{\sigma} \cdot \hat{S} \cdot \vec{\sigma} < 0 \quad (2.3)$$

¹The alignment of vorticity with strain tensor in the turbulent flow was observed long ago³⁰ and studied in the DNS since then.

We call these equations the Confined Vortex Surface or CVS equations. They are supposed to hold at every point of the vortex surface, thus imposing extra boundary conditions on the Euler equations.

As conventional Neumann boundary conditions for potential flow on each side of a fixed vortex surface (the first CVS equation) uniquely determine the local strain tensor, the two additional CVS boundary conditions restrict the allowed shapes of vortex surfaces.

The first CVS equation is simply a statement that the surface is steady. Only the normal velocity must vanish for such a steady surface– the tangent flow around the surface reparametrizes its equation but does not move it in the Euler-Lagrange dynamics.

The second CVS equation is an enhanced version of the vanishing eigenvalue requirement. The velocity gap $\Delta\vec{v} = \vec{v}_+ - \vec{v}_-$ should be a null vector for this zero eigenvalue. This requirement is stronger than $\det \hat{S} = 0$.

The third equation demands that the strain move the fluid towards both sides of the surface.

With negative normal strain and zero strain in the direction of the velocity gap, the flow effortlessly slides along the surface on both sides without leakage and pile-up.

Here is an intuitive explanation of the CVS conditions– they provide permanent tangential flow around the surface, confining vorticity inside the boundary layer.

Once these requirements are satisfied in the local tangent plane, one could solve the Navier-Stokes equation in the (flat) boundary layer and obtain the Gaussian Burgers-Townsend solution, vindicating the stability hypothesis. The error function of the normal coordinate will replace the velocity gap, and the delta function of tangent vorticity will become the Gaussian profile with viscous width.

The flow in the boundary layer surrounding the local tangent plane

has the form³¹ (with $\Phi_{\pm}(r)$ being velocity potentials on both sides)

$$\vec{v}(\vec{r}_0 + \vec{\sigma}_0 \zeta) = \frac{1}{2}(\vec{v}_+(\vec{r}_0) + \vec{v}_-(\vec{r}_0)) + \frac{1}{2}(\vec{v}_+(\vec{r}_0) - \vec{v}_-(\vec{r}_0)) \operatorname{erf}\left(\frac{\zeta}{h\sqrt{2}}\right); \quad (2.4)$$

$$\vec{\sigma}_0 = \vec{\sigma}(\vec{r}_0); \quad (2.5)$$

$$\vec{v}_{\pm}(\vec{r}_0) = \vec{\nabla} \Phi_{\pm}(\vec{r}_0); \quad (2.6)$$

$$\vec{\omega}(\vec{r}_0 + \vec{\sigma}_0 \zeta) = \frac{\sqrt{2}}{h\sqrt{\pi}} \vec{\sigma}_0 \times (\vec{v}_+(\vec{r}_0) - \vec{v}_-(\vec{r}_0)) \exp\left(-\frac{\zeta^2}{2h^2}\right); \quad (2.7)$$

$$h = \sqrt{\frac{\nu}{-\vec{\sigma}_0 \cdot \hat{S}(\vec{r}_0) \cdot \vec{\sigma}_0}}; \quad (2.8)$$

$$\hat{S}_{\alpha\beta}(\vec{r}_0) = \frac{1}{2} \partial_{\alpha} \partial_{\beta} \Phi_+(\vec{r}_0) + \frac{1}{2} \partial_{\alpha} \partial_{\beta} \Phi_-(\vec{r}_0) \quad (2.9)$$

With the inequality $S_{nn} = \vec{\sigma}_0 \cdot \hat{S}(\vec{r}_0) \cdot \vec{\sigma}_0 < 0$ satisfied, this width h will be real positive.

It is important to understand that this inequality breaks the reversibility of the Euler equation: the strain is an odd variable for time reflection, although it is even for space reflection.

Thus, we have found a dynamic mechanism for the irreversibility of the turbulent flow: the vorticity can collapse only to the surface with negative normal strain; otherwise, it is unstable.

Another way of saying this is as follows. The strain tensor has three local eigenvalues, adding up to zero. We sort them in decreasing order. The first one is positive, the last one is negative, and the second one lies in between and can, in principle, have any sign.

The stable vortex sheet orients itself locally normal to the last eigenvector and distorts the flow so that the middle eigenvalue vanishes. The velocity gap in this flow is aligned with the middle eigenvector, the one with the vanishing eigenvalue.

Let us systematically describe this theory, starting from the vortex sheet dynamics.

3. Hamiltonian Dynamics of Vortex Sheets

The vortex sheets (velocity gaps) have a long history, with various famous scientists contributing to the theory. The vortex surfaces recently

came to our attention after it was argued^{18,9} that they provide the basic fluctuating variables in turbulent statistics.

Let us define here the necessary equations.

Navier-Stokes equations

$$\partial_t \vec{v} + (\vec{v} \cdot \vec{\nabla}) \vec{v} + \vec{\nabla} p = \nu \vec{\nabla}^2 \vec{v}; \quad (3.1a)$$

$$\vec{\nabla} \cdot \vec{v} = 0; \quad (3.1b)$$

can be rewritten as the equation for vorticity

$$\vec{\omega} = \vec{\nabla} \times \vec{v}; \quad (3.2a)$$

$$\partial_t \vec{\omega} + (\vec{v} \cdot \vec{\nabla}) \vec{\omega} - (\vec{\omega} \cdot \vec{\nabla}) \vec{v} = \nu \vec{\nabla}^2 \vec{\omega}; \quad (3.2b)$$

As for the velocity, it is given by a Biot-Savart integral

$$\vec{v}(r) = -\vec{\nabla} \times \int d^3 r' \frac{\vec{\omega}(r')}{4\pi|r-r'|} \quad (3.3)$$

which is a linear functional of the instant value of vorticity. There is, in general, a solution of the Laplace equation to be added to the Biot-Savart integral.

The energy dissipation is related to the enstrophy (up to total derivative terms, vanishing by the Stokes theorem)

$$-\partial_t H = \mathcal{E} = \nu \int d^3 r \vec{\omega}^2 \quad (3.4)$$

The Euler equation corresponds to setting $\nu = 0$ in (3.1a), (3.2b). This limit is known not to be smooth, leading to a statistical distribution of vortex structures, which is the whole turbulence problem.

Within the Euler-Lagrange equations, the shape S of the vortex surface is arbitrary, as well as the density $\Gamma(\vec{r} \in S)$ parametrizing the velocity discontinuity $\Delta \vec{v} = \vec{\nabla} \Gamma$. The corresponding vortex surface dynamics^{3,4} represents a special case of the Hamiltonian dynamics in 2 dimensions with parametric invariance similar to the string theory.

3.1. Kelvin-Helmholtz instability

In conventional Euler-Lagrange dynamics, the vortex surface's shape is evolving, subject to Kelvin-Helmholtz instability, while Γ stays constant due to the Kelvin theorem.

The steady solution for the vortex surface \mathcal{S} , as we recently argued in^{18,9} would correspond to a particular potential gap $\Gamma(\mathcal{S}) = \Phi_+(\mathcal{S}) - \Phi_-(\mathcal{S})$ minimizing the fluid Hamiltonian.

This minimization is equivalent to the Neumann boundary condition for the potential flow $\vec{v}(\vec{r}) = \vec{\nabla}\Phi_{\pm}(\vec{r})$ inside and outside the vortex surface

$$\partial_n \Phi_+(\mathcal{S}) = \partial_n \Phi_-(\mathcal{S}) = 0 \quad (3.5)$$

The local normal displacement z of the surface² satisfies the Lagrange equation

$$\partial_t z = v_n = S_{nn} z + O(z^2) \quad (3.6)$$

$$S_{nn} = \frac{1}{2} \left(\partial_n^2 \Phi_+(\mathcal{S}) + \partial_n^2 \Phi_-(\mathcal{S}) \right) \quad (3.7)$$

The positive normal strain \hat{S}_{nn} would lead to the (trivial version of) Kelvin-Helmholtz instability, but in case

$$\hat{S}_{nn}(\mathcal{S}) < 0, \quad (3.8)$$

this steady vortex surface would be stable against smooth variations in a normal direction.

The Kelvin-Helmholtz instability remains when we allow high wavelength variations, but in certain cases, it is stabilized by viscosity (see below).

In the conventional analysis of the Kelvin-Helmholtz instability,³² Chapter 7, the variation of the displacement in the tangent direction is taken into account, which leads to a more general equation

$$\partial_t z = -az - \hat{b}z \quad (3.9)$$

where \hat{b} is a linear differential operator. The normal strain $-az$ was ignored in that book.

The equation is linear and can be solved in Fourier space where $\hat{b}z \Rightarrow \omega(k)\tilde{z}(k)$

$$\tilde{z}(k) = c_1 \exp \left(-(a + \omega(k))t \right) \quad (3.10)$$

²the tangent displacement is equivalent to reparametrization of the surface and, as such, can be discounted.¹⁹

This $\omega(k)$ has two eigenvalues $\pm k\Delta v_t$, of opposite sign, and the negative eigenvalue leads to the Kelvin-Helmholtz instability. This instability happens at large enough wave vectors $k \sim \frac{a}{\Delta v_t}$, invalidating the Euler vortex sheets.

However, the smearing of the vortex sheet in the boundary layer by viscosity stabilizes it under certain conditions, which we discuss below.

3.2. The Burgers-Townsend vortex sheet

We know some exact solutions of the Navier-Stokes equations where a boundary layer replaces the vortex sheet with the width $h \sim \sqrt{\frac{\nu}{a}}$.

The Burgers-Townsend solution reads

$$\vec{v} = \{ax, bF_h(z), -az\}; \quad (3.11a)$$

$$S_{\alpha\beta} = \text{diag}(a, 0, -a); \quad (3.11b)$$

$$\vec{\omega} = \{-bF'_h(z), 0, 0\}; \quad (3.11c)$$

$$F'_h(z) = \frac{1}{h\sqrt{2\pi}} \exp\left(-\frac{z^2}{2h^2}\right); \quad (3.11d)$$

$$F_h(z) = \text{erf}\left(\frac{z}{h\sqrt{2}}\right); \quad (3.11e)$$

$$h = \sqrt{\frac{\nu}{a}}; \quad (3.11f)$$

We verified this solution analytically in various coordinate systems in a *Mathematica*® notebook³³ for the reader's convenience. In the Euler limit of $\nu \rightarrow 0$, the vorticity reduces to $\delta(z)$, and the velocity gap reduces to $\text{sign}(z)$.

The dissipation in this limit is proportional to the area of the sheet

$$\mathcal{E} = b\sqrt{\frac{2a\nu}{\pi}} \int dS; \quad (3.12)$$

This result disappointed Burgers, who was looking for a finite limit of anomalous dissipation at $\nu \rightarrow 0$. In this solution, that finite limit would require ab^2 to grow as $1/\nu$, for which there were no physical reasons at the time.

We shall return to this issue later, considering it from the modern view of the self-consistent background strain.

3.3. Clebsch variables

Before going into details of the vortex sheet dynamics, let us mention the relation between vortex sheets and so-called Clebsch variables. These variables play an important role in solving the Euler equations with nontrivial topology.

We parameterize the vorticity by two-component Clebsch field $\phi = (\phi_1, \phi_2) \in R_2$:

$$\omega_\alpha = \frac{1}{2} e_{\alpha\beta\gamma} e_{ij} \partial_\beta \phi_i \partial_\gamma \phi_j \quad (3.13)$$

The Euler equations are then equivalent to passive convection of the Clebsch field by the velocity field (modulo gauge transformations, as we argue below):

$$\partial_t \phi_a = -v_\alpha \partial_\alpha \phi_a \quad (3.14)$$

$$v_\alpha(r) = \frac{1}{2} e_{ij} \left(\phi_i \partial_\alpha \phi_j \right)^\perp \quad (3.15)$$

Here V^\perp denotes projection to the transverse direction in Fourier space, or:

$$V_\alpha^\perp(r) = V_\alpha(r) + \partial_\alpha \partial_\beta \int d^3 r' \frac{V_\beta(r')}{4\pi|r-r'|} \quad (3.16)$$

One may check that projection (3.15) is equivalent to the Biot-Savart law (3.3).

The conventional Euler equations for vorticity:

$$\partial_t \omega_\alpha = \omega_\beta \partial_\beta v_\alpha - v_\beta \partial_\beta \omega_\alpha \quad (3.17)$$

follow from these equations.

The Clebsch field maps R_3 to R_2 and the velocity circulation around the loop $C \in R_3$:

$$\Gamma(C) = \oint_C dr_\alpha v_\alpha = \oint_{\gamma_2} \phi_1 d\phi_2 = \text{Area}(\gamma_2) \quad (3.18)$$

becomes the oriented area inside the planar loop $\gamma_2 = \phi(C)$. We will discuss this later when we build the Kelvinon.

The most important property of the Clebsch fields is that they represent a p, q (canonical) pair in this generalized Hamiltonian dynamics. The

phase-space volume element $D\phi = \prod_x d\phi_1(x)d\phi_2(x)$ is time-independent, as the Liouville theorem requires.

The generalized Beltrami flow (GBF) corresponding to steady vorticity is described by $G_\alpha(x) = 0$ where:

$$G_\alpha \stackrel{\text{def}}{=} \omega_\beta \partial_\beta v_\alpha - v_\beta \partial_\beta \omega_\alpha \quad (3.19)$$

These three conditions are, in fact, degenerate, as $\partial_\alpha G_\alpha = 0$. So, there are only two independent conditions, the same as the number of local Clebsch degrees of freedom. However, as we see below, the relation between vorticity and Clebsch field is not invertible.

3.4. Gauge invariance

Our system possesses some gauge invariance (canonical transformation in the Hamiltonian dynamics or area preserving diffeomorphisms geometrically).

$$\phi_a(r) \Rightarrow M_a(\phi(r)) \quad (3.20)$$

$$\det \frac{\partial M_a}{\partial \phi_b} = \frac{\partial(M_1, M_2)}{\partial(\phi_1, \phi_2)} = 1. \quad (3.21)$$

These transformations manifestly preserve vorticity and, therefore, velocity.
3

In terms of field theory, this is an exact gauge invariance, much like color gauge symmetry in QCD, which is why back in the early 90-ties, we referred to Clebsch fields as "quarks of turbulence." To be more precise, they are both quarks and gauge fields simultaneously.

It may not be very clear that there is another gauge invariance in fluid dynamics, namely the **volume** preserving diffeomorphisms of Lagrange dynamics. Due to incompressibility, the element of the fluid, while moved

³These variables and their ambiguity were known for centuries,³⁴ but they were not utilized within hydrodynamics until the pioneering work of Khalatnikov³⁵ and subsequent publications of Kuznetsov and Mikhailov³⁶ and Levich³⁷ in early 80-ties. The modern mathematical formulation in terms of symplectomorphisms was initiated in.³⁸ Yakhot and Zakharov³⁹ derived the K41 spectrum in weak turbulence using some approximation to the kinetic equations in Clebsch variables.

by the velocity field, preserved its volume. However, these diffeomorphisms are not the symmetry of the Euler dynamics, unlike the **area** preserving diffeomorphisms of the Euler dynamics in Clebsch variables.

One could introduce gauge fixing, which we will discuss later. The main idea is to specify the metric g_{ij} in Clebsch space as a gauge condition. The symplectomorphisms varies the metric while preserving its determinant.

At the same time, the topology of Clebsch space is specified by this gauge condition. We are going to choose the simplest topology of S_2 without handles. This gauge fixing is investigated in Appendix C. It does not require Faddeev-Popov ghosts.

As we argue in the later sections, the topology of the Clebsch space is not a matter of taste. There are two different phases of the turbulent flow – weak and strong turbulence. The weak turbulence corresponds to R_2 as the Clebsch target space, and strong turbulence, which we study here – to S_2 .

The R_2 Clebsch field can exist in a form of the waves in physical space R_3 with some conserved charge corresponding to the $O(2) = U(1)$ rotation group in the target space.³⁹

The S_2 Clebsch field is confined to a sphere and cannot exist as a wave in physical space.

As we argue later, this compactification phase transition $R_2 \Rightarrow S_2$ is the origin of the intermittency phenomena in strong turbulence.

Let us come back to the Clebsch field on a sphere.

Note that the GBF condition comes from the Poisson bracket with Hamiltonian $H = \int d^3r \frac{1}{2} v_\alpha^2$

$$G_\alpha(r) = [\omega_\alpha, H] = \quad (3.22)$$

$$\int d^3r' \frac{\delta \omega_\alpha(r)}{\delta \phi_i(r')} e_{ij} \frac{\delta H}{\delta \phi_j(r')} = \quad (3.23)$$

$$- \int d^3r' \frac{\delta \omega_\alpha(r)}{\delta \phi_i(r')} v_\lambda(r') \partial_\lambda \phi_i(r') \quad (3.24)$$

In the GBF, we only demand that this integral vanish. The steady solution for Clebsch would mean that the integrand vanishes locally, which is too strong. We could not find any finite steady solution for Clebsch field even in the limit of large circulation over a large loop.

The Euler evolution of vorticity does not mean the passive advection of the Clebsch field: the solution of a more general equation

$$\partial_t \phi_i = -v_\alpha \partial_\alpha \phi_i + e_{ij} \frac{\partial h(\phi)}{\partial \phi_j} \quad (3.25)$$

with some unknown function $h(\phi)$ would still provide the same Euler evolution of vorticity:

$$\partial_t \omega_\alpha = \int d^3 r' \frac{\delta \omega_\alpha(r)}{\delta \phi_i(r')} \partial_t \phi_i(r) = [\omega_\alpha, H] \quad (3.26)$$

The last term in $\partial_t \phi_i$ drops from here in virtue of infinitesimal gauge transformation $\delta \phi_a = \epsilon e_{ab} \frac{\partial h(\phi)}{\partial \phi_b}$ which leave vorticity invariant.

This invariance means that the Clebsch field is being gauge transformed while carried by the flow.

This motion's topology will play a central role in our theory of intermittency.

3.5. Spherical parametrization of Clebsch field

To find configurations with nontrivial topology, we have to assume that at least one of the two independent Clebsch fields, say, ϕ_2 is multivalued. The most natural representation was first suggested by Ludwig Faddeev and was used in subsequent works of Kuznetsov and Mikhailov³⁶ and Levich³⁷ in the early '80s.

$$\vec{\omega} = Z e_{abc} S_a \vec{\nabla} S_b \times \vec{\nabla} S_c; \quad (3.27)$$

$$S_1^2 + S_2^2 + S_3^2 = 1; \quad (3.28)$$

$$\phi_2 = \arg(S_1 + i S_2); \phi_1 = Z S_3; \quad (3.29)$$

where Z is some global constant with the dimension of viscosity, which becomes an **integral of motion** in vortex dynamics⁴.

⁴It plays a very important role in our theory: it absorbs all the randomness of the turbulent flow driven by random forces at the boundary. From the point of view of the Clebsch dynamics, it is the integral of motion; however, in the stochastic approach, one can take a particular realization of the external Gaussian forces, compute Z from the energy balance and later average the solution of the loop equation over these realizations of random forces.

The field ϕ_2 is defined modulo 2π . We shall assume it is discontinuous across a vortex sheet shaped as a disk \mathcal{D} .

Note also that this parametrization of vorticity is invariant to the shift $\phi_2 \Rightarrow \phi_2 + \pi$, corresponding to reflection of the complex field $\Psi = S_1 + \iota S_2$

$$\Psi \Rightarrow -\Psi; \quad (3.30)$$

$$\vec{\omega} = \text{inv} \quad (3.31)$$

This reflection symmetry allows us to look for the Clebsch field configurations with Ψ changing sign when the coordinate goes around some loop, like the Fermion wave function in quantum mechanics.

These configurations with an ambiguous sign of Ψ will play an important role in our theory later.

Let us now look at the helicity integral

$$H = \int_{R_3 \setminus \mathcal{D}} d^3 r \vec{v} \vec{\omega} \quad (3.32)$$

Note that velocity

$$v_i = \phi_2 \partial_i \phi_1 + \partial_i \phi_3 \quad (3.33)$$

will have discontinuity $\Delta \vec{v} = 2\pi n \vec{\nabla} \phi_1$

The ϕ_3 can be written as an integral

$$\phi_3(r) = \partial_\beta \int d^3 r' \frac{\phi_2(r') \partial_\beta \phi_1(r')}{4\pi |r - r'|} \quad (3.34)$$

plus an arbitrary solution of the Laplace equation.

If there is a discontinuity of the phase ϕ_2 and the corresponding discontinuity of velocity field on some surface \mathcal{S}_{disc} , the solution of the Laplace equation for ϕ_3 must satisfy Neumann boundary conditions (vanishing normal derivative at this surface).

In that case, this discontinuity surface will be steady in the Euler dynamics, as our theory requires (see later).

The same conditions apply to the other two components of the Clebsch field

$$\partial_n \phi_i(\mathcal{S}_{disc}) = 0; \quad (3.35)$$

The helicity integral could now be written as a map $R_3 \mapsto (\phi_1, \phi_2, \phi_3)$

$$H = \int_{R_3 \setminus \mathcal{D}} d^3r (\phi_1 \partial_i \phi_2 + \partial_i \phi_3) e_{ijk} \partial_j \phi_1 \partial_k \phi_2 = \quad (3.36)$$

$$\int_{R_3 \setminus \mathcal{D}} d\phi_1 \wedge d\phi_2 \wedge d\phi_3 \quad (3.37)$$

Here is the most important point. There is a following surgery performed in three-dimensional Clebsch space. An incision is made along the surface $\phi(\mathcal{D})$ and n more copies of the same space are glued to this incision like sheets of a Riemann surface of $f(z) = z^{k+\frac{1}{2}}$, except this time the three-dimensional spaces are glued at the two-dimensional boundary, rather than the two-dimensional Riemann sheets glued at a one-dimensional cut in the complex plane.

Best analogy: this disk is a portal to other Clebsch universes like in science fiction movies. The winding number of ϕ_2 counts these parallel universes when passing through that surface.

Integrating over ϕ_2 in (3.37), using discontinuity $\Delta\phi_2(\mathcal{D}) = 2\pi n$ and then integrating $\int_{\mathcal{D}} d\phi_3 \wedge d\phi_1$ we find a simple formula

$$H = 2\pi n \oint_C \phi_3 d\phi_1 \quad (3.38)$$

This helicity is 2π times the number of parallel universes times the area of the portal.

Later we shall consider less trivial configurations (Alice String) where the winding number is half-integer so that the complex variable $\Psi = S_1 + \iota S_2$ changes the sign after crossing the disk.

3.6. Euler flow as Clebsch flow in product space

In virtue of gauge invariance of the Clebsch parametrization of vorticity (3.27), the most general Clebsch dynamics involve time-dependent gauge transformation, as we have seen in Section 3.4.

The Euler-Lagrange flow passively carries the Clebsch field in addition to its gauge transformation. For the vector $\vec{S} \in S_2$, this flow becomes:

$$\partial_t S_i + (\vec{v} \cdot \vec{\nabla}) S_i + [h, S_i] = 0; \quad i = 1, 2, 3; \quad (3.39)$$

$$[A, B] = \frac{\partial A}{\partial \phi_1} \frac{\partial B}{\partial \phi_2} - \frac{\partial A}{\partial \phi_2} \frac{\partial B}{\partial \phi_1} \quad (3.40)$$

As discussed above, this equation, with arbitrary gauge function $h(\phi_1, \phi_2)$, leads to the usual Euler equations for vorticity and velocity. We call this equation Clebsch Flow Equation. The h - terms all cancel in the Euler equations for $\vec{\omega}, \vec{v}$.

Geometrically, this equation describes the passive flow in direct product space $R_3 \otimes S_2$ with velocity

$$V = \left(v_1, v_2, v_3, -\frac{\partial h}{\partial \phi_2}, \frac{\partial h}{\partial \phi_1} \right) \quad (3.41)$$

This flow conserves the volume element in each of the two spaces.

$$\text{div} V = \partial_i v_i + \partial_a e_{ab} \partial_b h = 0 + 0 = 0 \quad (3.42)$$

This flow corresponds to the vector $\vec{S}(\vec{r})$ being rotated while transported along the flow line in R_3 , thereby covering the target space S_2 .

This rotation is nonlocal in the target space, as it involves derivatives $\frac{\partial S_i}{\partial \phi_a}$. Geometrically, the point \vec{S} moves on a sphere while being carried by the Euler flow in physical space.

This gauge transformation accompanying the flow is a significant modification of the traditional view of the passive advection of the Clebsch field.

When solving Euler equations for the velocity field in Clebsch parametrization, one has also to fix this unknown velocity $u_a = e_{ab} \frac{\partial h}{\partial \phi_b}$ in target space.

3.7. Topological Invariants for closed surface

Let us now consider the case of a closed vortex sheet.

In that case, the first Clebsch field ϕ_2 takes constant values: $-\Delta\phi_2$ inside the surface and zero outside would lead to velocity gap $\Delta\vec{v} = \Delta\phi_2 \vec{\nabla}\phi_1$, corresponding to the potential gap $\Gamma = \phi_1 \Delta\phi_2$.

In short, the closed vortex surface (if it exists) is the bubble of the Clebsch field.

The values of the Clebsch field ϕ_1 outside the surface drop from the equation. One can take any smooth interpolating field ϕ_1 between closed vortex surfaces, and the vorticity field will stay zero outside and inside the surfaces.

Furthermore, the velocity circulation around any contractible loop at each surface vanishes because there is no normal vorticity on these surfaces.

The Clebsch topology plays no role in the case of closed surfaces with the spherical topology, unlike the case with open surfaces with edges $C_n = \partial S_n$ we considered above (see also¹⁸). There, the normal component of vorticity at the surface was present (and finite).

Still, our collection of closed vortex sheets in the general case has some nontrivial helicity (3.38). This helicity is pseudoscalar, but it preserves time-reversal symmetry. The higher genus surfaces say the torus, will have nontrivial circulation around its cycles, corresponding to conserved vorticity flux through the skin of the handle.

The parity transformation P changes the sign of velocity, keeping vorticity invariant, whereas the time-reversal T changes the signs of both velocity and vorticity.

The helicity integral is T -even and PT -odd. It measures the knotting of vortex lines between these surfaces.

As noted in,⁴ the surfaces avoid each other and themselves, so these are not just random surfaces. This property was studied in their time evolution and recently in their statistics.¹⁸

The circulation around each contractible loop on the surface will still be zero. However, the loop winding around a handle would produce a topologically invariant circulation $n\Delta\Gamma$ for any loop winding n times.

This $\Delta\Gamma$ is the period of $\Gamma(\xi)$ when the point ξ goes around this handle.³ This period depends upon the surface's size and shape, but it does not change when the path varies along the surface as long as it winds around the handle.

There is a flux through the handle related to tangential vorticity inside the skin of the surface. This flux through any surface intersecting the handle is topologically invariant and equals $\Delta\Gamma$.

Considering the circulation around some fixed loop in space will reduce to an algebraic sum of the circulations around closed surfaces' handles encircled by this loop. It will be topologically invariant when the loop moves in space without crossing any surfaces.

In particular, the closed vortex tube (topological torus) encircled by a fixed loop C in space would produce the circulation $\oint_C \vec{v} \cdot d\vec{r} = \Delta\Gamma$, which is equal to the period of Γ around the α cycle, corresponding to shrinking of C .

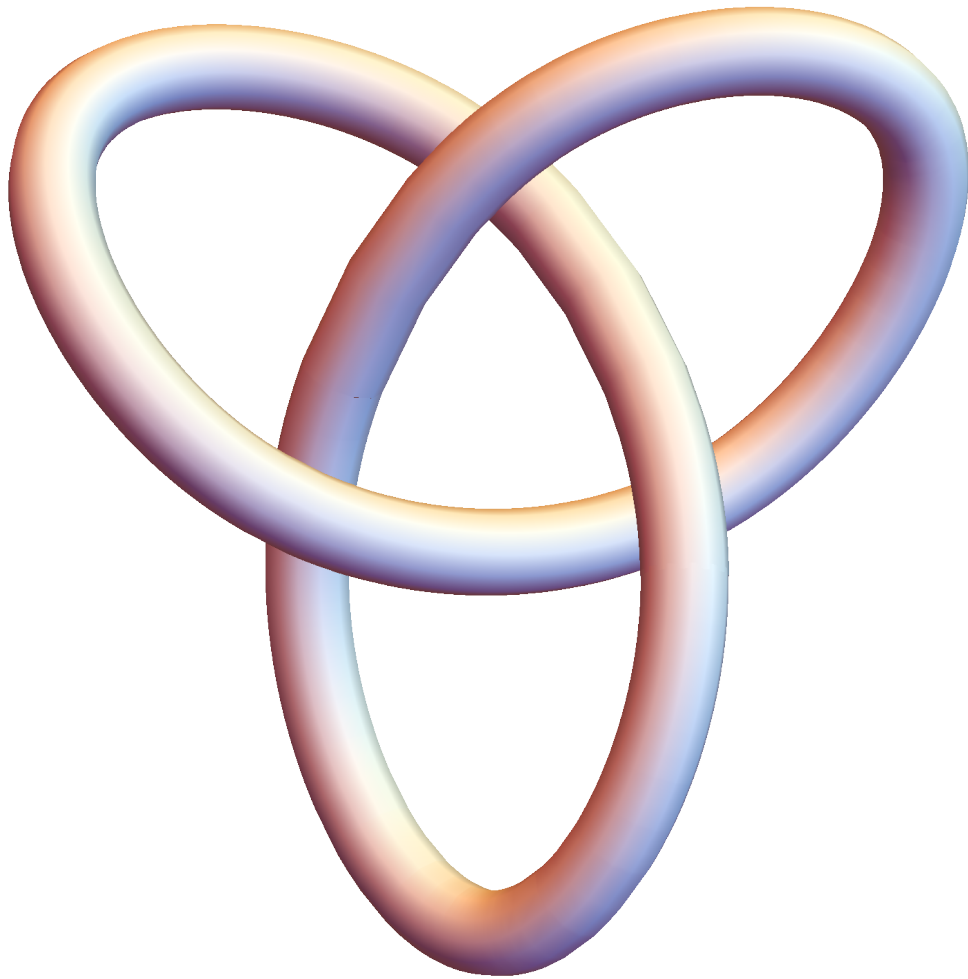


Figure 1: The torus is knotted to produce nontrivial helicity.

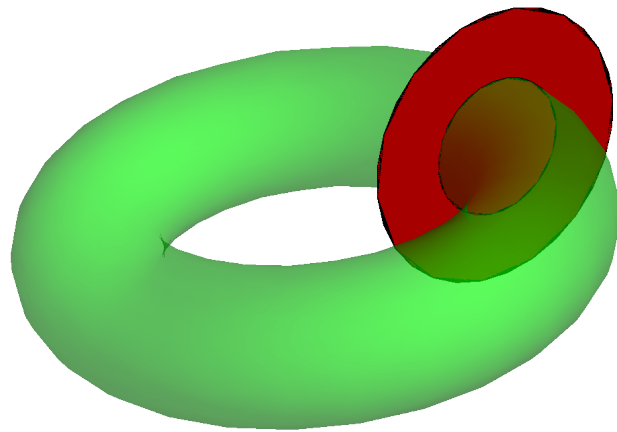


Figure 2: The green vortex tube T cut vertically by a red disk D_C . The vorticity flux through the disk reduces to the integral of velocity discontinuity over the α cycle.

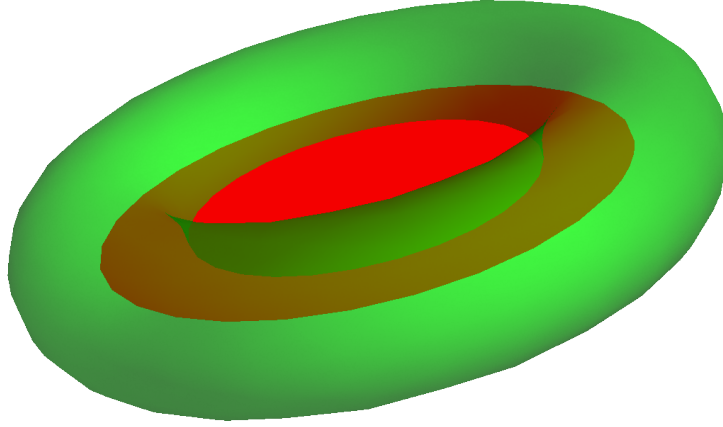


Figure 3: The green vortex tube T cut horizontally by a red disk D_C . The vorticity flux through the disk reduces to the integral of velocity discontinuity over the β cycle.

Another cross-section of the same vortex tube leads to circulation around another cycle of the torus.

To prove the relation between circulation over the disk edge C and $\Delta\Gamma$ over the corresponding cycle of the handle, let us consider the vorticity flux through the disk D_C bounded by C intersecting this torus T .

By Stokes' theorem, this flux equals the circulation on the external side of T minus the internal side. On the other hand, it is equal to the circulation around the edge C of this disk

$$\oint_C \vec{v} \cdot d\vec{r} = \oint_{\gamma \in T} \Delta \vec{v} d\vec{r} = \oint d\Gamma = \Delta\Gamma \quad (3.43)$$

3.8. The vortex sheet dynamics and parametric invariance

As we know, since the times of Euler and Lagrange, the Euler equations are equivalent to the statement that every element of any vortex structure is moving with the local velocity.

However, the mathematical meaning of this remarkable equivalency

was not elaborated initially. In particular, how does this statement apply to the singular vortex structures, where the local velocity is not defined?

In the case of the vortex line, the Euler velocity diverges at every point at the line; therefore, the Navier-Stokes equation must be used. It produces some exact solutions with an infinite velocity at the line in the vanishing viscosity limit.

We will not study these solutions here: our goal is the vortex sheet, where the Euler velocity is finite on both sides of the surface, with the tangent velocity gap.

In this case, the velocity driving each point of the vortex surface is an arithmetic mean of the velocities on both sides, in other words, the principal value of the Biot-Savart integral.

As we discussed in^{3,4} the velocity at the surface

$$\vec{v}^S(\vec{r}) = \frac{1}{2} \left(\vec{v}(\vec{X}^+(\xi)) + \vec{v}(\vec{X}^-(\xi)) \right) \quad (3.44)$$

The normal component v_n of velocity describes the surface's genuine change— its global motion or the change of its shape. This normal component must vanish at every surface point in a steady flow.

On the other hand, the remaining two tangent components \vec{v}_t of the velocity move points along the surface without changing the surface position or shape. To see that, we rewrite the tangent part \vec{v}_t^S of the surface velocity $\vec{v}^S(\vec{r})$ as time-dependent re-parametrization $\xi \Rightarrow \xi(t)$:

$$\vec{v}_t^S = \partial_t \vec{X}(\xi(t)) = \partial_a \vec{X} \partial_t \xi^a; \quad (3.45)$$

$$\partial_t \xi^a = g^{ab} \partial_b \vec{X} \cdot \vec{v}_t^S; \quad (3.46)$$

$$g_{ab} = \partial_a \vec{X} \cdot \partial_b \vec{X}; \quad (3.47)$$

Here g_{ab} is an induced metric, and g^{ab} is its inverse. To verify this identity, one has to expand \vec{v}_t^S in the two local plane vectors $\partial_1 \vec{X}, \partial_2 \vec{X}$ and use two identities

$$\partial_b \vec{X} \cdot \partial_c \vec{X} = g_{bc}; \quad (3.48)$$

$$g^{ab} g_{bc} = \delta_{ac} \quad (3.49)$$

For a closed surface, these tangent motions will never leave the surface. For the surface with the fixed edge C there is a boundary condition that

velocity normal to the edge vanishes $\vec{v}_t \times d\vec{r} = 0; \forall \vec{r} \in C$. In this case, the fluid will slide along C leading to its reparametrization, but it never leaves the surface.

We will restrict ourselves to the parametric invariant functionals, which do not depend on this tangent flow and will stay steady.

3.9. Multivalued Action

We introduced the Lagrange action of vortex sheets in the old paper.³ In that paper, we also conjectured the relation of turbulence to Random Surfaces.⁵

In the next paper,⁴ this Lagrange vortex dynamics was simulated using a triangulated surface. We calculated each triangle's contributions to the velocity field in terms of elliptic integrals. The positions of the triangle vertices served as dynamical degrees of freedom.

There were conserved variables related to the velocity gap as a function of a point at the surface. These points passively moved with the surface by the mean velocity on the surface's two sides.

Later, our equations were recognized and reiterated in traditional terms of fluid dynamics⁵ and simulated with a larger number of triangles⁴⁰ with similar results regarding the Kelvin-Helmholtz instability of the vortex sheet. There were dozens of publications using various versions of the discretization of the surface and various simulation methods.

Let us reproduce this theory for the reader's convenience before advancing it further.

The following ansatz describes the vortex sheet vorticity:

$$\vec{\omega}(\vec{r}) = \int_{\Sigma} d\vec{\Omega} \delta^3(\vec{X} - \vec{r}) \quad (3.50)$$

where the 2-form

$$d\vec{\Omega} \equiv d\Gamma \wedge d\vec{X} = d\tilde{\zeta}_1 d\tilde{\zeta}_2 e_{ab} \frac{\partial \Gamma}{\partial \tilde{\zeta}_a} \frac{\partial \vec{X}}{\partial \tilde{\zeta}_b}; \quad (3.51)$$

This vorticity is zero everywhere in space except the surface, where it is infinite. This ansatz must satisfy the divergence equation (the conservation

⁵I could not find³ anywhere online, but it exists in university libraries such as Princeton University Library and U.C. Berkeley Library.

of the "current" $\vec{\omega}$ in the language of statistical field theory) to describe the physical vorticity of the fluid,

$$\vec{\nabla} \cdot \vec{\omega} = 0; \quad (3.52)$$

This relation is built into this ansatz for arbitrary $\Gamma(\xi)$, as can be verified by direct calculation. In virtue of the singular behavior of the Dirac delta function, it may be easier to understand this calculation in Fourier space

$$\vec{\omega}^F(\vec{k}) = \int d^3r e^{i\vec{k} \cdot \vec{r}} \vec{\omega}(\vec{r}) = \int_{\Sigma} d\vec{\Omega} e^{i\vec{k} \cdot \vec{X}}; \quad (3.53)$$

$$i\vec{k} \cdot \vec{\omega}^F(\vec{k}) = \int_{\Sigma} d\Gamma \wedge d\vec{X} \cdot (i\vec{k}) e^{i\vec{k} \cdot \vec{X}} = \int_{\partial\Sigma} d\Gamma e^{i\vec{k} \cdot \vec{X}}; \quad (3.54)$$

If there is a surface boundary, this $\Gamma(\xi)$ must be a constant at this boundary for the identity $\vec{k} \cdot \vec{\omega}^F(\vec{k}) = 0$ to hold. Transforming to R_3 from Fourier space, we confirm the desired relation $\vec{\nabla} \cdot \vec{\omega} = 0$ in the sense of distribution, like the delta function itself.

It may be instructive to write down an explicit formula for the tangent components of vorticity in the local frame, where x, y is a local tangent plane and z is a normal direction

$$\omega_j(x, y, z) = \partial_i \Gamma e_{ij} \delta(z); \quad (3.55)$$

$$\omega_z(x, y, z) = 0; \quad (3.56)$$

In particular, outside the surface, $\vec{\omega} = 0$, so that its divergence vanishes trivially.

The divergence is manifestly zero in this coordinate frame

$$\vec{\nabla} \cdot \vec{\omega} = \delta(z) \partial_j \partial_i \Gamma e_{ij} = 0; \quad (3.57)$$

Let us compare this with the Clebsch representation

$$\omega_\alpha = e_{\alpha\beta\gamma} \partial_\beta \phi_1 \partial_\gamma \phi_2, \quad (3.58)$$

We see that in case ϕ_2 takes one space-independent value ϕ_2^{in} inside the surface and another space-independent value ϕ_2^{out} outside, the vorticity will have the same form, with

$$\Gamma = \phi_1(\phi_2^{in} - \phi_2^{out}) \quad (3.59)$$

Neither⁴ nor any subsequent papers noticed this relation between Clebsch field discontinuity and vortex sheets.

As we already noted in,^{3,4} the function $\Gamma(\xi_1, \xi_2)$ is defined modulo diffeomorphisms $\xi \Rightarrow \eta(\xi); \det \partial_i \eta_j > 0$ and is conserved in Lagrange dynamics:

$$\partial_t \Gamma = 0; \quad (3.60)$$

This function is related to the 1-form of velocity discontinuity

$$d\Gamma = \Delta \vec{v} \cdot d\vec{X} \quad (3.61)$$

where the velocity gap

$$\Delta \vec{v}(\xi) = \vec{v}(X_+(\xi)) - \vec{v}(X_-(\xi)) \quad (3.62)$$

Another way of writing the relation for Γ is to note that the velocity field is purely potential outside the surface because there is no vorticity.

However, the potential Φ^- inside is different from the potential Φ^+ outside.

In this case, the velocity discontinuity equals the difference between the gradients of these two potentials or, equivalently

$$\Gamma(\vec{r}) = \Phi^+(\vec{r}) - \Phi^-(\vec{r}); \forall \vec{r} \in S \quad (3.63)$$

The surface is driven by the self-generated velocity field (mean of velocity above and below the surface). Let us substitute our ansatz for vorticity into the Biot-Savart integral for the velocity field and change the order of integration

$$\begin{aligned} \vec{v}(\vec{r}) = & -\frac{1}{4\pi} \vec{\nabla} \times \int d^3 r' \frac{1}{|\vec{r} - \vec{r}'|} \int d\vec{\Omega} \delta^3(X - \vec{r}') = \\ & \frac{1}{4\pi} \int d\vec{\Omega} \times \vec{\nabla} \frac{1}{|\vec{r} - \vec{X}|} \end{aligned} \quad (3.64)$$

3.10. Steady State as a Minimum of the Hamiltonian

The Lagrange equations of motion for the surface

$$\partial_t \vec{X}(\xi) = \vec{v}(\vec{X}(\xi)) \quad (3.65)$$

were shown in^{3,4} to follow from the action

$$S = \int \Gamma dV - \int H dt; \quad (3.66)$$

$$dV = d\tilde{\zeta}_1 d\tilde{\zeta}_2 dt \frac{\partial \vec{X}}{\partial \tilde{\zeta}_1} \times \frac{\partial \vec{X}}{\partial \tilde{\zeta}_2} \cdot \partial_t \vec{X}; \quad (3.67)$$

$$H = \frac{1}{2} \int d^3 r \vec{v}^2 = \frac{1}{2} \int_S \int_S \frac{d\vec{\Omega} \cdot d\vec{\Omega}'}{4\pi |\vec{X} - \vec{X}'|}; \quad (3.68)$$

This dV is the 3-volume swept by the surface area element in its movement for the time dt .

The easiest way to derive the vortex sheet representation for the Hamiltonian is to go in Fourier space where the convolution becomes just multiplication and use the incompressibility condition $\vec{k} \cdot \vec{v}^F(\vec{k}) = 0$

$$\vec{\omega}^F(\vec{k}) = \iota \vec{k} \times \vec{v}^F(\vec{k}); \quad (3.69)$$

$$\vec{v}^F(\vec{k}) \cdot \vec{v}^F(-\vec{k}) = \frac{\vec{\omega}^F(\vec{k}) \cdot \vec{\omega}^F(-\vec{k})}{\vec{k}^2} \quad (3.70)$$

In the case of the handle on a surface, Γ acquires extra term $\Delta\Gamma = \oint_\gamma \Delta\vec{v} \cdot d\vec{r}$ when the point goes around one of the cycles $\gamma = \{\alpha, \beta\}$ of the handle.

This $\Delta\Gamma$ does not depend on the path shape because there is no normal vorticity at the surface, and thus there is no flux through the surface. This topologically invariant $\Delta\Gamma$ represents the flux through the handle cross-section.

This ambiguity in Γ makes our action multivalued as well.

Let us check the equations of motion emerging from the variation of the surface at fixed Γ :

$$\delta \int H dt = \int d\vec{\Omega} \times \delta \vec{X} \cdot \vec{v}(\vec{X}) dt; \quad (3.71)$$

$$\delta \int \Gamma dV = \int d\vec{\Omega} \times \delta \vec{X} \cdot \partial_t \vec{X} dt \quad (3.72)$$

As we discussed above, the tangent components of velocity at the surface create tangent motion, resulting in the surface's reparametrization.

One of the two tangent components of the velocity (along the line of constant $\Gamma(\tilde{\zeta})$) does not contribute to the variation of the action so that the

correct Lagrange equation of motion following from our action reads

$$\partial_t \vec{X}(\xi) = \vec{v}(\vec{X}(\xi)) \mod e^{ij} \partial_i \Gamma \partial_j \vec{X} \quad (3.73)$$

We noticed this gauge invariance before in.³ Now we see that both tangent components of the velocity could be absorbed into the reparametrization of a surface; therefore, these components do not represent an observable change.

However, the normal component of the velocity must vanish in a steady solution, which provides a linear integral equation for the conserved function $\Gamma(\xi)$.⁶

In the general case, when there is an ensemble of such surfaces $S_n, n = 1, \dots, N$ each has its discontinuity function $\Gamma_n(\xi)$. At each point on each surface $\vec{r} \in S_n$, the net normal velocity adding up from all surfaces, including this one in the Biot-Savart integral, must vanish:

$$\vec{\Sigma}_n(\xi) \cdot \vec{v}(\vec{X}_n(\xi)) = 0; \quad (3.74)$$

$$\vec{\Sigma}_n(\xi) = e^{ij} \partial_i \vec{X}_n \times \partial_j \vec{X}_n; \quad (3.75)$$

$$\vec{v}(\vec{r}) = \frac{1}{4\pi} \sum_m \int d\vec{\Omega}_m \times \vec{\nabla} \frac{1}{|\vec{r} - \vec{X}_m|} \quad (3.76)$$

This requirement provides a linear set of N linear integral equations (called Master Equation in¹⁸) relating N independent surface functions $\Gamma_1 \dots \Gamma_N$. With this set of equations satisfied, the collection of surfaces $S_1 \dots S_N$ will remain steady up to reparametrization.

Here is an essential new observation we have found in that paper.

The Master Equation is equivalent to the minimization of our Hamiltonian by $\Gamma_n, n = 1 \dots N$

$$H[\Gamma, \vec{X}] = \frac{1}{2} \sum_{n,m} \int_{S_n} \int_{S_m} \frac{d\vec{\Omega}_n \cdot d\vec{\Omega}_m}{4\pi |\vec{X}_n - \vec{X}_m|}; \quad (3.77)$$

$$\frac{\delta H[\Gamma, \vec{X}]}{\delta \Gamma_n(\xi)} = \vec{\Sigma}_n(\xi) \cdot \vec{v}(\vec{X}_n(\xi)); \quad (3.78)$$

⁶To be more precise, in the case of a uniform global motion of a fluid, the normal component of the velocity field must coincide with the normal component of this uniform global velocity \vec{v}^G .

The tangential components of velocity \vec{v}_t are included in the parametric transformations, as noted above. They are equivalent to variations of the Hamiltonian by the parametrization of Γ, \vec{X} and are, therefore, the tangent components of Lagrange equations of motion satisfied by parametric invariance.

Therefore, the normal surface velocity in the general case is equal to the Hamiltonian variation by Γ , as if Γ is the conjugate momentum corresponding to the surface's normal displacement. To be more precise, Γ in our action (3.66) is a conjugate momentum to the volume, which is locally equivalent – the variation of volume equals the area element times the normal displacement.

In other words, we can consider an extended dynamical system with the same Hamiltonian (3.77) but a wider phase space $\Gamma, \vec{X} \mod Diff$. We can introduce an extended Hamiltonian dynamics with our action (3.66).

This system is degenerate because for an arbitrary evolution of \vec{X} providing an extremum of the action, the evolution for Γ is absent, i.e., Γ is constant. It is a conserved momentum in our Hamiltonian dynamics with volume as a coordinate.

This conservation of Γ is a consequence of Kelvin's theorem. To see this relation,⁴ we rewrite this Γ as a circulation over the loop C puncturing the surface in two points A, B and going along some curve γ_{AB} on one side, then back on the same curve γ_{BA} on another side. The circulation does not depend upon the shape of γ_{AB} because there is no normal vorticity at the surface.

Another way to arrive at the conservation of Γ is to notice that it is related to the Clebsch field on the discontinuity surface, as we mentioned in the introduction.

The steady solution for $\vec{X} \mod Diff$ corresponds to the Hamiltonian minimum as a (quadratic) functional of Γ .

3.11. Does Steady Surface mean Steady Flow?

There is a subtle difference between the steady discontinuity surface and steady flow. After all, the flow around a steady object is not necessarily steady. There could be time-dependent motions in the bulk while the flow's normal component vanishes at the solid surface (as it always does).

This logic applies to the generic flow around steady solid objects but does not apply here. The big difference is that, by our assumption, there is no vorticity outside these discontinuity surfaces.

The Biot-Savart integral for the velocity field (3.64) is manifestly parametric invariant, if we transform **both** Γ, \vec{X}

$$\Gamma(\xi) \Rightarrow \Gamma(\eta(t, \xi)); \quad (3.79)$$

$$\vec{X}(\xi) \Rightarrow \vec{X}(\eta(t, \xi)); \quad (3.80)$$

$$\partial_t \eta_a = u_a(\eta); \quad (3.81)$$

This transformation describes the flux of coordinates η in parametric space with the velocity field $u_a(\eta)$. The tangent flow around the surface is equivalent to the transformation of \vec{X} , as demonstrated in (3.45).

However, in the Lagrange dynamics of vortex sheets, the function $\Gamma(\xi)$ remains constant, not constant up to reparametrization. However, an absolute constant so that $\partial_t \Gamma(\xi) = 0$ where time derivative goes at fixed ξ .

Therefore, the velocity field $\vec{v}(\vec{r})$ generally changes when the surface gets re-parametrized, but Γ does not. Naturally, one could not get a steady solution without solving some equations first :).

However, in our steady manifold, $\Gamma^*(\xi)$ is related to the surface by the Master Equation. Let us write it down once again

$$0 = \vec{\Sigma}_n \cdot \sum_m \int_{S_m} d\Gamma_m^* \wedge d\vec{X}_m \times \vec{\nabla}_n \frac{1}{|\vec{X}_n - \vec{X}_m|}; \quad (3.82)$$

$$\vec{\Sigma}_n = e^{ab} \partial_a \vec{X}_n \times \partial_b \vec{X}_n \quad (3.83)$$

This equation is invariant under the parametric transformation of both variables Γ^*, \vec{X} . This invariance means that the solution of this equation for Γ^* would come out as a parametric invariant functional of \vec{X} , also invariant by translations of \vec{X} .

As we have seen, this Master Equation leads to a vanishing normal velocity $\vec{\Sigma}_n \cdot \partial_t \vec{X}_n = 0$. The remaining tangent velocity leaves \vec{X} steady up to reparametrization. Therefore, in virtue of this Master Equation, the velocity field will also be steady.

We introduced a family of steady solutions of Lagrange equations, parametrized by an arbitrary set of discontinuity surfaces $\vec{X}_n(\xi)$ with discontinuities $\Gamma_n^*(\xi)$ determined by the minimization of the Hamiltonian.

The surfaces are steady up to time-dependent reparametrization (diffeomorphism). The equivalence of Lagrange and Euler dynamics suggests that these are steady solutions to the Euler equations.

The above arguments are too formal to accept our steady solution of the Euler equation. These are weak solutions with tangent discontinuities of velocity, and thus they require some care to investigate the equivalence between the Lagrange and Euler solutions.

We will investigate these solutions' stability in the following sections.

4. Clebsch Bubbles

4.1. New Steady Solutions of the Navier-Stokes equations

It was recently observed¹⁹ that in addition to the Burgers-Townsend sheet with the symmetric Gaussian profile of vorticity, there is an asymmetric solution expressed in the Hermite function with the negative fractional index. The solution for vorticity decays as a Gaussian on one side of the sheet; on the other, it grows or decays as a power.

In other words, vorticity leaks from that sheet, unlike the Burgers-Townsend sheet, where it collapses to a thin layer.

As for the velocity field, it does not have a finite gap at the asymmetric sheet. It grows or decays as power on one side while tending to a constant on another side.

Thus, this is not a vortex sheet in the sense of an Euler solution with a finite velocity gap.

Later, another important observation was made.²² The asymmetric sheet turned out to be the general solution of the Navier-Stokes equation for the constant background strain

$$S_{\alpha\beta} = \frac{1}{2}(\partial_\alpha v_\beta + \partial_\beta v_\alpha) \quad (4.1)$$

The eigenvalues of the strain add up to zero by incompressibility, so there are two independent parameters here.

$$\hat{S} = \text{diag}(a, b, -(a+b)) \quad (4.2)$$

We can always assume that the third eigenvalue corresponds to the eigenvector in the normal direction.

The asymmetric solution exists when

$$a + b > 0 \quad (4.3)$$

as required by Kelvin-Helmholtz stability.

The special case considered in¹⁹ corresponds to $a = b > 0$. The vorticity of the generic solution is proportional to the Hermite function

$$\omega_x \propto \exp\left(-\frac{z^2}{2h^2}\right) H_\mu\left(\frac{z}{h\sqrt{2}}\right); \quad (4.4)$$

$$\mu = -\frac{b}{a+b}; \quad (4.5)$$

$$\omega_x(z \rightarrow +\infty) \propto (z)^\mu \exp\left(-\frac{z^2}{2h^2}\right); \quad (4.6)$$

$$\omega_x(z \rightarrow -\infty) \propto (-z)^{\mu-1}; \quad (4.7)$$

$$v_y(z \rightarrow +\infty) \rightarrow 0; \quad (4.8)$$

$$v_y(z \rightarrow -\infty) \propto (-z)^\mu; \quad (4.9)$$

For every finite a, b vorticity decays negative z side as negative fractional power. The velocity at negative z grows or decays as z^μ . This decay makes any finite μ unacceptable for the vortex surface, which assumes a finite velocity gap.

There is also a mirror solution with $z \Rightarrow -z$.

The solution with odd velocity and even vorticity as a function of z

$$\omega_x \propto \exp\left(-\frac{z^2}{2h^2}\right) \left(H_\mu\left(\frac{z}{h\sqrt{2}}\right) + H_\mu\left(-\frac{z}{h\sqrt{2}}\right) \right); \quad (4.10)$$

has symmetric power tails $v_y \propto \pm|z|^\mu, \omega_x \propto |z|^{\mu-1}$.

4.2. The CVS as a linear boundary problem

The requirement that the Euler vortex sheet comes as a limit of the Navier-Stokes flow with vanishing viscosity is an obvious requirement for the classical fluid where viscosity is always finite so that the vortex sheet is an approximation to the smooth viscous flow.

Mathematically, this is a requirement of stability of the Euler equation against infinitesimal viscosity perturbation $\nu \vec{\nabla}^2 \vec{v}$.

We recently understood that this matching requirement is equivalent to a linear boundary problem.

In general, for the Euler vortex sheet with vanishing normal derivative the velocity gap and the mean strain are

$$\Delta \vec{v} = (\alpha, \beta, 0); \quad (4.11)$$

$$\hat{S} = (a, b, -a - b); \quad (4.12)$$

with four independent constant parameters α, β, a, b .

The matching NS Ansatz with planar symmetry has arbitrary dependence on the normal coordinate z

$$\vec{v} = \{ax, by + sS(z), -(a + b)z\}; \quad (4.13)$$

$$p = -\frac{1}{2}(ax)^2 - \frac{1}{2}(by)^2 - \frac{1}{2}(z(a + b))^2; \quad (4.14)$$

$$S(-\infty) = -1; \quad (4.15)$$

$$S(\infty) = 1 \quad (4.16)$$

The Galilean invariance makes the constant part of $S(z)$ arbitrary. We choose zero for simplicity, but this could be some local parameter at the tangent plane.

The NS equation within this Ansatz (dictated by the incompressibility and the planar geometry) reduces to the hypergeometric equation

$$S(z) = f(z/h); \quad (4.17)$$

$$h = \sqrt{\frac{v}{(a + b)}}; \quad (4.18)$$

$$f''(\xi) + \xi f'(\xi) - \frac{b}{a + b} f(\xi) = 0; \quad (4.19)$$

$$f(-\infty) = -1; \quad (4.20)$$

$$f(\infty) = 1; \quad (4.21)$$

The boundary condition $f(\pm\infty) = \pm 1, f'(\pm\infty) = 0$ is only possible at $b = 0, a > 0$, in which case the solution reduces to the error function (Burgers).

In the general case of $b \neq 0$, the solution reduces to the Hermite function, with power tail $\text{sign}(z)|z|^{-b/(a+b)}$ at infinity. We present this solution in *Mathematica*[®] file (attached).

In other words, Navier-Stokes equation with finite velocity gap represents the linear boundary problem for the y component of velocity. This

problem only has a nonzero solution in the case of the background Euler strain's vanishing middle eigenvalue b .

Matching Euler and NS solution at fixed z and $\nu \rightarrow 0$, we find

$$b = 0; \quad (4.22)$$

$$\alpha = 0; \quad (4.23)$$

$$\beta = 2s; \quad (4.24)$$

which leads to the CVS equation.

$$\hat{S} \cdot \Delta \vec{v} = (0, 0, 0) \quad (4.25)$$

We also observe that there is no gap in the pressure.

Note that the normal part (the last component) of the CVS constraint vanishes already as a consequence of the vanishing normal gap; only the transverse part of CVS requires the NS equation to vanish.

However, as it follows from this analysis, all three components of the CVS must vanish for the Euler vortex sheet to come up as $\nu \rightarrow 0$ limit of the solution of the NS.

The weaker CVS without the last component does not agree with the Navier-Stokes equation.

The Burgers-Townsend solution corresponds to the exceptional case $a > 0, b = 0$. The solution reads

$$\vec{v} = \{ax, \beta S_h(z), -az\}; \quad (4.26a)$$

$$S_{\alpha\beta}^0 = \text{diag}(a, 0, -a); \quad (4.26b)$$

$$\vec{\omega} = \{-\beta S'_h(z), 0, 0\}; \quad (4.26c)$$

$$S'_h(z) = \frac{1}{h\sqrt{2\pi}} \exp\left(-\frac{z^2}{2h^2}\right); \quad (4.26d)$$

$$S_h(z) = \text{erf}\left(\frac{z}{h\sqrt{2}}\right); \quad (4.26e)$$

$$a = \frac{\nu}{h^2}; \quad (4.26f)$$

We verified this solution analytically in various coordinate systems in a *Mathematica*[®] notebook³³ for the reader's convenience. In this case, the vorticity becomes Gaussian, and the velocity gap becomes an error function. In the limit of $h \rightarrow 0$, the vorticity reduces to $\delta(z)$, and the velocity gap reduces to $\text{sign}(z)$.

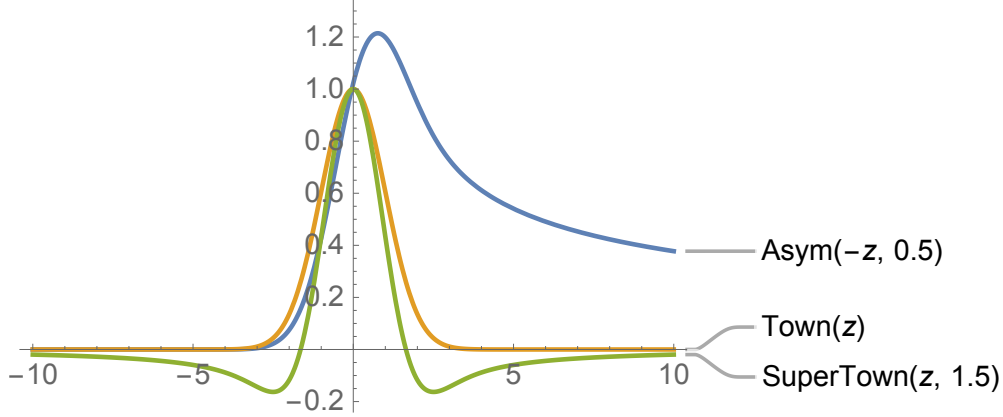


Figure 4: The vorticity profiles for asymmetric, Townsend, and super-Townsend strains

4.3. Numerical Simulations and stability properties

These solutions for various ratios μ of eigenvalues were investigated in.²² An interesting case is negative b (super-Townsend in²²). In that case, $\mu < -1$ so that power decay is even stronger than in the case of positive b .

The vorticity starts from the peak at $z = 0$ and then decays as a Gaussian to some level, after which the power terms take over. These power terms in the super-Townsend case are negative, so the vorticity approaches zero from the opposite side after reaching the minimum.

The authors of²² also studied time evolution. In the asymmetric case, $b > 0$ in our notation, the peak of vorticity decays. This decay happens due to leaks on one or both sides. The solution moves from the steady state to zero vorticity.

The super-Townsend case $-a < b < 0$ turns out to be unstable. Rather than decaying, the vorticity accumulates in the negative pockets and leaks from there. This solution moves away from the steady state, making it unstable.

Only the exceptional Townsend case $b = 0$ proves stable (up to some finite-size effects). Vorticity in the Gaussian peak does not decay nor grow on the sides; it stays the same.

The vortex sheets with Gaussian core and small pockets outside, like in the super-Townsend case, were also observed in simulations of real isotropic turbulence.²²

Presumably, these observed pockets are finite Reynolds effects; they will disappear in the extreme turbulence when the peak grows to infinity.

4.4. Topological stability of CVS and the Euler limit of NS

There is a simple topological reason for the stability of CVS.

This velocity gap

$$\Delta v_y(x, y) = v_y(x, y, +\infty) - v_y(x, y, -\infty) \quad (4.27)$$

is not affected by variation of the velocity field in any compact region (finite z).

On the contrary, continuous transformation (time evolution) in a compact region can reduce to zero the solution with a vanishing velocity gap.

Now, let us consider the two mutually reflected surfaces with opposite velocity gaps, separated by a finite distance $\Delta z = 2L$ in the vanishing viscosity limit.

At any finite viscosity, the total velocity gap is exactly zero. When we go from $z = -\infty$ to $z = +\infty$, we change velocity from 0 to $+\Delta v_y(x, y)$ at $z = -L$ then it stays constant for a long interval $-L < z < L$, then it goes back to 0 at $z = +\infty$.

The continuous transformation of velocity in a compact region covering the interval $(-L, L)$ can reduce velocity to zero, unlike the case of a single velocity gap.

However, the solution of the Navier-Stokes equation is topologically stable in the vicinity of each of two vortex surfaces: one in $-\infty < z < -L$ and another one in $L < z < \infty$ in the Euler limit $\nu \rightarrow 0$.

Within the Navier-Stokes equation, the size of the region between the vortex surfaces is infinite, as the solution depends on the ratio z/h .

From the point of view of Euler dynamics, two opposite vortex surfaces would annihilate in finite time, given enough normal velocity in the direction of the collision.

However, our stable solutions have zero normal velocity at each surface.

So, an infinitesimal variation of the velocity field will take infinite time to decay in the Euler dynamics.

This decay time grows as some negative viscosity power.

This finite though large decay time makes our pair of reflected surfaces micro-stable but not necessarily macro-stable.

4.5. Velocity gap on a curved surface

The Burgers-Townsend solution for a planar velocity gap has a clear mathematical meaning. Let us discuss the meaning of the velocity gap at the curved surface.

At finite viscosity, we expect the velocity field to be smooth, with infinite vorticity replaced by the peak with growing amplitude and shrinking width— Gaussian approximation of the delta function around the surface in three dimensions.

In the case of the smooth curved surface, every point at the surface has a local flat vicinity. The curvature is negligible compared to the inverse thickness of the boundary layer (the width h of the normal distribution of the vorticity around the surface).

Locally, the surface equation can involve the first quadratic form (with an implied sum over repeated indexes $i, j = 1, 2$)

$$z = \frac{1}{2}Q_{ij}x_ix_j + \dots; \quad (4.28)$$

$$x_i = (x, y) \quad (4.29)$$

where \dots stand for higher order terms.

One can flatten the surface by the transformation of coordinates in R_3

$$x \Rightarrow x; \quad (4.30)$$

$$y \Rightarrow y; \quad (4.31)$$

$$z \Rightarrow z - \frac{1}{2}Q_{ij}x_ix_j; \quad (4.32)$$

After this transformation of coordinates in the Navier-Stokes equation, the boundary conditions become planar, just like in a Burgers-Townsend case

$$v_z(x, y, 0) = 0 \quad (4.33)$$

The Navier-Stokes equation is perturbed by the terms proportional to powers of Q . This perturbation expansion's effective (tensor) expansion parameter is h^2Q .

We computed the leading (linear) terms in the Navier-Stokes equation. We get corresponding perturbations of the Burgers-Townsend solution of

the form

$$\vec{v} = \vec{v}_{BT} + \delta\vec{v} + O(Q^2); \quad (4.34)$$

$$\vec{L}(\delta\vec{v}) = \vec{R}(\hat{Q}) \quad (4.35)$$

with some linear operators \vec{L}, \vec{R} determined by the Burgers-Townsend solution. One can analytically find some of the terms in $\delta\vec{v}$; others reduce to solutions of the linear inhomogeneous ODE for functions of z with zero boundary conditions at $|z| \rightarrow \infty$.

This problem was addressed by a Ph.D. student.⁴¹

We do not need the explicit form of this perturbation here, just because for a smooth surface with finite quadratic form, these terms of perturbation expansion are finite and calculable using *Mathematica*[®].

In the following, we neglect these corrections, assuming that the expansion parameter is infinitesimal.

In this approximation, the Burgers-Townsend solution depends on invariants of the local strain, local normal vector, and local velocity gap.

4.6. Invariant form of CVS constraints

If we would like to match the Euler vortex surface with the Navier-Stokes equation in a boundary layer, we must ensure a finite velocity gap, which requires one vanishing eigenvalue. Furthermore, we need the normal strain to be negative to squeeze the vorticity into the sheet.

The sorted (in decreasing order) eigenvalues will be $(\lambda, 0, -\lambda)$. We can always choose the local coordinate system so that the normal to the surface is parallel to one of the strain's remaining eigenvectors.

One of the two remaining eigenvectors (corresponding to the vanishing eigenvalue) must be directed along the velocity gap (y -axis in the Burgers-Townsend solution), which provides another condition for stability.

Then we would have $\hat{S}_{nn} = \pm\lambda$. The flow direction change while preserving its geometry would change this sign in front of λ . Only the negative sign is acceptable, as only then the real solution for the width h would exist. The velocity gap points towards the vanishing component of the strain in its diagonal frame.

Generalizing these observations, we suggest a new scenario for a vortex sheet in extreme turbulence, which we call Confined Vortex Surface, or CVS.

The turbulent vorticity collapses along the closed surface where the normal velocity vanishes, the tangent strain annihilates the tangent velocity gap but the normal strain is negative. This required negative normal strain breaks the time-reversal but preserves the space symmetries, including parity.

One can rewrite these conditions for stability in invariant form

$$\vec{\sigma} \cdot \vec{\sigma} = 0; \quad (4.36)$$

$$\hat{S} \cdot \Delta \vec{\sigma} = 0; \quad (4.37)$$

$$\vec{\sigma} \cdot \hat{S} \cdot \vec{\sigma} < 0; \quad (4.38)$$

where $\vec{\sigma}$ is a local normal vector to the vortex surface.

In the rest of this chapter, we study the CVS and its implications for the vortex surface dynamics.

4.7. The CVS Equations in depth

The steady closed vortex surface \mathcal{S} can be treated within the framework of hydrostatics, as we recently advocated.¹⁹

In the 3D space inside and outside the surface $\mathcal{V}^\pm : \partial \mathcal{V}^\pm = \mathcal{S}$ there is no vorticity so one can describe the flow by a potential $\Phi_\pm(\vec{r})$

$$v_\alpha(\vec{r}) = \partial_\alpha \Phi_\pm(\vec{r}); \quad \forall \vec{r} \in \mathcal{V}^\pm \quad (4.39)$$

The incompressibility $\partial_\alpha v_\alpha = 0$ would be satisfied provided both potentials satisfied the Laplace equation with the Neumann boundary conditions at the surface. The steady surface requires vanishing normal velocity^{18,9}

$$\partial_\alpha v_\alpha(\vec{r}) = \partial_\alpha^2 \Phi_\pm(\vec{r}) = 0; \quad \forall \vec{r} \in \mathcal{V}^\pm \quad (4.40)$$

$$\partial_n \Phi_+(\vec{r}) = 0; \quad \forall \vec{r} \in \mathcal{S} \quad (4.41)$$

$$\partial_n \Phi_-(\vec{r}) = 0; \quad \forall \vec{r} \in \mathcal{S} \quad (4.42)$$

The potential is given by the Coulomb integral with dipole density Γ plus a background constant strain potential

$$\Phi_\pm(\vec{r}_0) = P(\vec{r}_0) - \frac{1}{4\pi} \int_S \Gamma_\pm(\vec{r}) d^2 \sigma_\alpha(\vec{r}) \partial_\alpha \frac{1}{|\vec{r} - \vec{r}_0|}; \quad (4.43)$$

$$d^2 \sigma_\alpha(\vec{r}) = e_{\alpha\beta\gamma} dr_\beta \wedge dr_\gamma; \quad (4.44)$$

$$P(\vec{r}_0) = \sum_n -\frac{1}{4\pi} \int_{\vec{r} \in S_n} \Gamma_+(\vec{r}) d^2 \sigma_\alpha(\vec{r}) \partial_\alpha \frac{1}{|\vec{r} - \vec{r}_0|} \quad (4.45)$$

The P term represents the contribution from similar dipole density terms from other remote vortex surfaces. The point \vec{r}_0 is presumed outside of these closed surfaces.

Assuming these surfaces to be far away, we expand $P(\vec{r}_0)$ in Taylor series in r_0 .

$$P(\vec{r}_0) \rightarrow \vec{V}_0 \cdot \vec{r}_0 + \frac{1}{2} \vec{r}_0 \cdot \hat{W} \cdot \vec{r}_0 + \dots \quad (4.46)$$

The leading term is some constant velocity \vec{V}_0 which a Galilean transformation can eliminate, so it does not have any physical effect.

We will stop the expansion at this first nontrivial W term. This term represents the background strain created by other remote vortex structures, which slowly vary in space.

The higher gradients of this background potential will be inversely proportional to the distance to these remote structures, which is the next order in the (assumed) small parameter R_0/R , where R_0 is the size of this vortex surface, and R is the typical distance between such surfaces.

The potential satisfies the Laplace equation in \mathcal{S}^\pm with a continuous normal derivative of the potential at the surface.

One can compute the velocity field as a gradient of this potential. Simple computations lead to the following expression

$$\vec{v}(\vec{r}_0) = \hat{W} \cdot \vec{r}_0 + \frac{1}{4\pi} \int d\Gamma \wedge d\vec{r} \times \vec{\nabla} \frac{1}{|\vec{r} - \vec{r}_0|}; \quad (4.47)$$

$$\Gamma = \Gamma_+ - \Gamma_- \quad (4.48)$$

The normal component of this velocity is continuous at the surface, as one can verify by direct computation.

In the CVS theory, we require that this normal velocity vanishes at every point on the surface

$$\vec{\sigma}(\vec{r}) \cdot \vec{v}(\vec{r}) = 0; \forall \vec{r} \in \mathcal{S} \quad (4.49)$$

We need this condition for a steady surface in vortex sheet dynamics.

The gap in potential at the surface equals Γ by construction. The velocity $\vec{v} = \vec{\nabla}\Phi$ has tangent discontinuity :

$$\Delta\Phi = \Gamma; \forall \vec{r} \in S; \quad (4.50)$$

$$\Delta\vec{v} = \vec{\nabla}\Gamma(\vec{r}); \forall \vec{r} \in S; \quad (4.51)$$

$$\vec{\sigma} \cdot \vec{\Delta}\vec{v} = 0; \forall \vec{r} \in S; \quad (4.52)$$

Taking the curl of velocity in the linear vicinity of a surface point in the tangent frame x, y, z , with z directed at the local normal, we have

$$\Delta v_i = \partial_i \Gamma; i = 1, 2 \quad (4.53)$$

$$\Delta v_z = 0; \quad (4.54)$$

$$\omega_i(x, y, z) = \delta(z) e_{ij} \partial_j \Gamma; \quad (4.55)$$

$$\omega_z(x, y, z) = 0 \quad (4.56)$$

It is straightforward to verify the divergence equation $\vec{\nabla} \cdot \vec{\omega} = 0$.

The invariant integral (3.50) generalizes this formula for an arbitrary continuous surface. With the vortex sheet dynamics, the condition of vanishing normal velocity represents a linear integral equation for Γ with a symmetric kernel.

It corresponds to the minimization of the quadratic Hamiltonian

$$H_0 = \int_{\vec{r}_1, \vec{r}_2 \in \mathcal{S}} d\Gamma(\vec{r}_1) \wedge d\vec{r}_1 \cdot d\Gamma(\vec{r}_2) \wedge d\vec{r}_2 \frac{1}{8\pi|\vec{r}_1 - \vec{r}_2|} \quad (4.57)$$

with an extra linear term

$$H_1 = \int_{\mathcal{S}} \Gamma(\vec{r}) d^2\vec{\sigma}(\vec{r}) \cdot \hat{W} \cdot \vec{r} \quad (4.58)$$

This equation is the first of the three basic equations of the CVS theory.

The regular part of the strain is the arithmetic mean of the strains at two sides of the surface; it is given by

$$S_{\alpha\beta}(\vec{r}) = \frac{1}{4} \partial_\alpha v_\beta(\vec{r}^+) + \frac{1}{4} \partial_\alpha v_\beta(\vec{r}^-) + \{\alpha \Longleftrightarrow \beta\}; \forall \vec{r} \in \mathcal{S}; \quad (4.59)$$

Here \vec{r}^\pm corresponds to the limit taken from the outside/inside of the surface.

The vector CVS equation

$$\hat{S} \cdot \vec{\nabla} \Gamma = 0 \quad (4.60)$$

provides two more relations between the surface and the potential gap Γ .

Thus, we have three algebraic/differential equations for the unknown functions of coordinates: the parametric equation $\vec{r} = \vec{X}(\xi) = 0$ of the surface \mathcal{S} and the boundary data $\Gamma(\xi)$ for the singular part of the potential.

At each surface point, the CVS condition reduces to the following. One of the two eigenvalues of the tangent part of the strain tensor S_{ij} , $i, j = 1, 2$ must vanish. The velocity gap is directed along the eigenvector of this vanishing eigenvalue, i.e., the null vector of the surface strain.

Locally, the surface is described by two functions of two variables $\Gamma(x, y), z(x, y)$, where $z(x, y)$ is the equation for the normal coordinate as a function of the two tangent coordinates x, y .

However, the CVS equation is nonlocal, as it involves the derivatives of velocity, which depend on the vorticity distribution over the whole surface. This argument leads to an integral equation for the unknown variables: Γ, S .

This solution depends on the random constant strain tensor W , which comes from the "thermostat" of the remaining vortex structures in the turbulent flow. We discuss this issue in the next chapters of this report.

4.8. Anomalous dissipation

The role of stable, steady solutions of the Navier-Stokes equations is to provide the subspace of attractors in phase space. We expect the evolution of the solution to cover this subspace with a uniform measure like Newton's dynamics covers the surface of constant energy.

The situation is more complex in turbulence. The energy E of the fluid is not conserved; it rather dissipates. This dissipation is proportional to the enstrophy

$$\partial_t E = -\mathcal{E} = -\nu \int d^3r \omega_\alpha^2 \quad (4.61)$$

We have a steady state of constant energy dissipation in the turbulent limit, with the constant energy supply from external forces on the system's boundary, like the submarine moving in the ocean or the water pumped into the pipe.

Although ultimately related to the viscous effects, one can study this dissipation in the turbulent limit within the framework of the Euler-Lagrange dynamics.

Large vorticity in certain regions of space where dissipation predominantly occurs will offset the vanishing factor ν in front of the enstrophy.

Our theory starts with the conjecture that dissipation occurs in vortex surfaces, like the Burgers-Townsend sheet. In that case, the Euler-Lagrange

equations describe the dynamics everywhere except the turbulent layer surrounding the vortex sheet, as discussed above.

Using the Burgers-Townsend vortex sheet solution in the linear vicinity of the local tangent plane to the surface, as in,^{18,9} we get the following integral for the dissipation

$$\mathcal{E} \propto \nu \int_D d^2\zeta \sqrt{g} (\vec{\nabla}\Gamma)^2 \int_{-\infty}^{\infty} d\eta (\delta_h(\eta))^2; \quad (4.62)$$

Here η is a local normal direction to the surface and

$$\delta_h(\eta) = \frac{1}{h\sqrt{2\pi}} \exp\left(-\frac{\eta^2}{2h^2}\right) \quad (4.63)$$

is the normal distribution. The (local!) width h is determined by

$$h = \sqrt{\frac{\nu}{\lambda}} \quad (4.64)$$

Here $\lambda = -\hat{S}_{nn} = S_i^i$.

Naturally, we assume that the local normal $\vec{\sigma}$ points on the third axis of the strain, where the finite eigenvalue is negative.

An important new phenomenon is the possibility of the variation of this eigenvalue along the surface.

The square of the Gaussian is also a Gaussian:

$$\delta_h(\eta)^2 = \frac{1}{2h\sqrt{\pi}} \delta_{\tilde{h}}(\eta); \quad (4.65)$$

$$\tilde{h} = h/\sqrt{2}. \quad (4.66)$$

In the limit $\tilde{h} \rightarrow 0$, we are left with the surface integral

$$\mathcal{E} = \frac{\sqrt{\nu}}{2\sqrt{\pi}} \int_D d^2\zeta \sqrt{g} \sqrt{-\hat{S}_{nn}} (\vec{\nabla}\Gamma)^2; \quad (4.67)$$

In the paper,⁹ we also found an expression for the time derivative of the viscosity anomaly for the Euler equation.

Repeating these steps with our local width h , we find (fixing wrong sign in⁹)

$$(\partial_t \mathcal{E})_{Euler} = 2\nu \int d^3r \left(-\partial_\beta \left(\frac{1}{2} v_\beta \omega_\alpha^2 \right) + \omega_\alpha \omega_\beta \partial_\beta v_\alpha \right) \rightarrow$$

$$+ \frac{\sqrt{\nu}}{2\sqrt{\pi}} \int_D d^2\zeta \sqrt{g} \sqrt{S_i^i} \tilde{\partial}^i \Gamma S_{ij} \tilde{\partial}^j \Gamma; \quad (4.68)$$

$$\tilde{\partial}^i = \epsilon_k^i \partial_k \quad (4.69)$$

We did not add the viscous term of the Navier-Stokes equation in that paper, which was a mistake. Adding it now, we get, after a simple algebra

$$(\partial_t \mathcal{E})_{NS} = (\partial_t \mathcal{E})_{Euler} + 2\nu^2 \int d^3r \vec{\omega} \cdot \vec{\nabla}^2 \vec{\omega} \rightarrow$$

$$+ \frac{\sqrt{\nu}}{2\sqrt{\pi}} \int_D d^2\zeta \sqrt{g} \sqrt{S_k^k} \tilde{\partial}^i \Gamma \tilde{\partial}^j \Gamma (S_{ij} - S_k^k g_{ij}) \quad (4.70)$$

We transform this expression into a simpler one using the properties of two-dimensional tensors

$$(\partial_t \mathcal{E})_{NS} = -\frac{\sqrt{\nu}}{2\sqrt{\pi}} \int_D d^2\zeta \sqrt{g} \sqrt{S_k^k} \partial^i \Gamma S_{ij} \partial^j \Gamma \quad (4.71)$$

In the general case, this expression is not zero and could have an arbitrary sign because the tangent eigenvalues must be both signs, given that their sum is positive.

However, in the CVS case, the Euler and Navier-Stokes terms in the time derivative of the enstrophy cancel so that the surface dissipation integral is conserved!

4.9. The Surface enstrophy conservation

The CVS equation, derived from the microscopic stability of the Euler dynamics in the turbulent limit, also provides a new turbulent motion integral: the surface dissipation (4.67).

Unlike the energy functional, this is an *integral of motion of the Navier-Stokes dynamics*, but not the Euler dynamics.

The CVS surface is unique in having these two effects: vortex stretching and diffusion cancel each other, making the surface enstrophy an integral on motion of the Navier-Stokes dynamics in the turbulent limit.

Naturally, the enstrophy is constant on every steady solution of the Navier-Stokes equation, simply by the definition of a steady solution. What is not trivial and is quite fortunate for the vortex sheet dynamics is that the *surface* enstrophy is conserved.

The energy could be dissipated all over the space, not just on the vortex surface. This phenomenon happens for every vortex sheet except the CVS. The time derivative of the enstrophy is either negative on these surfaces, which means that vorticity is leaking outside, or it is positive, meaning an instability of the surface.

The total enstrophy integral, in that case, would not be dominated by a surface, which would make the theory incomplete.

The simple idea that the turbulent statistics is a Gibbs distribution with surface dissipation in the effective Hamiltonian was advocated in our recent paper.⁹ The conservation of the surface dissipation was unknown at that time, which was the problem.

Now we have this problem solved in CVS dynamics. However, the Gibbs distribution with surface enstrophy in place of Gibbs energy was not confirmed.

As we shall see in the last section, an extreme turbulence statistical distribution is even simpler. It is three-dimensional statistical distribution as opposed to the functional integral of the Gibbs theory.

The CVS constraints reduce the arbitrary surface and arbitrary potential gap Γ to some family of solutions with a finite number of parameters. This family of solutions is no longer the functional phase space of the general vortex sheet dynamics.^{3,4}

A finite-dimensional attractor could be the Holy Grail of the turbulence quest, but first, we must thoroughly investigate this hypothesis.

In the next chapter, we make the first step by finding a family of exact solutions of the CVS equations with cylindrical geometry, parametrized by two eigenvalues of a background strain tensor.

We have found only non-compact CVS surfaces. Our surfaces extend to infinity in the Euler limit, and only a finite viscosity cuts them off. De Lellis and Brué subsequently proved that no compact CVS surfaces can exist.

In the next chapters, we study Euler solutions with vorticity spreading outside the vortex sheet. This sheet forms a minimal surface S_C bounded by a 3D loop (the Clebsch domain wall). The singular vorticity, confined to the vortex sheet, still dominates the enstrophy.

These solutions have a nontrivial topology of the Clebsch field, leading to the circulation conservation for the loop bounding the vortex sheet. As we argue, these solutions (Kelvinons) dominate the tails of the PDF of velocity circulation.

Are they the Holy Grail? Time will tell.

4.10. *Mathematical Studies of CVS*

After the talk on this subject in IAS last December, I had extensive discussions with Camillo De Lellis and Elia Brué from IAS about the mathematical meaning of the CVS equations and the exact cylindrical solution of these equations.

The physics ideas flew one way over the abyss between Theoretical Physics and Pure Math, and mathematical theorems were flying back. This method turned out quite productive.

As a result of this investigation, Camillo and Elia confirmed our analytical solution and came up with three interesting theorems, which we quote here without proof. The proofs are presented in Appendix D.6 with their generous permission.

Before presenting these theorems, let us add an important implied condition to the CVS definition.

Definition 1. The CVS is a C^1 surface (i.e., the one with a unique continuously varying normal vector) satisfying all three CVS equations for potential flow on both sides of the surface.

The C^1 condition is essential, as neither the normal velocity nor the normal component of the strain tensor exists otherwise.

Theorem 1. There is no CVS with spherical topology.

Theorem 2. There is no cylindrical CVS with a bounded cross-section.

Theorem 3. There is no compact closed CVS.

These three theorems eliminate any compact CVS.

There is a simple extension of the **Theorem 3**, which eliminates the surfaces with boundaries (say, the disk) unless the velocity field is singular at these boundaries.

The steady solutions require the vanishing velocity in the normal direction to the bounding curves of these holes and the vanishing normal velocity to each surface point.

The **Theorem 3** is based on the Gauss theorem applied to the surface integral of the divergence of the velocity field.

With vanishing normal velocity, this integral is zero for the surface with holes and the closed surface.

Therefore, the normal strain cannot be negative definite, violating the stability of the vortex sheet.

The unbounded CVS are allowed by these theorems. Another exception is the singularity at the boundary, such as our monopole loop in the Kelvinon.

The unbounded cylindrical CVS is presented in the next chapter. It is allowed by these theorems, but there is a nontrivial limiting behavior of the Navier-Stokes solution when viscosity ν goes to zero. At any finite viscosity, the region of finite velocity gap in the "unbounded" solution is finite, but this region grows with $\nu \rightarrow 0$.

In that sense, there is no such thing as the Euler limit of the Navier-Stokes equation. Viscosity always plays a key role in some domains of large vorticity.

5. CVS Equation for Cylindrical Geometry

The motivation for cylindrical geometry is as follows.

- This is the only known case of exactly solvable stability equations.
- Several numerical simulations^{26,25} indicate vortex structures shaped as long tubes corresponding to the cylindrical geometry.
- Three theorems by De Lellis and Brué severely limit the space of possible CVS. There is no compact closed CVS, moreover, there are no cylindrical CVS with bounded cross-section.

Our cylindrical unbounded solutions are (post-factum) allowed by these three theorems. A uniform strain tensor on one side allows the overdetermined system of equations to have a solution.

This solution heavily relies on complex analysis, thanks to the cylindrical geometry. There is no known analog of this analysis in full three-dimensional geometry.

Given the exceptional nature of this solution, we put forward the following conjecture:

Conjecture 1. The only CVS are unbounded cylindrical ones, with uniform strain tensor on one side.

We cannot prove this conjecture, so we leave it for further study. With this conjecture proven, we would have the complete solution to the vortex sheet stability problem.

Before studying the associated turbulent statistics, let us describe, generalize and solve the cylindrical CVS equations.

In cylindrical geometry, the piecewise harmonic potential has the following form:

$$\Phi_{\pm}(x, y, z) = \frac{1}{2}ax^2 + \frac{1}{2}by^2 + \frac{1}{2}cz^2 + \mathbf{Re} \phi_{\pm}(\eta); \quad (5.1)$$

$$a + b + c = 0, a \leq b \leq c; c > 0, a < 0; \quad (5.2)$$

$$\eta = x + \imath y; \quad (5.3)$$

$$\phi_{\pm}(\eta) = \frac{1}{2\pi\imath} \int d\Gamma_{\pm}(\theta) \log(\eta - C(\theta)); \quad (5.4)$$

$$v_z = cz; \quad (5.5)$$

$$V_{\pm}(x, y) = v_x - \imath v_y = ax - \imath by + F_{\pm}(x + \imath y); \quad (5.6)$$

$$F_{\pm}(\eta) = \phi'_{\pm}(\eta); \quad (5.7)$$

Here $C(\theta)$ is a complex periodic function of the angle $\theta \in (0, 2\pi)$ parametrizing the closed loop C . We simplified the notations compared to,²⁰ and now we denote the ordered eigenvalues of the background strain tensor as a, b, c .

The geometry is as follows. The vortex surface corresponds to the parallel transport of the xy loop C in the third dimension z . Thus, at some point on the surface, the local tangent frame is

$$\vec{E}_1 = \left(\frac{\mathbf{Re} C'}{|C'|}, \frac{\mathbf{Im} C'}{|C'|}, 0 \right); \quad (5.8)$$

$$\vec{E}_2 = (0, 0, 1); \quad (5.9)$$

$$\vec{E}_3 = \left(\frac{\mathbf{Im} C'}{|C'|}, -\frac{\mathbf{Re} C'}{|C'|}, 0 \right) \quad (5.10)$$

The first two orthogonal vectors define the tangent plane, and the third one $\vec{E}_3 = \vec{E}_1 \times \vec{E}_2$ corresponds to the normal $\vec{\sigma}$ to the surface. Do not confuse the z direction with the normal – this is one of the two tangent directions.

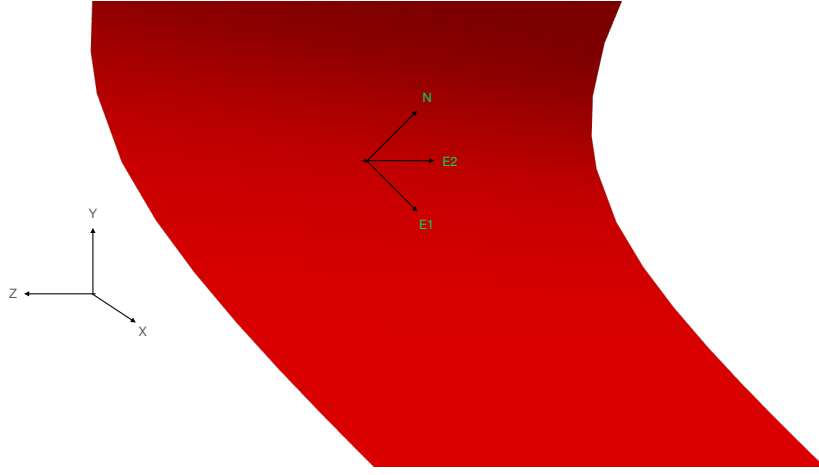


Figure 5: The local tangent plane E_1, E_2, N and the global Cartesian frame X, Y, Z .

In this solution, the functions $\Gamma_{\pm}(\theta)$ can be complex, but the circulation will depend on the real part.

The double-layer potential studied in the previous paper,²⁰ corresponds to the real $\Gamma_+(\theta) = \Gamma_-(\theta)$. In that case, the reparametrization of the curve would eliminate this function so that the solution would be parametrized by the loop $C(\theta)$ modulo diffeomorphisms.

As we see it now, the condition of real and equal $\Gamma_{\pm}(\theta)$ is unnecessary. We shall find simple analytic solutions by dropping this restriction.

One can reduce the condition of vanishing normal velocity at each side of the steady surface to two real equations

$$\text{Im } C'(\theta) V_+(C(\theta)) = 0; \quad (5.11)$$

$$\text{Im } C'(\theta) V_-(C(\theta)) = 0; \quad (5.12)$$

with V_{\pm} denoting the boundary values at each side of the surface.

The second CVS equation was reduced in²⁰ to the complex equation

$$V_+(C(\theta)) + V_-(C(\theta)) = 0; \quad (5.13)$$

These two equations were derived in²⁰ under assumptions of real $d\Gamma_{\pm}(\theta)$ in (5.5) which we find unnecessary and drop now.

In Appendix A, we re-derive these two equations without extra assumptions.

It follows from equation (5.13) that one of the two eigenvalues of the local tangent strain at the surface vanishes. This vanishing eigenvalue corresponds to the velocity gap $\Delta V = V_+ - V_- = -2V_-$ as an eigenvector.

The way to prove this is to note that differentiation of (5.13) by θ reduces to projecting the complex derivatives of $V_+(C) + V_-(C)$ on the complex tangent vector $C'(\theta)$. As the θ derivative of $V_+(C) + V_-(C)$ is zero in virtue of (5.13), so is the projection of the strain in the direction of the curve tangent vector $C'(\theta)$.

There is no normal velocity gap (as both normal velocities are zero), nor is there any gap in the z component of velocity $v_z = cz$. Thus, the velocity gap aligns with the curve tangent vector $C'(\theta)$, and the strain along the velocity gap vanishes. Direct calculation in Appendix A supports this argument.

The other eigenvalue \hat{S}_{nn} , corresponding to the eigenvector $\vec{\sigma} = \vec{E}_3$ normal to the surface, is then uniquely fixed by the condition of vanishing trace of the local strain tensor.

The third eigenvalue c corresponds to our cylindrical tube's eigenvector \vec{E}_2 .

Therefore, the normal component of the strain tensor is

$$\hat{S}_{nn} = -c \quad (5.14)$$

5.1. Spontaneous breaking of time-reversal symmetry and Normal strain

As the largest c of the three ordered numbers a, b, c with the sum equal to 0 is always positive (unless all three are zero), we have a negative normal strain as required by the stability of the Navier-Stokes equation in the local tangent plane.

Contrary to our previous statements, this condition does not restrict the background strain tensor. The irreversibility of turbulence manifests itself in the negative sign of the normal strain on the surface, which is true for arbitrary finite eigenvalues a, b, c .

The stability conditions restrict the vortex tube shape: its axis aligns with the leading eigenvector of the background strain, and its profile loop adjusts to the local strain to annihilate its projection on the velocity gap.

Unlike the general shape of the vortex tube, the cylindrical shape guarantees the negative sign of the normal strain. We may be dealing with the spontaneous emergence of cylindrical symmetry at the expense of breaking the time-reversal symmetry from the stability condition.

The maximal value of the normal strain on the closed vortex surface represents a functional of its shape. So, the problem is to find under which conditions this maximal value is negative. The potential being harmonic, this normal strain equals minus the surface Laplacian of the boundary value of potential.

Thus, we are dealing with the minimal value of the surface Laplacian of a boundary value of harmonic potential on a closed surface. Under which conditions is this minimal value positive?

The third theorem by De Lellis and Brué answers this question. This minimal value cannot be positive for any bounded smooth surface of an arbitrary genus because the average over such surface vanishes by the Gauss theorem.

So, this leaves us with unbounded surfaces. We conjecture that these are cylindrical ones, with uniform strain on one side. This condition is sufficient for CVS, as we shall see below, but we cannot prove it is necessary.

The Euler equation is invariant under time reversal, changing the sign of the strain. Without the CVS boundary conditions, both signs of the normal strain would satisfy the steady Euler equation. Therefore, this CVS vortex sheet represents a dynamical breaking of the time-reversal symmetry.

Out of the two time-reflected solutions of the Euler equation, only the one with the negative normal strain survives. If virtually created as a metastable phase, the other dissolves in the turbulent flow, but this remains stable.

Technically this instability displays itself in the lack of the real solutions of the steady Navier-Stokes equation for positive \hat{S}_{nn} . The Gaussian profile of vorticity as a function of normal coordinate formally becomes complex at positive \hat{S}_{nn} , which means instability or decay in the time-dependent equation.

In,²² the authors verified this decay/instability process. They solved the time-dependent Navier-Stokes equation numerically in the vicinity of the steady solution with arbitrary background strain. Only the Burgers-Townsend solution corresponding to our CVS conditions on the strain was

stable.

No external forces drive the breaking of the time-reversal symmetry of the Euler dynamics; it rather emerges spontaneously by the stability requirement of internal Navier-Stokes dynamics. The result of this microscopic stability mechanism of the Navier-Stokes dynamics is the CVS boundary conditions added to the ambiguous Euler dynamics of the vortex sheets.

5.2. Complex Curves

Let us proceed with the exact solution of the CVS equations.

The CVS equations for the cylindrical geometry reduce to the equation (5.11) for the boundary loop $C(\theta)$ plus a complex equation $V_+(x, y) + V_-(x, y) = 0$ at the loop $(x, y) \in C$.

Consider two holomorphic functions involved in this equation: $F_-(\eta)$ inside the loop, $F_+(\eta)$ outside. The boundary condition relates these two functions

$$F_+(\eta) + F_-(\eta) + (a - b)\eta - c\bar{\eta} = 0; \forall \eta \in C; \quad (5.15)$$

Let us look for the linear solution of the Laplace equation inside (constant strain):

$$F_-(\eta) = (p + \imath q)\eta \quad (5.16)$$

with some real p, q .

The vanishing normal velocity from the inside leads to the differential equation for $C(\theta)$.

$$\mathbf{Im} \left((2p + a - b + 2\imath q)C(\theta) - c\bar{C}(\theta) \right) C'(\theta) = 0 \quad (5.17)$$

This equation is integrable for arbitrary parameters. We shall use two dimensionless parameters γ, β to parametrize p, q as follows:

$$p + \imath q = \frac{b - a}{2} + \frac{ce^{-2\imath\beta}}{2(2\gamma + 1)}; \quad (5.18)$$

The general solution of (5.17) in polar coordinates reads⁴² (up to an arbitrary normalization constant)

$$C(\theta) = e^{\imath\beta}(1 + \imath\tau)\tau^\gamma; \quad (5.19)$$

$$\tau = \tan \theta \quad (5.20)$$

This solution applies when τ^γ is real.

5.3. Parabolic curves

Let us consider positive γ first (the parabolic curves).

This solution passes through the origin and will have no singularity at $\tau = 0$ in case $\gamma = n, n \in \mathbb{Z}, n \geq 0$.

The case $n = 0$ corresponds to a tilted straight line. This case is just a Burgers-Townsend planar vortex sheet. The next cases are already nontrivial

However, not all positive n are acceptable. For even positive n we have a cusp in a curve because only positive $r(\theta)$ exist at $\theta \rightarrow 0$. This cusp is visible at the $n = 2$ curve.

For odd positive $n = 2k + 1$, there is a linear relation between x, y at small τ provided $\beta \neq 0$. The slope of the curve $y(x)$ at $x = \pm 0$ is the same.

Higher derivatives are singular, as we have

$$x \sim \tau^{2k+1} \cos(\beta) (1 - \tan(\beta) \tau); \quad (5.21)$$

$$y \sim \tau^{2k+1} \sin(\beta) (1 + \cot(\beta) \tau); \quad (5.22)$$

$$y \rightarrow \tan(\beta) x \left(1 + \frac{2 \operatorname{sign} x}{\sin \beta} \left(\frac{|x|}{\cos(\beta)} \right)^{\frac{1}{2k+1}} \right); \quad (5.23)$$

$$\frac{dy}{dx} \rightarrow \tan(\beta) \text{ at } x \rightarrow \pm 0 \quad (5.24)$$

As the slopes $\frac{dy}{dx}$ are the same at $x = \pm 0$, the vortex sheet reduces to a plane up to higher-order terms. Thus, the Burgers-Townsend solution, assuming the infinitesimal thickness of the vorticity layer, will still apply here. Ergo, the sheet will be stable at this point and the points on the rest of the surface.

Thus, we have found the discrete parametric family of CVS shapes. It simplifies in terms of $\tau = \tan \theta$.

$$\eta(\tau) = e^{i\beta} (1 + i\tau) \tau^{2k+1}; \quad (5.25)$$

$$k \in \mathbb{Z}, k \geq 0; \quad (5.26)$$

$$-\infty < \tau < \infty; \quad (5.27)$$

We have a conformal map from the τ plane to the plane of $\eta = x + iy$, with our curve C corresponding to the real axis. The physical

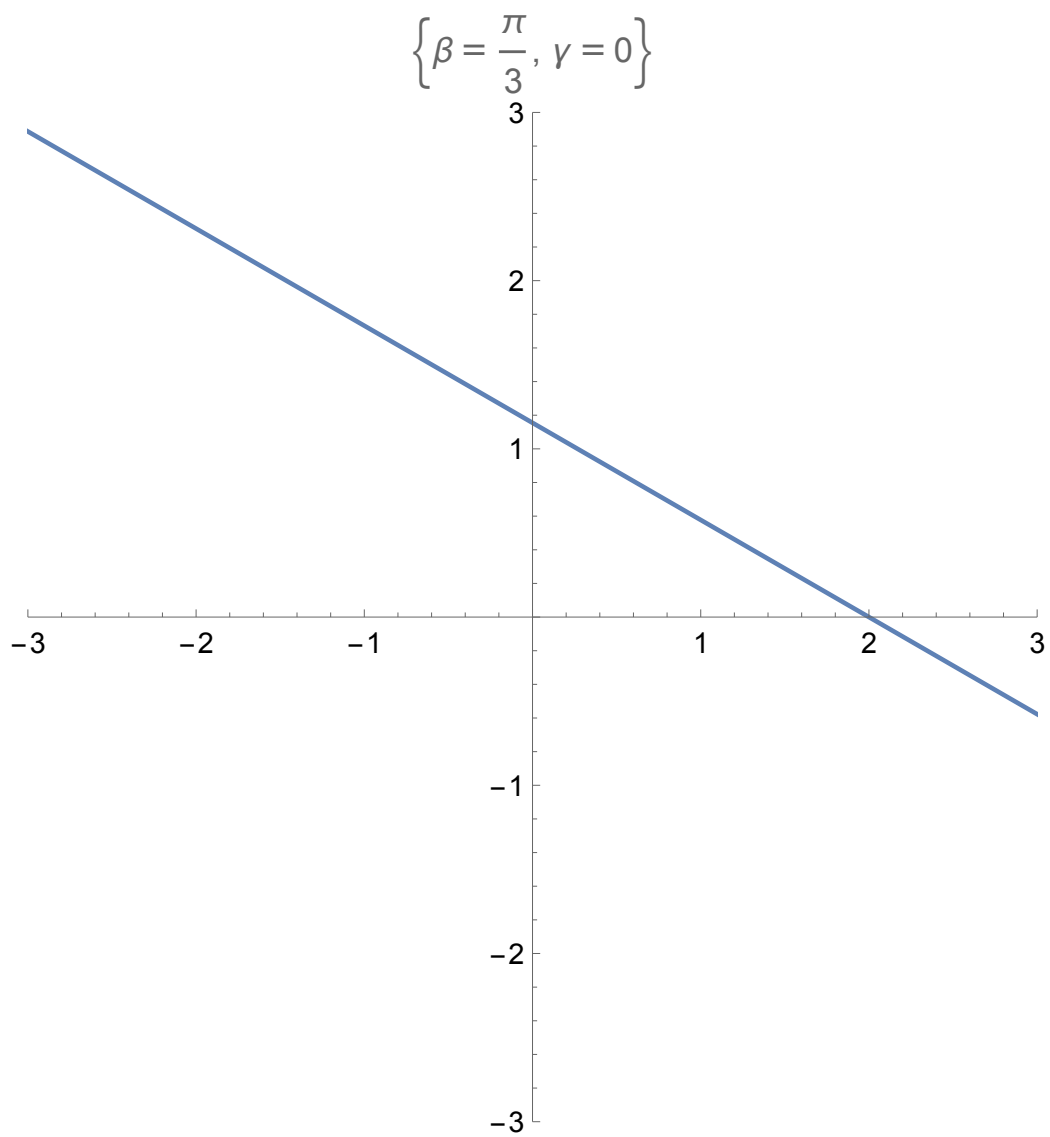


Figure 6: The Burgers-Townsend case, $n = 0$.

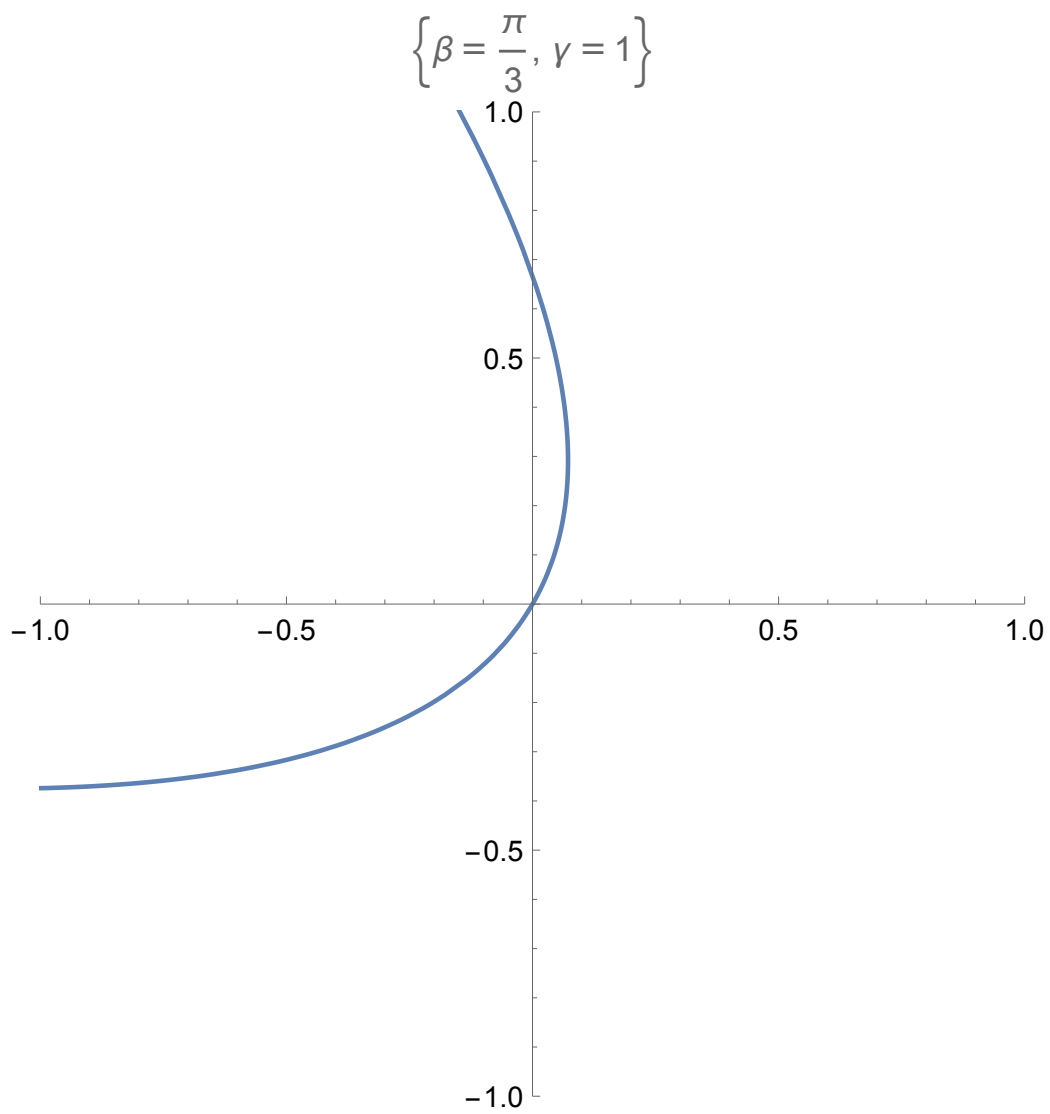


Figure 7: The CVS for $n = 1$.

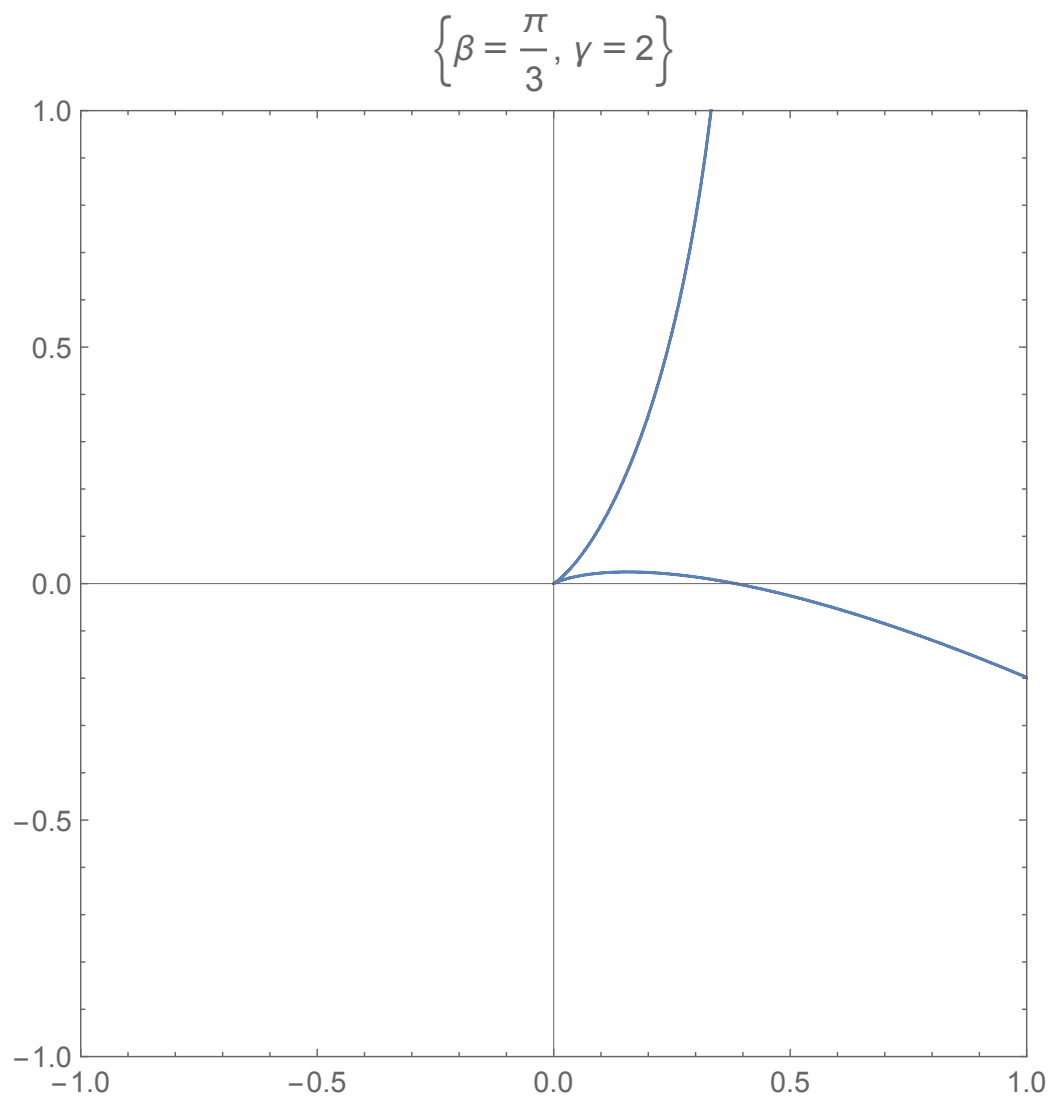


Figure 8: The CVS for $n = 2$.

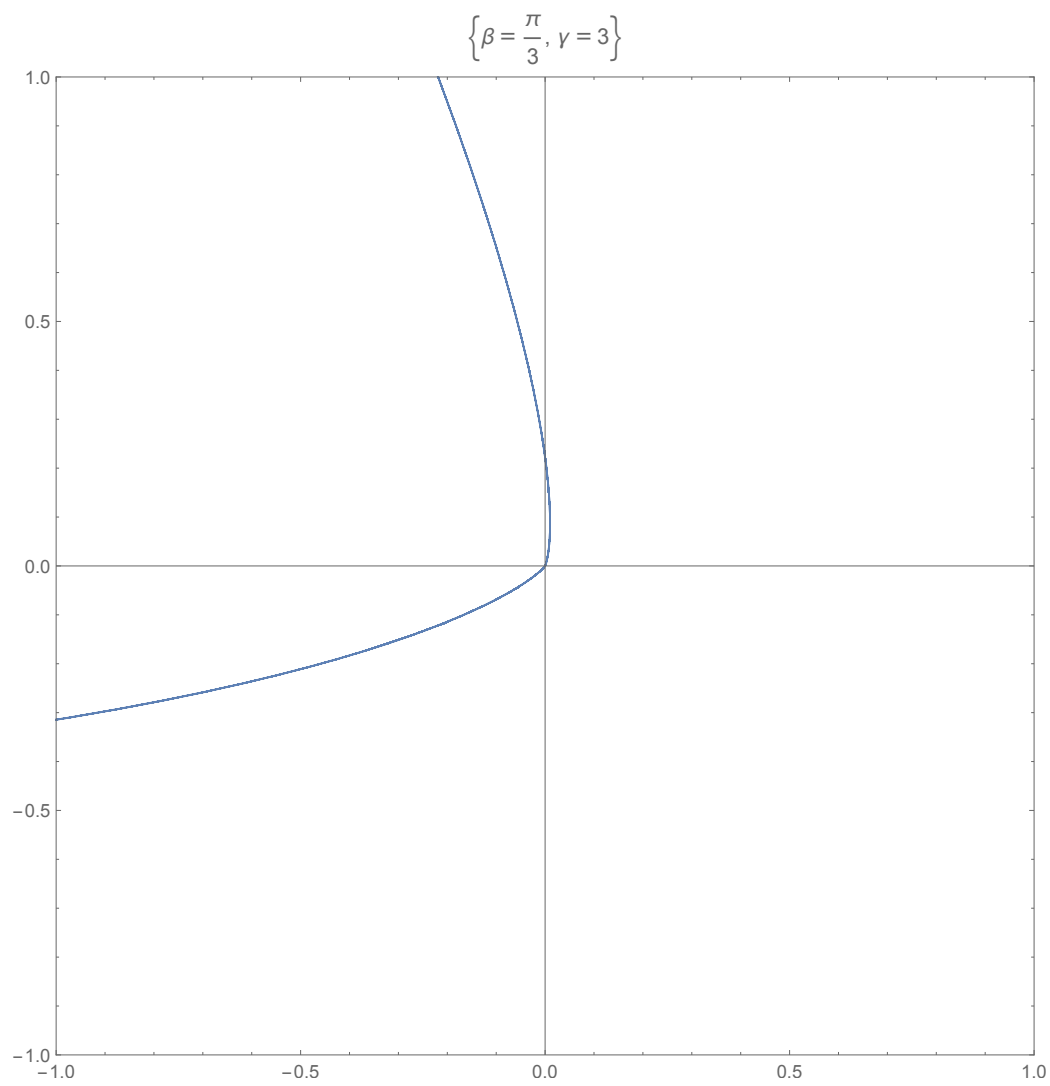


Figure 9: The CVS for $n = 3$.

region outside the loop corresponds to the sector in the lower semiplane, $-\frac{\pi}{(k+1)} < \arg \tau < 0$.

The infinity in the physical space corresponds to infinity in the τ plane.

Two singular points correspond to the vanishing derivative $\eta'(\tau) = 0$. The singularity happens at

$$\tau = 0; \quad (5.28)$$

$$\tau = \frac{\imath(2k+1)}{2(k+1)}; \quad (5.29)$$

The first one maps to the origin in the η plane. The second one is in the upper τ semiplane, so it does not affect the inverse function $\tau(\eta)$ in the physical sector of the lower semiplane.

The next step is to find the holomorphic function $F_+(\eta)$, which defines the complex velocity on the external side of the sheet (the internal side has linear velocity $F_-(\eta) = (p + \imath q)\eta$).

From the CVS equation, we get the boundary values, which we express in terms of η, η^*

$$F_+(\eta) = -(p + a - b + \imath q)\eta + c\eta^*; \quad \forall \eta \in C \quad (5.30)$$

We have to continue this function from the curve (5.25) into the part of the complex plane outside this curve.

Let us express the right side in terms of τ

$$f(\tau) = -(p + a - b + \imath q)\eta(\tau) + c\tilde{\eta}(\tau) \quad (5.31)$$

Here $\tilde{\eta}(\tau)$ is the complex conjugate expression for η

$$\tilde{\eta}(\tau) = e^{-\imath\beta} (1 - \imath\tau) \tau^{2k+1}; \quad (5.32)$$

$$(5.33)$$

At the real axis of τ the variables $\eta(\tau), \tilde{\eta}(\tau)$ will be complex conjugates, and the boundary value

$$f(\tau) = F_+(\eta(\tau)); \quad \forall \text{Im } \tau = 0 \quad (5.34)$$

Now we have an obvious analytic continuation to the lower semiplane

of τ . After some algebra, we get⁴²

$$\eta(\tau) = e^{i\beta} (1 + i\tau) \tau^{2k+1}; \quad (5.35)$$

$$f(\tau) = \frac{1}{2} e^{-i\beta} \tau^{2k+1} \left(\frac{c(-i(8k+7)\tau + 8k+5)}{4k+3} - ie^{2i\beta}(\tau - i)(2a+c) \right) \quad (5.36)$$

This parametric function in the sector $-\frac{\pi}{(k+1)} < \arg \tau < 0$ of the complex τ plane represents an implicit solution of the CVS equation.

Now, let us consider the limit $\tau \rightarrow \infty$ corresponding to $\eta \rightarrow \infty$. In this limit, the function $F_+(\eta(\tau))$ linearly grows

$$F_+(\eta) \rightarrow B\eta; \quad (5.37)$$

$$B = -a + \frac{1}{2}c \left(-1 - \frac{e^{-2i\beta}(8k+7)}{4k+3} \right) \quad (5.38)$$

This linear growth means that the true value of the xy components of strain at infinity is not $\text{diag}(a, -c-a)$ we thought it was. It is instead

$$\hat{S} = \begin{pmatrix} -\frac{c((8k+7)\cos(2\beta)+4k+3)}{8k+6} & -\frac{c(8k+7)\sin(2\beta)}{8k+6} \\ -\frac{c(8k+7)\sin(2\beta)}{8k+6} & \frac{c((8k+7)\cos(2\beta)-4k-3)}{8k+6} \end{pmatrix} \quad (5.39)$$

The eigenvalues of this strain are

$$\left\{ -\frac{c(6k+5)}{4k+3}, \frac{2c(k+1)}{4k+3} \right\} \quad (5.40)$$

The angle β dropped from the eigenvalues because it can be eliminated by the $U(1)$ transformation $\eta \rightarrow \eta e^{-i\beta}$, which leaves the eigenvalues invariant.

The parabolic solution does not decrease at infinity, which is inadequate for the turbulent statistics we develop later in this paper.

5.4. Hyperbolic curves

Let us now consider the hyperbolic curves with negative $\gamma < 0$, which do not need to be half-integer. We redefine our parameters as follows:

$$\eta(\xi) = \pm e^{i\beta} \left(\xi + i \xi^{-\mu} \right); \quad (5.41)$$

$$\xi = \tau^\gamma; \quad (5.42)$$

$$\mu = -1 - \frac{1}{\gamma}; \mu > 0; \quad (5.43)$$

$$0 < \xi < \infty \quad (5.44)$$

These two curves correspond to various μ, β .

Note that there are no singularities at the origin, as both curves are going around it.

The inverse function is singular at the point ξ_0 in the upper semiplane where $\eta'(\xi_0) = 0$:

$$\xi_0 = (i\mu)^{\frac{1}{\mu+1}} \quad (5.45)$$

Therefore, we need to use the lower semiplane as a physical domain for $f(\xi) = F_+(\eta(\xi))$.

The holomorphic function $f(\xi)$ is reconstructed employing the same steps as in the parabolic case. We get

$$\begin{aligned} f(\xi) = & \frac{1}{2} e^{-i\beta} \xi \left(\frac{c(\mu-3)}{\mu-1} - e^{2i\beta}(2a+c) \right) - \\ & \frac{ie^{-i\beta} \xi^{-\mu} \left(c(3\mu-1) + e^{2i\beta}(\mu-1)(2a+c) \right)}{2(\mu-1)} \end{aligned} \quad (5.46)$$

Let us now find the limit at $\xi \rightarrow \infty$, when η and f both linearly grow

$$f \rightarrow \eta B; \quad (5.47)$$

$$B = -a + \frac{1}{2}c \left(-1 + \frac{e^{-2i\beta}(\mu-3)}{\mu-1} \right) \quad (5.48)$$

We want this coefficient to be zero so that $f(\eta)$ decreases at infinity.

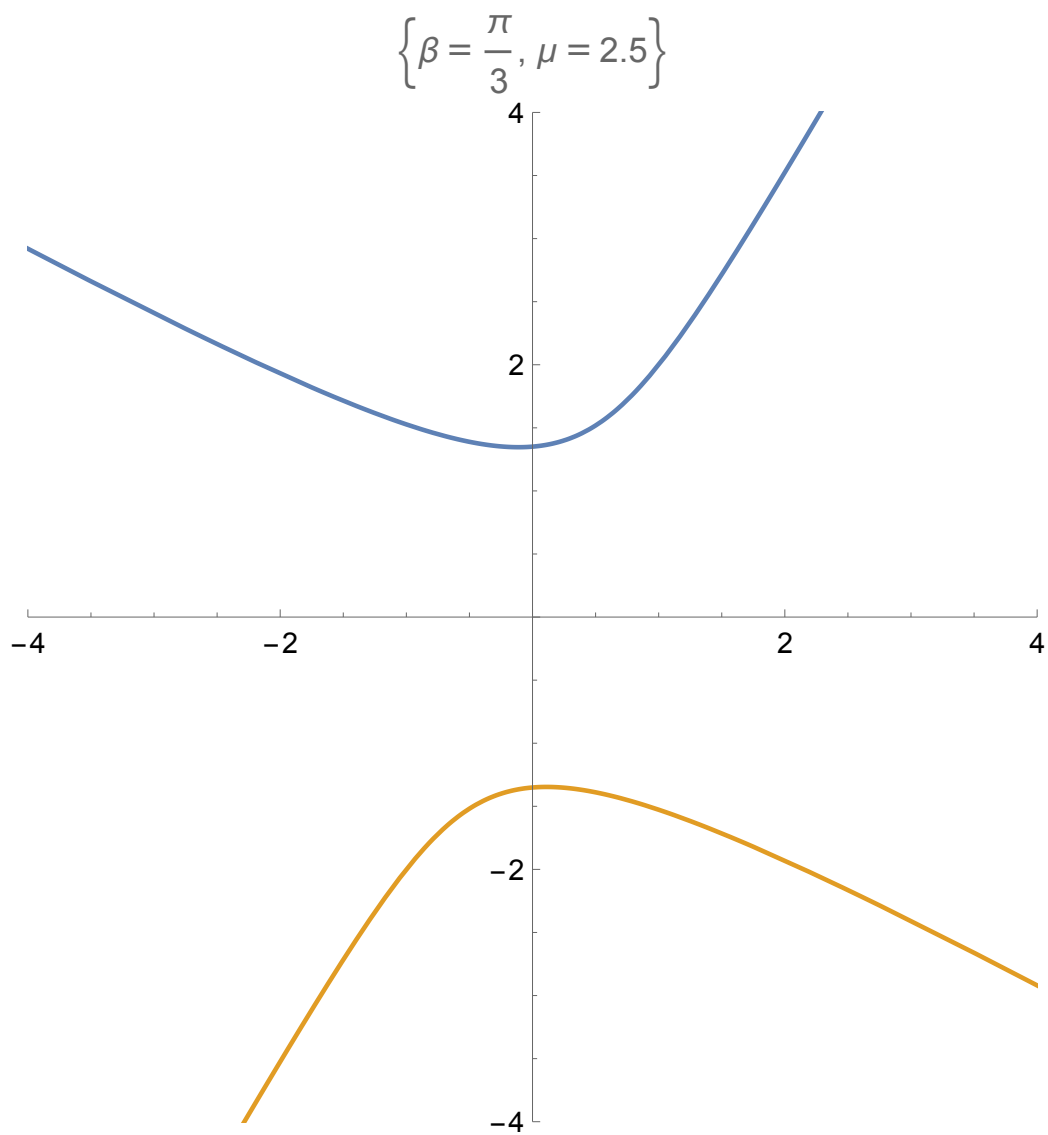


Figure 10: The hyperbolic CVS for $\beta = \pi/3, \mu = 2.5$.

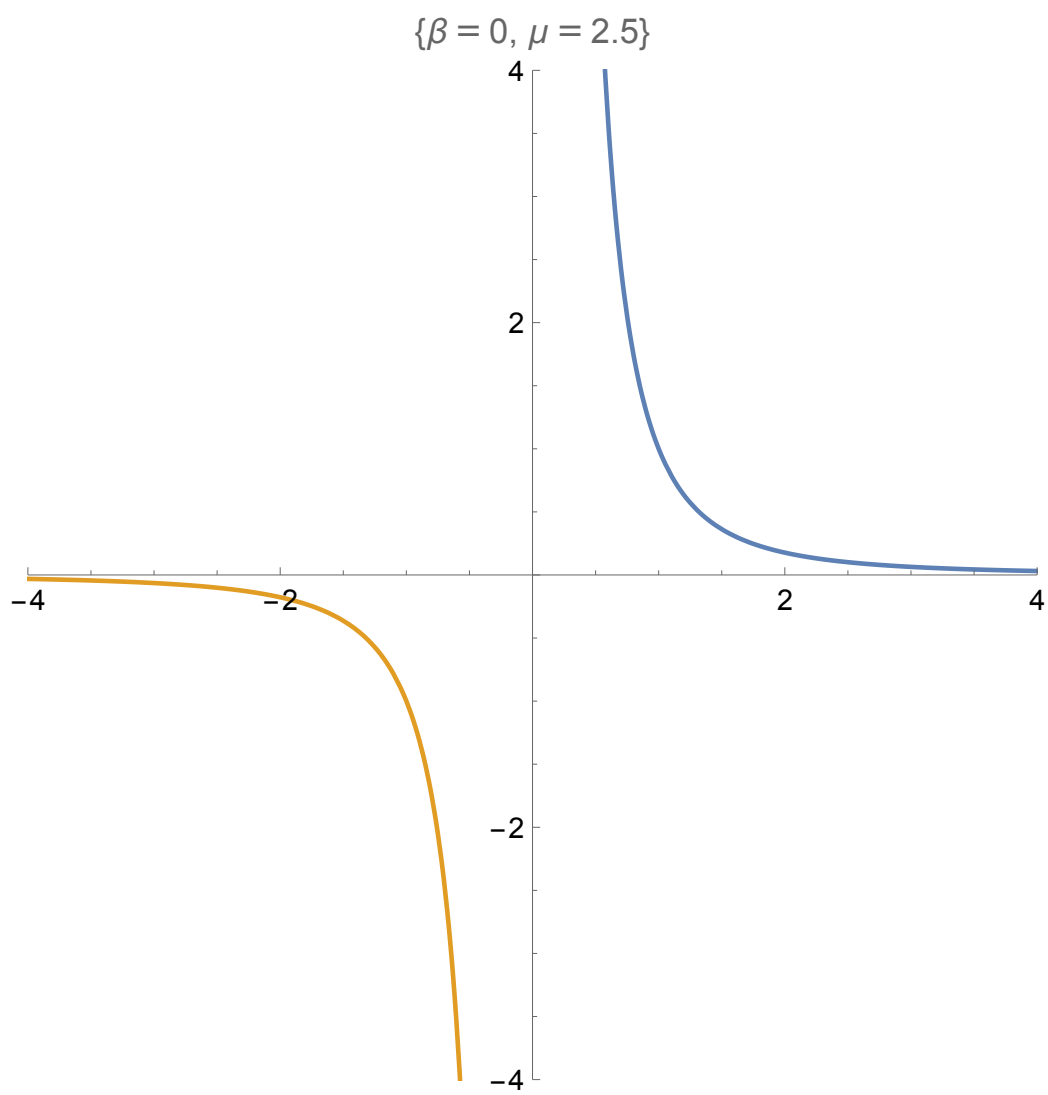


Figure 11: The hyperbolic CVS for $\beta = 0, \mu = 2.5$

The solution of this complex equation for β, μ is

$$\begin{cases} \beta = 0; & \mu = 1 - \frac{c}{a}; \\ \beta = \frac{1}{2}\pi; & \mu = 1 - \frac{c}{b}; \end{cases} \quad (5.49)$$

From the inequalities between the three eigenvalues $a < b < c$ adding to zero, we get

$$-2c < a < -\frac{c}{2}; \quad (5.50)$$

$$-\frac{c}{2} < b < c; \quad (5.51)$$

which makes this index μ limited to the intervals

$$\begin{cases} \beta = 0; & \frac{3}{2} < \mu < 3; \\ \beta = \frac{1}{2}\pi; & -\infty < \mu < \infty; \end{cases} \quad (5.52)$$

We choose the first solution, as in this case, μ varies in the positive region where there are no singularities.

Now, we observe that at $\beta = 0, \frac{1}{2}\pi$, which means $q = 0$ there is an extra symmetry in the equation (5.17)

$$C \Rightarrow C^* \quad (5.53)$$

This symmetry means that now all four branches of the hyperbola

$$|y||x|^\mu = \text{const}; \quad (5.54)$$

are the parts of a single periodic (unbounded) solution $C(\theta)$ (Fig 19).

These four branches define the domain inside the loop C where the holomorphic velocity

$$F_-(\eta) = -2a\eta; \quad (5.55)$$

As for the function F_+ it is just a negative power

$$F_+ \left(x \pm i |x|^{-\mu} \right) = +2i c |x|^{-\mu}; \quad (5.56)$$

The loop $C(\theta)$ defined by these four branches is a periodic function with singularities at $\theta = k\pi/2$.

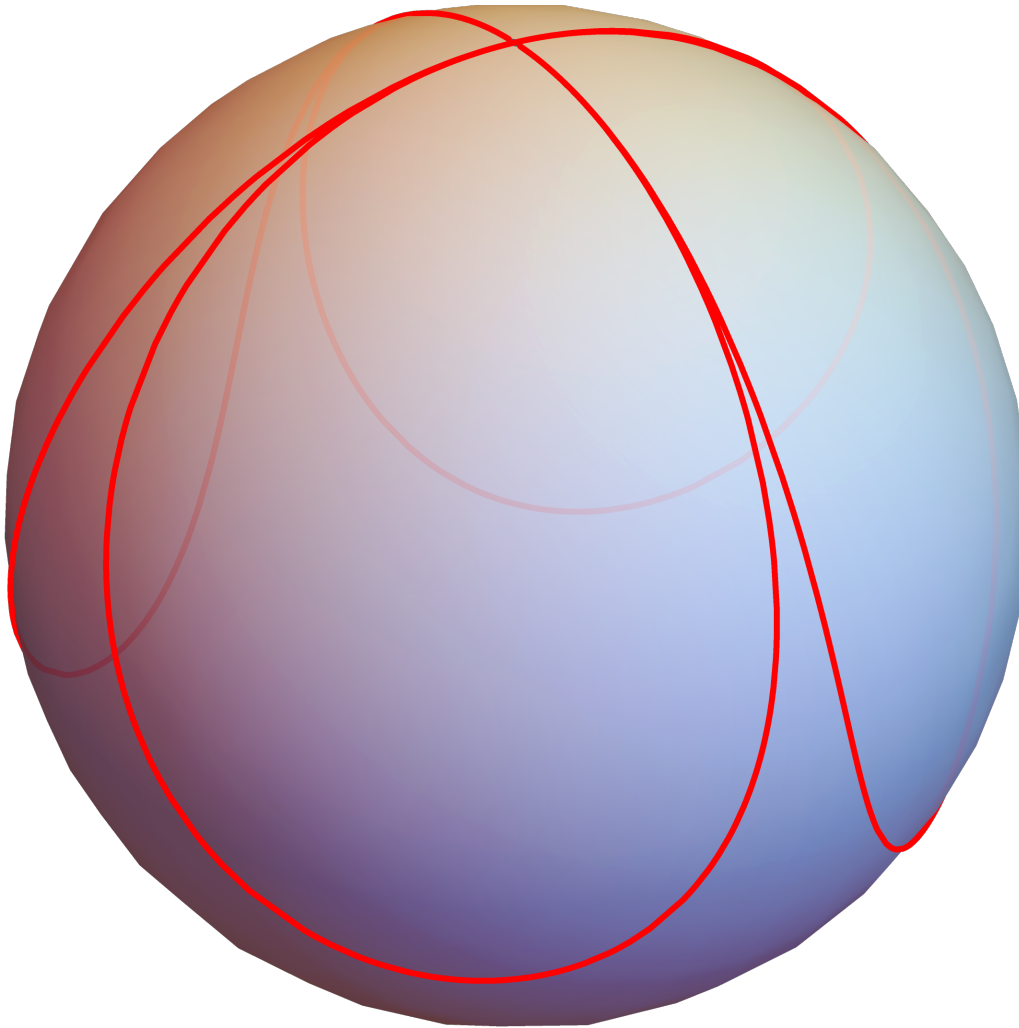


Figure 12: The stereographic projection of four hyperbola branches on the Riemann sphere.

Topologically, on a Riemann sphere S_2 , these four branches divide the sphere into five regions. There is an inside region, with the boundary touching Riemann infinity four times.

Each of the four remaining outside regions is bounded by a hyperbola, starting and ending at infinity.

Let us consider the lower right hyperbola with $y = -x^{-\mu}, x > 0$

The values of $F_+(\eta)$ in three other external regions will be obtained from this one by reflection against the x or y axis.

$$F_+(-\eta) = -F_+(\eta); \quad (5.57)$$

$$F_+(\eta^*) = F_+^*(\eta); \quad (5.58)$$

We can continue the above parametric equation for the function f to the complex plane for the variable w , with the cut from $-\infty$ to 0. The phase of the multivalued function $w^{-\mu}$ is set to $\arg w^{-\mu} = 0, w > 0$.

$$\eta = w - \imath w^{-\mu}; \quad (5.59)$$

$$F_+ = 2\imath c w^{-\mu}; \quad (5.60)$$

This parametric function has a square root singularity at the point where derivative $\partial_w \eta = 1 + \imath \mu w^{-\mu-1}$ vanishes:

$$w_c = (-\imath \mu)^{\frac{1}{\mu+1}} \quad (5.61)$$

For positive μ , this singularity is located in the lower semiplane of w , leaving the upper semiplane as a physical domain.

We have drawn the complex maps⁷ of the derivative $\partial_w \eta = 1 + \imath \mu w^{-\mu-1}$ for $\mu = 1.51, 2, 2.99$

; .

We indicate the zeros of $\partial_w \eta$ as holes on the surface (white circles).

To check whether these singularities penetrate the physical region, we have drawn in black the boundaries of the physical regions

$$\mathbf{Re} \eta^\mu \mathbf{Im} \eta = \pm 1 \quad (5.62)$$

⁷Complex map in *Mathematica*[®] is a 3D surface of $x, y, |f(x + \imath y)|$ for complex function $f(z)$ with its phase $\arg f(x + \imath y)$ as color of the point at this surface.

$$\eta = 1 + \frac{0. + 1.51i}{w^{2.51}}$$

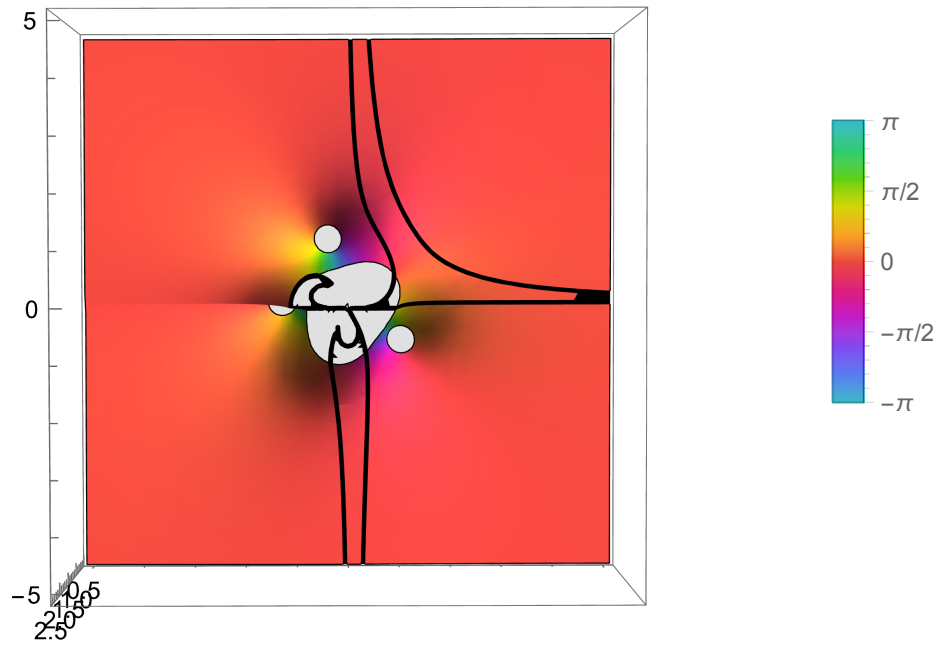


Figure 13: The complex Map3D of the holomorphic function $\eta'(w) = 1 + i\mu w^{\mu-1}$ for $\mu = 1.51$. The height is $|\eta'|$, the color is $\arg \eta'$. The square root singularities of inverse function $\eta(w)$ lie at the points where $\eta'(w) = 0$. We indicate them as holes on the surface (white circles). The black lines are described by $(\mathbf{Re} \eta(w))^\mu \mathbf{Im} \eta(w) = \pm 1$. The physical region is outside the black line in the first quadrant, and there are no singularities.

$$\eta = 1 + \frac{0.+2.i}{w^3.}$$

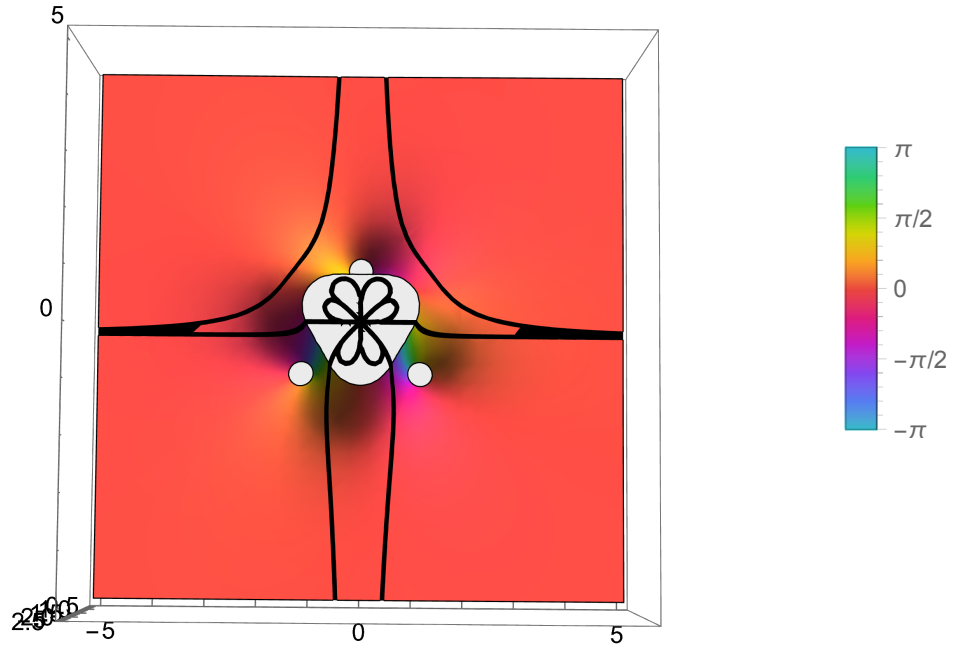


Figure 14: The complex Map3D of the holomorphic function $\eta'(w) = 1 + i\mu w^{-\mu-1}$ for $\mu = 2$. The height is $|\eta'|$, the color is $\arg \eta'$. The square root singularities of inverse function $\eta(w)$ lie at the points where $\eta'(w) = 0$. We indicate them as holes on the surface (white circles). The black lines are described by $(\operatorname{Re} \eta(w))^\mu \operatorname{Im} \eta(w) = \pm 1$. The physical region is outside the black line in the first quadrant, and there are no singularities.

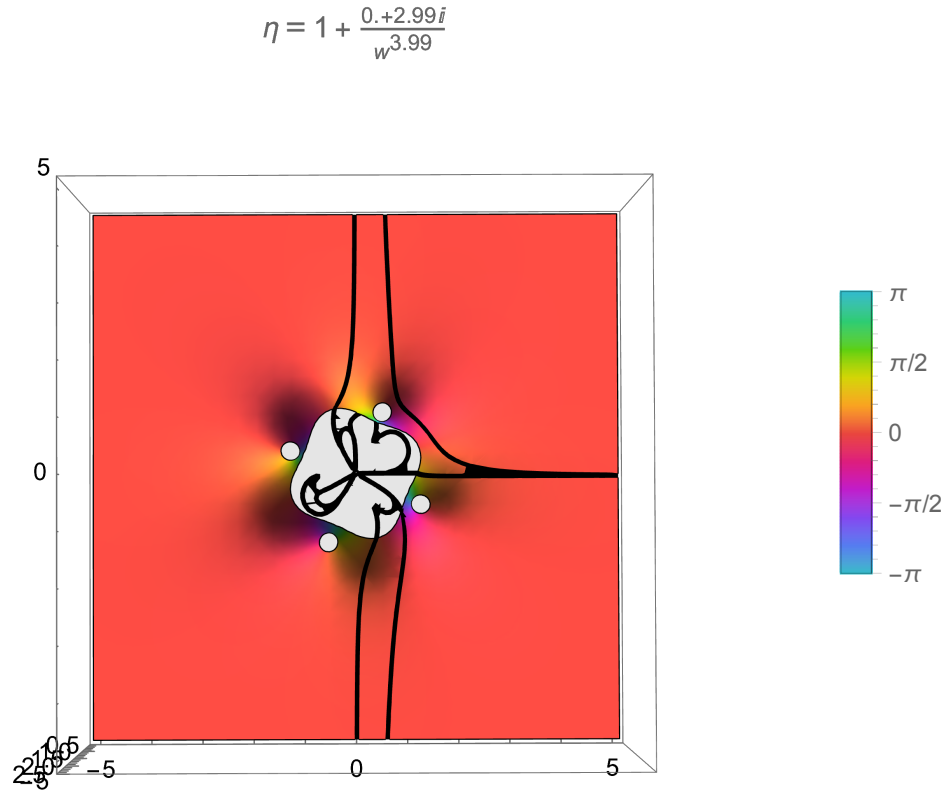


Figure 15: The complex Map3D of the holomorphic function $\eta'(w) = 1 + i\mu w^{-\mu-1}$ for $\mu = 2.99$. The height is $|\eta'|$, the color is $\arg \eta'$. The square root singularities of inverse function $\eta(w)$ lie at the points where $\eta'(w) = 0$. We indicate them as holes on the surface (white circles). The black lines are described by $(\text{Re } \eta(w))^\mu \text{Im } \eta(w) = \pm 1$. The physical region is outside the black line in the first quadrant, and there are no singularities.

We observe that these square root singularities lie outside the physical region. This physical region is above the black line in the first quadrant, and there are no singular points there.

Inside the tube, the velocity is linear, and an extra linear term $F_-(\eta) = -2a\eta$; is a potential flow, which preserves the incompressibility

$$V^- = ax - \imath by - 2a(x + \imath y) = -ax + \imath(c - a)y \quad (5.63)$$

To summarize, the velocity field $\vec{v}(x, y, z)$ and complex coordinates $\eta = x + \imath y$ are parametrized as a function of a complex variable w as follows

$$v_z = cz; \quad (5.64a)$$

$$v_x - \imath v_y = ax - \imath by + F_{\pm} \left(\frac{x + \imath y}{R_0} \right); \quad (5.64b)$$

$$F_-(\eta) = -2a\eta; \quad (5.64c)$$

$$F_+(\eta) = 2\imath cw(\eta)^{-\mu}; \quad \mathbf{Re} \, \eta > 0, \mathbf{Im} \, \eta < 0; \quad (5.64d)$$

$$F_+(-\eta) = -F_+(\eta); F_+(\eta^*) = F_+^*(\eta); \quad (5.64e)$$

$$w(\eta) : \eta = w - \imath w^{-\mu}; \quad (5.64f)$$

$$C : |x|^{\mu}|y| = R_0^{1+\mu}; \quad (5.64g)$$

$$\mu = 1 - \frac{c}{a}; \quad \frac{3}{2} < \mu < 3; \quad (5.64h)$$

$$\Delta\Gamma = \oint_C \vec{v}(\vec{r})d\vec{r} = 0; \quad (5.64i)$$

We show the flow at Figs.16, 16. . The stream plot of this flow is projected in the xy plane.

We performed analytical and numerical computations in.⁴³

While computing the complex velocity and coordinates using parametric equations, we restricted w to the physical region and populated this region with an irregular grid in angular variables in the w plane.

After that, we used *ListStreamPlot* method of *Mathematica*[®].

The grid resolution does not allow tracking the boundary's immediate vicinity, but we computed the normal velocity numerically at the boundary. It turned out to be less than 10^{-15} on both sides of the sheet.

5.5. Clipping the Cusps

Let us consider the hyperbolic cylindrical CVS $|x|^{\mu}|z| = 1, \mu = 2 + \frac{b}{a}$ (in proper units, with cylinder axis, parallel to y , and decreasing eigenvalues

$$\{V, \mu = 1.7, v_n \leq 4.32199 \times 10^{-16}\}$$

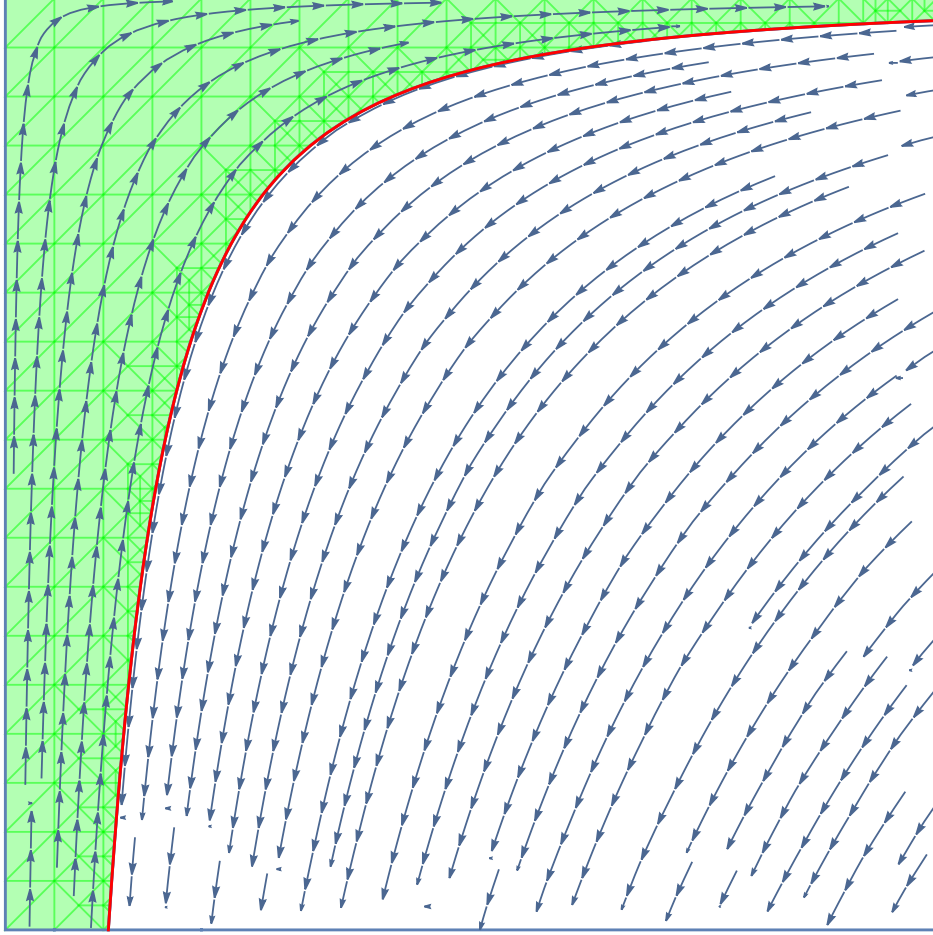


Figure 16: The stream plot in IV quadrant of xy plane for $\mu = 1.7$. The green fluid is inside; the clear fluid is outside the vortex surface (red). One can obtain the flow in other quadrants by reflection against the x and y axes. The normal velocity vanishes at the vortex sheet on both sides, with accuracy $\sim 10^{-16}$.

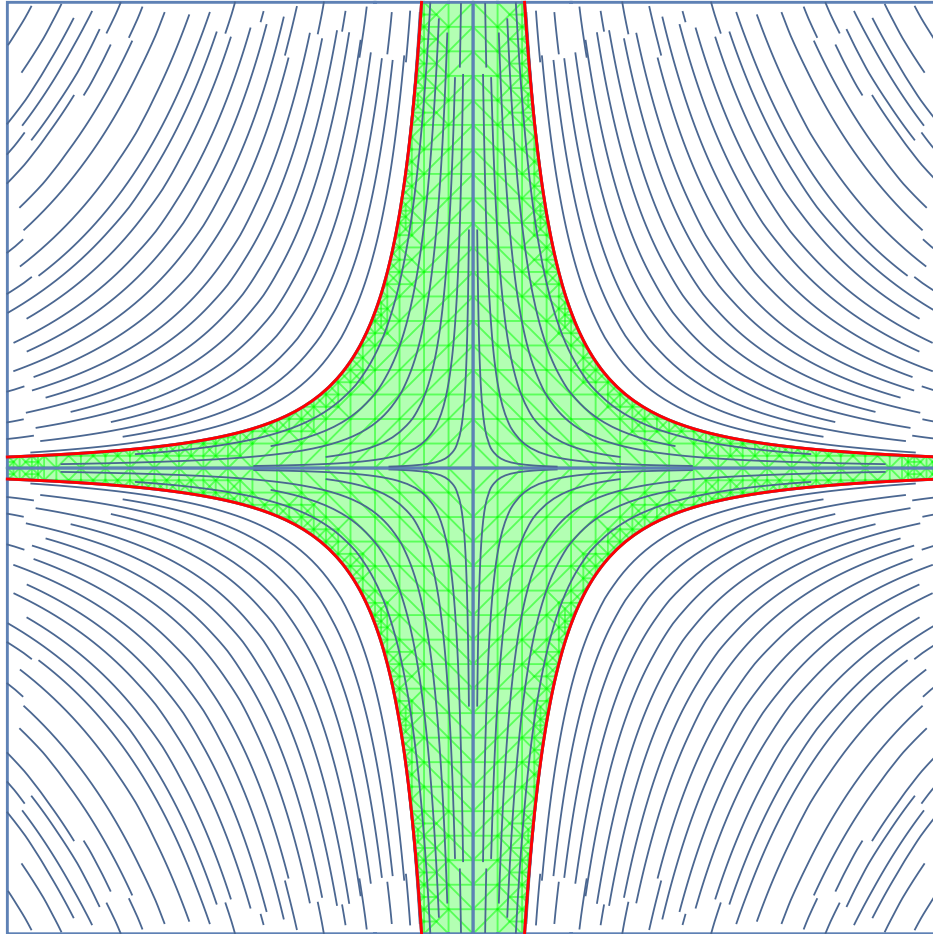


Figure 17: The stream plot in xy plane for $\mu = 1.7$. The green fluid is inside; the clear fluid is outside the vortex surface (red)

of background strain being $(a, b, -a - b)$.

With finite viscosity, in the Navier-Stokes system, there is a thickness $h = \sqrt{\nu/(a+b)}$ of the vortex sheet, which goes to zero at $\nu \rightarrow 0$. We are not assuming that $a+b$ is finite at $\nu \rightarrow 0$, only that $h \rightarrow 0$.

There are three domains on the positive z axis⁸:

$$I : 0 < z < z_0; \quad (5.65)$$

$$II : z_0 < z < z_1; \quad (5.66)$$

$$III : z_1 < z < \infty; \quad (5.67)$$

where

$$z_0 \ll h \ll z_1; \quad (5.68)$$

In the third region, the two opposite velocity gaps $\pm \Delta v_y$ at the mirror branches of hyperbola $|x|^\mu |z| = 1$ are present. In the first region, there is no gap, and the opposite gaps annihilated each other.

The solution in the intermediate (second) region has the same geometry as the Burgers sheet, but the velocity has no gap. In fact, up to the higher correction terms, the hyperbola is horizontal, with the CVS normals aligned at $z > 0, z < 0$, so the same Ansatz $v_y = f(z/h)$ applies, but this time the velocity is an even solution of the same equation

$$f''(\xi) + \xi f'(\xi) - \alpha f(\xi) = 0; \quad (5.69)$$

$$\xi = \frac{z}{h}; \quad (5.70)$$

$$\alpha = \frac{b}{a+b}; \quad (5.71)$$

$$f(\pm\infty) = 0; \quad (5.72)$$

With these boundary conditions, the only restriction on parameters is an inequality $\alpha < 0$.

Hypergeometric functions give this solution for velocity and vorticity

$$v_y = {}_1F_1 \left(\frac{\alpha}{2}; \frac{1}{2}; -\frac{\xi^2}{2} \right); \quad (5.73)$$

$$\omega_x = -\partial_z v_y = \frac{\alpha}{h} \xi {}_1F_1 \left(\frac{\alpha}{2} + 1; \frac{3}{2}; -\frac{\xi^2}{2} \right) \quad (5.74)$$

⁸and, likewise on any other axis

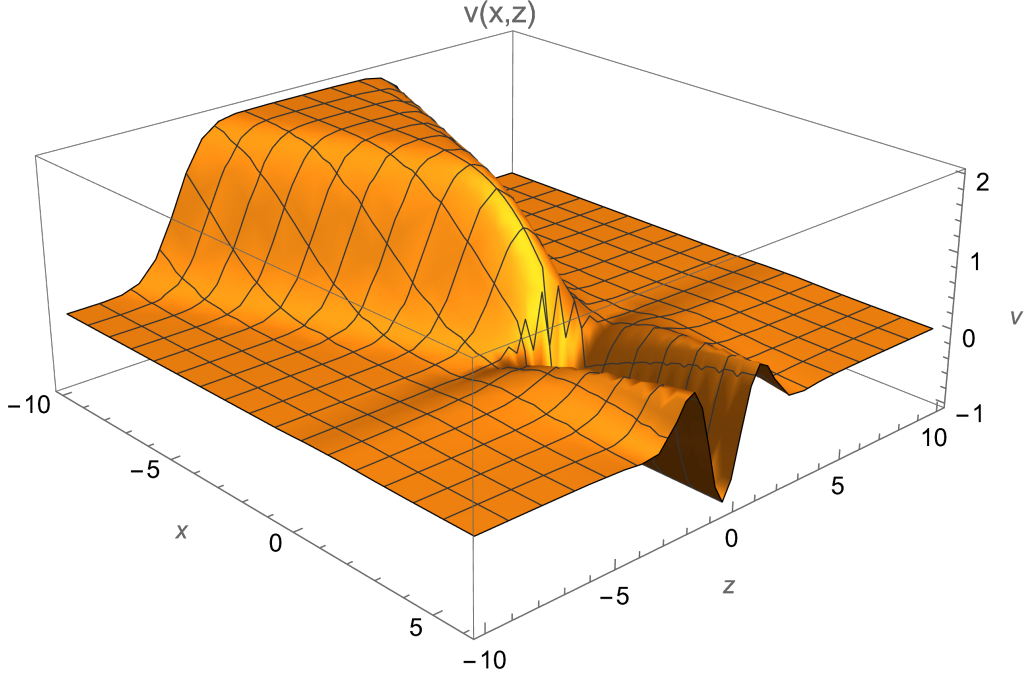


Figure 18: The velocity profile $v_y(x, z)$

The positions $\xi = \pm\Xi(\alpha)$ of the extrema of vorticity are given by the position of the extremum

$$\Xi(\alpha) = \arg \max_{\xi} \left(\xi {}_1F_1 \left(\frac{\alpha}{2} + 1; \frac{3}{2}; -\frac{\xi^2}{2} \right) \right) \quad (5.75)$$

Now, matching the position of these symmetric extrema with the positions of the extrema of the vorticity for the Burgers solution for two separated vortex sheets, we find

$$z_0 = h|\Xi(\alpha)| \quad (5.76)$$

In the region $z_0 < z < z_1$, there is a nontrivial velocity field structure in the boundary layer proportional to h . However, at the distances $z < z_0$, the gaps are mutually annihilated, and velocity and its derivatives are all finite in the Euler limit.

This analysis is only a partial solution in the whole plane x, z . We just studied two regions out of the three. The intermediate region where the two-gap solution deforms into the one with no gaps is yet to be studied.

The curve has an infinite length, and it encircles an infinite area because of the infinite cusps at $x = \pm 0, y = \pm 0$ (see Fig.19).

At a large upper limit $x_{max} \rightarrow \infty$ and small lower limit $x_{min} \rightarrow 0$ the perimeter of the loop goes as

$$P = 4R_0 \int_{x_{min}}^{x_{max}} dx \sqrt{1 + \mu^2 x^{-2(\mu+1)}} \rightarrow 4 \left(x_{min}^{-\mu} + x_{max} \right) R_0; \quad (5.77)$$

Of course, these infinities will not occur in the viscous fluid with finite ν . Our solution applies only as long as the spacing between the two branches of the hyperbola is much larger than the viscous thickness of the vortex sheet.

$$h = \sqrt{\frac{\nu}{c}}; \quad (5.78)$$

$$x_{min} = \frac{h}{R_0}; \quad (5.79)$$

$$x_{max} = \left(\frac{R_0}{h} \right)^{\frac{1}{\mu}}; \quad (5.80)$$

$$P \rightarrow 4R_0 \left(\frac{R_0}{h} \right)^{\mu} + 4R_0 \left(\frac{R_0}{h} \right)^{\frac{1}{\mu}} \rightarrow 4R_0^{\mu+1} h^{-\mu} \quad (5.81)$$

To keep the perimeter fixed in the extreme turbulent limit, we have to tend the parameter R_0 to zero as

$$R_0 = \left(\frac{P}{4} \right)^{\frac{1}{\mu+1}} \left(\frac{\nu}{c} \right)^{\frac{\mu}{2(\mu+1)}} \rightarrow 0; \quad (5.82)$$

The cross-section area of the tube

$$\text{Area} = 4R_0^2 \int_{x_{min}}^{\infty} dx x^{-\mu} = \frac{4}{\mu-1} R_0^2 x_{min}^{1-\mu} \propto Ph \sim P \left(\frac{\nu}{c} \right)^{\frac{1}{2}} \quad (5.83)$$

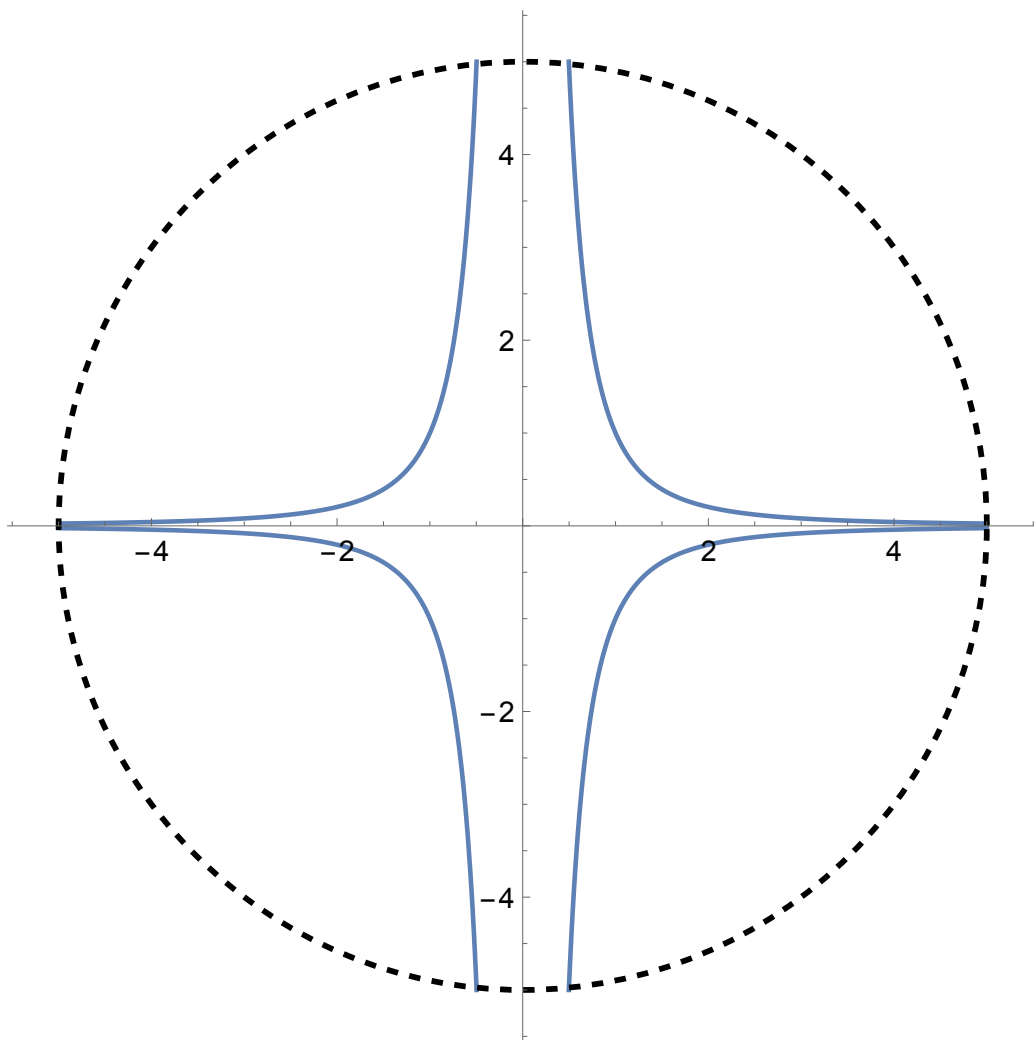


Figure 19: The loop is made of four hyperbola branches.

5.6. Velocity Gap and Circulation

Once the equation is solved, the parametric solution for Γ is straightforward (with factors of R_0 restored from dimensional counting)

$$\Gamma = \int (-2aXX' + 2(a-c)YY')dx = -aR_0^2 \left(x^2 - \mu|x|^{-2\mu} \right); (5.84)$$

$$\Delta V = \frac{\Gamma'}{C'} = -2aR_0x \left(1 + \mu|x|^{-\mu-1} \right) \quad (5.85)$$

We have not expected to find such a singular vortex tube, but it satisfies all requirements and must be accepted.

In,²⁰ we appealed to the Brouwer theorem⁴⁴ to advocate the existence of solutions of the CVS equations. This theorem does not tell us how many fixed points are on a sphere made of the normalized Fourier coefficients when their number goes to infinity.

De Lellis and Brué have proven that there are no compact solutions.

Our non-compact solution is not normalizable, and it has no circulation

$$\Delta\Gamma = \frac{cR_0^2}{\mu-1} \left(x^2 - \mu|x|^{-2\mu} \right)_{x=-\infty}^{x=\infty} = 0 \quad (5.86)$$

We assumed finite circulation in;²⁰ thus, the Brouwer theorem does not apply. On the other hand, we no longer need an existence theorem once we have found an analytic solution.

Note that the net circulation would be infinite unless we combine all four branches of our hyperbola into a single closed loop (with infinite wings at the real and imaginary axes, but still closed).

5.7. Minimizing Euler Energy

Let us now compute the energy of the vortex surface as a Hamiltonian system.^{3/4} There is a regular part related to the background strain. This part is not involved in the minimization we are interested in; it depends on a, b, c , which are external parameters for our problem.

The internal part of the Hamiltonian is directly related to the potential gap Γ we have computed in the previous section.

As shown in the previous sections, the extremum equations for the fluid Hamiltonian as a functional of Γ are locally equivalent to the Laplace equation for the external and internal potentials with Neumann boundary conditions.

$$H_{int} = \int_{\vec{r}_1, \vec{r}_2 \in \mathcal{S}} d\Gamma(\vec{r}_1) \wedge d\vec{r}_1 \cdot d\Gamma(\vec{r}_1) \wedge d\vec{r}_1 \frac{1}{8\pi|\vec{r}_1 - \vec{r}_2|} \quad (5.87)$$

One determines the remaining parameters in the solution from the global minimum condition.

In our case, we have a cylindrical surface

$$d\Gamma(\vec{r}_1) \wedge d\vec{r}_1 = d\Gamma(\theta) \{0, 0, dz\} \quad (5.88)$$

and a separation of variables θ, z .

The integration over z_1, z_2 provides the total length $L \rightarrow \infty$ of the cylinder times logarithmically divergent integral over $z_1 - z_2$. We limit this integral to the interval $(-L, L)$ and compute it exactly

$$\int_{-L}^L \frac{1}{8\pi\sqrt{\eta^2 + z^2}} dz = \frac{\log\left(\frac{2L(\sqrt{\eta^2 + L^2} + L)}{\eta^2} + 1\right)}{8\pi} \quad (5.89)$$

Then we expand it for large L

$$\int_{-L}^L \frac{1}{8\pi\sqrt{\eta^2 + z^2}} dz \rightarrow \frac{\log(2L) - \log|\eta|}{4\pi} + O\left(\frac{\eta^2}{L^2}\right) \quad (5.90)$$

Thus we get in our case, with $\Gamma'(w)$ from (5.84)

$$\begin{aligned} \frac{H_{int}}{L} &= \log(2L) \frac{(\Delta\Gamma)^2}{4\pi} - \\ &\frac{1}{8\pi} \int_{-\infty}^{\infty} dw_1 \Gamma'(w_1) \int_{-\infty}^{\infty} dw_2 \Gamma'(w_2) \log|\xi_1 - \xi_2|; \end{aligned} \quad (5.91)$$

$$\xi_{1,2} = w_{1,2} - \imath |w_{1,2}|^{-\mu}; \quad (5.92)$$

$$\Gamma'(w) = \frac{2cR_0^2 w}{\mu - 1} \left(1 + \mu^2 |w|^{-2\mu-2}\right) \quad (5.93)$$

The first term is the leading one at $L \rightarrow \infty$. Minimization of the energy leads to the condition

$$\Delta\Gamma = 0 \quad (5.94)$$

Therefore, our solution with zero circulation is singled out among other combinations of hyperbolic vortex sheets by the requirement of minimization of energy.

Once the divergent term vanishes, one can compute the rest of the energy.

The remaining principal value integral over x_1, x_2 converges at infinity. In the local limit, when $R_0 \rightarrow 0$, it goes to zero.

We do not see a point in this computation compared to observable quantities such as the energy dissipation and the loop functional.

5.8. *The induced background strain*

What is the physical origin of the constant background strain $W_{\alpha\beta}$ which we used in our solution?

Usually, the external Gaussian random forces are added to the Navier-Stokes equation to trigger the effects of the unknown inner randomness.

In the above theory, the random forces come from many remote vortex structures, contributing to the background velocity field via the Biot-Savart law.

There is no contradiction: in the case of spontaneous magnetization of ferromagnetic, one can introduce an infinitesimal external magnetic field, which is enhanced by infinite susceptibility to produce finite magnetization.

One may also write the self-consistent equation for the mean field, which is analogous to our background strain.

Ultimately, the randomness and the energy flow originate from the external forces at the boundary. These forces trigger internal randomness to be enhanced by the large vorticity structures in bulk.

Let us assume that the space is occupied by some localized vortex structures (not necessarily the CVS surfaces) far from each other. In other words, let us consider an ideal gas of vortex bubbles.

We shall see below that the mean size R_0 of the surface is small compared to the mean distance \bar{R} between them in the turbulent limit $\nu \rightarrow 0, \mathcal{E} = \text{const}$. This vanishing size vindicates the assumptions of the low-density ideal gas.

In such an ideal gas, we can neglect the collision of these extended particles but not the long-range effect of the strain they impose on each other.

The Biot-Savart formula (3.3) for the velocity field induced by the set of remote localized vorticity bubbles B

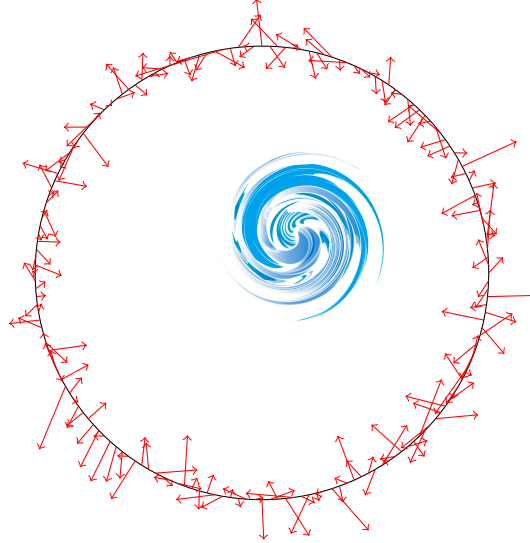
$$\vec{v}(\vec{r}) = \sum_B \int_B d^3 r' \frac{\vec{\omega}(\vec{r}') \times (\vec{r}' - \vec{r})}{4\pi |\vec{r} - \vec{r}'|^3} \quad (5.95)$$

falls off as $1/r^2$ for each bubble, like an electric field from the charged body.

All vortex structures in our infinite volume contribute to this background velocity field, adding up to many small terms at every point in space.

While the Navier-Stokes equation is nonlinear, this relation between the local strain and contributions from each vortex tube is **perfectly linear**, as it follows from the linear Poisson equation relating velocity to vorticity.

Therefore, the interaction between bubbles decreases with distance by the power law, which justifies the ideal gas picture in the case of sparsely distributed vortex tubes.



This picture symbolizes the vortex tube under consideration (blue vortex symbol) surrounded by other remote tubes on a large sphere (orange arrows). The arrows indicate the directions of these remote tubes, which are aligned with the main axis of local strain. We expect the positions and directions of these tubes to be random and uncorrelated when they are far from each other.

If many such bubbles populate space with small but finite density, we would have the "night sky paradox." The bubbles spread on the far away sphere will compensate the inverse distance squared for a divergent distribution like $\int R^2 dR/R^2$.

This estimate is, of course, wrong, as the velocity contributions from various bubbles are uncorrelated, so there is no coherent mean velocity.

Moreover, a Galilean transformation would remove the finite background velocity, so it does not have any physical effects.

However, with the strain, there is another story. Strain coming from remote vortex bubbles

$$W_{\alpha\beta}(\vec{r}) = \frac{1}{2} e_{\alpha\mu\gamma} \partial_\beta \partial_\gamma \sum_B \int_B d^3 r' \frac{\omega_\mu(\vec{r}')}{4\pi|\vec{r} - \vec{r}'|} + \{\alpha \leftrightarrow \beta\}; \quad (5.96)$$

falls off as $1/r^3$, and this time, there could be a mean value \bar{W} , coming from a large number of random terms from various bubbles with distribution $R^2 dR/R^3 \sim dR/R$.

The space symmetry arguments and Laplace equation $\vec{\nabla}^2 1/|\vec{r}| = 0$ outside the origin tell us that averaging over the directions of the bubble centers $\vec{R} = \vec{r}' - \vec{r}$ completely cancels this mean value.

The Central Limit Theorem suggests (within our ideal vortex gas model) that such a strain would be a Gaussian tensor variable, satisfying the normal distribution of a symmetric traceless matrix with zero mean value (see Appendix B.)

$$dP_\sigma(W) \propto \prod_i dW_{ii} \prod_{i < j} dW_{ij} \delta \left(\sum_i W_{ii} \right) \exp \left(-\frac{\text{tr } W^2}{2\sigma^2} \right) \quad (5.97)$$

The parameter σ is related to the mean trace of the square of the random matrix. In n dimensional space

$$\frac{(n+2)(n-1)}{2} \sigma^2 = \langle \text{tr } W^2 \rangle \quad (5.98)$$

The Gaussian random matrices were studied extensively in physics and mathematics. For example, in⁴⁵ the distribution of the Gaussian random symmetric matrix (Gaussian Orthogonal Ensemble, $GOE(n)$) is presented.

We achieve the extra condition of zero matrix trace by inserting the delta function of the matrix trace into the invariant measure. This projection preserves the measure's $O(n)$ symmetry as the trace is invariant to

orthogonal transformations. We tried to find references for this straightforward extension of the $GOE(n)$ to the space of traceless symmetric matrices.

Separating SO_3 rotations $\Omega \in S_2$, we have the measure for eigenvalues a, b, c :

$$dP_\sigma(W) = \frac{1}{4\pi} d\Omega da db dc \delta(a + b + c) P_\sigma(a, b, c); \quad (5.99)$$

$$P_\sigma(a, b, c) = \sqrt{\frac{3}{\pi}} \theta(b - a) \theta(c - b) (b - a)(c - a)(c - b) \exp\left(-\frac{a^2 + b^2 + c^2}{2\sigma^2}\right) \quad (5.100)$$

The moments $\left\langle \left(\frac{a}{\sigma}\right)^m \left(\frac{b}{\sigma}\right)^n \right\rangle$ of this distribution are calculable analytically (see⁴⁶). Here is the table for $m, n = 0, 1, 2, 3, 4$:

$$\begin{pmatrix} 1 & 0 & \frac{1}{6} & 0 & \frac{1}{12} \\ \frac{3\sqrt{\frac{3}{\pi}}}{2} & -\frac{1}{12} & \frac{3\sqrt{\frac{3}{\pi}}}{2} - \frac{2\sqrt{\pi}}{3} & -\frac{1}{24} & 5\sqrt{\frac{3}{\pi}} - \frac{8\sqrt{\pi}}{3} \\ \frac{29}{12} & \frac{2\sqrt{\pi}}{3} - \frac{3\sqrt{\frac{3}{\pi}}}{2} & \frac{13}{24} & \frac{8\sqrt{\pi}}{3} - 5\sqrt{\frac{3}{\pi}} & \frac{49}{144} \\ \frac{9\sqrt{\frac{3}{\pi}}}{2} & -\frac{19}{24} & 6\sqrt{\frac{3}{\pi}} - \frac{8\sqrt{\pi}}{3} & -\frac{71}{144} & 25\sqrt{\frac{3}{\pi}} - \frac{40\sqrt{\pi}}{3} \\ \frac{209}{24} & \frac{8\sqrt{\pi}}{3} - 7\sqrt{\frac{3}{\pi}} & \frac{373}{144} & \frac{40\sqrt{\pi}}{3} - \frac{77}{\sqrt{3}\pi} & \frac{1747}{864} \end{pmatrix} \quad (5.101)$$

The mean traces of powers of the strain, as well as the powers of its determinant, are also calculable. Odd powers yield zero, and the even

powers yield the following tables

$$\left\langle \text{tr} \left(\frac{\hat{W}}{\sigma} \right)^{2n} \right\rangle = \left\{ 3, 5, \frac{35}{2}, \frac{1015}{12}, \frac{37345}{72}, \frac{185185}{48}, \dots \right\}; \quad (5.102a)$$

$$\left\langle \left(\det \frac{\hat{W}}{\sigma} \right)^{2n} \right\rangle = \left\{ 1, \frac{35}{18}, \frac{5005}{108}, \frac{8083075}{1944}, \frac{32534376875}{34992}, \frac{29248404810625}{69984} \right\} \quad (5.102b)$$

The estimate of the variance of the background strain can be done as follows.

$$\sigma^2 = \langle \text{tr} (\hat{W}^2) \rangle \sim \left\langle \left(\int_{V_B} d^3 \vec{r}' \vec{\omega}(\vec{r}') \right)^2 \right\rangle / \Delta R_B^6 \quad (5.103)$$

where the first factor is the mean value of the variance of volume vorticity of the blob, and ΔR_B is the average distance between blobs.

Later we shall use this estimate to get an estimate of the vortex sheet thickness.

5.9. Energy dissipation and its distribution

As we noticed in the previous work²⁰ (see previous sections), the total surface dissipation is conserved on CVS surfaces.

$$\mathcal{E}_{tot} = \sum_S \mathcal{E}_S = \text{const} \quad (5.104)$$

Without CVS as a stability condition, the surface dissipation would not be motion integral. The energy would leak from the vortex surfaces and dissipate in the rest of the volume. Thus, the CVS condition is necessary for the vortex sheet turbulence.

While the total dissipation is conserved, the individual contributions to this sum from each tube are not. The long-term interactions between the vortex tubes, arising due to the Gaussian fluctuations of the background

strain, lead to the statistical distribution of the energy dissipation of an individual tube.

From analogy with the Gibbs-Boltzmann statistical mechanics, one would expect that the dissipation distribution would come out exponential, with some effective temperature. We put forward this hypothesis in our previous work.

However, the interaction between our tubes is different from that of the Gibbs mechanics. While the background strain is a Gaussian (matrix) variable, the shapes of the tubes and the corresponding dissipation are not.

These tubes in our incompressible fluid instantly adjust to the realization of the random background strain. Our exact solutions of the Euler equations with the CVS boundary conditions describe this adjustment.

The general formula²⁰ for the surface dissipation was derived above ((4.67).

For our hyperbolic loop solution, the energy dissipation integral reduces to the following expression (where we restore the implied spatial scale R_0 and express the cutoffs in terms of the perimeter P of the loop by (5.82))

$$\frac{\mathcal{E}}{L\sqrt{\nu}} = 4 \frac{2a^2\sqrt{c}}{\sqrt{\pi}} R_0^3 \int_{x_{min}}^{x_{max}} dw w^2 \left| 1 - \mu w^{-\mu-1} \right|^3 \rightarrow$$

$$P^3 \frac{a^2\sqrt{c}}{24\sqrt{\pi}} \quad (5.105)$$

The normalized distribution $W(\zeta)$ for the scaling variable $\zeta = \frac{a^2\sqrt{c}}{\sigma^2}$ takes the form⁴⁶

$$W(\zeta) = 2\zeta^{9/5} \sqrt{\frac{3}{\pi}} \int_{2^{-1/5}}^{2^{1/5}} dy \frac{(2-y^5)(y^5+1)(2y^5-1)}{y^{14}}$$

$$\exp\left(\frac{(-y^{10}+y^5-1)\zeta^{4/5}}{y^8}\right) \quad (5.106)$$

$$\zeta = \frac{24\sqrt{\pi}\mathcal{E}}{LP^3\sqrt{\nu}\sigma^5}; \quad (5.107)$$

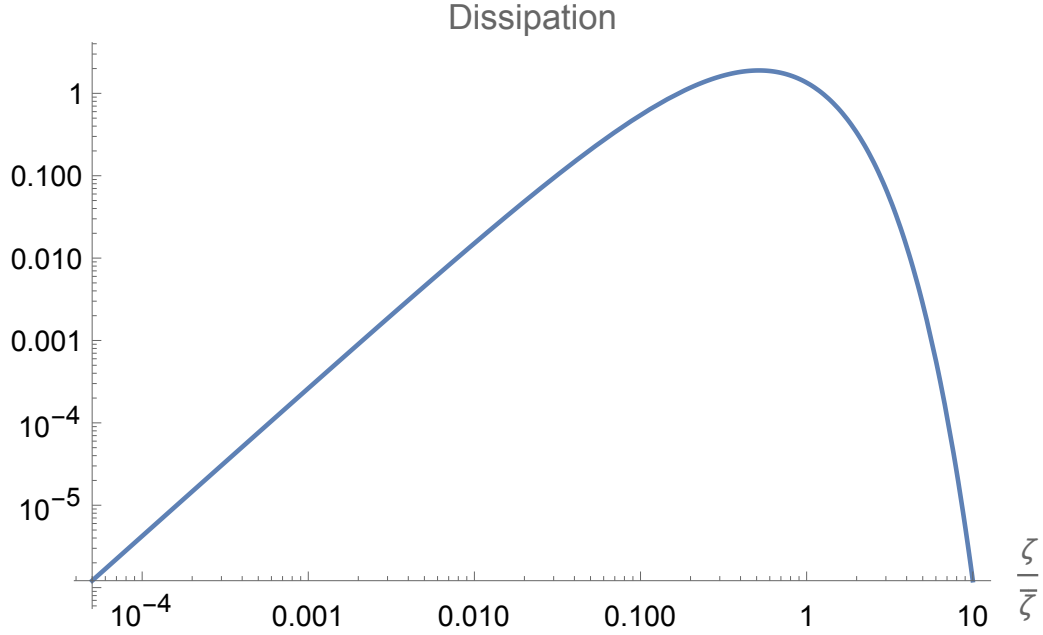


Figure 20: The energy dissipation PDF (fixed perimeter) in log-log scale

The expectation value of this scaling variable equals to

$$\bar{\zeta} = 4.90394 \quad (5.108)$$

We show at the log-log plot of this distribution.

This $W(\zeta)$ is a completely universal function. We will verify this prediction when the distribution of energy dissipation and tube sizes in numerical or real experiments in the extreme turbulent regime becomes available.

The perimeter P of the loop remains a free parameter of our theory. We need some extra restrictions to find the distribution of these perimeters. This additional restriction of the fixed perimeter of the cross-section makes it quite tedious to compare our distribution of the energy dissipation with numerical simulation.

Moreover, we need to find out if these vortex tubes with non-compact cross-sections, though stable, are indeed realized in a turbulent flow.

As we shall see in the next sections, the stable solutions are characterized by topological numbers.

These solutions nicely describe the tails of PDF of velocity circulation, which makes them the best candidates for the dominant classical Clebsch fields (Kelvinons).

6. Energy pumping

Let us review various methods of pumping energy to the turbulent flow and choose the one most appropriate for our Clebsch confinement phase of turbulence.

6.1. Kolmogorov Anomaly

There is a famous Kolmogorov anomaly that relates a certain triple correlation function to the same energy flow in an arbitrary space dimension d :

$$\langle \mathcal{E} \rangle = \lim_{\vec{r} \rightarrow 0} \frac{\partial}{\partial r_\beta} \int d^3 r_0 \left\langle v_\alpha(\vec{r}_0) v_\beta(\vec{r}_0) v_\alpha(\vec{r} + \vec{r}_0) \right\rangle \quad (6.1)$$

The general triple correlation with two coinciding points can be reconstructed from symmetry, incompressibility, and this relation:

$$\left\langle v_\alpha(\vec{r}_0) v_\beta(\vec{r}_0) v_\gamma(\vec{r} + \vec{r}_0) \right\rangle = \quad (6.2)$$

$$\frac{\langle \mathcal{E} \rangle}{(d-1)(d+2)V} \left(\delta_{\alpha\gamma} r_\beta + \delta_{\beta\gamma} r_\alpha - \frac{2}{d} \delta_{\alpha\beta} r_\gamma \right); \quad (6.3)$$

We split points in the Kolmogorov formula to resolve the singularity. Formally, at $\vec{r} = 0$ there is a total derivative

$$v_\alpha(\vec{r}_0) v_\beta(\vec{r}_0) \partial_\beta v_\alpha(\vec{r}_0) = \partial_\beta \left(v_\beta \frac{\vec{r}^2}{2} \right) \quad (6.4)$$

so that the integral vanishes in an infinite box with periodic boundary conditions.

Therefore, this relation holds at distances \vec{r} larger than the viscous scale.

Let us see how this relation applies to vortex sheets.

The general identity, which follows from the Navier-Stokes if one multiplies both sides by \vec{v} and averages over an infinite time interval,

reads:

$$\begin{aligned}\langle \mathcal{E}_V \rangle &= \int_V d^3r \langle \nu \vec{\omega}^2 \rangle \\ &= - \int_V d^3r \partial_\beta \left\langle v_\beta \left(p + \frac{1}{2} v_\alpha^2 \right) + \nu v_\alpha (\partial_\beta v_\alpha - \partial_\alpha v_\beta) \right\rangle\end{aligned}\quad (6.5)$$

By the Stokes theorem, the right side equals the flux over the boundary ∂V of the integration region V . The left side is the dissipation in this volume, so we find:

$$\langle \mathcal{E}_V \rangle = - \int_{\partial V} d\vec{\sigma} \cdot \left\langle \vec{v} \left(p + \frac{1}{2} v_\alpha^2 \right) + \nu \vec{\omega} \times \vec{v} \right\rangle \quad (6.6)$$

This identity holds for an arbitrary volume. The left side represents the viscous dissipation inside V , while the right represents the energy flow through the boundary ∂V .

In case there is a finite collection of vortex sheets (or other localized vortex structures), we can expand this volume to an infinite sphere, in which case the $\vec{\omega} \times \vec{v}$ term drops as there is no vorticity at infinity.

Furthermore, the velocity in the Biot-Savart law decreases as $|\vec{r}|^{-3}$ at infinity, so that only the $\vec{v}p$ term survives

$$\langle \mathcal{E}_V \rangle \rightarrow - \int_{\partial V} d\vec{\sigma} \cdot \langle \vec{v}p \rangle \quad (6.7)$$

This energy flow on the right side will stay finite in the limit of the expanding sphere in case the pressure grows as $p \rightarrow -\vec{f} \cdot \vec{r}$.

$$\langle \mathcal{E} \rangle = \vec{f}_\alpha R^3 \int_{S_2} n_\alpha n_\beta \langle v_\beta(R\vec{n}) \rangle \quad (6.8)$$

This expression is, of course, equal to our definition of energy pumping

$$\begin{aligned}\langle \mathcal{E}_\infty \rangle &= \int d^3r \vec{f} \cdot \vec{v} = \\ &= \int_V d^3r \vec{\nabla} \cdot (\vec{v}(\vec{f} \cdot \vec{r})) = \int_{\partial V} d\vec{\sigma} \cdot \vec{v}(\vec{r} \cdot \vec{f})\end{aligned}\quad (6.9)$$

Where did we lose the Kolmogorov energy flow? It is still there for any finite volume surrounding the vortex sheet

$$\langle \mathcal{E}_V \rangle = - \int_V d^3r \langle v_\beta \partial_\beta p + v_\alpha v_\beta \partial_\beta v_\alpha \rangle = \quad (6.10)$$

$$- \int_V d^3r \langle v_\alpha v_\beta \partial_\beta v_\alpha \rangle - \int_{\partial V} d\vec{\sigma} \cdot \langle \vec{v} p \rangle \quad (6.11)$$

The first term is the Kolmogorov energy flow inside the volume V , and the second is the energy flow through the boundary.

The pressure can also be expressed in terms of velocity from incompressibility and the Navier-Stokes equation

$$p = -\vec{f} \cdot \vec{r} + \int d^3\vec{r}' \frac{\partial_\alpha v_\beta \partial_\beta v_\alpha}{4\pi|\vec{r} - \vec{r}'|} \quad (6.12)$$

We see that without finite force \vec{f} acting on the boundary, say, with periodic boundary conditions, the boundary integral would be absent, and we would recover the Kolmogorov relation.

In the conventional approach, based on the time averaging of the Navier-Stokes equations, the periodic Gaussian random force $\vec{f}(\vec{r})$ is added to the right side. In this case, with periodic boundary conditions

$$\langle \mathcal{E}_V \rangle = - \int_V d^3r \langle v_\beta \partial_\beta p - v_\beta f_\beta(\vec{r}) + v_\alpha v_\beta \partial_\beta v_\alpha \rangle = \quad (6.13)$$

$$\int_V d^3r \langle v_\beta f_\beta(\vec{r}) \rangle \quad (6.14)$$

In the limit when the force becomes uniform in space, we recover our definition as $\mathcal{E} = \vec{f} \cdot \vec{P}$.

So, our formula is another way to specify the energy flow, generalizing rather than contradicting the Kolmogorov triple correlation.

6.2. Alternative energy pumping

Naturally, we assume that turbulence is a universal phenomenon, so it should not depend upon the mechanism of random forcing or the boundary conditions.

As long as there is an energy flow from the large wavelengths or the boundary, the confined turbulence in bulk would dissipate this energy flow in singular vortex structures.

We expect the distribution of these structures to be universal at a given energy flow, regardless of how the energy is pumped in.

These assumptions were confirmed in a beautiful experimental work by William Irvine and collaborators at Chicago University ⁽⁴⁷⁾.

They measured the Kolmogorov energy spectrum, proving that periodic boundary conditions were unnecessary.

This universality allows us to use yet another way to pump energy at large scales.

Namely, let us add a uniform shift in the velocity field.

In terms of the spherical representation of Clebsch field (without Z factor)

$$v_\alpha = Z\tilde{v}_\alpha; \quad (6.15)$$

$$\tilde{v}_\alpha = (\phi\partial_\alpha S_3 + \partial_\alpha\Phi); \quad (6.16)$$

$$\partial_\alpha^2\Phi = -\partial_\alpha(\phi\partial_\alpha S_3); \quad (6.17)$$

$$(6.18)$$

we add the linear solution of the Laplace equation to potential Φ

$$\Phi = \vec{G}(\vec{f}) \cdot \vec{r} + \vec{\nabla} \cdot \int d^3r' \frac{\phi(r') \vec{\nabla} S_3(r')}{4\pi|r-r'|} \quad (6.19)$$

Here the vector $\vec{G}(\vec{f})$ represents the result of the forcing. It is uniform in space, but with a time-dependent Clebsch field, evolving by the Clebsch Flow Equation it will also depend on time.

This forcing is equivalent to adding the volume term to the net momentum of the fluid

$$\vec{P} = \int_V d^3r \vec{v} \rightarrow ZV\vec{G}(\vec{f}) \quad (6.20)$$

This term corresponds to the linear term in the pressure

$$p = -\vec{f} \cdot \vec{r} + \int d^3r' \frac{\partial_\alpha v_\beta \partial_\beta v_\alpha}{4\pi|\vec{r}-\vec{r}'|} \quad (6.21)$$

Comparing the space-independent terms in the time-dependent Euler equations for the velocity field with the above linear term in the velocity

representation, we find the following estimation

$$\partial_t G_\alpha + M_{\alpha\beta} G_\beta \approx f_\alpha; \quad (6.22)$$

$$M_{\alpha\beta} \approx \left\langle \partial_\beta \tilde{v}_\alpha \right\rangle_{R_3}; \quad (6.23)$$

$$(6.24)$$

Here we made some approximations to be removed below.

The vorticity part of velocity gradient $\partial_\beta \tilde{v}_\alpha$ vanishes after spacial averaging, so we are left with background strain \hat{S} in the vicinity of our vortex sheet

$$\hat{M} \approx \hat{S} \quad (6.25)$$

This background strain is the same one we studied for Clebsch bubbles, but here we have the external force fixed rather than random, which is why the mean strain is not zero.

Assuming that the average over space R_3 is time-independent, we can compute the time average of this $\vec{G}(t)$

$$\left\langle \vec{G}(t) \right\rangle_t \approx \hat{S}^{-1} \cdot \vec{f}; \quad (6.26a)$$

$$\mathcal{E} \approx ZV \vec{f} \cdot \hat{S}^{-1} \cdot \vec{f} \quad (6.26b)$$

In a complete theory, we have to study the dynamics of the velocity field, perturbed by constant force at the boundary. Only then can we relate the time average of the constant term in velocity with the force term in the pressure.

However, this relation will also be linear with the small force we need, with some general tensor $\hat{Q} \neq \hat{S}^{-1}$.

The corresponding perturbation of velocity field $\delta \vec{v}$ and pressure δp by a weak force at the boundary satisfies the linearized Euler equation (we omit the tilde in \vec{v}):

$$\partial_t \delta \vec{v} + (\vec{v} \cdot \nabla) \delta \vec{v} + (\delta \vec{v} \cdot \nabla) \vec{v} + \vec{\nabla} \delta p = 0; \quad (6.27)$$

$$\vec{\nabla} \cdot ((\vec{v} \cdot \nabla) \delta \vec{v} + (\delta \vec{v} \cdot \nabla) \vec{v}) + \vec{\nabla}^2 \delta p = 0; \quad (6.28)$$

$$\delta p(\vec{r} \rightarrow \infty) \rightarrow -\vec{f} \cdot \vec{r} \quad (6.29)$$

The linear force term in mean velocity is equal to the time and volume average of this perturbation

$$\langle \vec{G} \rangle_t = \langle \langle \delta \vec{v} \rangle_V \rangle_t = \hat{Q} \cdot \vec{f} \quad (6.30)$$

Later we average energy pumping over Gaussian force \vec{f} assuming the existence of \hat{Q} , and we obtain the mean energy pumping. The quadratic dependence of Z as a function of external force \vec{f} (see below) will be considered. The resulting Gaussian average will involve $\langle (\vec{f} \cdot \hat{Q} \cdot \vec{f})^2 \rangle \sim \sigma^4$.

We shall denote \hat{Q} as \hat{S}^{-1} keeping in mind that it is an averaged tensor density for the linear perturbation of the Kelvinon flow.

This average tensor would be proportional to \hat{I} in the empty space due to space symmetry. However, the steady discontinuity surface \mathcal{S}_C (see below) violates the space symmetry, so this average value $\hat{Q}(C)$ is some finite functional of C .

7. Kelvinon as Clebsch domain wall

We suggested in a recent work¹⁸ a certain weak solution (domain wall bounded by a monopole) to the Euler equations. This solution is more general than the pure vortex sheet we studied in the previous section.

That vortex sheet corresponds to the bubble of a constant phase ϕ_2 of the Clebsch field while this new vortex sheet corresponds to a phase gap $\Delta\phi_2 = \pi(2k + 1)$.

The new Euler flow also contains a vortex sheet, but there is also some vorticity in bulk.

This singular flow does not belong to the Generalized Beltrami flow ($\vec{\nabla} \times \vec{\omega} \times \vec{v} = 0$).

Moreover, it does not correspond to a steady solution for the Clebsch field. This field evolves with time while preserving its circulation over a fixed loop in space. It also undergoes time-dependent gauge transformations while being carried by the self-generated flow.

The vorticity stays invariant under the gauge transformations (i.e., symplectomorphisms invariance).

Geometrically, the vortex sheet looks like a disk, but the shape of the surface does not have to satisfy the CVS conditions.

Those conditions were derived above as the solution of the linear boundary problem for the steady Navier-Stokes equation in a very specific geometry; there was zero vorticity outside the boundary layer and only tangential vorticity inside this layer.

In the case of the Kelvinon, there is some normal vorticity at the surface, violating the simple geometry of the solution of the Navier-Stokes equation needed for the CVS condition. In addition, this solution is not steady: it only has a stationary circulation Γ_C .

We formulated this solution using S_2 Clebsch variables (3.27).

After extensive discussions with Grigory Volovik, we concluded that this solution is topologically equivalent to the so-called KLS domain wall bounded by the Alice string, initially suggested for the early universe.

Volovik summarized these discussions in a short paper (unpublished), which we attach with his generous permission as a section, "Topological defects in Turbulent flows," to this review.

Such topological defects^{48,24} were observed in real experiments in liquid ^3He , which is an example of a (quantum) fluid with zero viscosity. The dynamic variables in the liquid ^3He are different from our Clebsch variables, but the topology is the same.

The vortex surface is a disk D bounded by some loop C .

In terms of Clebsch variables, the disk is a domain wall such that S_3 stays continuous, but the complex field $\Psi = S_1 + i S_2$ rotates $2k + 1$ times by π in a complex plane when crossing this disk.

To be more precise, the angular variable $\phi = \arg \Psi$ in target space S_2 is related to two angular variables in R_3

$$\phi = m\alpha + n\beta; \quad (7.1)$$

$$n = k + \frac{1}{2}; \quad (7.2)$$

where α, β are two cycles for the loop C . α is the angle along the loop, and β is the angle along the dual loop \tilde{C} encircling C .

7.1. Initial data for the Kelvinon

Let us present an explicit example of the Clebsch field with required topology, which could serve as initial data for the Clebsch Flow Equation.

We introduce a surface of the minimal area bounded by our loop C

$$\mathcal{S}_{min}(C) = \arg \min_{S: \partial S = C} \int_S dS \quad (7.3)$$

For every point $\vec{r} \in R_3$, there is the nearest point \vec{r}_1 at the minimal surface $\mathcal{S}_{min}(C)$.

$$\vec{r}_1 = \arg \min_{\vec{r}' \in \mathcal{S}_{min}(C)} (\vec{r} - \vec{r}')^2; \quad (7.4)$$

For this point \vec{r}_1 at the surface there is also a nearest point \vec{r}_0 at its edge C , minimizing the geodesic distance $d(a, b)$ along the surface from \vec{r}_1 to the edge

$$s_0 = \arg \min_s d(\vec{r}_1, \vec{C}(s)); \quad (7.5)$$

$$\vec{r}_0 = \vec{C}(s_0); \quad (7.6)$$

Let us also introduce the local frame with vectors $\vec{t}(s), \vec{n}(s), \vec{\sigma}(s)$ at the loop:

$$\vec{C}'(s)^2 = 1; \quad (7.7a)$$

$$\vec{t}(s) = \vec{C}'(s); \quad (7.7b)$$

$$\vec{n}(s) = \frac{\vec{C}''(s)}{|\vec{C}''(s)|} \quad (7.7c)$$

$$\vec{\sigma}(s) = \vec{t}(s) \times \vec{n}(s); \quad (7.7d)$$

Our field is then defined as follows:

$$\alpha = \frac{2\pi s_0}{\oint |d\vec{C}|}; \quad (7.8a)$$

$$\beta = \arg \left((\vec{r} - \vec{r}_0) \cdot (\vec{n}(s_0) + \imath \vec{\sigma}(s_0)) \right); \quad (7.8b)$$

$$\rho = \sqrt{(\vec{r} - \vec{r}_1)^2 + d(\vec{r}_1, \vec{r}_0)^2}; \quad (7.8c)$$

$$S_1 + \imath S_2 = \frac{2\lambda\rho}{\lambda^2 + \rho^2} e^{\imath m\alpha + \imath n\beta}; \quad (7.8d)$$

$$S_3 = \frac{\lambda^2 - \rho^2}{\lambda^2 + \rho^2}; \quad (7.8e)$$

The parameter λ plays the role of the size of the Kelvinon in physical space R_3 .

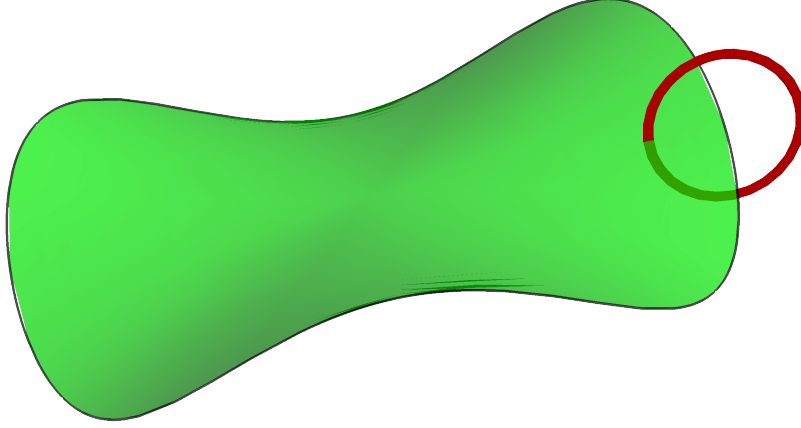


Figure 21: Kelvinon cycles. The β cycle (red) around the α cycle (black) of the vortex sheet (green).

When the point \vec{r} approaches the nearest point \vec{r}_1 at the minimal surface, the difference $\vec{\eta} = \vec{r} - \vec{r}_1$ is normal to this surface.

When the point \vec{r}_1 approaches the nearest point \vec{r}_0 at the edge C of the surface, the geodesic becomes a straight line in R_3 , tangent to the surface and ρ becomes Euclidean distance to the loop

$$d(\vec{r}_1, \vec{r}_0) \rightarrow |\vec{r}_1 - \vec{r}_0|; \quad (7.9)$$

$$\rho^2 \rightarrow |\vec{r} - \vec{r}_1|^2 + |\vec{r}_1 - \vec{r}_0|^2 = |\vec{r} - \vec{r}_0|^2 \quad (7.10)$$

Note that all variables $s_0, \vec{r}_0, \vec{r}_1, \alpha, \beta, \rho, \vec{S}$ depend on $\vec{r} \in R_3$ through the minimization of the distance to the surface and the loop. By construction, $\rho = |\vec{r} - \vec{r}_0|$ away from the surface, when $\vec{r}_1 = \vec{r}_0, d(\vec{r}_1, \vec{r}_0) = 0$.

The Clebsch field $\vec{S}(\vec{r})$ takes the boundary value $\vec{S}(C) = (0, 0, 1)$ at the loop and $\vec{S}(\infty) = (0, 0, -1)$.

Let us move \vec{r} along the normal from the surface at \vec{r}_1 . Our parametriza-

tion of S_3 does not change in the first order in normal shift $\vec{\eta} = \vec{r} - \vec{r}_1$, as ρ^2 has only quadratic terms in $\vec{\eta}$.

We conclude that the normal derivative of the Clebsch field $\phi_1 = Z(1 + S_3)$ vanishes

$$\partial_n \phi_1 = 0; \quad (7.11)$$

We requested vanishing normal velocity at the discontinuity surface for this surface to be steady. In terms of Clebsch parametrization (3.33) the normal velocity would vanish provided

$$\partial_n \phi_3 = 0; \quad (7.12)$$

As for the angular field $\phi_2 = \phi$ in (7.8), its normal derivative does not vanish in the general case. The angle α does not change when the point \vec{r} moves in normal direction $\vec{N}(\vec{r}_1)$ from the surface projection \vec{r}_1 by infinitesimal shift $\vec{\eta} = \epsilon \vec{N}(\vec{r}_1)$. However, another angle β changes in the linear order in ϵ as

$$\vec{N}(\vec{r}_1) \cdot (\vec{n}(s_0) + \iota \vec{\sigma}(s_0)) \neq 0 \quad (7.13)$$

The angle β varies when the point \vec{r} goes around anti-clockwise along the β cycle, starting from the lower side of the surface. When \vec{r} approaches initial point \vec{r}_1 from the upper side, β changes by 2π .

$$\beta(\vec{r}_1 + \epsilon \vec{N}(\vec{r}_1)) = \beta(\vec{r}_1 - \epsilon \vec{N}(\vec{r}_1)) + 2\pi; \quad (7.14)$$

$$\Psi(\vec{r}_1 + \epsilon \vec{N}(\vec{r}_1)) = \Psi(\vec{r}_1 - \epsilon \vec{N}(\vec{r}_1)) e^{2\iota \pi n}; \quad (7.15)$$

$$\Psi(\vec{r}) = S_1(\vec{r}) + \iota S_2(\vec{r}); \quad (7.16)$$

At the boundary C of the discontinuity surface, the Clebsch field has a singularity but remains finite and tends to the sphere's north pole.

Thus, the loop C maps into an infinitesimal circle around the north pole of S_2 . The velocity circulation around the north pole is reduced to the area outside this circle, i.e., the sphere's whole area 4π . It is finite despite the singularity of the Clebsch field at the loop.

This field is a particular example of the topology of the Kelvinon. The general solution would have the same topology but evolve with time by the Clebsch Flow Equation(3.39). This example provides proper initial data for the Clebsch Flow Equation.

The solution maps the minimal surface $S_{min}(C) \in R_3, C = \partial S$ with the disk topology into the region σ outside the loop $\gamma \in S_2$.

In our paper,¹⁸ we assumed that there was an integer number n of full β rotations. However, as we see it now, the half-integer numbers are also allowed, as they change the sign of Ψ leaving velocity and vorticity invariant.

There is no continuous deformation of the Clebsch field, which could change its half-integral winding number.

The disk then is a 2D version of the branch cut in the complex plane between two singularities at $\pm a$ of the function $f(z) = (z^2 - a^2)^{k+\frac{1}{2}}$.

The tangent vorticity in this solution is the same as with ordinary vortex sheets.

In the local tangent frame

$$\omega_i(x, y, z) = (2k + 1)\pi Z \delta(z) e_{ij} \partial_j S_3(x, y) + \text{regular terms}; \quad (7.17)$$

This ω is the same tangent vorticity we had in vortex sheets with the local gap of potential at the disk

$$\Phi^+ - \Phi^- = \Gamma = (2k + 1)\pi Z S_3 \quad (7.18)$$

The azimuth angle $\phi = \arg(S_1 + \iota S_2)$ has $(2k + 1)\pi$ discontinuity at two sides of the wall corresponding to tangent velocity discontinuity

$$\Delta \vec{v}_i = \partial_i \Gamma = (2k + 1)\pi Z \partial_i S_3(x, y) \quad (7.19)$$

There is also a finite normal component ω_z of vorticity, also related to the same function $S_3(x, y)$.

$$\omega_z = Z e_{ij} \partial_i \phi \partial_j S_3(x, y) \quad (7.20)$$

7.2. Discontinuity surface vs. minimal surface

Our Clebsch field $\phi_2 = \phi$ has $2\pi n$ discontinuity across some surface S_C bounded by C . We remind that $\phi_1 = Z(1 + S_3), S_3 = \cos \theta$. As we argued in papers^{8, 17, 18} (see also the next sections), the minimal surface is compatible with Clebsch parametrization of conserved vorticity ($\partial_\alpha \omega_\alpha = 0$).

One can describe a minimal surface by Enneper-Weierstrass parametrization:⁴⁹

$$\vec{X}(\rho, \theta) = \mathbf{Re} \vec{F}(\rho e^{i\theta}); \quad (7.21)$$

$$\vec{F}'(z) = \left\{ \frac{1}{2}(1 - g^2)f, \frac{i}{2}(1 + g^2)f, gf \right\} \quad (7.22)$$

with $g(z), f(z)$ being analytic functions inside the unit circle $|z| < 1$. Such surface is shown at Fig.22 for $f = 1, g = z$:

However, solutions of the Euler equation could exist with Clebsch discontinuity at arbitrary, non-minimal surfaces.

Let us discuss this important point in some detail. Let us assume that the Clebsch field is discontinuous across some generic smooth surface S_{disc} , bounded by the loop C where we specify the circulation.

In the quadratic vicinity of the local tangent plane to the surface, its equation reads (with K_1, K_2 being principal curvatures at this point)

$$S_{disc}(x, y, z) = z - \frac{K_1}{2}x^2 - \frac{K_2}{2}y^2 = 0 \quad (7.23a)$$

$$n_\alpha = \frac{(-K_1x, -K_2y, 1)}{\sqrt{1 + K_1^2x^2 + K_2^2y^2}} \rightarrow (-K_1x, -K_2y, 1); \quad (7.23b)$$

$$\partial_\alpha n_\alpha = -(K_1 + K_2) \quad (7.23c)$$

The minimal surface would correspond to $K_1 + K_2 = 0$, which means a divergence-less normal vector along the surface.

In case the normal derivatives of both Clebsch fields ϕ_1, ϕ_2 vanish, the vorticity at the surface will be directed along the local normal vector, as follows from Clebsch parametrization of vorticity.

In the general case, the Clebsch Flow Equation equations do not support vanishing normal derivatives of the Clebsch field, only the vanishing normal velocity.

Vanishing normal velocity is achieved by the Neumann boundary condition for the Poisson equation for the pressure, compensating the normal component of the convection term $v_\alpha \partial_\alpha v_\beta$ in the Euler equation. In terms of the Clebsch variables, a similar role is played by ϕ_3 potential.

It is easy to see that the Euler equations (3.25) demand that the normal velocity vanishes at the surface to cancel the term $2\pi n v_z \delta(z)$ in advection term $v_\alpha \partial_\alpha \phi_2$.

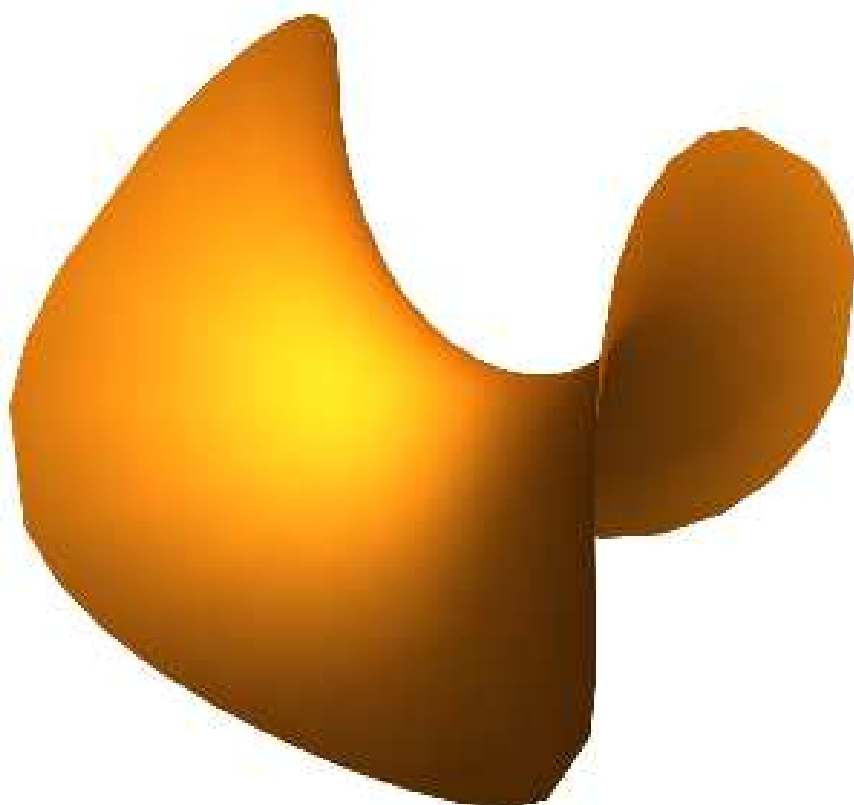


Figure 22: The Enneper's Minimal surface with $f = 1, g = z$.

$$n_\alpha v_\alpha(\vec{r} \in \mathcal{S}_{disc}) = 0 \quad (7.24)$$

The tangent derivatives $v_i \partial_i \phi_2$ are generally finite and can balance with the gauge transformation term and the time derivative.

From the point of view of the Euler dynamics in Clebsch variables, the discontinuity surface could be any smooth surface. It is the Loop Equation, which we study in the next sections, which provides the missing relation between discontinuity and the minimal surface for Kelvinon as a fixed point of the Loop Equation.

Once ϕ_3 is adjusted to nullify the normal velocity at the surface, the discontinuity surface will not move with the flow.

The $\delta(z)$ term in vorticity is orthogonal to the normal vector to the surface and thus does not contribute to the flux through the minimal surface, so this flux is still determined by the second (regular) term, and circulation is related to this $S_3|_{\vec{r} \in C} = 1$

$$\Gamma_C = \oint_C v_\alpha dr_\alpha = Z \oint_\gamma d\alpha (1 + S_3) = 4\pi m Z \quad (7.25)$$

The extra term 1 in $1 + S_3$ comes from integration by parts with boundary value $S_3(\infty) = -1$.

The relation of the circulation for the domain wall to the winding number was discussed in the context of the quantum liquid (see appendix by Volovik, where different normalization of circulation was used).

Here, we claim the quantization of **classical** circulation in terms of Z , which is no longer related to Planck's constant. It is related, instead, to the external forcing, causing energy dissipation.

The Stokes theorem ensures that the flux through any other surface bounded by the loop C would be the same, but in that case, the singular tangent component of vorticity would also contribute. The simplest computation corresponds to choosing the flux through the discontinuity surface.

The fact that circulation is a number multiplied by the Z factor, which is **an integral of motion** in the Euler dynamics, is another way to prove that this circulation is conserved in the Euler dynamics.

This conservation, in turn, means that the exponential of this circulation satisfies the loop equation in the WKB limit $\nu \rightarrow 0$ (at fixed external force \vec{f}).

It is remarkable that the circulation of the **static** loop C , as opposed to the loop moving with the flow, is conserved.

We computed it in terms of Z by purely topological arguments without using the explicit form of this solution.

The relation of the constant Z to the constant external forces comes outside of the Euler dynamics.

It relies on the energy balance in the full Navier-Stokes equation, which is made possible by anomalous dissipation (4.67).

Without anomalous dissipation, the energy of the Euler solution would be formally conserved rather than dissipated and balanced by the energy pumping from the boundaries.

The Kelvinon velocity field reduces to the surface integral

$$v_{\beta}^{Kelv}(r) = 2\pi n \left(\delta_{\beta\gamma} \partial_{\alpha} - \delta_{\alpha\beta} \partial_{\gamma} \right) \int_{S_C} d\sigma_{\gamma}(\xi) \partial_{\alpha} \Phi(\xi) \frac{1}{4\pi |\vec{X}(\xi) - \vec{r}|} + \dots \quad (7.26)$$

The dots represent the volume contribution to the Biot-Savart integral, determined by the bulk solution for the Clebsch field.

7.3. Topology of the Kelvinon

The topological invariant, which depends on these winding numbers, was suggested in,⁸ where it was argued that it was distinguishing our solution from the generic Clebsch field.

Consider the circulation $\Gamma_{\delta C(\alpha)}$ around the infinitesimal β cycle $\delta C(\alpha)$ which encircles our loop at some point with angular variable α (Fig.23).

It is straightforward to compute

$$\Gamma_{\delta C(\alpha)} = \oint_{\delta C(\alpha)} \phi_1 d\phi_2 = 2\pi n \phi_1 \quad (7.27)$$

This circulation stays finite in a limit of shrinking loop δC because of singular vorticity at the loop C .

Now, integrating this over the loop C with $d\phi_2 = m d\alpha$ we get our original circulation

$$\oint_C \Gamma_{\delta C(\alpha)} d\phi_2(\alpha) = 2\pi n \oint_C \phi_1 d\phi_2 = 2\pi n \Gamma_C \quad (7.28)$$

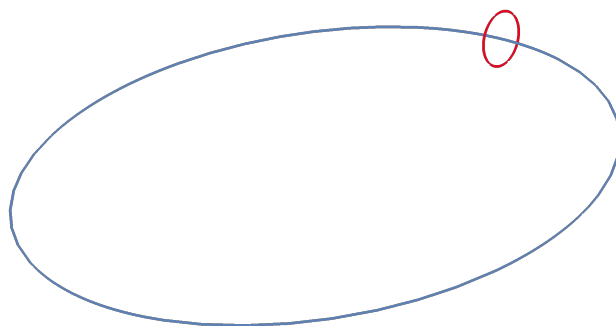


Figure 23: The infinitesimal β loop δC (red) encircling original loop C (blue).

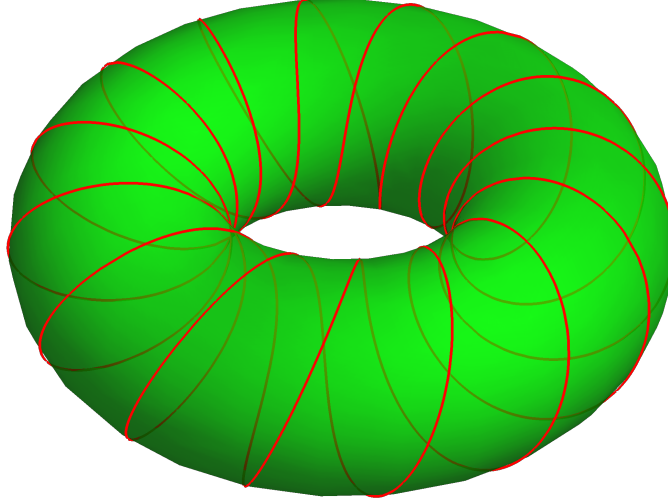


Figure 24: The torus mapped into Clebsch space

Geometrically, this is an area of the torus \mathcal{T}_C in Clebsch space mapped from the tube made by sweeping the infinitesimal circle around our loop (see Fig.24).

This circulation is an oriented area inside the loop in Clebsch space, which is m times the geometric area, as the area is covered m times by the Kelvinon field.

$$|\mathcal{T}_C| = 8\pi^2 nmZ \quad (7.29)$$

This area is mapped from the infinitesimal torus in physical space R_3 around a singular loop C but is finite and quantized.

This finite area is a generalization of the pole residue in a complex plane. In the case of a pole, the integral over an infinitesimal 1-loop in 2-plane yields a finite result proportional to the winding number. In the

present case, the integral over the infinitesimal 2-torus in 3-space yields a finite result proportional to the product of two winding numbers.

Let us look at the topology of the mapping from the physical space to the Clebsch space S_2 .

We cut out of R_3 the infinitesimal solid torus (inside the above torus) around our loop – this remaining space topologically also represents a solid torus. We cut this solid torus along the discontinuity surface S_C bounded by C , and then glue it back with $2\pi n$ twist around the polar axis (path inside the solid torus).

This solid torus with the cut is now topologically equivalent to a ball (inside of S_2 sphere). This ball is mapped on a stereographic sphere S_2 with its pole corresponding to that axial path. The field does not have a singularity on this path.

The two sides of the discontinuity surface are mapped to two spheres S_2 glued at the North pole. One of these spheres is rotated around the polar axis by $2\pi n$. When we go through the discontinuity surface of the viscous thickness $h \sim \nu^{\frac{1}{2}}$ we cover this S_2 precisely n times.

This evolution of $\vec{S}(x, y, z)$ when z goes from $-h$ to $+h$ describes this rapid rotation around the vertical axis. The tangential vorticity is related to the angular speed of this rotation, which goes to infinity as $1/h$.

The corresponding vortex lines come from $z = -\infty$, enter the surface at $z \sim -h$ in the normal direction, then coil n times, then exit at $z \sim h$ and go to $+\infty$ as shown at Fig.25.

Note that each of these lines is coiling in space, but they are not interlinked. As we shall see below, this property leads to vanishing helicity: there is no knotting of the vortex lines.

In the appendix "Topological defects in Turbulent flows," Grigory Volovik describes various topological configurations of Clebsch field and related tetrad field in superfluid Helium.

We expect some smooth field $\vec{S}(\vec{r})$, which tends to $(0, 0, -1)$ at spatial infinity. $\Psi = S_1 + \iota S_2$ has $(2k + 1)\pi$ winding around the β cycle, and $2m\pi$ winding number along the loop (α cycle).

An example of this field (7.8) with proper topology and vanishing normal derivatives was presented in the previous section. This example can serve as initial data for the time evolution of the Clebsch field, according to Clebsch Flow Equation.

The boundary condition at the edge says that the velocity field is

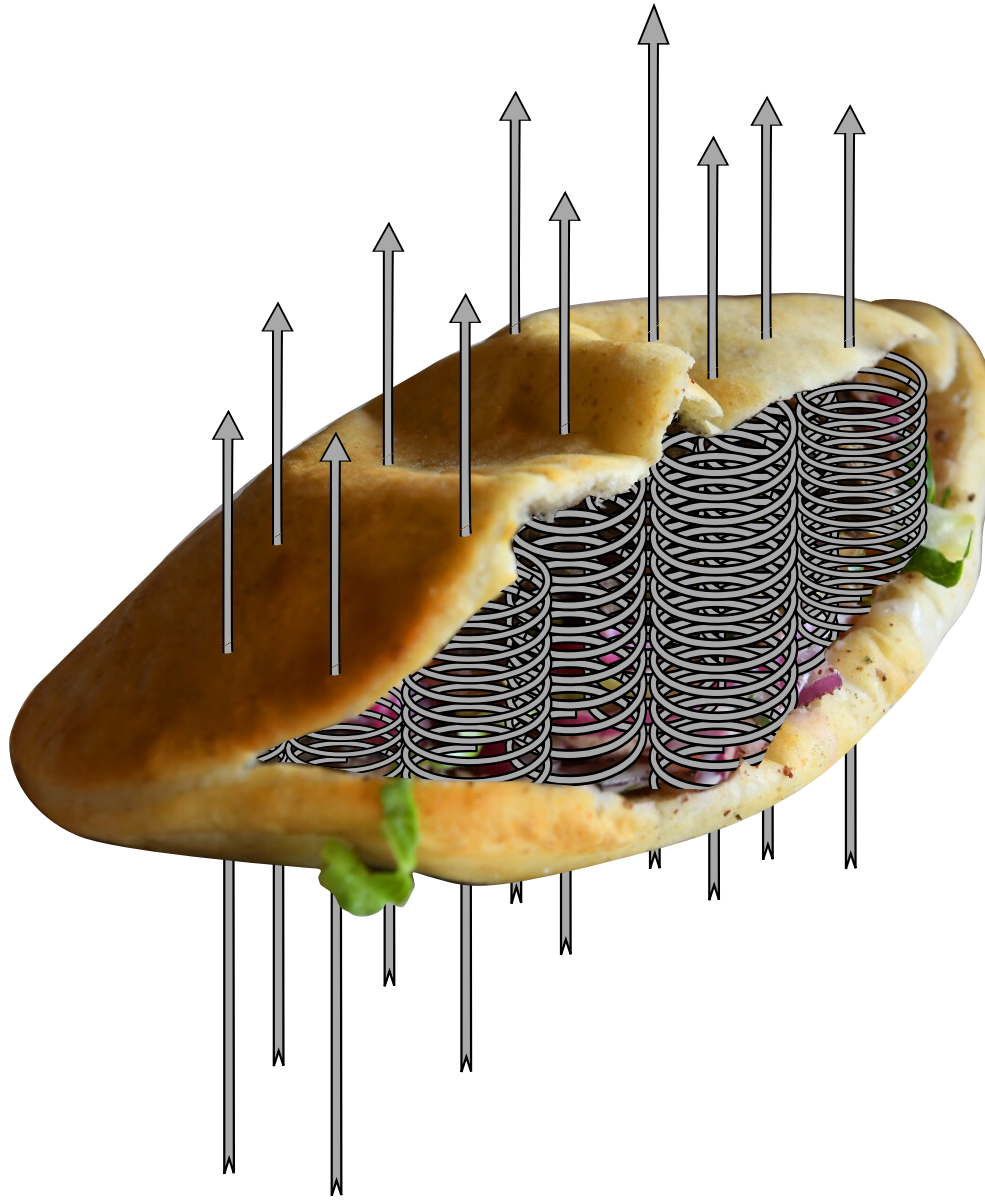


Figure 25: The vortex lines coiling inside the vortex sheet (Zeldovich pancake⁵⁰ stuffed with vortex coils) in our Kelvinon solution. We depicted this pancake as a pita bread– its American version.

tangent to the bounding loop. This way, the flow goes around rather than leaks off the disk.

With no gap at the edge and no normal velocity, we have the constant value of the Clebsch vector \vec{S} at C . As $S_1 + \iota S_2$ changes the sign when crossing the disk, it must vanish at the boundary, just as the velocity gap vanishes.

This requirement leads us to the boundary conditions at the edge ∂D of the disk

$$\vec{S}(\vec{r} \in \partial D) = (0, 0, 1); \quad (7.30)$$

With this boundary condition, the helicity integral (3.38) for this solution is zero

$$H = 2\pi n Z \oint_C \phi_3 dS_3 = 0 \quad (7.31)$$

as expected for the vortex lines, which coil but do not link.

Thus, we have tangent vorticity peaking at $\eta = 0$ with a Gaussian profile in the normal direction η , plus we have the normal vorticity, finite at $\eta = 0$.

The normal component of vorticity contributes to the flux through the disk. However, it does not contribute to the enstrophy in the turbulent limit $\nu \rightarrow 0, h \rightarrow 0$ because the tangent term dominates the integral of the square of vorticity.

The normal term yields the next correction at $\nu \rightarrow 0$.

7.4. Kelvinon equation and WKB approximation for the Hopf equation

Let us now consider the time-dependent Clebsch Flow Equation (3.39) derived in⁸

$$\partial_t \phi_a + v_\alpha \partial_\alpha \phi_a = e_{ab} \frac{\partial h(\phi)}{\partial \phi_b};; a, b = 1, 2 \quad (7.32)$$

$$v_\alpha = \phi_2 \partial_\alpha \phi_1 + \partial_\alpha \phi_3; \quad (7.33)$$

$$\partial_\alpha v_\alpha = 0; \quad (7.34)$$

Here the gauge function $h(\phi)$ is an arbitrary local function of the Clebsch field, independent of the point in space R_3 ; it must be determined from the consistency of the equation.

As discussed in the previous section (3.39), the equation describes the passive flow of the Clebsch field in the direct product space $R_3 \otimes S_2$. The 5- component velocity field in this space $V = (v_1, v_2, v_3, -\partial_2 h, \partial_1 h)$ is divergence-less in each of R_3, S_2 . The Clebsch field is passively transported by this velocity in the product space.

The leading term in these equations near the discontinuity surface is the normal flow restriction

$$v_\alpha(r)n_\alpha(r) = 0; r \in S_C \quad (7.35)$$

which annihilates the $\delta(\eta)$ term on the left side of (7.32) for $a = 2$.

The next order terms will involve the gauge function $h(\phi)$.

The idea behind the instanton in stochastic equations⁵¹ is that the intermittent phenomena, i.e., rare events responsible for the tails of PDF, are related to certain classical (meaning non-random) field configurations minimizing effective Action, **including the random force**. The classical value of the random force turns out to be imaginary, which corresponds to the saddle point in functional integral.

There is no functional integral for the turbulence theory (not counting Wyld's integral, which is inappropriate in the turbulent limit). Instead, we have an exact loop equation, which plays the role of the Schrödinger equation, and we could develop the WKB expansion in that equation.

We study the loop equation in more detail in the following sections.

At the moment, we assume that at a fixed value of the external random force \vec{f} , the relevant field configuration is the domain wall, bounded by an Alice string with the same shape as our loop C . The circulation is related to the flux $4\pi mZ$ through that disk; thus, at fixed winding numbers m, n , the remaining problem is to find the relation between Z and \vec{f} .

In the conventional formulation, with Wyld's functional integral over velocity \vec{v} , pressure p , and auxiliary vector field \vec{u} , the instanton is determined by the minimum of the Action, i.e., classical solution in extended phase space.

Those equations are hard to solve, plus they are too general: the dynamics of the potential part of velocity are very complex and even possibly non-universal.

Instead of Wyld's integral, our theory has the Hopf equation for the loop functional (see Section 8). It has the form of the Schrödinger equation in loop space, and the classical approximation for the loop functional is also related to the classical solution of the non-stationary Euler equation.

We shall find out that the usual instantons (solutions of the forced Navier-Stokes equation with imaginary time) are irrelevant to the intermittency in the circulation statistics.

We **do not need** to assume the fixed point (i.e., steady solution) of the Clebsch Flow Equation. We have different solutions - Kelvinons, which are time-dependent but conserve the circulation around a particular loop. This conservation makes Kelvinon a fixed point of the loop equation.

It suffices to know that Clebsch field covers a compact manifold S_2 ; therefore, its time averages could have a finite limit as time goes to infinity.

Another, stronger hypothesis, which we do not need now, would be a uniform measure on this compact manifold.

We need nontrivial winding numbers for the existence and stability of the Kelvinon, the same as with instantons in the gauge theory.

Regardless of this unknown measure, the Euler dynamics says that the parameter Z is an integral of motion of this Clebsch Flow Equation, so it can be taken out of time averaging.

The energy balance (6.5),(6.26a) says:

$$\mathcal{E} = Z^2 A(\vec{f}) = Z B(\vec{f}); \quad (7.36)$$

$$A(\vec{f}) = \nu \left\langle \int_V \left(\vec{\nabla} \phi \times \vec{\nabla} S_3 \right)^2 \right\rangle_t; \quad (7.37)$$

$$B(\vec{f}) = V \vec{f} \cdot \hat{S}^{-1} \cdot \vec{f}; \quad (7.38)$$

Note that all time averages in the above formulas are taken at fixed (rather than randomized) external force \vec{f} .

The \vec{f} dependence of these functions $A(\vec{f}), B(\vec{f})$ comes from the random forces in the boundary condition for the potential part Φ in the velocity dependence of the Clebsch variables on S_2 .

The energy balance determines the normalization constant Z .

This energy balance follows from the time averaging of the time derivative of the Euler energy $\frac{1}{2} \int \vec{v}^2$ over the solution of the Navier-Stokes equation at fixed constant external force \vec{f} .

We exploited that Z is an integral of Euler motion, so it can be taken out of time averaging and thus related to time averages of certain functionals of the vector $\vec{S}(\vec{r}, t)$.

The Gaussian averaging over \vec{f} will be performed as the last step.

Note that here is where we radically deviate from the standard approach to the Euler equation. In the Generalized Beltrami flow, which is the non-singular steady solution of the Euler equation, there is no parameter of a dimension of viscosity to relate Z to, so it remains a free parameter of the flow.

We specify this parameter by replacing the Euler flow with the limit of the Navier-Stokes flow at viscosity going to zero at a fixed energy dissipation rate. Such a limit is significantly different from conventional Euler flow, as seen in the previous sections.

Moreover, our flow is a weak solution of the Euler equation rather than a conventional Generalized Beltrami flow. The singularities are resolved by viscosity, and this is how we get the necessary parameters to fix arbitrary constant Z of the spherical parametrization of vorticity by Clebsch field.

The non-zero solution of the quadratic equation yields:

$$Z = \frac{B(\vec{f})}{A(\vec{f})} \quad (7.39)$$

At small \vec{f} (we justify this extra assumption below), these functions expand in the Taylor series, with A starting from a constant and B by construction having only quadratic terms.

Thus we have in the leading order

$$A(\vec{f}) \rightarrow A(\vec{0}); \quad (7.40)$$

$$Z \rightarrow \frac{\vec{f} \cdot \hat{S}^{-1} \cdot \vec{f}}{A(\vec{0})/V}; \quad (7.41)$$

In the turbulent limit $\nu \rightarrow 0$ at fixed \mathcal{E} , the width of the turbulent layer goes to zero as $h \sim \sqrt{\nu}$ which makes the surface part of enstrophy integral $A(\vec{0}) \sim \sqrt{\nu}$. This decrease disappointed Burgers in the last century, as his theory had no Z factor.

The contribution from the bulk to $A(0)$ takes over the surface contribution, assuming other vortex structures are filling the volume.

$$\frac{A(0)}{V} = \rho \nu \left\langle \left\langle \int_B (\vec{\nabla} \phi \times \vec{\nabla} S_3)^2 \right\rangle_t \right\rangle_B ; \quad (7.42a)$$

$$\rho = \frac{\sum_B 1}{V} \quad (7.42b)$$

Here $\langle \dots \rangle_B$ stands for averaging over a single vortex structure in our volume, and $\sum_B 1$ is the total number of these structures.

7.5. Stability of Kelvinon and the first De Lellis-Brué theorem

One comment about the stability of the domain wall in the Euler-Lagrange equation. There is the rotational part of velocity at the surface and the potential part; therefore, the stability analysis now also involves normal vorticity ω_γ .

$$\partial_t \delta r_\alpha = \partial_\beta v_\alpha \delta r_\beta; \quad (7.43)$$

$$\partial_\beta v_\alpha = S_{\alpha\beta} + \frac{1}{2} e_{\alpha\beta\gamma} \omega_\gamma; \quad (7.44)$$

$$\sigma_\alpha v_\alpha = 0 \quad (7.45)$$

The three complex eigenvalues of the non-symmetric derivative matrix $H_{\alpha\beta} = \partial_\beta v_\alpha$ add up to zero because of incompressibility. There is one real and two complex-conjugate ones.

The normal motion will be stable if the real eigenvalue is negative and its eigenvector points along the normal to the surface.

$$\hat{H} \cdot \vec{\sigma} = \lambda \vec{\sigma}; \quad (7.46)$$

$$\lambda = \vec{\sigma} \cdot \hat{H} \cdot \vec{\sigma} = \hat{S}_{nn} < 0 \quad (7.47)$$

The transverse motion does not need to be stable, as it reduces to reparametrization of the surface, not resulting in observable quantities in virtue of gauge invariance.

Once this stability condition is satisfied, the estimate $h \rightarrow \sqrt{\nu / (-\hat{S}_{nn})}$ still holds by estimating the cancellation of the singular terms in the Navier-Stokes equation in the presence of normal vorticity.

The normal component \hat{S}_{nn} , in this case, can be negative everywhere on the surface except the loop $C = \partial S$, where it is singular.

This singularity invalidates assumptions of the theorem by De Lellis and Brué. This theorem claims that for a non-singular surface velocity field tangent to C , the normal strain cannot be negative everywhere on the surface.

The tangent to the boundary $\partial S = C$ velocity component can stay finite.

Lack of proof of instability does not prove stability, unfortunately. The missing proof of the stability of Kelvinon with minimal discontinuity surface remains a problem for future research.

7.6. Estimates of parameters

Let us continue analyzing the factors $A(\vec{f}), B(\vec{f})$.

The enstrophy $A(\vec{0})$ is dominated by the contribution from the vortex sheets B , which grows as $1/h = \sqrt{-\hat{S}_{nn}/\nu}$

$$\frac{1}{V}A(\vec{0})_{\nu \rightarrow 0} \rightarrow \frac{\rho\sqrt{\nu}(2\pi n)^2}{2\sqrt{\pi}} \left\langle \left\langle \int_{S(B)} |d\vec{\sigma}| \left(\vec{\nabla} S_3 \right)^2 \sqrt{-\hat{S}_{nn}} \right\rangle_t \right\rangle_B \quad (7.48)$$

Therefore, the energy balance leads to the growth of Z in the turbulent limit. Here is the estimate after averaging over the Gaussian random force

$$\begin{aligned} \frac{\langle \mathcal{E} \rangle_f}{V} &= \frac{\left\langle \left(\vec{f} \cdot \hat{S}^{-1} \cdot \vec{f} \right)^2 \right\rangle_f}{A(\vec{0})/V} = \\ &= \frac{\sigma^2 \left(2\text{tr} \left(\hat{S}^{-2} \right) + (\text{tr} \hat{S}^{-1})^2 \right)}{A(\vec{0})/V} \end{aligned} \quad (7.49)$$

The variance of the random force is then determined from this relation and $A(\vec{0})/V \sim \sqrt{\nu}\rho$

$$\sigma^2 \sim \frac{(\langle \mathcal{E} \rangle_f / V)(A(\vec{0})/V)}{\left(2\text{tr} \left(\hat{S}^{-2} \right) + (\text{tr} \hat{S}^{-1})^2 \right)}; \quad (7.50)$$

$$\sigma \sim \nu^{\frac{1}{4}} \sqrt{\rho \langle \mathcal{E} \rangle_f / V} \quad (7.51)$$

This estimate justifies keeping the leading terms in Taylor expansion of unknown functions $A(\vec{f}), B(\vec{f})$.

In estimating $A(\vec{0})$ one should keep in mind that the thickness of the viscous layer at the vortex sheet is determined by the local normal strain $h = \sqrt{-\nu/\hat{S}_{nn}}$.

Let us estimate the local normal strain \hat{S}_{nn} as the background strain $W_{\alpha\beta}$ in (5.103):

$$\hat{S}_{nn} \sim \sqrt{\langle \hat{W}^2 \rangle_f} \sim \sqrt{\langle Z^2 \rangle_f} R_B \rho \quad (7.52)$$

where R_B is the size of the blob, and ρ is their density in space

We treat \hat{S}_{nn}, R_B as independent parameters, finite in the turbulent limit. Then, from the latter estimate and the relation (7.40), we find the estimate for the variance σ

$$\sqrt{\langle Z^2 \rangle_f} \sim \frac{\sigma}{\rho \sqrt{\nu}}; \quad (7.53)$$

$$\sigma \sim \frac{\sqrt{\nu}}{R_B} \sim \sqrt{\nu}; \quad (7.54)$$

$$\rho R_B^3 \sim \frac{\sigma^2}{\sqrt{\nu}} = \sqrt{\nu} \quad (7.55)$$

With these estimates, the variance of the random force vanishes in the turbulent limit as $\sigma \sim \sqrt{\nu} \rightarrow 0$, making turbulence a spontaneous statistical phenomenon, like critical phenomena in solid-state physics.

The small external force $f \sim \sqrt{\sigma} \sim \nu^{1/4}$ is enhanced in the energy dissipation by large "susceptibility" factor $\mathcal{E} \sim \sigma^2 / (\rho \sqrt{\nu}) \sim 1$.

At the same time, we see that the mean distance between ΔR_B vortex blobs is large compared with their average size R_B

$$\Delta R_B \sim \rho^{-1/3} \sim \nu^{-1/6} R_B \quad (7.56)$$

7.7. PDF for the velocity circulation

Now, the Gaussian distribution $\exp\left(-\frac{\vec{f}^2}{2\sigma}\right)$ of the random force yields the following Fourier transform of the distribution of the circulation (7.25).

$$\Psi_{nm}(\gamma) = \left\langle \exp\left(i 4\pi m \gamma Z(\vec{f})\right) \right\rangle_f = \frac{1}{\sqrt{\det\left(1 - i \frac{m}{n^2} \gamma \hat{\Sigma}[C]\right)}}; \quad (7.57)$$

$$\Sigma[C] = \frac{\sqrt{\pi \nu \rho}}{4\sigma} \left\langle \left\langle \int_{S(B)} |d\vec{\sigma}| \left(\vec{\nabla} S_3\right)^2 \sqrt{-\hat{S}_{nn}} \right\rangle_t \right\rangle_B \quad (7.58)$$

Here \det is 3×3 determinant of the constant symmetric matrix, not the functional determinant of the field theory.

The PDF tail from the Fourier transform of this function would be determined by the largest eigenvalue $q_{\pm}(C)$ of Q on the corresponding side of the real axis in Fourier integral

$$P_{mn}(\Gamma, C) = \int_{-\infty}^{\infty} \frac{d\gamma}{2\pi} e^{-i\gamma\Gamma} \Psi_{nm}(\gamma) \\ \propto \frac{1}{\sqrt{|\Gamma| |\Sigma[C]|}} \exp \left(-\frac{n^2 |\Gamma| |\Sigma[C]|}{|mq_{\pm}(C)|} \right) \quad (7.59)$$

So, there is an exponential tail with a pre-exponential power factor $1/\sqrt{|\Gamma|}$.

We shall have an infinite sum from Kelvinons with growing winding numbers $m, n = k + \frac{1}{2}$ with some unknown coefficients.

The time reversal breaking in this solution corresponds to the lack of symmetry between Kelvinon (positive m) and anti-Kelvinon (negative m).

7.8. Discussion. Comparing with Numerical Simulations

We identified the Kelvinon mechanism of enhancement of infinitesimal random force in the Euler equation and demonstrated how this enhancement occurs at small viscosity.

The required random force to create the energy flow and asymptotic exponential distribution of circulation has the variance $\sigma \sim \nu^{\frac{1}{4}}$. This small force is enhanced by large susceptibility $Z \sim \nu^{-\frac{1}{4}}$.

This large susceptibility originates from the singular behavior of the vorticity field at the domain wall in the Euler limit of Navier-Stokes equations.

We presented an explicit solution for the shape of the circulation PDF generated by Kelvinon. We claim it occurs in high Reynolds flows for the large loops and large circulations, not as a model but as an exact asymptotic law.

The dependence $|\Gamma| \propto \sqrt{A_C}$ was predicted earlier¹³ based on the Loop equations (see the next sections). We compared the raw data from¹⁰ with this prediction. We took the ratio of the moments $M_p = \langle \Gamma^p \rangle$ at largest available p and defined the circulation scale as $S = \sqrt{\frac{M_8}{M_6}}$.

We fitted using *Mathematica*[®] $S(r)$ as a function of the size $r = \frac{a}{\eta}$ of the square loop measured in the Kolmogorov scale η . The quality of a linear

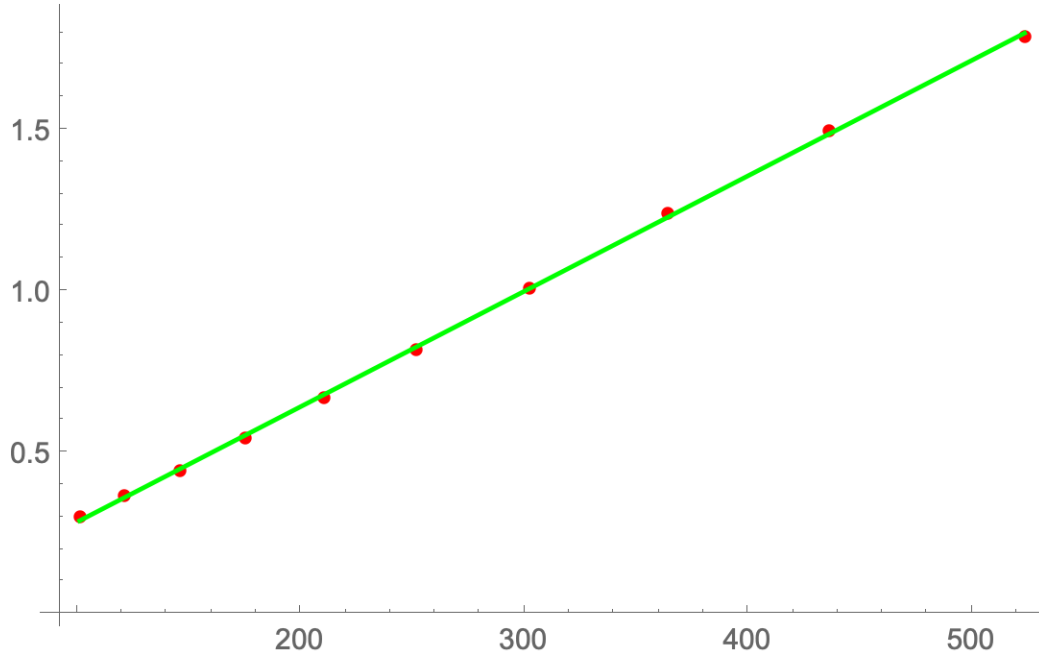


Figure 26: Linear fit of the circulation scale $S = \sqrt{\frac{M_8}{M_6}}$ (with $M_p = \langle \Gamma^p \rangle$) as a function of the a/η for inertial range $100 \leq a/\eta \leq 500$. Here a is the side of the square loop C , and η is a Kolmogorov scale. The linear fit $S = -0.073404 + 0.00357739a/\eta$ is almost perfect: adjusted $R_2 = 0.999609$

fit was very high with adjusted $R_2 = 0.9996$. The so-called ANOVA table summarizes this fit as follows

	DF	SS	MS	F-Statistic	P-Value
R	1	2.30567	2.30567	22984.4	$4.008150477989548 \times 10^{-15}$
Error	8	0.000802519	0.000100315	Null	Null
Total	9	2.30648	Null	Null	Null

(7.60)

The linear fit is shown in Fig.26 .

The errors are most likely artifacts of random forcing at an 8K cubic lattice⁹.

⁹This is not to say that some other nonlinear formulas cannot fit this data equally well or maybe even better, for example, fitting $\log S$ by $\log R$ would produce a very good

The $m = 1$ term matches very well numerical experiments. We found that our formula fits the latest data by Kartik Iyer within error bars of DNS with adjusted $R_2 = 0.9999$, (see Fig.27, 28, 29).¹⁰

The ANOVA table is as good as it gets

	DF	SS	MS	F-Statistic	P-Value
x	1	474.656	474.656	34991.5	$3.3022757147320016 \times 10^{-50}$
Error	32	0.434077	0.0135649	Null	Null
Total	33	475.091	Null	Null	Null

(7.61)

With circulation here being the sum of normal components of a large number of local circulations over the minimal surface, it is nontrivial for this circulation to have an exponential distribution, regardless of the local circulation PDF, as long as it has a finite variance.

The Central Limit theorem tells us that unless these local vorticities are all strongly correlated, the resulting flux (i.e., circulation) will have a Gaussian distribution. The deviation from this Gaussian distribution is the essence of critical phenomena in statistical mechanics, and we have it here in turbulence.

The spectacular violation of this Gaussian distribution in the DNS¹⁰ with seven decades of exponential tails strongly suggests that large spatial structures with correlated vorticity are relevant for these tails.

We identified these spatial structures as coherent vorticity spread thin over the minimal surface. We computed the resulting PDF matching this DNS, including the pre-exponential $1/\sqrt{|\Gamma|}$ factor.

The sum over integers emerges here by the same mechanism as in Planck's distribution in quantum physics. There we had to sum over all occupation numbers in Bose statistics. Here we sum over all winding numbers of the Clebsch field across the minimal surface in physical space.

In Bose statistics, the discreteness of quantum numbers is related to the compactness of the domain for the corresponding degree of freedom.

linear fit with the slope 1.1 instead of our 1. Data fitting cannot derive the physical laws – it can only verify them against some null hypothesis, especially in the presence of a few percent of systematic errors related to finite size effects and harmonic quasi-random forcing. We believe that distinguishing between 1.1 and 1 is an over-fit in such a case.

¹⁰Again, some nonlinear power fit with log/log slope different from 1 could also fit these data, but as we mentioned above, with systematic errors present we cannot reliably distinguish linear law from power close to 1.

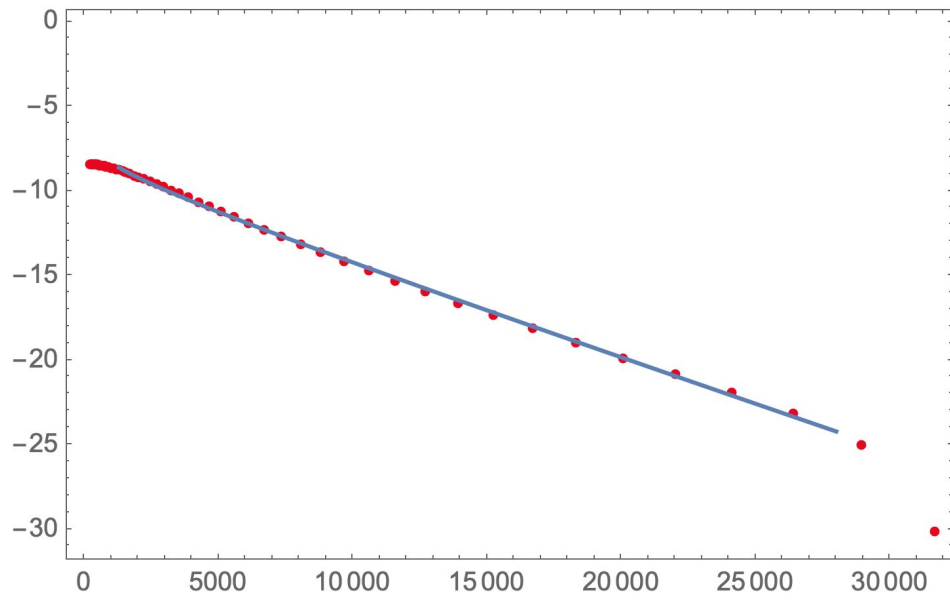


Figure 27: $\log P(x)$ (red dots) together with fitted line $\log P \approx -0.000526724x - 4.3711 - 0.5 \log(x) \pm 0.116469$, $1300 < x < 28000$. Here $x = \frac{|\Gamma|}{\nu}$. We discarded from fit the last two points with low statistics in DNS. The remaining data match the theoretical formula within statistical errors of DNS. Adjusted $R_2 = 0.999929$

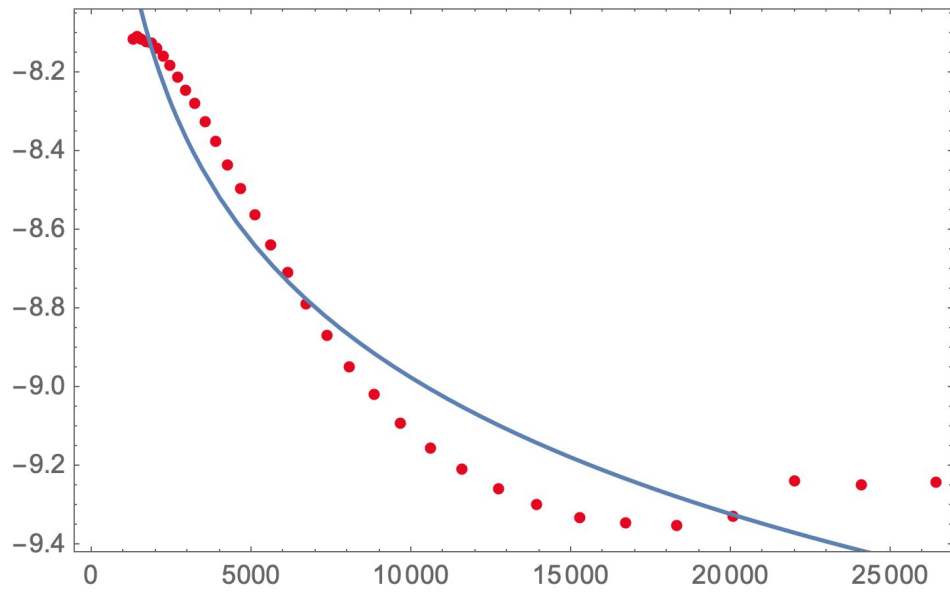


Figure 28: Subtracting the slope. $0.000526724x + \log P(x)$ (red dots) together with fitted line $-4.3711 - 0.5 \log(x)$, $1300 < x < 28000$. Here $x = |\Gamma|$ in some obscure units used by.¹⁰ We see that the pre-exponential factor $1/\sqrt{|\Gamma|}$ fits the data, though with less accuracy, after subtracting the leading term.

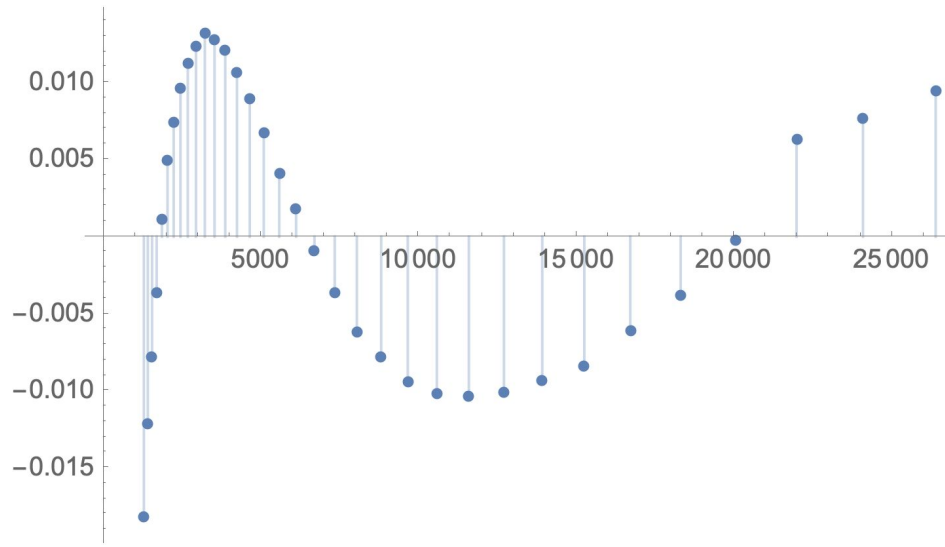


Figure 29: The relative residuals of the log fit of PDF. The harmonic wave behavior suggests that these are artifacts of random harmonic forcing on a $16K^3$ cubic lattice rather than genuine oscillations in an infinite isotropic system. Such residuals do not imply contradictions with the theory.

In our case, this also follows from the compactness of the domain for the Clebsch fields, varying on S_2 . The velocity circulation in physical space becomes the area inside the oriented loop in Clebsch space S_2 , times the winding number m .

Many of the assumptions and arguments of this section are unjustified and unconventional. Our theory goes against many dogmas accepted in turbulence studies since Kolmogorov.

We are presenting a dual view of the same system, complementing rather than contradicting these dogmas. The phenomenon of duality is known in QFT but is unfamiliar in 3D fluid mechanics.

Still, there are examples of duality in low-dimensional flows. The Burgers equation describes 1D compressible flow. It is dual to the statistics of shocks,^{52,53,54} which are 1D versions of our vortex sheets.

Topology in the 1D case is much more primitive than in 3D, but this duality still holds. These shocks are responsible for the intermittency in Burgers equations, which inspired us to look for topological defects in 3D Euler.

In the next sections, we describe the general theory used to justify these assumptions and (in principle) compute the terms of the WKB expansion in the extreme turbulent limit of the Navier-Stokes equation.

8. The Loop equation and its turbulent limit

We reproduce the lectures in Cargese Summer School and Chernogolovka Summer School in '93.

Many questions raised then are now answered (see next sections). The Area law was justified (with some restrictions) theoretically and observed in the DNS 25 years later.

We present these lectures almost the same as they were delivered back in '93, with minimal corrections and occasional comments relating to future work. This theory's natural chronological evolution may be easier to digest than its advanced state.

8.1. Introduction

Incompressible fluid dynamics underlies the vast majority of natural phenomena. It is described by the famous Navier-Stokes equation

$$\dot{v}_\alpha = \nu \partial_\beta^2 v_\alpha - v_\beta \partial_\beta v_\alpha - \partial_\alpha p; \quad \partial_\alpha v_\alpha = 0 \quad (8.1)$$

which is nonlinear and, therefore, hard to solve. This nonlinearity makes life more interesting, as it leads to turbulence. Solving this equation with appropriate initial and boundary conditions, we expect to obtain the chaotic behavior of the velocity field.

The simplest boundary conditions correspond to infinite space with vanishing velocity at infinity. We are looking for the translation invariant probability distribution for the velocity field with an infinite range of wavelengths. In order to compensate for the energy dissipation, we add the usual random force to the Navier-Stokes equations, with the long wavelength support corresponding to large-scale energy pumping.

One may attempt to describe this probability distribution by the Hopf generating functional (the angular bracket denotes time averaging or ensemble averaging over realizations of the random forces)

$$Z[J] = \left\langle \exp \left(\int d^3r J_\alpha(r) v_\alpha(r) \right) \right\rangle \quad (8.2)$$

which is known to satisfy the linear functional differential equation

$$\dot{Z} = H \left[J, \frac{\delta}{\delta J} \right] Z \quad (8.3)$$

similar to the Schrödinger equation for Quantum Field Theory, and equally hard to solve. Nobody managed to go beyond the Taylor expansion in source J , which corresponds to the obvious chain of equations for the equal time correlation functions of the velocity field at various points in space. One could obtain the same equations directly from Navier-Stokes equations, so the Hopf equation looks useless.

In this work¹¹ we argue that one could significantly simplify the Hopf functional without losing information about correlation functions. This simplified functional depends upon the set of 3 periodic functions of one variable

$$C : r_\alpha = C_\alpha(\theta); 0 < \theta < 2\pi \quad (8.4)$$

which set describes the closed loop in coordinate space. The correlation functions reduce to certain functional derivatives of our loop functional with respect to $C(\theta)$ at vanishing loop $C \rightarrow 0$.

¹¹see also⁷ where this approach was initiated and⁵⁵ where its relation with the generalized Hamiltonian dynamics and the Gibbs-Boltzmann statistics was established

The properties of the loop functional at large loop C also have physical significance. Like the Wilson loops in Gauge Theory, they describe the statistics of large-scale structures of the vorticity field, which is analogous to the gauge field strength.

In Appendix A, we recover the expansion in inverse powers of viscosity by direct iterations of the loop equation.

In Appendix B, we study the matrix formulation of the Navier-Stokes equation, which may serve as a basis for the random matrix description of turbulence.

In Appendix C, we study the reduced dynamics corresponding to the functional Fourier transform of the loop functional. We argue that instead of 3D Navier-Stokes equations, one can use the 1D equations for the Fourier loop $P_\alpha(\theta, t)$.

In Appendix D, we discuss the relation between the initial data for velocity field and the P field, and we find particular realization for these initial data in terms of the Gaussian random variables.

In Appendix F, we discuss the possible numerical implementations of the reduced loop dynamics.

In Appendix G, we show the uniqueness of the tensor area law within a certain class of functionals.

In Appendix H, we present the modern view of the old problem of the minimal surface.

In Appendix I, we show that the triple Kolmogorov correlation function corresponds to a vanishing correlation of vorticity with two velocity fields.

8.2. The Loop Calculus

We suggest using in turbulence the following version of the Hopf functional

$$\Psi[C] = \left\langle \exp \left(\frac{t}{\nu} \oint dC_\alpha(\theta) v_\alpha(C(\theta)) \right) \right\rangle \quad (8.5)$$

which we call the loop functional or the loop field. It is implied that all angular variable θ run from 0 to 2π and that all the functions of this variable are 2π periodic.¹² The viscosity ν was inserted in the denominator in exponential as the only parameter of proper dimension.

¹²This parametrization of the loop is a matter of convention, as the loop functional, is parametric invariant.

As we shall see below, viscosity plays the role of the Planck's constant in Quantum mechanics and the turbulence corresponds to the WKB limit $\nu \rightarrow 0$. It is not an accident that viscosity has the same dimension as Planck's constant!

The ratio of the circulation to viscosity is one definition of the Reynolds number (invariant to Galilean transformations).

As for the imaginary unit ι , there are two reasons to insert it in the exponential.

First, it makes the motion compact: the phase factor goes around the unit circle in the evolution of the solution of the Navier-Stokes equations. So, at large times one may expect the ergodicity, with a well-defined average functional bounded by 1 by absolute value.¹³

Second, with this factor of ι , the irreversibility of the problem is manifest. The time reversal corresponds to the complex conjugation of Ψ so that the imaginary part of the asymptotic value of Ψ at $t \rightarrow \infty$ measures the effects of dissipation.

The loop orientation reversal $C(\theta) \rightarrow C(2\pi - \theta)$ also leads to the complex conjugation, so the loop reversal is equivalent to the time reversal. This symmetry implies that any correlator of an odd/even number of velocities should be integrated an odd/even number of times over the loop, and it must enter with an imaginary/real factor. Later, we shall use this property in the area law.

We shall use the field theory notations for the loop integrals,

$$\Psi[C] = \left\langle \exp \left(\frac{\iota}{\nu} \oint_C dr_\alpha v_\alpha \right) \right\rangle \quad (8.6)$$

This loop integral can be reduced to the surface integral of the vorticity field

$$\omega_{\mu\nu} = \partial_\mu v_\nu - \partial_\nu v_\mu \quad (8.7)$$

by the Stokes theorem

$$\Gamma_C[v] \equiv \oint_C dr_\alpha v_\alpha = \int_S d\sigma_{\mu\nu} \omega_{\mu\nu}; \quad \partial S = C \quad (8.8)$$

¹³Otherwise, the loop average would not exist: as we show later (also confirmed by DNS), the PDF for circulation decreases only exponentially.

This integral is the well-known velocity circulation, which measures the net strength of the vortex lines passing through the loop C . Would we fix the initial loop C and let it move with the flow, the loop field would be conserved by the Euler equation so that only the viscosity effects would be responsible for its time evolution.

However, this is not what we are trying to do. We take the Euler rather than Lagrange dynamics so that the loop is fixed in space; hence, Ψ is time-dependent already in the Euler equations. The difference between Euler and Navier-Stokes equations is the time irreversibility, which leads to complex average Ψ in Navier-Stokes dynamics.

It is implied that this field $\Psi[C]$ is invariant under translations of the loop $C(\theta) \rightarrow C(\theta) + \text{const.}$

The asymptotic behavior at the large time with proper random forcing reaches certain fixed point, governed by the translation- and scale invariant equations, which we derive in this paper.

The general Hopf functional (8.2) for the following imaginary singular source

$$J_\alpha(r) = \frac{l}{\nu} \oint_C dr'_\alpha \delta^3(r' - r) \quad (8.9)$$

reduces to the Schrödinger equation.

The Ψ functional involves connected correlation functions of the powers of circulation at equal times.

$$\Psi[C] = \exp \left(\sum_{n=2}^{\infty} \frac{l^n}{n! \nu^n} \langle \langle \Gamma_C^n[v] \rangle \rangle \right) \quad (8.10)$$

This expansion goes in powers of effective Reynolds number, so it diverges in a turbulent regime. There, the opposite WKB approximation will be used.

Let us come back to the general case of the arbitrary Reynolds number. What could be the use of such restricted Hopf functional? At first glance, it seems that we lost most of the information described by the Hopf functional, as the general Hopf source J depends upon three variables x, y, z , whereas the loop C depends on only one parameter θ . Still, this information can be recovered by taking the loops of the singular shape, such as two infinitesimal loops R_1, R_2 , connected by a couple of wires.

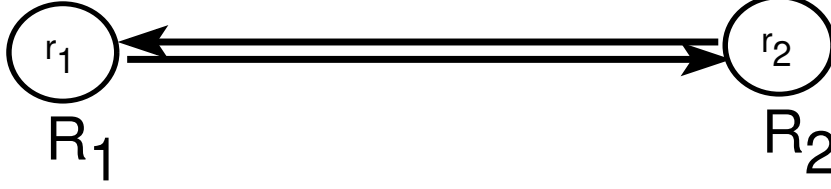


Figure 30: Wires between two loops

The loop field, in this case, reduces to

$$\Psi [C] \rightarrow \left\langle \exp \left(\frac{i}{2\nu} \Sigma_{\mu\nu}^{R_1} \omega_{\mu\nu}(r_1) + \frac{i}{2\nu} \Sigma_{\mu\nu}^{R_2} \omega_{\mu\nu}(r_2) \right) \right\rangle \quad (8.11)$$

where

$$\Sigma_{\mu\nu}^R = \oint_R dr_\nu r_\mu \quad (8.12)$$

is the tensor area inside the loop R . Taking functional derivatives with respect to the shape of R_1 and R_2 prior to shrinking them to points, we can bring down the product of vorticities at r_1 and r_2 . Namely, the variations yield

$$\delta \Sigma_{\mu\nu}^R = \oint_R (dr_\nu \delta r_\mu + r_\mu d\delta r_\nu) = \oint_R (dr_\nu \delta r_\mu - dr_\mu \delta r_\nu) \quad (8.13)$$

where integration by parts was used in the second term.

One may introduce the area derivative $\frac{\delta}{\delta \sigma_{\mu\nu}(r)}$, which brings down the vorticity at the given point r at the loop.

$$-\nu^2 \frac{\delta^2 \Psi [C]}{\delta \sigma_{\mu\nu}(r_1) \delta \sigma_{\lambda\rho}(r_2)} \rightarrow \left\langle \omega_{\mu\nu}(r_1) \omega_{\lambda\rho}(r_2) \right\rangle \quad (8.14)$$

The careful definition of these area derivatives is of paramount importance to us. The corresponding loop calculus was developed in⁵⁶ in

the context of the gauge theory. Here we rephrase and further refine the definitions and relations established in that work.

The basic element of the loop calculus is what we suggest calling the spike derivative, namely the operator which adds the infinitesimal Λ shaped spike to the loop

$$D_\alpha(\theta, \epsilon) = \int_\theta^{\theta+2\epsilon} d\phi \left(1 - \frac{|\theta + \epsilon - \phi|}{\epsilon} \right) \frac{\delta}{\delta C_\alpha(\phi)} \quad (8.15)$$

The finite spike operator

$$\Lambda(r, \theta, \epsilon) = \exp(r_\alpha D_\alpha(\theta, \epsilon)) \quad (8.16)$$

adds the spike of the height r . This spike is the straight line from $C(\theta)$ to $C(\theta + \epsilon) + r$, followed by another straight line from $C(\theta + \epsilon) + r$ to $C(\theta + 2\epsilon)$,

Note that the loop remains closed, and the slopes remain finite. Only the second derivatives diverge. The continuity and closure of the loop eliminate the a potential part of velocity; as we shall see below, this closure is necessary to obtain the loop equation.

In the limit $\epsilon \rightarrow 0$, these spikes are invisible, at least for the smooth vorticity field, as one can see from the Stokes theorem (the area inside the spike goes to zero as ϵ). However, taking certain derivatives prior to the limit $\epsilon \rightarrow 0$ we can obtain the finite contribution.

Let us consider the operator

$$\Pi(r, r', \theta, \epsilon) = \Lambda\left(r, \theta, \frac{1}{2}\epsilon\right) \Lambda(r', \theta, \epsilon) \quad (8.17)$$

By construction, it inserts the smaller spike on top of a bigger one, in such a way, a polygon appears (see Fig. 32).

Taking the derivatives by the vertices of this polygon r, r' , setting $r = r' = 0$ and anti-symmetrizing, we find the tensor operator

$$\Omega_{\alpha\beta}(\theta, \epsilon) = -i\nu D_\alpha\left(\theta, \frac{1}{2}\epsilon\right) D_\beta(\theta, \epsilon) - \{\alpha \leftrightarrow \beta\} \quad (8.18)$$

which brings down the vorticity when applied to the loop field

$$\Omega_{\alpha\beta}(\theta, \epsilon) \Psi[C] \xrightarrow{\epsilon \rightarrow 0} \omega_{\alpha\beta}(C(\theta)) \Psi[C] \quad (8.19)$$

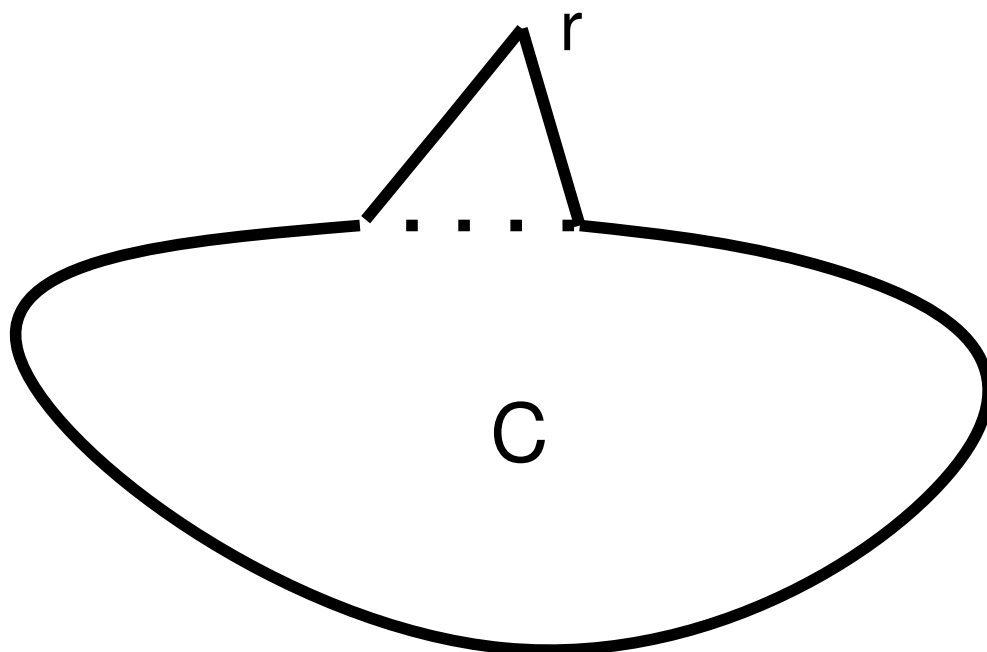


Figure 31: Λ variation of the loop.

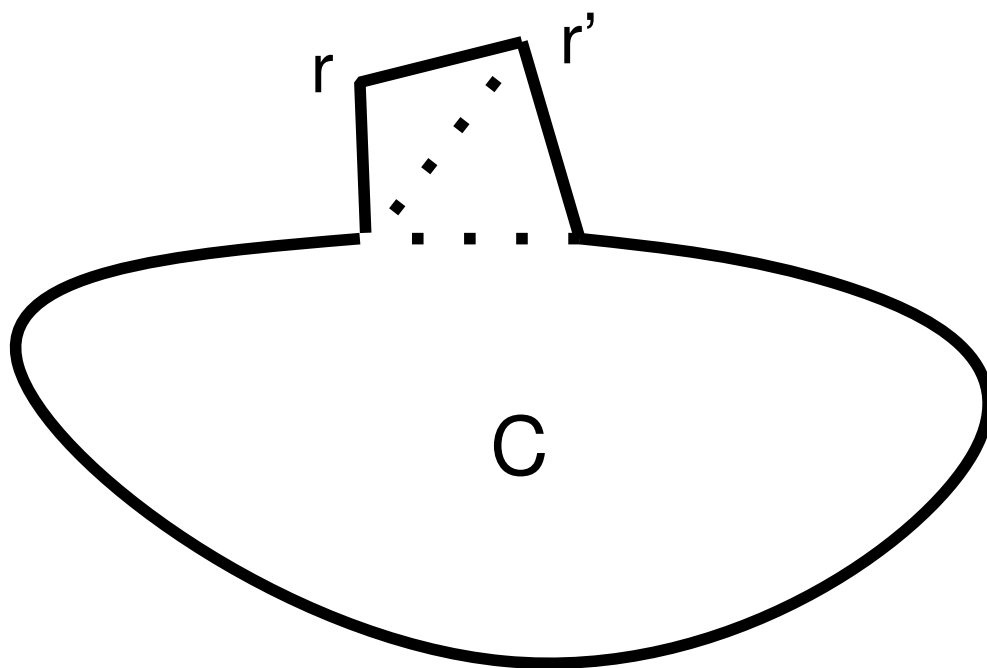


Figure 32: Π variation of the loop

The quick way to check these formulas is to use formal functional derivatives

$$\frac{\delta \Psi [C]}{\delta C_\alpha(\theta)} = C'_\beta(\theta) \frac{\delta \Psi [C]}{\delta \sigma_{\alpha\beta}(C(\theta))} \quad (8.20)$$

Taking one more functional derivative, we find the term with vorticity times the first derivative of the δ function, coming from the variation of $C'(\theta)$

$$\begin{aligned} \frac{\delta^2 \Psi [C]}{\delta C_\alpha(\theta) \delta C_\beta(\theta')} &= \delta'(\theta - \theta') \frac{\delta \Psi [C]}{\delta \sigma_{\alpha\beta}(C(\theta))} + \\ &C'_\gamma(\theta) C'_\lambda(\theta') \frac{\delta^2 \Psi [C]}{\delta \sigma_{\alpha\gamma}(C(\theta)) \delta \sigma_{\beta\lambda}(C(\theta'))} \end{aligned} \quad (8.21)$$

This term is the only one that survives the limit $\epsilon \rightarrow 0$ in our relation (8.19).

So, the area derivative can be defined from the antisymmetric tensor part of the second functional derivative as the coefficient in front of $\delta'(\theta - \theta')$. Still, it has all the properties of the first functional derivative, as it can also be defined from the above first variation.

The advantage of dealing with spikes is the control over the limit $\epsilon \rightarrow 0$, which might be quite singular in applications.

So far, we have managed to insert the vorticity at the loop C by variations of the loop field. Later we shall need the vorticity off the loop, in an arbitrary point in space. This result can be achieved by the following the sequence of the spike operators

$$\Lambda(r, \theta, \epsilon) \Pi(r_1, r_2, \theta + \epsilon, \delta); \delta \ll \epsilon \quad (8.22)$$

This operator inserts the Π shaped little loop at the top of the bigger spike. In other words, this little loop is translated by a distance r by the big spike.

Taking derivatives, we find the operator of finite translation of the vorticity

$$\Lambda(r, \theta, \epsilon) \Omega_{\alpha\beta}(\theta + \epsilon, \delta) \quad (8.23)$$

and the corresponding infinitesimal translation operator

$$D_\mu(\theta, \epsilon) \Omega_{\alpha\beta}(\theta + \epsilon, \delta) \quad (8.24)$$

which inserts $\partial_\mu \omega_{\alpha\beta}(C(\theta))$ when applied to the loop field.



Figure 33: Backtracking wires

Coming back to the correlation function, we are going now to construct the operator, which would insert two vorticities separated by a distance. Let us note that the global Λ spike

$$\Lambda(r, 0, \pi) = \exp \left(r_\alpha \int_0^{2\pi} d\phi \left(1 - \frac{|\phi - \pi|}{\pi} \right) \frac{\delta}{\delta C_\alpha(\phi)} \right) \quad (8.25)$$

when applied to a shrunk loop $C(\phi) = 0$ does nothing but the backtracking from 0 to r (see Fig. 33).

This backtracking means that the operator

$$\Omega_{\alpha\beta}(0, \delta) \Omega_{\lambda\rho}(\pi, \delta) \Lambda(r, 0, \pi) \quad (8.26)$$

when applied to the loop field for a shrunk loop yields the vorticity correlation function

$$\Omega_{\alpha\beta}(0, \delta) \Omega_{\lambda\rho}(\pi, \delta) \Lambda(r, 0, \pi) \Psi[0] = \left\langle \omega_{\alpha\beta}(0) \omega_{\lambda\rho}(r) \right\rangle \quad (8.27)$$

The higher correlation functions of vorticities could be constructed in a similar fashion, using the spike operators. As for the velocity, one should solve the Poisson equation

$$\partial_\mu^2 v_\alpha(r) = \partial_\beta \omega_{\beta\alpha}(r) \quad (8.28)$$

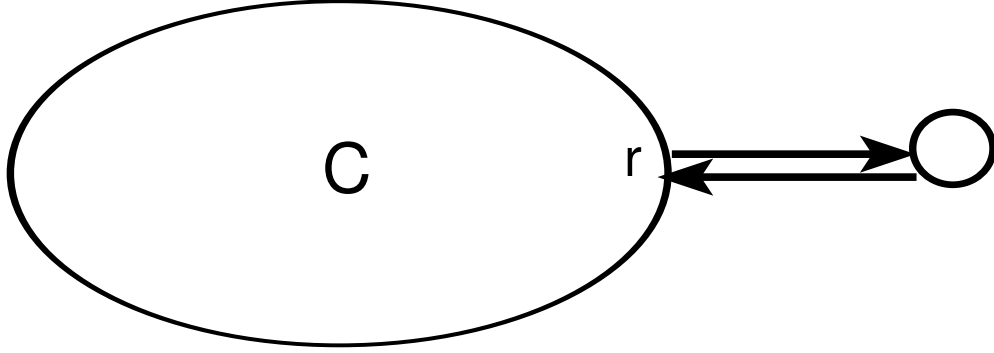


Figure 34: Area derivative

with the proper boundary conditions, say, $v = 0$ at infinity. Formally,

$$v_\alpha(r) = \frac{1}{\partial_\mu^2} \partial_\beta \omega_{\beta\alpha}(r) \quad (8.29)$$

This formula suggests the following definition of the velocity operator

$$V_\alpha(\theta, \epsilon, \delta) = \frac{1}{D_\mu^2(\theta, \epsilon)} D_\beta(\theta, \epsilon) \Omega_{\beta\alpha}(\theta, \delta); \delta \ll \epsilon \quad (8.30)$$

$$V_\alpha(\theta, \epsilon, \delta) \Psi[C] \xrightarrow{\delta, \epsilon \rightarrow 0} v_\alpha(C(\theta)) \Psi[C] \quad (8.31)$$

Another version of this formula is the following integral

$$V_\alpha(\theta, \epsilon, \delta) = \int d^3\rho \frac{\rho_\beta}{4\pi|\rho|^3} \Lambda(\rho, \theta, \epsilon) \Omega_{\alpha\beta}(\theta + \epsilon, \delta) \quad (8.32)$$

where the Λ operator shifts the Ω by a distance ρ off the original loop at the point $r = C(\theta + \epsilon)$, (see Fig. 34).

8.3. Loop Equation

Let us now derive an exact equation for the loop functional. Taking the time derivative of the original definition and using the Navier-Stokes equation we get in front of exponential

$$\oint_C dr_\alpha \frac{\iota}{\nu} \left(\nu \partial_\beta^2 v_\alpha - v_\beta \partial_\beta v_\alpha - \partial_\alpha p \right) \quad (8.33)$$

The term with the pressure gradient yields zero after integration over the closed loop, and the velocity gradients in the first two terms could be expressed in terms of vorticity up to the irrelevant gradient terms so that we find

$$\oint_C dr_\alpha \frac{\iota}{\nu} \left(\nu \partial_\beta \omega_{\beta\alpha} - v_\beta \omega_{\beta\alpha} \right) \quad (8.34)$$

Replacing the vorticity and velocity by the operators discussed in the previous Section 8.2, we find the following loop equation (in explicit notations)

$$\begin{aligned} -\iota \nu \dot{\Psi}[C] &= \oint dC_\alpha(\theta) \\ &\left(\nu D_\beta(\theta, \epsilon) \Omega_{\beta\alpha}(\theta, \epsilon) + \int d^3\rho \frac{\rho_\gamma \left(\Lambda(\rho, \theta, \epsilon) \Omega_{\gamma\beta}(\theta + \epsilon, \delta) \Omega_{\beta\alpha}(\theta, \delta) \right)}{4\pi|\rho|^3} \right) \Psi[C] \end{aligned} \quad (8.35)$$

The more compact form of this equation, using the notations of,⁵⁶ reads

$$\iota \nu \dot{\Psi}[C] = \mathcal{H}_C \Psi; \quad (8.36a)$$

$$\mathcal{H}_C = \mathcal{H}_C^{(1)} + \mathcal{H}_C^{(2)} \quad (8.36b)$$

$$\mathcal{H}_C^{(1)} = \nu \oint_C dr_\alpha \partial_\beta \frac{\delta}{\delta \sigma_{\beta\alpha}(r)}; \quad (8.36c)$$

$$\mathcal{H}_C^{(2)} = \oint_C dr_\alpha \int d^3r' \frac{r'_\gamma - r_\gamma}{4\pi|r - r'|^3} \frac{\delta^2}{\delta \sigma_{\beta\alpha}(r) \delta \sigma_{\beta\gamma}(r')} \quad (8.36d)$$

We observe viscosity ν appearing in front of time and spatial derivatives, like the Planck constant \hbar in Quantum mechanics. The first term $\mathcal{H}_C^{(1)}$ in our loop Hamiltonian is local in the loop space. The second term $\mathcal{H}_C^{(2)}$

contains the second loop derivatives, acting as a (nonlocal!) kinetic term in loop space.

The first term came from the viscous diffusion term; as we shall see later, it violates the time symmetry.

8.4. External forces and Dissipation

So far, we have considered so-called decaying turbulence without external energy source. The energy

$$E = \int d^3r \frac{1}{2} v_\alpha^2 \quad (8.37)$$

would eventually all dissipate so that the fluid would stop. In this case the loop wave function Ψ would asymptotically approach 1

$$\Psi[C] \xrightarrow{t \rightarrow \infty} 1 \quad (8.38)$$

In order to reach the steady state, we add to the right side of the Navier-Stokes equation the usual Gaussian random forces $f_\alpha(r, t)$ with the space dependent correlation function

$$\langle f_\alpha(r, t) f_\beta(r', t') \rangle = \delta_{\alpha\beta} \delta(t - t') F(r - r') \quad (8.39)$$

concentrated at small wavelengths, i.e., slowly varying with $r - r'$.

Using the identity

$$\langle f_\alpha(r, t) \Phi[v(\cdot)] \rangle = \int d^3r' F(r - r') \frac{\delta \Phi[v(\cdot)]}{\delta v_\alpha(r')} \quad (8.40)$$

which is valid for arbitrary functional Φ we find the following imaginary potential term in the loop Hamiltonian

$$\delta \mathcal{H}_C \equiv i U[C] = \frac{i}{\nu} \oint_C dr_\alpha \oint_C dr'_\alpha F(r - r') \quad (8.41)$$

Note that orientation reversal, followed by complex conjugation, changes the sign of the loop Hamiltonian, as it should. The potential part involves double loop integration times an imaginary constant.

The first term in the kinetic part has one loop integration and one loop derivative times a real constant.

The second kinetic term has one loop integration, two loop derivatives, and a real constant. The left side of the loop equation has no loop integration and no loop derivatives but has a factor of ι .

The relation between the potential and kinetic parts of the loop Hamiltonian depends on viscosity, or, better to say, it depends upon the Reynolds number, which is the ratio of the typical circulation to viscosity.

When the Reynolds number is small, the loop wave function is close to 1. The perturbation expansion in $\frac{1}{\nu}$ goes in powers of the potential, in the same way, as in Quantum mechanics. The second (nonlocal) term in the kinetic part of the Hamiltonian also serves as a small perturbation (it corresponds to the nonlinear term in the Navier-Stokes equation). The first term of this perturbation expansion is just

$$\Psi[C] \rightarrow 1 - \int \frac{d^3k}{(2\pi)^3} \frac{\tilde{F}(k)}{2\nu^3 k^2} \left| \oint_C dr_\alpha e^{\iota k r} \right|^2 \quad (8.42)$$

with $\tilde{F}(k)$ being the Fourier transform of $F(r)$. This term is real, as it corresponds to the two-velocity correlation. The next term comes from the triple correlation of velocity, and this term is purely imaginary so that the dissipation shows up.

Direct iterations in the loop space can derive this expansion as in,⁵⁶ inverting the operator in the local part of the kinetic term in the Hamiltonian. This expansion is discussed in Appendix A. The results agree with the straightforward iterations of the Navier-Stokes equations in powers of the random force, starting from zero velocity.

So, we have a familiar situation, like in QCD, where the perturbation theory breaks because of the infrared divergencies. For an arbitrarily small force in a large system, the region of small k would yield a large contribution to the terms of the perturbation expansion. Therefore, one should take the opposite WKB limit $\nu \rightarrow 0$.

In this limit, the wave function should behave as the usual WKB wave function, i.e., as an exponential

$$\Psi[C] \rightarrow \exp \left(\frac{\iota S[C]}{\nu} \right) \quad (8.43)$$

The effective loop Action $S[C]$ satisfies the loop space Hamilton-Jacobi

equation

$$\dot{S}[C] = -\imath U[C] + \oint_C dr_\alpha \int d^3r' \frac{r'_\gamma - r_\gamma}{4\pi|r - r'|^3} \frac{\delta S}{\delta \sigma_{\beta\alpha}(r)} \frac{\delta S}{\delta \sigma_{\beta\gamma}(r')} \quad (8.44)$$

The imaginary part of $S[C]$ comes from imaginary potential $\imath U[C]$, which distinguishes our theory from reversible Quantum mechanics. The sign of $\mathbf{Im} S$ must be positive definite since $|\Psi| < 1$. As for the real part of $S[C]$, it changes the sign under the loop orientation reversal $C(\theta) \rightarrow C(2\pi - \theta)$.

At finite viscosity, there would be an additional term

$$-\nu \oint_C dr_\alpha \partial_\beta \frac{\delta S[C]}{\delta \sigma_{\beta\alpha}(r)} - \imath \nu \oint_C dr_\alpha \int d^3r' \frac{r'_\gamma - r_\gamma}{4\pi|r - r'|^3} \frac{\delta^2 S[C]}{\delta \sigma_{\beta\alpha}(r) \delta \sigma_{\beta\gamma}(r')} \quad (8.45)$$

on the right of (8.44). As for the term

$$- \oint_C dr_\alpha \imath \left(\partial_\beta S[C] \right) \frac{\delta S[C]}{\delta \sigma_{\beta\alpha}(r)} \quad (8.46)$$

which formally arises in the loop equation: this term vanishes, since $\partial_\beta S[C] = 0$. This operator inserts backtracking at some point at the loop without first applying the loop derivative at this point. It was discussed in the previous Section that such backtracking does not change the loop functional. This issue was discussed at length in,⁵⁶ where the Leibnitz rule for the operator $\partial_\alpha \frac{\delta}{\delta \sigma_{\beta\gamma}}$ was established

$$\partial_\alpha \frac{\delta f(g[C])}{\delta \sigma_{\beta\gamma}(r)} = f'(g[C]) \partial_\alpha \frac{\delta g[C]}{\delta \sigma_{\beta\gamma}(r)} \quad (8.47)$$

In other words, this operator acts as a first-order derivative on the loop functional with finite area derivative (so-called Stokes type functional). Then, the above term does not appear.

The Action functional $S[C]$ describes the distribution of the large-scale vorticity structures; hence, it should not depend on viscosity. In terms of the connected correlation functions of the circulation this regime corresponds to the limit when the effective Reynolds number $\frac{\Gamma_C[v]}{\nu}$ goes to infinity, but the sum of the divergent series tends to the finite limit. According to the standard picture of turbulence, the large-scale vorticity structures depend upon the energy pumping, rather than energy dissipation.

It is understood that both time t and the loop size¹⁴ $|C|$ should be greater than the viscous scales

$$t \gg t_0 = \nu^{\frac{1}{2}} \mathcal{E}^{-\frac{1}{2}}; |C| \gg r_0 = \nu^{\frac{3}{4}} \mathcal{E}^{-\frac{1}{4}} \quad (8.48)$$

where \mathcal{E} is the energy dissipation rate.

The energy balance equation defines it

$$0 = \partial_t \left\langle \frac{1}{2} v_\alpha^2 \right\rangle = \nu \left\langle v_\alpha \partial^2 v_\alpha \right\rangle + \left\langle f_\alpha v_\alpha \right\rangle \quad (8.49)$$

which we can transform to

$$\frac{1}{4} \nu \left\langle \omega_{\alpha\beta}^2 \right\rangle = 3F(0) \quad (8.50)$$

The left side represents the energy dissipated at a small scale due to viscosity, and the right side - represents the energy pumped in from a large scale due to random forces. Their common value is \mathcal{E} .

We see that constant $F(r - r')$, i.e., $\tilde{F}(k) \propto \delta(k)$ is sufficient to provide the necessary energy pumping. However, such forcing does not produce vorticity, which we readily see in our equation. The contribution from this constant part to the potential in our loop equation drops out (this is a closed loop integral of the total derivative). This reduction of the constant term is important because it would have the wrong order of magnitude in the turbulent limit - it would grow as the Reynolds number.

Dropping this term, we arrive at a remarkably simple and universal functional equation

$$\dot{S}[C] = \oint_C dr_\alpha \int d^3 r' \frac{r'_\gamma - r_\gamma}{4\pi|r - r'|^3} \frac{\delta S}{\delta \sigma_{\beta\alpha}(r)} \frac{\delta S}{\delta \sigma_{\beta\gamma}(r')} \quad (8.51)$$

The steady solution of this equation describes the steady distribution of the circulation in the strong turbulence.

¹⁴As a measure of the loop size, one may take the square root of the minimal area inside the loop.

8.5. Loop Equation for the Circulation PDF

The loop field could serve as the generating function for the PDF $P_C(\Gamma)$ for the circulation. The Fourier integral

$$P_C(\Gamma) = \int_{-\infty}^{\infty} \frac{dg}{2\pi\nu} \exp \left(i g / \nu \left(\oint_C dr_\alpha v_\alpha(r) - \Gamma \right) \right) \quad (8.52)$$

can be analyzed in the same way as the loop field before. The only difference is that instead of constant $1/\nu$ we have a variable g/ν . These factors can be replaced by

$$g \rightarrow i \nu \frac{\partial}{\partial \Gamma} \quad (8.53)$$

acting on $P_C(\Gamma)$.

As a result, we find

$$\begin{aligned} \frac{\partial}{\partial \Gamma} P_C(\Gamma) = & - \oint_C dr_\alpha \int d^3 r' \frac{r'_\gamma - r_\gamma}{4\pi|r - r'|^3} \frac{\delta^2 P_C(\Gamma)}{\delta \sigma_{\beta\alpha}(r) \delta \sigma_{\beta\gamma}(r')} \\ & + \nu \frac{\partial}{\partial \Gamma} \oint_C dr_\alpha \partial_\beta \frac{\delta P_C(\Gamma)}{\delta \sigma_{\beta\alpha}(r)} - U[C] \frac{\partial^3 P_C(\Gamma)}{\partial \Gamma^3} \end{aligned} \quad (8.54)$$

All the imaginary units disappear as they should. The viscosity and force terms can be neglected in the inertial range in the same way as before. The only new thing is that one has to assume that $\Gamma \gg \nu$ is in the inertial range in addition to the above assumptions about the loop size.

In the absence of these terms, there are no dimensional parameters, so the following scaling laws hold (with the same index κ as before)

$$P_C(\Gamma) = t^{1-2\kappa} F \left[\frac{C}{t^\kappa}, \frac{\Gamma}{t^{2\kappa-1}} \right] \quad (8.55)$$

The factor $t^{1-2\kappa}$ came from the normalization of probability density. Note that this is more general law than before. Here we do not have to use the WKB approximation for the PDF. In other words, rather than its decay at large Γ , the whole PDF satisfies the scaling law.

The steady distribution would have the form of

$$P_C(\Gamma) \rightarrow \frac{1}{\Gamma} \Phi \left[\frac{C}{\Gamma^{\frac{\kappa}{2\kappa-1}}} \right] \quad (8.56)$$

where the scaling functional Φ satisfies the homogeneous equation

$$\oint_C dr_\alpha \int d^3 r' \frac{r'_\gamma - r_\gamma}{4\pi|r - r'|^3} \frac{\delta^2 \Phi[C]}{\delta \sigma_{\beta\alpha}(r) \delta \sigma_{\beta\gamma}(r')} = 0 \quad (8.57)$$

with the normalization condition

$$1 = \int_{-\infty}^{\infty} \frac{d\Gamma}{\Gamma} \Phi \left[\frac{C}{\Gamma^{\frac{\kappa}{2\kappa-1}}} \right] \quad (8.58)$$

There could be different scaling functions for positive and negative Γ , rather than just absolute value $|\Gamma|$ prescription. This asymmetry would correspond to a violation of the time-reversal symmetry. However, as we mentioned above, there is no exact relation that would eliminate the symmetric solution.

The Kolmogorov triple correlation function vanishes for vorticities (see Appendix I) so that there is no restriction on the asymmetric part of the circulation PDF. Nevertheless, the Kolmogorov scaling $\kappa = \frac{3}{2}$ seems the most likely possibility, for the reasons discussed in the previous Section.

The homogeneous loop equation requires boundary conditions at large loops to provide a meaningful solution. The asymptotic decrease of PDF

$$P_C(\Gamma) \sim \exp \left(-Q \left[\frac{C}{\Gamma^{\frac{\kappa}{2\kappa-1}}} \right] \right), Q \rightarrow \infty \quad (8.59)$$

would lead to the same WKB equation as before

$$\oint_C dr_\alpha \int d^3 r' \frac{r'_\gamma - r_\gamma}{4\pi|r - r'|^3} \frac{\delta Q[C]}{\delta \sigma_{\beta\alpha}(r)} \frac{\delta Q[C]}{\delta \sigma_{\beta\gamma}(r')} = 0 \quad (8.60)$$

We are studying this equation in the next Section.

8.6. How could classical statistics be exactly equivalent to quantum mechanics?

Let us stop here and think about this remarkable analogy with quantum mechanics.

What is this analogy– a poetic metaphor or perhaps something deeper, like the Hawking radiation or the ADS/CFT duality?

First of all, this analogy is not a word game – it is precise mathematical correspondence between two theories: the statistics of classical fluid and the quantum mechanics in loop space.

The wave function of the quantum theory is related to the probability of the classical turbulence by inverse Fourier transformation with the frequency set to inverse viscosity (Planck's constant of our loop space quantum mechanics)

$$\Psi_C(\Gamma) = \int_{-\infty}^{\infty} \frac{d\omega}{2\pi} \exp(i\omega\Gamma) P_C(\Gamma) \Big|_{\omega=\frac{1}{\nu}} \quad (8.61)$$

In the same way as Hawking's interpretation of the period β in the black hole solution as inverse temperature, we start with formal relation between two theories by analytical continuation in a complex plane.

The constant \hbar also enters the Schrödinger equation directly, so one cannot use it as a Fourier frequency for the direct transfer. However, with inverse transform, the correspondence involves **setting** frequency to $1/\nu$, which is a correct mathematical statement.

There are more transformations in our theory – the Clebsch variables, which look like ordinary fields described as a superposition of planar waves in $R_3 \mapsto R_2$, suddenly wrap up from a plane R_2 to a sphere S_2 . Now they map $R_3 \mapsto S_2$. They are now confined and exist only as internal degrees of freedom, never observable as waves.

The Clebsch waves were used by Yakhot, and Zakharov³⁹ in their approximate derivation of the K41 spectrum in the weak turbulence.

We argue that in strong turbulence, these Clebsch fields are confined to a sphere in internal space, unobservable as waves in physical space. The turbulence statistics is related to quantum mechanics in loop space, where the classical configurations of Clebsch field are related to the WKB limit of the wave function.

Still, do these relations represent a formal equivalence or are there some observable quantum effects in classical turbulence?

As we shall see later in this report, there are such quantum effects: quantization of the circulation created by Kelvinons (the winding numbers of classical solutions for Clebsch fields on a sphere S_2).

These Kelvinons are behind the dramatic intermittency effect: exponential decay of the circulation PDF over ten decades in probability. None of the conventional models of turbulence can explain this effect so far.

There are (not yet observed) contributions to PDF with a higher quantized decrement in exponential, like the terms of Planck's radiation, arising as a direct consequence of the quantization of the compact motion.

So, as we shall see later, this formal equivalence leads to observable effects, confirmed in DNS.

8.7. The loop equation in the WKB limit and weak Euler solutions

The loop equation's classical ($\nu \rightarrow 0$) limit can be related to the Euler equation.

If one takes any **non-steady** solution \vec{v}_{cl} of the Navier-Stokes equation and computes

$$P_{cl}[C; \Gamma] = \left\langle \delta \left(\Gamma - \oint_C \vec{v}_{cl} \cdot d\vec{r} \right) \right\rangle = \int_{-\infty}^{\infty} \frac{dg}{2\pi} \exp(-ig\Gamma) \left\langle \exp \left(ig \oint_C \vec{v}_{cl} \cdot d\vec{r} \right) \right\rangle \quad (8.62)$$

it will satisfy the **non-steady** loop equation. In the limit $\nu \rightarrow 0$ the right side of the loop equation (8.34) becomes

$$\left\langle \oint_C (\vec{\omega}_{cl} \times \vec{v}_{cl}) \cdot d\vec{r} \right\rangle = \left\langle \oint_C \vec{\omega}_{cl} \cdot (\vec{v}_{cl} \times d\vec{r}) \right\rangle \quad (8.63)$$

This integral will vanish for any classical steady solution of the **Euler** equation, which corresponds to GBF ($\vec{\nabla} \times \vec{v} \times \vec{\omega} = 0$).

However, we need a weaker condition: only the contour integral must vanish.

In case the velocity field is a solution of the time-dependent Euler equation with the boundary condition

$$\vec{v}_{cl}(\vec{r} = \vec{C}(\theta)) \times \vec{C}'(\theta) = 0 \quad (8.64)$$

the **steady** loop equation will also be satisfied.

We will discuss these boundary conditions in more detail later.

Now, note that we can use any steady vortex sheet providing finite circulation for this solution.

The steady vortex sheet requires the boundary value of velocity to be aligned with the boundary, plus it must be tangent to the vortex sheet inside the boundary.

The circulation will be conserved, as the steady loop equation requires.

This conservation is a manifestation of the Kelvin theorem. In the case of the steady boundary of the vortex sheet, the liquid contour along this boundary does not move. Thus, the Kelvin theorem says the circulation is conserved.

We suggest calling these circulation-conserving Euler solutions Kelvinons.

As we argue later, the KLS domain wall, which we discussed in the section 7, could be a realization of a Kelvinon.

8.8. *Kelvinon vs instanton*

In ordinary quantum mechanics, the tails of the PDF, such as the probability of the penetration through a potential barrier, are determined by the minimum of the classical Action A_{cl} for imaginary time.

One should perform analytic continuation $t \Rightarrow i\tau$ and find the classical trajectory (instanton) in the complex plane, corresponding to the saddle point in the functional integral $\int \exp(-A_{cl}/\hbar)$.

Then the amplitude of the transition under the potential barrier will be given by $\exp(-\min A_{cl}/\hbar)$ times some preexponential factor, determined by the integration over the quadratic vicinity of the saddle point.

However, in our theory, there is a different correspondence between the probability and the wave function. The wave function is an inverse Fourier integral of the probability PDF with Fourier frequency $\omega = \frac{1}{\hbar}$.

So, instead of PDF being the square of the absolute value of the quantum wave function, they are related linearly by the Fourier transform.

With this correspondence, the probability satisfies the evolution loop equation, which does not have any imaginary units. The tails of the PDF correspond to the steady solution of the loop equation, exponentially decaying with the size of the loop or the value of circulation around this loop.

Still, this is not a steady solution to the Euler equations but rather a solution with steady circulation for a given loop.

For such circulation to be steady, it is sufficient for this loop to be steady, as the circulation is known to be carried by the flow (Kelvin theorem). The circulation will be time-independent if the flow is stagnant at a particular loop (to be more precise, the normal velocity to the surface edge vanishes, but the tangent velocity is finite and produces finite time-independent circulation).

This stagnation happens if the loop is a boundary of a steady discontinuity surface (vortex sheet).

The flow around this surface can be time-dependent as long as this loop stays steady.

It will be equivalent to a time-dependent flow around a steady object.

When we study the loop equation by itself, we do not need to think about the flow- we have a closed functional equation in loop space, which can be investigated instead.

However, one can go only so far in this investigation- at some point, it becomes necessary to recall the underlying Euler dynamics to overcome mathematical problems.

8.9. Tensor Area law

The Wilson loop in QCD decreases as the exponential of the minimal area encircled by the loop. This decay leads to quark confinement. What is the similar asymptotic law in turbulence? The physical mechanisms leading to the area law in QCD are absent here. Moreover, there is no guarantee that $\Psi[C]$ always decreases with the size of the loop.

This observation makes it possible to look for the simple Ansatz, which was not acceptable in QCD, namely

$$S[C] = s \left(\Sigma_{\mu\nu}^C \right) \quad (8.65)$$

where

$$\Sigma_{\mu\nu}^C = \oint_C r_\mu dr_\nu \quad (8.66)$$

is the tensor area encircled by the loop C . The difference between this area, and the scalar area is the positivity property. The scalar area vanishes only for the loop, which can be contracted to a point by removal of all the backtracking. As for the tensor area, it vanishes for the 8 shaped loop, with the opposite orientation of petals.

Thus, there are some large contours with vanishing tensor areas, for which there would be no decrease in the Ψ functional. In QCD, the Wilson loops must always decrease at large distances due to the finite mass gap. Here, large-scale correlations play a central role in a turbulent flow. So, at this point, we see no convincing arguments to reject the tensor area Ansatz.

This Ansatz in QCD was not only unphysical, but it also failed to reproduce the correct short-distance singularities in the loop equation. In turbulence, there are no such singularities. Instead, there are the large-distance singularities, which all should cancel in the loop equation.

For this Ansatz, the (turbulent limit of the) loop equation is automatically satisfied without further restrictions. Let us verify this important property. The first area derivative yields

$$\omega_{\mu\nu}^C(r) = \frac{\delta S}{\delta \sigma_{\mu\nu}(r)} = 2 \frac{\partial s}{\partial \Sigma_{\mu\nu}^C} \quad (8.67)$$

The factor of 2 comes from the second term in the variation

$$\frac{\delta \Sigma_{\alpha\beta}^C}{\delta \sigma_{\mu\nu}(r)} = \delta_{\alpha\mu} \delta_{\beta\nu} - \delta_{\alpha\nu} \delta_{\beta\mu} \quad (8.68)$$

Note that the right side does not depend on r . Moreover, one can shift r aside from the base loop C with proper wires inserted. The area derivative would stay the same as the contribution of wires drops.

This observation implies that the corresponding vorticity $\omega_{\mu\nu}^C(r)$ is space independent, it only depends upon the loop itself. The velocity can be reconstructed from vorticity up to irrelevant constant terms

$$v_\beta^C(r) = \frac{1}{2} r_\alpha \omega_{\alpha\beta}^C \quad (8.69)$$

One can formally derive this relation from the above integral representation

$$v_\beta^C(r) = \int d^3 r' \frac{r_\alpha - r'_\alpha}{4\pi |r - r'|^3} \omega_{\alpha\beta}^C \quad (8.70)$$

as a residue from the infinite sphere $R = |r'| \rightarrow \infty$. One may insert the regularizing factor $|r'|^{-\epsilon}$ in ω , compute the convolution integral in Fourier space and check that in the limit $\epsilon \rightarrow 0^+$, the above linear term arises. So, one can use the above form of the loop equation, with the analytic regularization prescription.

Now, the $v \omega$ term in the loop equation reads

$$\oint_C dr_\gamma v_\beta^C(r) \omega_{\beta\gamma}^C \propto \Sigma_{\gamma\alpha}^C \omega_{\alpha\beta}^C \omega_{\beta\gamma}^C \quad (8.71)$$

This tensor trace vanishes because the first tensor is antisymmetric, and the product of the last two antisymmetric tensors is symmetric with respect to $\alpha\gamma$.

So, the positive and negative terms cancel each other in our loop equation, like the "income" and "outcome" terms in the usual kinetic equation. We see that there is an equilibrium in our loop space kinetics.

From the point of view of the notorious infrared divergencies in turbulence, the above calculation explicitly demonstrates how they cancel. By naive dimensional counting, these terms were linearly divergent. The space isotropy lowered this to logarithmic divergence in (8.70), which reduced to finite terms at closer inspection. Then, the explicit form of these terms was such that they were all canceled.

This cancellation originates from the angular momentum conservation in fluid mechanics. The large loop C creates the macroscopic eddy with constant vorticity $\omega_{\alpha\beta}^C$ and linear velocity $v^C(r) \propto r$. This eddy is a well-known static solution of the Navier-Stokes equation.

The eddy is conserved due to the angular momentum conservation. The only nontrivial thing is the eddy vorticity's functional dependence upon the loop's shape and size C . This expression is a function of the tensor area $\Sigma_{\mu\nu}^C$, rather than a general functional of the loop.

Combining this Ansatz with the space isotropy and the Kolmogorov scaling law, we arrive at the tensor area law

$$\Psi[C] \propto \exp \left(-B \left(\frac{\mathcal{E}}{\nu^3} \left(\Sigma_{\alpha\beta}^C \right)^2 \right)^{\frac{1}{3}} \right) \quad (8.72)$$

The universal constant B must be real and positive because of the symmetry of the loop orientation. When the orientation is reversed $C(\theta) \Rightarrow C(2\pi - \theta)$ The loop-integral changes sign, but its square, which enters here, stays invariant. Therefore, the constant in front must be real. The time reversal tells the same.

Moreover, the energy dissipation rate \mathcal{E} is time-odd. Therefore, the ratio $\frac{\mathcal{E}}{\nu^3}$ is time-even. Hence it must enter $\Psi[C]$ with the real coefficient. This coefficient B must be positive since $|\Psi[C]| < 1$.

Note, however, that we did not prove this law. The absence of decay for large twisted loops with zero tensor area is unphysical. Also, the physics seems to differ from what we expect in turbulence. The uniform vorticity,

even a random one, as in this solution, contrasts the observed intermittent distribution. Besides, there must be corrections to the asymptotic law, whereas the tensor area law is *exact*. This solution is far too simple: it is a trivial steady Euler flow rather than a flow with a steady loop we are seeking.

We discussed this unphysical solution mostly as a test of the loop technology.

8.10. Scalar Area law

Let us now study the scalar area law, which is a valid Ansatz for the asymptotic decay of the circulation PDF. We summarized in Appendix A the equations (the Weierstrass theory) for the minimal surface. All we need here is the following representation

$$A \rightarrow \frac{1}{2L_\Gamma^2} \int \int d\sigma_{\mu\nu}(x) d\sigma_{\mu\nu}(y) \exp \left(-\pi \frac{(x-y)^2}{L_\Gamma^2} \right) \quad (8.73)$$

where $L_\Gamma = |\Gamma|^{\frac{3}{4}} \mathcal{E}^{-\frac{1}{4}}$. The distance $(x-y)^2$ is measured in 3-space, and integration goes along the minimal surface. We implied that its size is much larger than L_Γ .

In this limit, one can perform the integration over, say, y along the local tangent plane at x in small vicinity $y-x \sim L_\Gamma$. Afterward, L_Γ factors cancel. We are left then with the ordinary scalar area integral

$$A \rightarrow \frac{1}{2} \int d\sigma_{\mu\nu}(x) d\sigma_{\mu\nu}(y) \delta^2(x-y) \rightarrow \int d^2x \sqrt{g} \quad (8.74)$$

In the previous, regularized form, the area represents the so-called Stokes functional,⁵⁶ which can be substituted into the loop equation. The area derivative of the area reads

$$\frac{\delta A}{\delta \sigma_{\mu\nu}(x)} = \frac{1}{L_\Gamma^2} \int d\sigma_{\mu\nu}(y) \exp \left(-\pi \frac{(x-y)^2}{L_\Gamma^2} \right) \quad (8.75)$$

In the local limit, this reduces to the tangent tensor

$$\frac{\delta A}{\delta \sigma_{\mu\nu}(x)} \rightarrow \int d\sigma_{\mu\nu}(y) \delta^2(x-y) = t_{\mu\nu}(x) \quad (8.76)$$

We implied that the point x approaches the contour from inside the surface so that the tangent tensor is well defined

$$t_{\mu\nu}(x) = t_\mu n_\nu - t_\nu n_\mu \quad (8.77)$$

Here t_μ is the local tangent vector of the loop, and n_ν is the inside normal to the loop along the surface.

The second area derivative of the regularized area in this limit is just the exponential

$$\frac{\delta^2 A}{\delta\sigma_{\alpha\beta}(x)\delta\sigma_{\gamma\delta}(y)} = \frac{\delta_{\alpha\gamma}\delta_{\beta\delta} - \delta_{\alpha\delta}\delta_{\beta\gamma}}{L_\Gamma^2} \exp\left(-\pi\frac{(x-y)^2}{L_\Gamma^2}\right) \quad (8.78)$$

Should we look for the higher terms of the asymptotic expansion at a large area, we would have to take into account the shape of the minimal surface, but in the thermodynamical limit, we could neglect the curvature of the loop and use the planar disk.

Let us use the general WKB form of PDF

$$P_C(\Gamma) = \frac{1}{\Gamma} \exp\left(-Q\left(\frac{A}{t^{2\kappa}}, \frac{\Gamma}{t^{2\kappa-1}}\right)\right) \quad (8.79)$$

We shall skip the arguments of effective action Q . We find on the left side of the loop equation

$$\partial_t Q \partial_\Gamma Q - \partial_t \partial_\Gamma Q \quad (8.80)$$

On the right side, we find the following integrand

$$\left((\partial_A Q)^2 - \partial_A^2 Q\right) \frac{\delta A}{\delta\sigma_{\alpha\beta}(r)} \frac{\delta A}{\delta\sigma_{\gamma\beta}(r')} - \partial_A Q \frac{\delta^2 A}{\delta\sigma_{\alpha\beta}(r)\delta\sigma_{\gamma\beta}(r')} \quad (8.81)$$

The last term drops after the r' integration in virtue of symmetry. The leading terms in the WKB approximation on both sides are those with the first derivatives. We find

$$\partial_t Q \partial_\Gamma Q = (\partial_A Q)^2 \oint_C dr_\alpha \frac{\delta A}{\delta\sigma_{\alpha\beta}(r)} \int d^3 r' \frac{r_\gamma - r'_\gamma}{4\pi|r - r'|^3} \frac{\delta A}{\delta\sigma_{\gamma\beta}(r')} \quad (8.82)$$

In the last integral, we substitute the above explicit form of the area derivatives and perform the $d^3 r'$ integration first. In the thermodynamical

limit only the small vicinity $r' - y \sim L_\Gamma$ contributes, and we find

$$\int d^3 r' \frac{r_\gamma - r'_\gamma}{4\pi|r - r'|^3} \frac{\delta A}{\delta \sigma_{\gamma\beta}(r')} \rightarrow L_\Gamma^2 \int d\sigma_{\gamma\beta}(y) \frac{r_\gamma - y_\gamma}{4\pi|r - y|^3} \quad (8.83)$$

This integral logarithmically diverges. We compute it with the logarithmic accuracy with the following result

$$\int d\sigma_{\gamma\beta}(y) \frac{r_\gamma - y_\gamma}{4\pi|r - y|^3} \propto \frac{t_\beta}{\pi} \ln \frac{L_\Gamma^2}{A} \quad (8.84)$$

The meaning of this integral is the average velocity in the WKB approximation. This velocity is tangent to the loop, up to the next correction terms at a large area.

Now, the emerging loop integral vanishes due to symmetry

$$\oint_C dr_\alpha t_\beta t_{\alpha\beta} = 0 \quad (8.85)$$

as the line element dr_α is directed along the tangent vector t_α , and the tangent tensor $t_{\alpha\beta}$ is antisymmetric. We used a similar mechanism in the tensor area solution; only there the cancellations emerged at the global level after the closed loop integration.

Here the right side of the loop equation vanishes locally at every point of the loop. Thus, we see that the scalar area represents the steady solution of the loop equation in the leading WKB approximation.

However, this steady solution no longer corresponds to a steady Euler flow– the circulation is conserved only for this specific loop.

The area conservation is the same phenomenon we discussed in the previous section 8.7. The loop equation is satisfied under the boundary condition for the velocity field: it is directed along the boundary, making this boundary steady.

It might be instructive to compare this solution with another known exact solution of the Euler dynamics, namely the Gibbs solution

$$P[v] = \exp \left(-\beta \int d^3 r \frac{1}{2} v_\alpha^2 \right) \quad (8.86)$$

For the loop functional it reads

$$\Psi_C(\gamma) = \exp \left(-\frac{\gamma^2}{2\beta} \oint_C dr_\alpha \oint_C dr'_\beta \delta^3(r - r') \right) \quad (8.87)$$

The integral diverges, and it corresponds to the perimeter law

$$\oint_C dr_\alpha \oint_C dr'_\beta \delta^3(r - r') \rightarrow r_0^{-2} \oint_C |dr| \quad (8.88)$$

where r_0 is a small distance cutoff. For the PDF it yields

$$P(\Gamma) \propto \exp \left(-\frac{\Gamma^2 \beta r_0^2}{2 \oint_C |dr|} \right) \quad (8.89)$$

We observe the same thing when substituting the Gibbs solution into the loop equation. Average velocity is tangent to the loop, which leads to a vanishing integrand in the loop equation. The difference is that in our case, this is true only asymptotically; there are the next corrections.

This equation does not fix the shape of the function Q in the leading WKB approximation. In a scale-invariant theory, it is natural to expect the power law

$$Q \left(\frac{A}{t^{2\kappa}}, \frac{\Gamma}{t^{2\kappa-1}} \right) \rightarrow \text{const} \left(\Gamma^{2\kappa} A^{1-2\kappa} \right)^\mu \quad (8.90)$$

There is one more arbitrary index μ involved. Even for the Kolmogorov law $\kappa = \frac{3}{2}$ the Γ dependence remains unknown.

8.11. Discussion

So, we found two asymptotic solutions of the loop equation in the turbulent limit, not counting the Gibbs solution. It remains to be seen which one (if any) is realized in turbulent flows. The tensor area solution is mathematically cleaner, but its physical meaning contradicts the intermittency paradigm. It corresponds to the uniform vorticity with random magnitude and random direction rather than the regions of high vorticity interlaced with regions of low vorticity observed in the turbulent flows.

The recent numerical experiments⁵⁷ favor the scalar area rather than the tensor one. Also, the Kolmogorov scaling was observed in these experiments. The Reynolds number was only ~ 100 , which was too small to conclude. We have to wait for the experiments (real or numerical) with the Reynolds numbers are a few orders of magnitude larger.

The scalar area is less trivial than the tensor one. The minimal area as a functional of the loop cannot be represented as any explicit contour integral of the Stokes type. Therefore it corresponds to an infinite number

of higher correlation functions present. Moreover, there could be several minimal surfaces for the same loop, as the equations for the minimal surface are nonlinear. The one with the least area should be accepted.

The condition of minimality of the area geometrically means that the normal vector is divergence-free in 3 dimensions. The surface variation can be viewed as the difference between the area of the surface $\delta_+ S$ with a little bump in the positive normal direction and the surface $\delta_- S$ with the same bump in the negative normal direction.

This difference is a surface integral of the normal vector n_μ over the closed surface $\delta S = \delta_+ S - \delta_- S$

$$\delta A = \int_{\delta S} d\sigma_\mu n_\mu \quad (8.91)$$

which, by the Stokes theorem, is equal to the volume integral of the divergence of vector N_μ with boundary value n_μ at δS .

$$\delta A = \int_{\delta V} \partial_\mu N_\mu; \quad (8.92)$$

$$\partial \delta V = \delta S; \quad (8.93)$$

$$N_\mu(\delta S) = n_\mu \quad (8.94)$$

The condition $\partial_\mu N_\mu = 0$ is equivalent to the usual requirement that the trace of external curvature tensor equals zero. We discuss this in the next sections in more detail.

In our case, this normal vector represents the vorticity in the local neighborhood of the surface. Thus, the vorticity is divergent-less.

8.12. Loop Expansion

Let us outline the method of direct iterations of the loop equation. A full description of the method can be found in.⁵⁶ The idea is to use the following representation of the loop functional

$$\Psi[C] = 1 + \sum_{n=2}^{\infty} \frac{1}{n} \left\{ \oint_C dr_1^{\alpha_1} \cdots \oint_C dr_n^{\alpha_n} \right\}_{\text{cyclic}} W_{\alpha_1 \dots \alpha_n}^n(r_1, \dots, r_n) \quad (8.95)$$

This representation holds for every translation invariant functional with finite area derivatives (so-called Stokes type functional). The coefficient

functions W can be related to these area derivatives. The normalization $\Psi[0] = 1$ for the shrunk loop is implied.

In general case the integration points r_1, \dots, r_n in (8.95) are cyclically ordered around the loop C . The coefficient functions can be assumed cyclicly symmetric without loss of generality. However, in the case of fluid dynamics, we are dealing with the so-called abelian Stokes functional. These functionals are characterized by completely symmetric coefficient functions, in which case the ordering of points can be removed at the expense of the extra symmetry factor in the denominator

$$\Psi[C] = 1 + \sum_{n=2}^{\infty} \frac{1}{n!} \oint_C dr_1^{\alpha_1} \cdots \oint_C dr_n^{\alpha_n} W_{\alpha_1 \dots \alpha_n}^n(r_1, \dots, r_n) \quad (8.96)$$

The incompressibility conditions

$$\partial_{\alpha_k} W_{\alpha_1 \dots \alpha_n}^n(r_1, \dots, r_n) = 0 \quad (8.97)$$

does not impose any further restrictions because of the gauge invariance of the loop functionals. This invariance (nothing to do with the symmetry of dynamical equations!) follows from the fact that the closed loop integral of any total derivative vanishes. So, the coefficient functions are defined modulo such derivative terms. In effect, this means that one may relax the incompressibility constraints (8.97), without changing the loop functional.

Let us note that the physical incompressibility constraints are not neglected to avoid confusion. They are, in fact, present in the loop equation, where we used the integral representation for the velocity in terms of vorticity. Still, the longitudinal parts of W drop in the loop integrals.

The loop calculus for the abelian Stokes functional is especially simple. The area derivative corresponds to the removal of one loop integration, and differentiation of the corresponding coefficient function

$$\frac{\delta \Psi[C]}{\delta \sigma_{\mu\nu}(r)} = \sum_{n=1}^{\infty} \frac{1}{n!} \oint_C dr_1^{\alpha_1} \cdots \oint_C dr_n^{\alpha_n} \hat{V}_{\mu\nu}^{\alpha} W_{\alpha, \alpha_1 \dots \alpha_n}^{n+1}(r, r_1, \dots, r_n) \quad (8.98)$$

where

$$\hat{V}_{\mu\nu}^{\alpha} \equiv \partial_{\mu} \delta_{\nu\alpha} - \partial_{\nu} \delta_{\mu\alpha} \quad (8.99)$$

In the nonabelian case, there would also be the contact terms, with W at coinciding points, coming from the cyclic ordering.⁵⁶ In the abelian case, these terms are absent since W is completely symmetric.

As a next step, let us compute the local kinetic term

$$\hat{L}\Psi[C] \equiv \oint_C dr_\nu \partial_\mu \frac{\delta\Psi[C]}{\delta\sigma_{\mu\nu}(r)} \quad (8.100)$$

Using the above formula for the loop derivative, we find

$$\hat{L}\Psi[C] = \sum_{n=1}^{\infty} \frac{1}{n!} \oint_C dr^\alpha \oint_C dr_1^{\alpha_1} \cdots \oint_C dr_n^{\alpha_n} \partial^2 W_{\alpha, \alpha_1 \dots \alpha_n}^{n+1}(r, r_1, \dots, r_n) \quad (8.101)$$

The net result is the second derivative of W by one variable. Note that the second term in $\hat{V}_{\mu\nu}^\alpha$ dropped as the total derivative in the closed loop integral.

As for the nonlocal kinetic term, it involves the second area derivative off the loop, at the point, r' , integrated over r' with the corresponding Green's function. Each area derivative involves the same operator \hat{V} , acting on the coefficient function. Again, the abelian Stokes functional simplifies the general framework of the loop calculus. The contribution of the wires cancels here, and the ordering does not matter so that

$$\begin{aligned} \frac{\delta^2 \Psi[C]}{\delta\sigma_{\mu\nu}(r) \delta\sigma_{\mu'\nu'}(r')} &= \sum_{n=0}^{\infty} \frac{1}{n!} \oint_C dr_1^{\alpha_1} \cdots \oint_C dr_n^{\alpha_n} \\ &\hat{V}_{\mu\nu}^\alpha \hat{V}_{\mu'\nu'}^{\alpha'} W_{\alpha, \alpha', \alpha_1 \dots \alpha_n}^{n+2}(r, r', r_1, \dots, r_n) \end{aligned} \quad (8.102)$$

Using these relations, we can write the steady-state loop equation as in the above figure.

Here the light dotted lines symbolize the arguments α_k, r_k of W , the big circle denotes the loop C ; the tiny circles stand for the loop derivatives and the pair of lines with the arrow denote the Green's function. The sum over the tensor indexes and the loop integrations over r_k are implied.

The first term is the local kinetic term, the second is the nonlocal kinetic term, and the right is the potential term in the loop equation. The heavy dotted line in this term stands for the correlation function F of the random forces. Note that this term is an abelian Stokes functional as well.

The iterations go in the potential term, starting with $\Psi[C] = 1$. In the next approximation, only the two-loop correction $W_{\alpha_1 \alpha_2}^2(r_1, r_2)$ is present. Comparing the terms, we note, that nonlocal kinetic term reduces to the total derivatives due to the space symmetry (in the usual terms, it would be $\langle v\omega \rangle$ at coinciding arguments), so we are left with the local one.

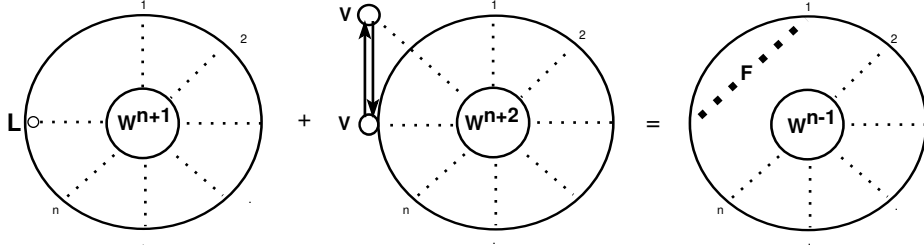


Figure 35: Loop equation for coefficient functions

This reasoning yields the equation

$$\nu^3 \partial^2 W_{\alpha\beta}^2(r - r') = F(r - r') \delta_{\alpha\beta} \quad (8.103)$$

modulo derivative terms. The solution is trivial in Fourier space

$$W_{\alpha\beta}^2(r - r') = - \int \frac{d^3 k}{(2\pi)^3} \exp(i k(r - r')) \delta_{\alpha\beta} \frac{\tilde{F}(k)}{\nu^3 k^2} \quad (8.104)$$

Note that we did not use the transverse tensor

$$P_{\alpha\beta}(k) = \delta_{\alpha\beta} - \frac{k_\alpha k_\beta}{k^2} \quad (8.105)$$

Though such a tensor is present in the physical velocity correlation, here we may use $\delta_{\alpha\beta}$ instead, as the longitudinal terms drop in the loop integral. This phenomenon is analogous to the Feynman gauge in QED. The correct correlator corresponds to the Landau gauge.

The potential term generates the four-point correlation $F W^2$, which matches the disconnected term in the W^4 on the left side

$$\begin{aligned} W_{\alpha_1 \alpha_2 \alpha_3 \alpha_4}^4(r_1, r_2, r_3, r_4) &\rightarrow W_{\alpha_1 \alpha_2}^2(r_1 - r_2) W_{\alpha_3 \alpha_4}^2(r_3 - r_4) + \\ &W_{\alpha_1 \alpha_3}^2(r_1 - r_3) W_{\alpha_2 \alpha_4}^2(r_2 - r_4) + W_{\alpha_1 \alpha_4}^2(r_1 - r_4) W_{\alpha_2 \alpha_3}^2(r_2 - r_3) \end{aligned} \quad (8.106)$$

The three-point function will appear in the same order in the loop expansion. The corresponding terms in the kinetic part must cancel, as

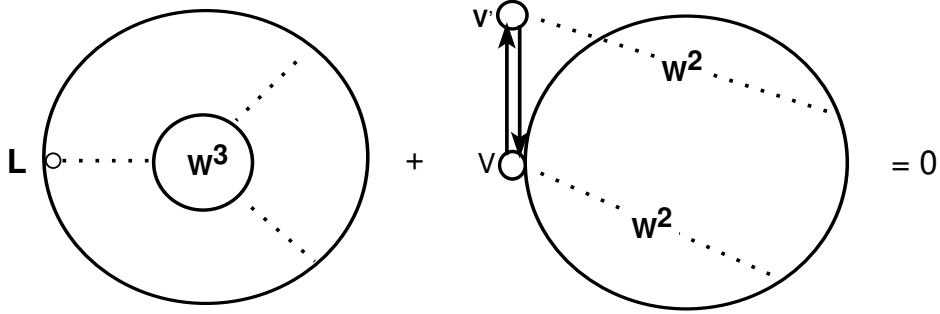


Figure 36: Relation between third and fourth coefficient functions

the potential term does not contribute. The local kinetic term yields the loop integrals of $\partial^2 W^3$, whereas the nonlocal one yields $\hat{V} W^2 \hat{V}' W^2$, integrated over $d^3 r'$ with the Greens's function $\frac{(r-r')}{4\pi|r-r'|^3}$. The equation has the structure (see Fig.36).

Now it is clear that the solution of this equation for W^3 would be the same three-point correlator, which one could obtain (much easier!) by direct iterations of the Navier-Stokes equation.

The purpose of this painful exercise was not to give one more method of developing the expansion in powers of the random force. We verified that the loop equations are capable of producing the same results, as the ordinary chain of the equations for the correlation functions.

In the above arguments, the loop functional needed to belong to the class of the abelian Stokes functionals. Let us check that our tensor area Ansatz

$$\Sigma_{\alpha\beta}^C = \oint_C r_\alpha dr_\beta \quad (8.107)$$

belongs to the same class. Taking the square, we find

$$\left(\Sigma_{\alpha\beta}^C\right)^2 = \oint_C dr_\beta \oint_C dr'_\beta r_\alpha r'_\alpha = -\frac{1}{2} \oint_C dr_\beta \oint_C dr'_\beta (r - r')^2 \quad (8.108)$$

where the last transformation follows from the fact that only the cross term in $(r - r')^2$ yields nonzero after double loop integration.

Any expansion in terms of the square of the tensor area, therefore, reduces to the superposition of multiple loop integral of the product of $(r_i - r_j)^2$; this is an example of the abelian Stokes functional. In the large area limit, this could reduce to a function of some loop integral. An example could be, say

$$\Psi[C] \stackrel{?}{=} \exp \left(B \left(1 - \left(1 + \frac{\mathcal{E} \left(\Sigma_{\alpha\beta}^C \right)^2}{\nu^3} \right)^{\frac{1}{3}} \right) \right) \quad (8.109)$$

One could explicitly verify all the properties of the abelian Stokes functional. This example is unrealistic, though, as it does not have the odd terms of expansion. In the real world, such terms are present at the viscous scales. According to our solution, this asymmetry disappears in the inertial range of loops (which does not apply to velocity correlators in the inertial range, as those correspond to shrunk loops).

8.13. Matrix Model

The Navier-Stokes equation represents a very special case of nonlinear PDE. There is a well-known Galilean invariance

$$v_\alpha(r, t) \rightarrow v_\alpha(r - ut, t) + u_\alpha \quad (8.110)$$

which relates the magnitude of the velocity field with the scales of time and space.¹⁵ Let us make this relation more explicit.

First, let us introduce the vorticity field

$$\omega_{\mu\nu} = \partial_\mu v_\nu - \partial_\nu v_\mu \quad (8.111)$$

and rewrite the Navier-Stokes equation as follows

$$\dot{v}_\alpha = \nu \partial_\beta \omega_{\beta\alpha} - v_\beta \omega_{\beta\alpha} - \partial_\alpha w; \quad w = p + \frac{v^2}{2} \quad (8.112)$$

¹⁵At the same time, it tells us that the constant part of velocity is frame-dependent, so it better be eliminated if we would like to have a smooth limit at large times. Most notorious large-scale divergencies in turbulence are due to this unphysical constant part.

This w is the well-known enthalpy density to be found from the incompressibility condition $\text{div} v = 0$, i.e.

$$\partial^2 w = \partial_\alpha v_\beta \omega_{\beta\alpha} \quad (8.113)$$

As a next step, let us introduce the "covariant derivative" operator

$$D_\alpha = v \partial_\alpha - \frac{1}{2} v_\alpha \quad (8.114)$$

and observe that

$$2 [D_\alpha D_\beta] = v \omega_{\beta\alpha} \quad (8.115)$$

$$2 D_\beta [D_\alpha D_\beta] + h.c. = v \partial_\beta \omega_{\beta\alpha} - v_\beta \omega_{\beta\alpha} \quad (8.116)$$

where $h.c.$ stands for hermitian conjugate.

These identities allow us to write down the following dynamical equation for the covariant derivative operator

$$\dot{D}_\alpha = D_\beta [D_\alpha D_\beta] - D_\alpha W + h.c. \quad (8.117)$$

As for the incompressibility condition, we can write it as follows

$$[D_\alpha D_\alpha^\dagger] = 0 \quad (8.118)$$

The enthalpy operator $W = \frac{w}{v}$ is to be determined from this condition, or, equivalently

$$[D_\alpha [D_\alpha W]] = [D_\alpha, D_\beta [D_\alpha D_\beta]] \quad (8.119)$$

We see that the viscosity disappeared from these equations. This paradox is resolved by extra degeneracy of this dynamics: the anti-hermitian part of the D operator is conserved. Its value at the initial time is proportional to viscosity.

The operator equations are invariant by the time independent unitary transformations

$$D_\alpha \rightarrow S^\dagger D_\alpha S; S^\dagger S = 1 \quad (8.120)$$

and, in addition, to the time-dependent unitary transformations with

$$S(t) = \exp \left(\frac{1}{2v} t u_\beta (D_\beta - D_\beta^\dagger) \right) \quad (8.121)$$

corresponding to the Galilean transformations.

One could view the operator D_α as the matrix

$$\langle i|D_\alpha|j\rangle = \int d^3r \psi_i^*(r) v \partial_\alpha \psi_j(r) - \frac{1}{2} \psi_i^*(r) v_\alpha(r) \psi_j(r) \quad (8.122)$$

where the functions $\psi_j(r)$ are the Fourier of Chebyshev functions depending upon the geometry of the problem.

The finite mode approximation would correspond to the truncation of this infinite size matrix to finite size N . This approximation is not the same as leaving N terms in the mode expansion of the velocity field. The number of independent parameters here is $O(N^2)$ rather than $O(N)$. Is the unitary symmetry worth paying such a high price in numerical simulations?

The matrix model of the Navier-Stokes equation has some theoretical beauty. Moreover, it raises hopes of a simple asymptotic probability distribution. The ensemble of random hermitian matrices was recently applied to the the problem of Quantum Gravity,⁵⁸ which led to a genuine breakthrough in the field.

Unfortunately, the model of several coupled random matrices, which is the case here, is much more complicated than the one-matrix model studied in Quantum Gravity. The dynamics of the eigenvalues are coupled to the dynamics of the "angular" variables, i.e., the unitary matrices S in the above relations. We could not directly apply the technique of orthogonal polynomials, which was so successful in the one matrix problem.

Another technique that proved to be successful in QCD and Quantum Gravity is the loop equation. This method, which we discuss at length in this paper, works in field theory problems with hidden geometric meaning. The turbulence is an ideal case, much simpler than QCD or Quantum Gravity.

8.14. *The Reduced Dynamics*

Let us now try to reproduce the dynamics of the loop field in a simpler Ansatz

$$\Psi[C] = \left\langle \exp \left(\frac{i}{v} \oint dC_\alpha(\theta) P_\alpha(\theta) \right) \right\rangle \quad (8.123)$$

The difference with the original definition (8.5) is that our new function $P_\alpha(\theta)$ depends directly on θ rather than through the function $v_\alpha(r)$ taken

at $r_\alpha = C_\alpha(\theta)$. This transformation is the $d \Rightarrow 1$ dimensional reduction we mentioned above. From the point of view of the loop functional, there is no need to deal with field $v(r)$; one could take a shortcut.

The reduced dynamics must be fitted to the Navier-Stokes dynamics of the original field. With the loop calculus developed above, we have all the necessary tools to build these reduced dynamics.

Let us assume some unknown dynamics for the P field

$$\dot{P}_\alpha(\theta) = F_\alpha(\theta, [P]). \quad (8.124)$$

Furthermore, compare the time derivatives of the original and reduced Ansatz. We find in (8.123) instead of (8.34)

$$\frac{\iota}{\nu} \oint dC_\alpha(\theta) F_\alpha(\theta, [P]) \quad (8.125)$$

Now we observe that P' could be replaced by the functional derivative, acting on the exponential in (8.123) as follows

$$\frac{\delta}{\delta C_\alpha(\theta)} \leftrightarrow -\iota \nu P'_\alpha(\theta) \quad (8.126)$$

This equation means that one could take the operators of the Section 2 which are expressing velocity and vorticity in terms of the spike operator, and replace the functional derivative as above. This transformation yields the following formula for the spike derivative

$$\begin{aligned} D_\alpha(\theta, \epsilon) = & \\ & -\iota \nu \int_\theta^{\theta+2\epsilon} d\phi \left(1 - \frac{|\theta + \epsilon - \phi|}{\epsilon} \right) P'_\alpha(\phi) = \\ & -\iota \nu \int_{-1}^1 d\mu \operatorname{sgn}(\mu) P_\alpha(\theta + \epsilon(1 + \mu)) \end{aligned} \quad (8.127)$$

We obtained the weighted discontinuity of the function $P(\theta)$, which, in the naive limit $\epsilon \rightarrow 0$, would become the true discontinuity. However, the function $P(\theta)$ has in general the stronger singularities, then discontinuity, so that this limit cannot be taken yet.

Thus, we arrive at the dynamical equation for the P field

$$\dot{P}_\alpha = \nu D_\beta \Omega_{\beta\alpha} - V_\beta \Omega_{\beta\alpha} \quad (8.128)$$

where the operators V, D, Ω of the Section 8.2 should be regarded as the ordinary numbers, with definition (8.127) of D in terms of P .

All the functional derivatives are gone! We needed them only to prove equivalence of reduced dynamics to the Navier-Stokes dynamics.

The function $P_\alpha(\theta)$ would become complex now, as the right side of the reduced dynamical equation is complex for real $P_\alpha(\theta)$.

Let us discuss this puzzling issue in more detail. The origin of imaginary units was the factor of ι in the exponential of the loop field. We had to insert this factor to make the loop field decrease at large loops due to oscillations of the phase factors. Later this factor propagated to the definition of the P field.

Our spike derivative D is purely imaginary for real P , and so is our Ω , operator. As a result, the velocity operator V is real. Therefore the $D\Omega$ term in the reduced equation (8.128) is real for real P whereas the $V\Omega$ term is purely imaginary.

This relation does not contradict the moment equations, as we saw before. The terms with even/odd numbers of velocity fields in the loop functional are real/imaginary, but the moments are real, as they should be. The complex dynamics of P doubles the number of independent variables.

There is one serious problem, however. Inverting the spike operator D_α we implicitly assumed that it was anti-hermitian and could be regularized by adding an infinitesimal negative constant to D_α^2 in denominator. Indeed, this prescription works perturbatively in each term of expansion in time or size of the loop, as we checked. However, beyond this expansion, there would be a problem of singularities, which arise when $D_\alpha^2(\theta)$ vanishes at some θ .

In general, this would occur for complex θ when the imaginary and real part of $D_\alpha^2(\theta)$ simultaneously vanish. One could introduce the complex variable

$$e^{\iota\theta} = z; \quad e^{-\iota\theta} = \frac{1}{z}; \quad \oint d\theta = \oint \frac{dz}{iz} \quad (8.129)$$

where the contour of z integration encircles the origin around the unit circle. Later, with time evolution, these contours must be deformed, to avoid complex roots of $D_\alpha^2(\theta)$.

8.15. Initial Data

Let us study the relation between the initial data for the original and reduced dynamics. Let us assume that the initial field is distributed

according to some translation invariant probability density, so that the initial value of the loop field does not depend on the constant part of $C(\theta)$.

One can expand the translation invariant loop field in functional Fourier transform

$$\Psi[C] = \int DQ \delta^3 \left(\oint d\phi Q(\phi) \right) W[Q] \exp \left(i \oint d\theta C_\alpha(\theta) Q_\alpha(\theta) \right) \quad (8.130)$$

which can be inverted as follows

$$\delta^3 \left(\oint d\phi Q(\phi) \right) W[Q] = \int DC \Psi[C] \exp \left(-i \oint d\theta C_\alpha(\theta) Q_\alpha(\theta) \right) \quad (8.131)$$

Let us take a closer look at these formal transformations. The functional measure for these integrations is defined according to the scalar product

$$(A, B) = \oint \frac{d\theta}{2\pi} A(\theta) B(\theta) \quad (8.132)$$

which diagonalizes in the Fourier representation

$$\begin{aligned} A(\theta) &= \sum_{-\infty}^{+\infty} A_n e^{in\theta}; \quad A_{-n} = A_n^* \\ (A, B) &= \sum_{-\infty}^{+\infty} A_n B_{-n} = \\ &= A_0 B_0 + \sum_{n=1}^{\infty} a'_n b'_n + a''_n b''_n \\ a'_n &= \sqrt{2} \text{Re } A_n, \quad a''_n = \sqrt{2} \text{Im } A_n \end{aligned} \quad (8.133)$$

The corresponding measure is given by an infinite product of the Euclidean measures for the imaginary and real parts of each Fourier component

$$DQ = d^3 Q_0 \prod_{n=1}^{\infty} d^3 q'_n d^3 q''_n \quad (8.134)$$

The orthogonality of Fourier transformation could now be explicitly

checked, as

$$\begin{aligned}
& \int DC \exp \left(i \int d\theta C_\alpha(\theta) (A_\alpha(\theta) - B_\alpha(\theta)) \right) \\
&= \int d^3 C_0 \prod_1^\infty d^3 c'_n d^3 c''_n \\
& \exp \left(2\pi i \left(C_0 (A_0 - B_0) + \sum_1^\infty c'_n (a'_n - b'_n) + c''_n (a''_n - b''_n) \right) \right) \\
&= \delta^3 (A_0 - B_0) \prod_1^\infty \delta^3 (a'_n - b'_n) \delta^3 (a''_n - b''_n)
\end{aligned} \tag{8.135}$$

Let us now check the parametric invariance

$$\theta \rightarrow f(\theta); f(2\pi) - f(0) = 2\pi; f'(\theta) > 0 \tag{8.136}$$

The functions $C(\theta)$ and $P(\theta)$ have zero dimension in the sense that only their argument transforms

$$C(\theta) \rightarrow C(f(\theta)); P(\theta) \rightarrow P(f(\theta)) \tag{8.137}$$

The functions $Q(\theta)$ and $P'(\theta)$ in above transformation have dimension one

$$P'(\theta) \rightarrow f'(\theta)P'(f(\theta)); Q(\theta) \rightarrow f'(\theta)Q(f(\theta)) \tag{8.138}$$

so that the constraint on Q remains invariant

$$\oint d\theta Q(\theta) = \oint df(\theta) Q(f(\theta)) \tag{8.139}$$

The invariance of the measure is easy to check for infinitesimal reparametrization

$$f(\theta) = \theta + \epsilon(\theta); \epsilon(2\pi) = \epsilon(0) \tag{8.140}$$

which changes C and the L_2 norm (C, C) as follows

$$\delta C(\theta) = \epsilon(\theta)C'(\theta) \tag{8.141}$$

$$\begin{aligned}
\delta(C, C) &= \oint \frac{d\theta}{2\pi} \epsilon(\theta) 2C_\alpha(\theta) C'_\alpha(\theta) \\
&= - \oint \frac{d\theta}{2\pi} \epsilon'(\theta) C_\alpha^2(\theta)
\end{aligned} \tag{8.142}$$

The corresponding Jacobian reduces to

$$1 - \oint d\theta \epsilon'(\theta) = 1 \quad (8.143)$$

in virtue of periodicity.

This relation proves the parametric invariance of the functional Fourier transformations. Using these transformations, we could find the probability distribution for the initial data of

$$P_\alpha(\theta) = -\nu \int_0^\theta d\phi Q_\alpha(\phi) \quad (8.144)$$

The simplest but still meaningful distribution of the initial velocity field is the Gaussian one, with energy concentrated in the macroscopic motions. The corresponding loop field reads

$$\Psi_0[C] = \exp \left(-\frac{1}{2} \oint dC_\alpha(\theta) \oint dC_\alpha(\theta') f(C(\theta) - C(\theta')) \right) \quad (8.145)$$

where $f(r - r')$ is the velocity correlation function

$$\langle v_\alpha(r) v_\beta(r') \rangle = \left(\delta_{\alpha\beta} - \partial_\alpha \partial_\beta \partial_\mu^{-2} \right) f(r - r') \quad (8.146)$$

The potential part drops out in the closed loop integral.

The correlation function varies at the macroscopic scale, which means that we could expand it in the Taylor series

$$f(r - r') \rightarrow f_0 - f_1(r - r')^2 + \dots \quad (8.147)$$

The first term f_0 is proportional to initial energy density,

$$\frac{1}{2} \langle v_\alpha^2 \rangle = \frac{d-1}{2} f_0 \quad (8.148)$$

and the second one is proportional to initial energy dissipation rate

$$\mathcal{E}_0 = -\nu \langle v_\alpha \partial_\beta^2 v_\alpha \rangle = 2d(d-1)\nu f_1 \quad (8.149)$$

where $d = 3$ is the dimension of space.

The constant term in (8.147) as well as $r^2 + r'^2$ terms drop from the closed loop integral, so we are left with the cross-term rr'

$$\Psi_0[C] \rightarrow \exp \left(-f_1 \oint dC_\alpha(\theta) \oint dC_\alpha(\theta') C_\beta(\theta) C_\beta(\theta') \right) \quad (8.150)$$

This distribution is almost Gaussian: it reduces to Gaussian one by extra integration

$$\Psi_0[C] \rightarrow \text{const} \int d^3\omega \exp \left(-\omega_{\alpha\beta}^2 \right) \exp \left(2i\sqrt{f_1}\omega_{\mu\nu} \oint dC_\mu(\theta) C_\nu(\theta) \right) \quad (8.151)$$

The integration here goes overall $\frac{d(d-1)}{2} = 3$ independent $\alpha < \beta$ components of the antisymmetric tensor $\omega_{\alpha\beta}$. Note that this is ordinary integration, not the functional one. The physical meaning of this ω is the random constant vorticity at the initial moment.

At fixed ω the Gaussian functional integration over C

$$\int DC \exp \left(i \oint d\theta \left(\frac{1}{\nu} C_\beta(\theta) P'_\beta(\theta) + 2\sqrt{f_1}\omega_{\alpha\beta} C'_\alpha(\theta) C_\beta(\theta) \right) \right) \quad (8.152)$$

can be performed explicitly, it reduces to the solution of the saddle point equation

$$P'_\beta(\theta) = 4\nu\sqrt{f_1}\omega_{\beta\alpha}C'_\alpha(\theta) \quad (8.153)$$

which is trivial for constant ω

$$C_\alpha(\theta) = \frac{1}{4\nu\sqrt{f_1}}\omega_{\alpha\beta}^{-1}P_\beta(\theta) \quad (8.154)$$

The inverse matrix is not unique in odd dimensions since $\text{Det } \omega_{\alpha\beta} = 0$. However, the resulting pdf for P is unique. This probability distribution is Gaussian, with the correlator

$$\langle P_\alpha(\theta) P_\beta(\theta') \rangle = 2i\nu\sqrt{f_1}\omega_{\alpha\beta}\text{sign}(\theta' - \theta) \quad (8.155)$$

Note that antisymmetry of ω compensates that of the sign function so that this correlation function is symmetric, as it should be. However, it is anti-hermitian, which corresponds to purely imaginary eigenvalues. The corresponding realization of the P functions are complex!

Let us study this phenomenon for the Fourier components. Differentiating the last equation by θ and Fourier transforming, we find

$$\langle P_{\alpha,n} P_{\beta,m} \rangle = \frac{4\nu}{m} \delta_{-nm} \sqrt{f_1} \omega_{\alpha\beta} \quad (8.156)$$

This relation cannot be realized with complex conjugate Fourier components $P_{\alpha,-n} = P_{\alpha,n}^*$ but we could take $\bar{P}_{\alpha,n} \equiv P_{\alpha,-n}$ and $P_{\alpha,n}$ as real random variables, with the correlation function

$$\langle \bar{P}_{\alpha,n} P_{\beta,m} \rangle = \frac{4\nu}{m} \delta_{nm} \sqrt{f_1} \omega_{\alpha\beta}; \quad n > 0 \quad (8.157)$$

The trivial realization is

$$\bar{P}_{\alpha,n} = \frac{4\nu}{n} \sqrt{f_1} \omega_{\alpha\beta} P_{\beta,n} \quad (8.158)$$

with $P_{\beta,n}$ being Gaussian random numbers with unit dispersion.

As for the constant part $P_{\alpha,0}$ of $P_{\alpha}(\theta)$, it is not defined, but it drops from equations by virtue of translational invariance.

8.16. Possible Numerical Implementation

The above general scheme is fairly abstract and complicated. Could it lead to any practical computation method? It would depend upon the success of the discrete approximations of the singular equations of reduced dynamics.

The most obvious approximation would be the truncation of Fourier expansion at some large number N . With Fourier components decreasing only as powers of n , this approximation is doubtful. In addition, such truncation violates the parametric invariance, which looks dangerous.

It is safer to approximate $P(\theta)$ by a sum of step functions so that it is piecewise constant. The parametric transformations vary the lengths of intervals of constant $P(\theta)$ but leave invariant these constant values. The corresponding representation reads

$$P_{\alpha}(\theta) = \sum_{l=0}^N (p_{\alpha}(l+1) - p_{\alpha}(l)) \Theta(\theta - \theta_l); \quad p(N+1) = p(1), \quad p(0) = 0 \quad (8.159)$$

It is implied that $\theta_0 = 0 < \theta_1 < \theta_2 \cdots < \theta_N < 2\pi$. By construction, the function $P(\theta)$ takes value $p(l)$ at the interval $\theta_{l-1} < \theta < \theta_l$.

We could take $\dot{P}(\theta)$ at the middle of this interval as approximation to $\dot{p}(l)$.

$$\dot{p}(l) \approx \dot{P}(\bar{\theta}_l); \bar{\theta}_l = \frac{1}{2} (\theta_{l-1} + \theta_l) \quad (8.160)$$

As for the time evolution of angles θ_l , one could differentiate (8.159) in time and find

$$\dot{P}_\alpha(\theta) = \sum_{l=0}^N (\dot{p}_\alpha(l+1) - \dot{p}_\alpha(l)) \Theta(\theta - \theta_l) - \sum_{l=0}^N (p_\alpha(l+1) - p_\alpha(l)) \delta(\theta - \theta_l) \dot{\theta}_l \quad (8.161)$$

from which one could derive the following approximation

$$\dot{\theta}_l \approx \frac{(p_\alpha(l) - p_\alpha(l+1))}{(p_\mu(l+1) - p_\mu(l))^2} \int_{\bar{\theta}_l}^{\bar{\theta}_{l+1}} d\theta \dot{P}_\alpha(\theta) \quad (8.162)$$

The extra advantage of this approximation is its simplicity. All the integrals involved in the definition of the spike derivative (8.127) are trivial for the stepwise constant $P(\theta)$. So, this approximation can be, in principle, implemented on the computer. This formidable task exceeds the scope of the present work, which we view as purely theoretical.

8.17. Uniqueness of the tensor area law

Let us address the issue of the uniqueness of the tensor area solution. Let us take the following Ansatz

$$S[C] = f \left(\oint_C dr_\alpha \oint_C dr'_\alpha W(r - r') \right) \quad (8.163)$$

When substituted into the static loop equation (with the area derivatives computed in Appendix A), it yields the following equation for the correlation function $W(r)$

$$\begin{aligned} 0 &= \oint_C dr_\alpha \oint_C dr'_\beta \oint_C dr''_\gamma U_{\alpha\beta\gamma}(r, r', r'') \\ U_{\alpha\beta\gamma}(r, r', r'') &= W(r - r') \hat{V}_{\beta\gamma}^\alpha W(r' - r'') + \text{permutations} \\ \hat{V}_{\mu\nu}^\alpha &= \delta_{\alpha\nu} \partial_\mu - \delta_{\alpha\mu} \partial_\nu \end{aligned} \quad (8.164)$$

The derivative f' of the unknown function drops from the static equation.

This equation should hold for arbitrary loop C . Using the Taylor expansion for the Stokes type functional,⁵⁶ we can argue that the coefficient function U must vanish up to the total derivatives. The equivalent statement is that the third area derivative of this functional must vanish. Using the loop calculus (see Appendix A), we find the following equation

$$0 = \hat{V}_{\mu\nu}^{\alpha} \hat{V}_{\mu'\nu'}^{\alpha'} \hat{V}_{\mu''\nu''}^{\alpha''} U_{\alpha\alpha'\alpha''}(r, r', r'') \quad (8.165)$$

which should hold for arbitrary r, r', r'' . These relations lead to the over-complete system of equations for $W(r)$ in general case. However, for the special case $W(r) = r^2$, which corresponds to the square of the tensor area

$$\Sigma_{\alpha\beta}^2 = -\frac{1}{2} \oint_C dr_{\alpha} \oint_C dr'_{\alpha} (r - r')^2 \quad (8.166)$$

the system is satisfied as a consequence of certain symmetry. In this case, we find in the loop equation

$$2 \oint_C dr_{\alpha} \oint_C dr'_{\beta} (r - r')^2 \oint_C dr''_{\alpha} (r'_{\beta} - r''_{\beta}) \propto \Sigma_{\alpha\beta}^C \oint_C dr_{\alpha} \oint_C dr'_{\beta} (r - r')^2 \quad (8.167)$$

The last integral is symmetric against permutations of α, β , whereas the first factor $\Sigma_{\alpha\beta}^C$ is antisymmetric, hence the sum over $\alpha\beta$ yields zero, as we already saw above.

It was assumed in the above arguments that the loop C consists of only one connected part. Let us now consider the more general situation, with arbitrary number n of loops C_1, \dots, C_n . The corresponding Ansatz would be

$$S_n [C_1, \dots, C_n] = s_n (\Sigma^1, \dots, \Sigma^n) \quad (8.168)$$

where Σ^i are tensor areas.

This function should obey the same WKB loop equations in each variable. Introducing the loop vorticities

$$\omega_{\mu\nu}^k = 2 \frac{\partial s_n}{\partial \Sigma_{\mu\nu}^k} \quad (8.169)$$

which are constant on each loop, we have to solve the following problem. What are the values of $\omega_{\mu\nu}^k$ such that the single velocity field $v_{\alpha}(r)$ could produce them?

We do not see any other solutions but the trivial one, with all equal $\omega_{\mu\nu}^k$ and linear velocity, as before. This property would correspond to

$$s_n(\Sigma^1, \dots, \Sigma^n) = s_1(\Sigma); \Sigma_{\mu\nu} = \sum_{k=1}^n \Sigma_{\mu\nu}^k = \oint_{\uplus C_k} r_\mu dr_\nu \quad (8.170)$$

The loop equation would be satisfied with $C = \uplus C_k$. This property corresponds to the additivity of loops

$$S_n[C_1, \dots, C_n] = S_1[\uplus C_k] \quad (8.171)$$

Note that such additivity is the opposite of the statistical independence, which would imply that

$$S_n[C_1, \dots, C_n] = \sum S_1[C_k] \quad (8.172)$$

The additivity could also be understood as a statement that any set of n loops is equivalent to a single loop for the abelian Stokes functional. Just connect these loops by wires, and note that the contribution of wires cancels. So, if the area law holds for *arbitrary* single loop, it must be additive.

However, this assumption may not be true, as it often happens in the WKB approximation. There is no single asymptotic formula but rather collections of different WKB regions, with quantum regions in between. In our case, this corresponds to the following situation.

Take the large circular loop, for which the WKB approximation holds, and try to split it into two large circles. One will have to twist the loop like the infinity symbol ∞ , in which case it intersects itself. The WKB approximation might break at this point, as the short-distance velocity correlation might be important near the self-intersection point. This phenomenon may explain the paradox of the vanishing tensor area for the ∞ shaped loop. From the point of view of our area law, such a loop is not large.

8.18. Minimal surfaces

Let us present the modern theoretical physicist's view of the classical Weierstrass theory of minimal surfaces. One can describe the minimal surface by a parametric equation

$$S : r_\alpha = X_\alpha(\xi_1, \xi_2) \quad (8.173)$$

The function $X_\alpha(\xi)$ should provide the minimum to the area functional

$$A[X] = \int_S \sqrt{d\sigma_{\mu\nu}^2} = \int d^2\xi \sqrt{\text{Det } G} \quad (8.174)$$

where

$$G_{ab} = \partial_a X_\mu \partial_b X_\mu, \quad (8.175)$$

is the induced metric. For general studies, it is sometimes convenient to introduce the unit tangent tensor as an independent field and minimize

$$A[X, t, \lambda] = \int d^2\xi \left(e_{ab} \partial_a X_\mu \partial_b X_\nu t_{\mu\nu} + \lambda (1 - t_{\mu\nu}^2) \right) \quad (8.176)$$

From the classical equations, we will find then

$$t_{\mu\nu} = \frac{e_{ab}}{2\lambda} \partial_a X_\mu \partial_b X_\nu ; t_{\mu\nu}^2 = 1, \quad (8.177)$$

which shows equivalence to the old definition.

For the actual computation of the minimal area, it is convenient to introduce the auxiliary internal metric g_{ab}

$$A[X, g] = \frac{1}{2} \int_S d^2\xi \text{tr } g^{-1} G \sqrt{\text{Det } g}. \quad (8.178)$$

The straightforward minimization by g_{ab} yields

$$g_{ab} \text{tr } g^{-1} G = 2G_{ab}, \quad (8.179)$$

which has a family of solutions

$$g_{ab} = \lambda G_{ab}. \quad (8.180)$$

The local scale factor λ drops from the area functional, and we recover the original definition. So, we could first minimize the quadratic functional (8.178) of $X(\xi)$ (the linear problem), and then minimize by g_{ab} (the nonlinear problem).

The crucial observation is the possibility of choosing conformal coordinates, with the diagonal metric tensor

$$g_{ab} = \delta_{ab} \rho, \quad g_{ab}^{-1} = \frac{\delta_{ab}}{\rho}, \quad \sqrt{\text{Det } g} = \rho; \quad (8.181)$$

after which the local scale factor ρ drops from the integral

$$A[X, \rho] = \frac{1}{2} \int_S d^2 \xi \partial_a X_\mu \partial_a X_\mu. \quad (8.182)$$

However, the ρ field is implicitly present in the problem, through the boundary conditions.

Namely, one has to allow an arbitrary parametrization of the boundary curve C . We shall use the upper half plane of ξ for our surface, so the boundary curve corresponds to the real axis $\xi_2 = 0$. The Boundary condition will be

$$X_\mu(\xi_1, +0) = C(f(\xi_1)), \quad (8.183)$$

where the unknown function $f(t)$ is related to the boundary value of ρ by the boundary condition for the metric

$$g_{11} = \rho = G_{11} = \left(\partial_1 X_\mu \right)^2 = C_\mu'^2 f'^2 \quad (8.184)$$

As it follows from the initial formulation of the problem, one should now solve the linear problem for the X field, compute the area and minimize it as a functional of $f(\cdot)$. As we shall see below, the minimization condition coincides with the diagonality of the metric at the boundary

$$\left[\partial_1 X_\mu \partial_2 X_\mu \right]_{\xi_2=+0} = 0 \quad (8.185)$$

The linear problem is nothing but the Laplace equation $\partial^2 X = 0$ in the upper half plane with the Dirichlet boundary condition (8.183). The solution is well known

$$X_\mu(\xi) = \int_{-\infty}^{+\infty} \frac{dt}{\pi} \frac{C_\mu(f(t)) \xi_2}{(\xi_1 - t)^2 + \xi_2^2} \quad (8.186)$$

The area functional can be reduced to the boundary terms in virtue of the Laplace equation

$$A[f] = \frac{1}{2} \int d^2 \xi \partial_a \left(X_\mu \partial_a X_\mu \right) = -\frac{1}{2} \int_{-\infty}^{+\infty} d\xi_1 \left[X_\mu \partial_2 X_\mu \right]_{\xi_2=+0} \quad (8.187)$$

Substituting here the solution for X , we find

$$A[f] = -\frac{1}{2\pi} \mathbf{Re} \int_{-\infty}^{+\infty} dt \int_{-\infty}^{+\infty} dt' \frac{C_\mu(f(t)) C_\mu(f(t'))}{(t - t' - i0)^2} \quad (8.188)$$

This formula can be rewritten in a nonsingular form

$$A[f] = \frac{1}{4\pi} \int_{-\infty}^{+\infty} dt \int_{-\infty}^{+\infty} dt' \frac{\left(C_\mu(f(t)) - C_\mu(f(t'))\right)^2}{(t - t')^2} \quad (8.189)$$

which is manifestly positive.

Another nice form can be obtained by integrating by-parts

$$A[f] = \frac{1}{2\pi} \int_{-\infty}^{+\infty} dt f'(t) \int_{-\infty}^{+\infty} dt' f'(t') C'_\mu(f(t)) C'_\mu(f(t')) \log |t - t'| \quad (8.190)$$

This form allows one to switch to the inverse function $\tau(f)$, which is more convenient for optimization

$$A[\tau] = \frac{1}{2\pi} \int_{-\infty}^{+\infty} df \int_{-\infty}^{+\infty} df' C'_\mu(f) C'_\mu(f') \log |\tau(f) - \tau(f')| \quad (8.191)$$

In the above formulas, it was implied that $C(\infty) = 0$. One could switch to more traditional circular parametrization by mapping the upper half plane inside the unit circle

$$\zeta_1 + \imath \zeta_2 = \imath \frac{1 - \omega}{1 + \omega}; \omega = r e^{\imath \alpha}; r \leq 1. \quad (8.192)$$

The real axis is mapped at the unit circle. Changing variables in above integral we find

$$X_\mu(r, \alpha) = \mathbf{Re} \int_{-\pi}^{\pi} \frac{d\theta}{\pi} C_\mu(\phi(\theta)) \left(\frac{1}{1 - r \exp(\imath \alpha - \imath \theta)} - \frac{1}{1 + \exp(-\imath \theta)} \right) \quad (8.193)$$

Here

$$\phi(\theta) = f \left(\tan \frac{\theta}{2} \right). \quad (8.194)$$

The last term represents an irrelevant translation of the surface, so it can be dropped. The resulting formula for the area reads

$$A[\phi] = \frac{1}{4\pi} \int_{-\pi}^{\pi} d\theta \int_{-\pi}^{\pi} d\theta' \frac{\left(C_\mu(\phi(\theta)) - C_\mu(\phi(\theta'))\right)^2}{|e^{\imath \theta} - e^{\imath \theta'}|^2} \quad (8.195)$$

or, after integration by parts and inverting parametrization

$$A[\theta] = \frac{1}{2\pi} \int_{-\pi}^{\pi} d\phi \int_{-\pi}^{\pi} d\phi' C'_\mu(\phi) C'_\mu(\phi') \log \left| \sin \frac{\theta(\phi) - \theta(\phi')}{2} \right| \quad (8.196)$$

Let us now minimize the area as a functional of the boundary parametrization $f(t)$ (we shall stick to the upper half plane). The straightforward variation yields

$$0 = \mathbf{Re} \int_{-\infty}^{+\infty} dt' \frac{C_\mu(f(t')) C'_\mu(f(t))}{(t - t' + i0)^2} \quad (8.197)$$

which duplicates the above diagonality condition (8.185). Note that in virtue of this condition, the normal vector $n_\mu(x)$ is directed towards $\partial_2 X_\mu$ at the boundary. Explicit formula reads

$$n_\mu(C(f(t))) \propto \mathbf{Re} \int_{-\infty}^{+\infty} dt' \frac{C_\mu(f(t'))}{(t - t' + i0)^2} \quad (8.198)$$

Let us have a closer look at the remaining nonlinear integral equation (8.197). In terms of inverse parametrization, it reads

$$0 = \mathbf{Re} \int_{-\infty}^{+\infty} df \frac{C'_\mu(f) C'_\mu(f')}{\tau(f) - \tau(f') + i0} \quad (8.199)$$

Introduce the vector set of analytic functions

$$F_\mu(z) = \int_{-\infty}^{+\infty} df \frac{C'_\mu(f)}{\pi \tau(f) - z} \quad (8.200)$$

which decrease as z^{-2} at infinity. The discontinuity in the real axis

$$\mathbf{Im} F_\mu(\tau + i0) = C'_\mu(f) f'(\tau) \quad (8.201)$$

Which provides the implicit equation for the parametrization $f(\tau)$

$$\int d\tau \mathbf{Im} F_\mu(\tau + i0) = C_\mu(f) \quad (8.202)$$

We see that the imaginary part points in the tangent direction at the boundary. As for the boundary value of the real part of $F_\mu(\tau)$ it points in the normal direction along the surface

$$\mathbf{Re} F_\mu \propto n_\mu \quad (8.203)$$

Inside the surface, there is no direct relation between the derivatives of $X_\mu(\xi)$ and $F_\mu(\xi)$.

The integral equation (8.197) reduces to the trivial boundary condition

$$F_\mu^2(t + i0) = F_\mu^2(t - i0) \quad (8.204)$$

In other words, there should be no discontinuity of F_μ^2 at the real axis. The solution, which is analytic in the upper half plane and z^{-2} decrease at infinity is

$$F_\mu^2(z) = (1 + \omega)^4 P(\omega); \quad \omega = \frac{i - z}{i + z} \quad (8.205)$$

where $P(\omega)$ defined by a series, convergent at $|\omega| \leq 1$. In particular, this could be a polynomial. The coefficients of this series should be found from an algebraic minimization problem, which cannot be pursued forward in the general case.

The flat loops are trivial, however. In this case, the problem reduces to the conformal transformation mapping the loop onto the unit circle. For the unit circle, we have

$$C_1 + i C_2 = \omega; \quad F_1 = i F_2 = -\frac{(1 + \omega)^2}{2}; \quad P = 0. \quad (8.206)$$

Small perturbations around the circle or any other flat loop can be treated systematically by a perturbation theory.

8.19. Kolmogorov triple correlation and time reversal

Are there any restrictions on PDF of circulation from the known asymmetry of velocity correlations, in particular, the Kolmogorov triple correlation? The answer is that the Kolmogorov correlation does not imply the asymmetry of *vorticity* correlations.

Taking the tensor version of the $\frac{4}{5}$ law in arbitrary dimension d

$$\langle v_\alpha(0) v_\beta(0) v_\gamma(r) \rangle = \frac{\mathcal{E}}{(d-1)(d+2)} \left(\delta_{\alpha\gamma} r_\beta + \delta_{\beta\gamma} r_\alpha - \frac{2}{d} \delta_{\alpha\beta} r_\gamma \right) \quad (8.207)$$

and differentiating, we find that

$$\left\langle v_\alpha(0)v_\beta(0)\omega_{\gamma\lambda}(r) \right\rangle = 0 \quad (8.208)$$

So, the odd vorticity correlations could be absent, despite the asymmetry of the velocity distribution.

9. Exact Scaling Index

This section is based on a recent paper published in the '20-ties, after the DNS¹⁰ confirmed area law.

9.1. Introduction

Let us summarize the main equations of the loop dynamics as viewed from the 21st Century. The basic variable in the Loop Equations is circulation around a closed loop in coordinate space.

$$\Gamma_C = \oint_C \vec{v} d\vec{r} \quad (9.1)$$

The PDF for velocity circulation as a functional of the loop

$$P(C, \Gamma) = \left\langle \delta \left(\Gamma - \oint_C \vec{v} d\vec{r} \right) \right\rangle \quad (9.2)$$

with brackets $\langle \rangle$ corresponding to time average or average over random forces, was shown to satisfy certain functional equation (loop equation).

$$\frac{\partial}{\partial \Gamma} \frac{\partial}{\partial t} P(C, \Gamma) = \oint_C dr_i \int d^3\rho \frac{\rho_j}{4\pi|\vec{\rho}|^3} \frac{\delta^2 P(C, \Gamma)}{\delta \sigma_k(r) \delta \sigma_l(r + \rho)} \left(\delta_{ij} \delta_{kl} - \delta_{jk} \delta_{il} \right) \quad (9.3)$$

The area derivative is defined using the difference between $P(C + \delta C, \Gamma) - P(C, \Gamma)$ where an infinitesimal loop δC around the 3d point r is added as an extra connected component of C . In other words, let us assume that the loop C consists of an arbitrary number of connected components $C = \sum C_k$. We add one more infinitesimal loop at some point

away from all C_k . In virtue of the Stokes theorem, the difference comes from the circulation $\oint_{\delta C} \vec{v} d\vec{r}$, which reduces to vorticity at r

$$P(C + \delta C, \Gamma) - P(C, \Gamma) = d\sigma_i(r) \left\langle \omega_i(r) \delta' \left(\Gamma - \oint_C \vec{v} d\vec{r} \right) \right\rangle \quad (9.4)$$

where

$$d\sigma_k(r) = \oint_{\delta C} e_{ijk} r_i dr_j, \quad (9.5)$$

is an infinitesimal vector area element inside δC . In general, for the Stokes type functional, by definition:

$$U[C + \delta C] - U[C] = d\sigma_i(r) \frac{\delta U[C]}{\delta \sigma_i(r)} \quad (9.6)$$

The Stokes condition $\oint_{\delta S} d\sigma_i \omega_i = 0$ for any closed surface δS translates into

$$\oint_{\delta S} d\sigma_i \frac{\delta U[C]}{\delta \sigma_i(r)} = 0 \quad (9.7)$$

The fixed point of the chain of the loop equations (8) was shown to have solutions corresponding to two known distributions: Gibbs distribution and (trivial) global random rotation distribution. In addition, we found the third, nontrivial solution, which is an arbitrary function of minimal area A_C bounded by C .

$$P(C, \Gamma) = F(A_C, \Gamma) \quad (9.8)$$

The Minimal Area can be reduced to the Stokes functional by the following regularization

$$A_C = \min_{S_C} \int_{S_C} d\sigma_i(r_1) \int_{S_C} d\sigma_j(r_2) \delta_{ij} \Delta(r_1 - r_2) \quad (9.9)$$

with

$$\Delta(r) = \frac{1}{r_0^2} \exp \left(-\pi \frac{r^2}{r_0^2} \right); r_0 \rightarrow 0 \quad (9.10)$$

representing two-dimensional delta function, and integration goes over minimized surface S_C (see Fig.37, created with *Mathematica*[®],⁵⁹).

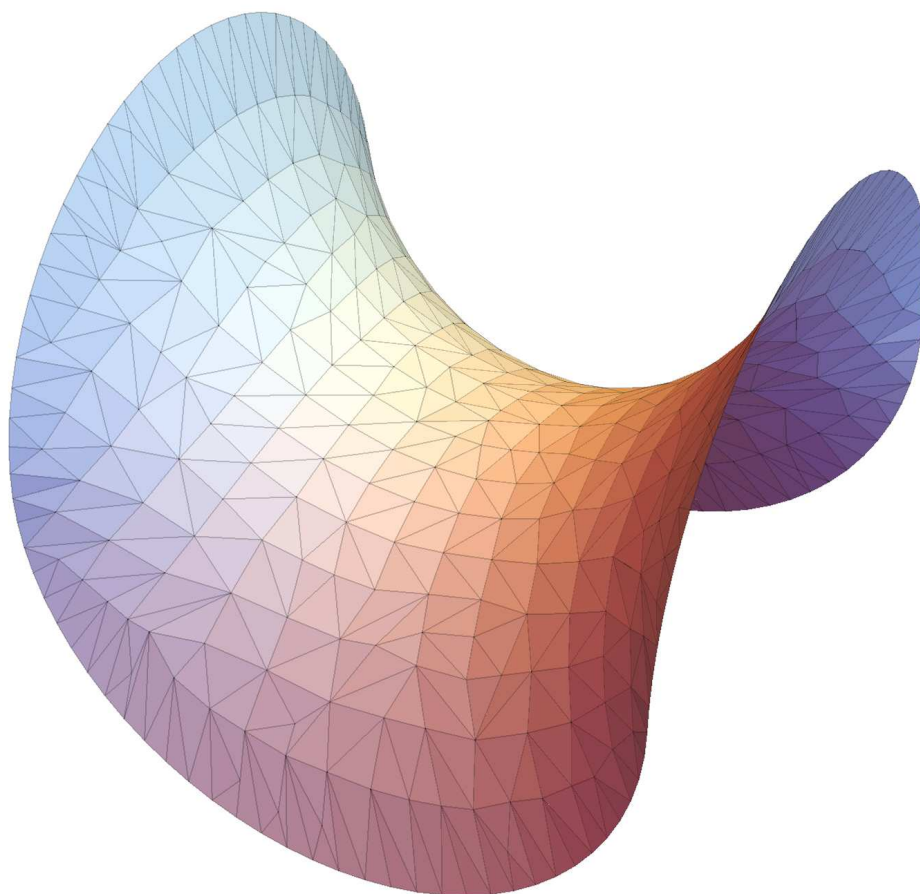


Figure 37: Minimal Surface, topologically equivalent to a disk (sphere with one hole), bounded by curved loop C.

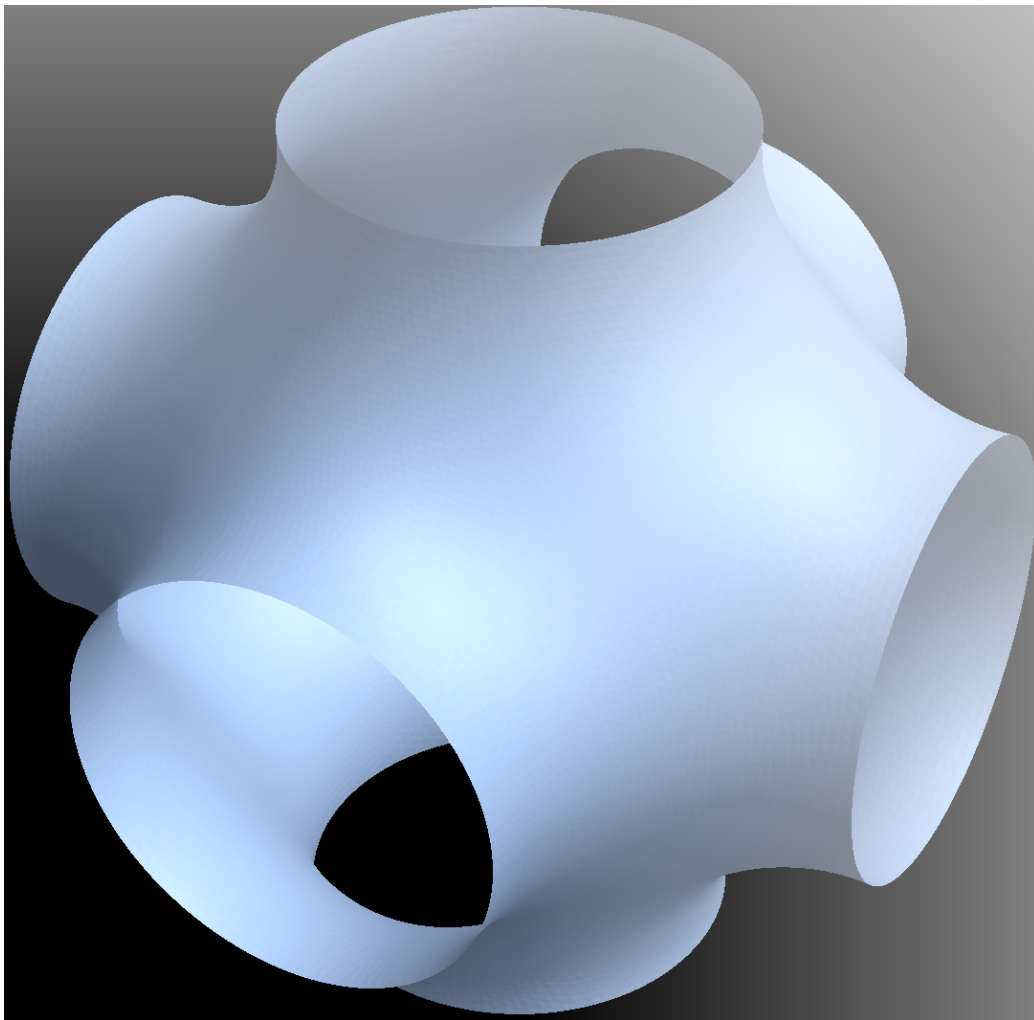


Figure 38: Minimal Surface, topologically equivalent to a sphere with $N = 6$ holes, bounded by loop $C = \sum_{k=1}^6 C_k$.

In the general case, the loop C consists of N closed pieces $C = \sum_{k=1}^N C_k$ and the surface S_C must connect them all so that it is topologically equivalent to a sphere with N holes and no handles (see Fig.37 created with *Mathematica*⁵⁹).

If some pieces are far from others, the minimal surface will make thin tubes reach from one closed loop C_k to another via some central hub where all the tubes grow out of the sphere. In our case, we need only two extra little loops, both close to the initial contour C , but for completeness, we must assume an arbitrary number of closed pieces in C .

In real world this r_0 would be the viscous scale $\left(\frac{\nu^3}{\varepsilon}\right)^{1/4}$. This is a positive definite functional of the surface, as one can easily verify using spectral representation:

$$\int_{S_C} d\sigma_i(r_1) \int_{S_C} d\sigma_j(r_2) \delta_{ij} \Delta(r_1 - r_2) \propto \int d^3k \exp\left(-\frac{k^2 r_0^2}{4\pi}\right) \left| \int_{S_C} d\sigma_i(r) e^{ikr} \right|^2 \quad (9.11)$$

In the limit $r_0 \rightarrow 0$, this definition reduces to the ordinary area:

$$A_C \rightarrow \min_{S_C} \int_{S_C} d^2\zeta \sqrt{g} \quad (9.12)$$

The Stokes condition ((9.7)) follows from the extremum condition. When the surface changes into S' , the linear variation reduces to the surface integral ((9.7)), with $\delta S = S' - S$ being the infinitesimal closed surface between S' and S . This linear variation must vanish by the definition of the minimal surface for the regularized area and its local limit.

The area derivative of the Minimal Area in regularized form, then, as before, reduces to the elimination of one integration (see (10.11))

With this regularization, the area derivative is defined everywhere in space but exponentially decreases away from the surface.

Precisely at the surface it reduces to twice the unit normal vector¹⁶.

¹⁶As for Stokes condition $\partial_i \frac{\delta A_C}{\delta \sigma_i(r)} = 0$ one can readily check in a local coordinate frame where $\vec{r} = (x, y, z)$ and the surface equation is $z = \frac{1}{2} (k_1 x^2 + k_2 y^2)$, that at $r_0 \rightarrow 0$ the Stokes condition reduces to $\int_{-\infty}^{\infty} dx \int_{-\infty}^{\infty} dy \partial_z \Delta(\vec{r}) \propto (k_1 + k_2) = 0$ which is the well-known equation of vanishing mean curvature at a minimal surface.

Should we go to the limit $r_0 \rightarrow 0$ first, we would have to consider the minimal surface connecting the original loop C and infinitesimal loop δC . Such a minimal surface would have a thin tube connecting the point r to \tilde{r} at the original minimal surface along its local normal \vec{n} (see Fig.39).

We are not going to investigate this complex problem here – with the regularized area, we have an explicit formula, and we need this formula only at the boundary in leading log approximation (see¹²).

As we argued in the old paper⁷ we expect scale-invariant solutions, depending on $\gamma = \Gamma A_C^{-\alpha}$ in our scale invariant equations, with some critical index α , yet to be determined. Let us stress again that the Kolmogorov value of the scaling index $\alpha_K = \frac{2}{3}$ does **not** follow from the loop equations; this is an additional assumption based on dimensional counting and Kolmogorov anomaly⁷ for the third moment of velocity. As we stressed in that paper, the Kolmogorov anomaly poses no restrictions on the vorticity correlations and cannot be used to determine our scaling index.

The Area law is expected to be an asymptotic solution at large enough circulations and areas where PDF is small. Such PDF tails are usually interpreted as Kelvinons, or classical solutions in some variables.⁵¹ In our variables, this is the minimal area as a functional of its boundary loops $C = \sum_k C_k$.

This Universal Area Law was confirmed in numerical experiments¹⁰ with Reynolds up to 10^4 with very high accuracy over the whole inertial range of circulations and areas with PDF from 1 down to 10^{-8} . See¹² for analysis of numerical results and their correspondence with Area Law.

Let us present a more conventional physical interpretation of this Area Law.

Let us consider the vorticity field ((10.11)) generated by a minimal surface with thickness r_0 . It rapidly decreases outside the surface and equals twice the normal vector at the surface. The corresponding velocity field will be defined everywhere in space by the integral

$$v_i(r) \propto e_{ijk} \int d^3 r' \frac{r'_j - r_j}{|\vec{r} - \vec{r}'|^3} n_k(\vec{r}') \Delta(r - r') \quad (9.13)$$

In particular, directly at the surface

$$v_i(r) \propto r_0 e_{ijk} \int_{S_C} d^2 r' \frac{r'_j - r_j}{|\vec{r} - \vec{r}'|^3} n_k(r') \quad (9.14)$$

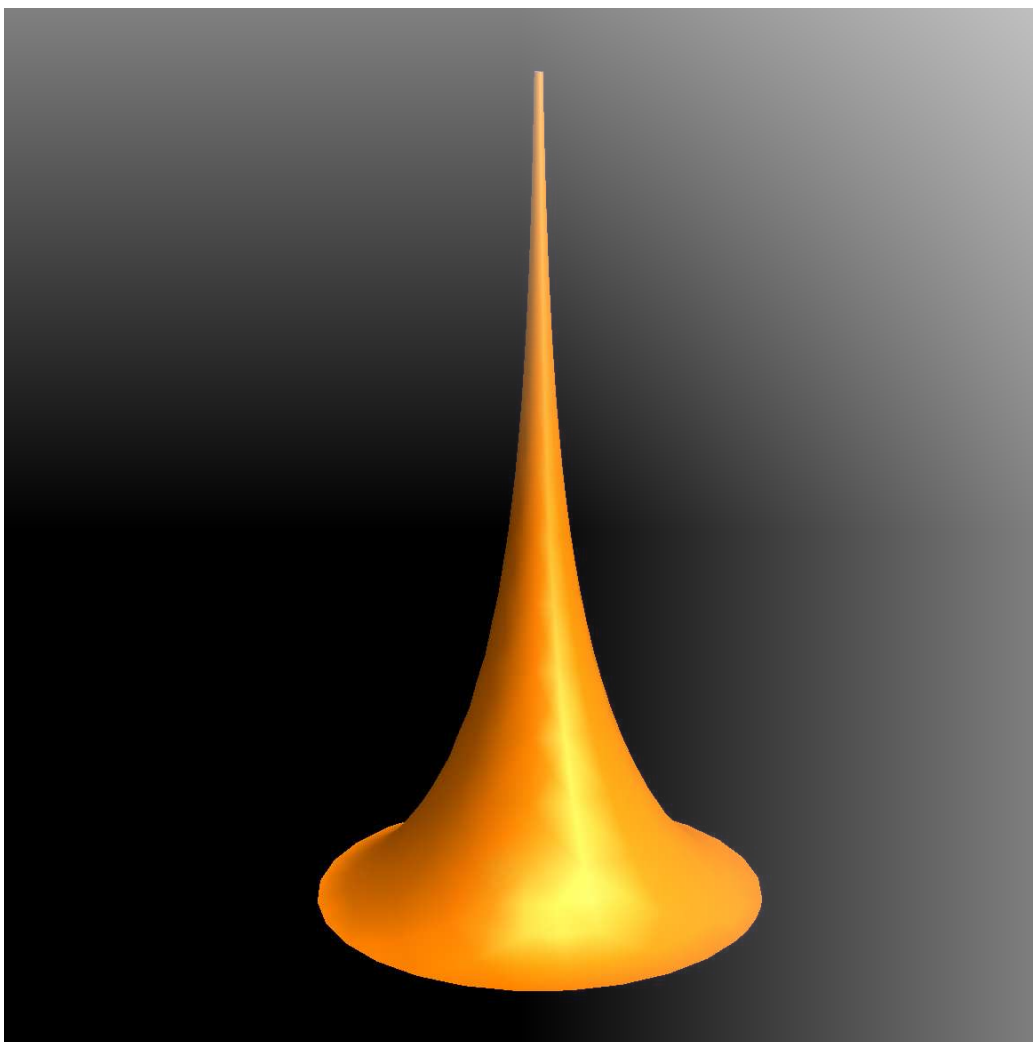


Figure 39: Minimal Surface, stretched to reach a remote point (infinitesimal loop)

If r approaches the edge, this integral logarithmically diverges (we use the frame where the surface normal is directed to z , the local tangent to C goes along x , and the inside tangent vector of the surface at its boundary $\partial S = C$ goes along y , and $\rho = x, y$ are local coordinates on the surface near its edge).

$$\begin{aligned} v_a(C - \epsilon) &\propto r_0 e_{ab} \int_{-\infty}^{\infty} dx \int_0^{\infty} dy \rho_b \left((y + \epsilon)^2 + x^2 \right)^{-\frac{3}{2}} \propto \\ &r_0 \delta_{a1} \int_0^{\infty} dy \frac{y}{(y + \epsilon)^2} \propto r_0 \delta_{a1} \ln \epsilon \end{aligned} \quad (9.15)$$

Now, as is well known (Kelvin theorem, see also¹²)

$$\partial_t \Gamma \propto e_{ijk} \int_C dr_i v_j \omega_k \quad (9.16)$$

In our coordinate frame, using the fact that $\vec{\omega} \propto \vec{n}$ is directed along z

$$\partial_t \Gamma \propto \int_C dx v_2 \quad (9.17)$$

which vanished as $v_2 = 0$. So, the circulation would be conserved for this particular vorticity distributed in an infinitesimal (i.e., viscous) layer around a minimal surface.

We have shown that this is indeed a steady PDF for circulation. However, the velocity field is not steady. The nonlinear term $v_k \partial_k v_i$ does not vanish anywhere in space, including the minimal surface with this vorticity field. Only after the cancellation of $\nabla \left(\frac{v^2}{2} + p \right)$ in the integral over closed loop for $\partial_t \Gamma$ do we get simple local term $e_{ijk} dr_i v_j \omega_k$ which, as we proved, cancels in a leading logarithmic approximation.

9.2. Equation for Scaling Index

Let us start without the assumption of scaling law, with a weaker assumption of some unknown function of the minimal area as the scale of Γ

$$P(C, \Gamma) \rightarrow G(\ln A_C) \Pi(\Gamma G(\ln A_C)) \quad (9.18)$$

The factor of $G(\ln A_C)$ in front of scaling function $\Pi(\gamma)$ follows from the fact that $\Gamma P(C, \Gamma)$ must be scale-invariant, regardless of how effective scale G depends on $\ln A_C$.

Let us derive the self-consistency equation for $G(\ln A)$.

On the one hand:

$$\left\langle \int_{S_C} d\vec{\sigma} \cdot \vec{\omega} \delta' \left(\Gamma - \int_{S_C} d\vec{\sigma} \cdot \vec{\omega} \right) \right\rangle = \partial_\Gamma \left(\left\langle \int_{S_C} d\vec{\sigma} \cdot \vec{\omega} \delta \left(\Gamma - \int_{S_C} d\vec{\sigma} \cdot \vec{\omega} \right) \right\rangle \right) \quad (9.19)$$

$$= \partial_\Gamma \left(\Gamma \left\langle \delta \left(\Gamma - \int_{S_C} d\vec{\sigma} \cdot \vec{\omega} \right) \right\rangle \right) \quad (9.20)$$

$$= \partial_\Gamma \left(\Gamma G(\ln A_C) \Pi \left(\Gamma G(\ln A_C) \right) \right) \quad (9.21)$$

On another hand:

$$\left\langle \int_{S_C} d\vec{\sigma} \cdot \vec{\omega} \delta' \left(\Gamma - \int_{S_C} d\vec{\sigma} \cdot \vec{\omega} \right) \right\rangle = - \left\langle \int_{S_C} d\vec{\sigma} \cdot \frac{\delta}{\delta \vec{\sigma}} \delta \left(\Gamma - \int_{S_C} d\vec{\sigma} \cdot \vec{\omega} \right) \right\rangle \quad (9.22)$$

$$= - \int_{S_C} d\vec{\sigma} \cdot \frac{\delta}{\delta \vec{\sigma}} \left\langle \delta \left(\Gamma - \int_{S_C} d\vec{\sigma} \cdot \vec{\omega} \right) \right\rangle \quad (9.23)$$

$$= - \int_{S_C} d\vec{\sigma} \cdot \frac{\delta}{\delta \vec{\sigma}} \left(G(\ln A_C) \Pi \left(\Gamma G(\ln A_C) \right) \right) \quad (9.24)$$

Recall that at the minimal surface

$$\frac{\delta A_C}{\delta \vec{\sigma}} = 2\vec{n} \quad (9.25)$$

$$\int_{S_C} d\vec{\sigma} \vec{n} = A_C \quad (9.26)$$

Moreover, we find in (9.21):

$$G \left(\Pi(\Gamma G) + \Gamma G \Pi'(\Gamma G) \right) \quad (9.27)$$

and in (9.24):

$$-2 \frac{\partial}{\partial \ln A_C} \left(G(\ln A_C) \Pi(\Gamma G(\ln A_C)) \right) = -2G' (\Pi(\Gamma G) + \Gamma G \Pi'(\Gamma G)) \quad (9.28)$$

Comparing these two expressions, we find the differential equation

$$G' = -\frac{1}{2}G \quad (9.29)$$

with solution

$$G \propto A_C^{-\frac{1}{2}} \quad (9.30)$$

Note that there is no restriction on the PDF scaling function $\Pi(\gamma)$.

Note also that as Γ changes sign on time reversal, we expect the dissipation reflects itself in the asymmetry of PDF. Indeed, as measured in,¹⁰ the left tail of the PDF decreases with a twice larger slope in stretched exponential decay compared to the right tail. As a consequence, the odd moments $\langle \Gamma^p \rangle$ are present even at large p where the right saddle point dominates, and the left saddle point provides exponentially small correction (see discussion below).

9.3. Higher Correlations

Now let us check that this remarkable solution is compatible with the higher correlations.

Let us recall the results:¹²

$$\left\langle \vec{\omega}_1 \dots \vec{\omega}_k \delta \left(\Gamma - \oint_C \vec{v} d\vec{r} \right) \right\rangle = \vec{n}_1 \dots \vec{n}_k A_C^{-\alpha-k(1-\alpha)} \Omega_k \left(\Gamma A_C^{-\alpha} \right) \quad (9.31)$$

The scaling functions $\Omega_k(\gamma)$ with $\Omega_0(\gamma) = \Pi(\gamma)$ being scaling PDF, satisfy recurrent equations :

$$\Omega_{k+1}(\gamma) = 2\alpha\gamma\Omega_k(\gamma) - 2(1-\alpha)k \int_{\gamma}^{\pm\infty} \Omega_k(y) dy \quad (9.32)$$

$$\left\langle \delta \left(\Gamma - \oint_C \vec{v} d\vec{r} \right) \right\rangle = A_C^{-\alpha} \Pi \left(\frac{\Gamma}{A_C^\alpha} \right) \quad (9.33)$$

$$\left\langle \vec{\omega} \delta \left(\Gamma - \oint_C \vec{v} d\vec{r} \right) \right\rangle = 2\alpha \vec{n} \frac{\Gamma}{A_C} \Pi \left(\frac{\Gamma}{A_C^\alpha} \right) \quad (9.34)$$

From the original derivation using the area derivative, it follows that this equation holds on **the whole surface** as well as at its edge C . Therefore, as pointed out in¹² we can integrate this equation over the surface:

$$\left\langle \int_{S_C} d\vec{\sigma}(r) \vec{\omega}(r) \delta \left(\Gamma - \oint_C \vec{v} d\vec{r} \right) \right\rangle = 2\alpha \int_{S_C} d\vec{\sigma}(r) \vec{n}(r) \frac{\Gamma}{A_C} \Pi \left(\frac{\Gamma}{A_C^\alpha} \right) \quad (9.35)$$

On the left side we obtain $\int_{S_C} d\vec{\sigma}(r) \vec{\omega}(r) = \Gamma$ in virtue of the δ function, and on the right side we get $\int_{S_C} d\vec{\sigma}(r) \vec{n}(r) = A_C$. As a result, after canceling Γ , we obtain the equation:

$$\Pi \left(\frac{\Gamma}{A_C^\alpha} \right) = 2\alpha \Pi \left(\frac{\Gamma}{A_C^\alpha} \right) \quad (9.36)$$

from which we conclude that

$$\alpha = \frac{1}{2} \quad (9.37)$$

as we already found in the previous section 9.

With the next equation, though, things are getting tricky, and this is where we got stuck in:¹²

$$\left\langle \omega_1 \omega_2 \delta \left(\Gamma - \oint_C \vec{v} d\vec{r} \right) \right\rangle = n_1 n_2 A_C^{-\frac{3}{2}} \Omega_2 \left(\Gamma A_C^{-\frac{1}{2}} \right) \quad (9.38)$$

with

$$\Omega_2(\gamma) = \gamma^2 \Pi(\gamma) - \int_{\gamma}^{\pm\infty} \Pi(y) y dy \quad (9.39)$$

Integrating over the surface, we get, as before, after going to scaling variables and setting $\alpha = \frac{1}{2}$, on the left :

$$\gamma^2 \Pi(\gamma) \quad (9.40)$$

and on the right

$$\gamma^2 \Pi(\gamma) - \int_{\gamma}^{\pm\infty} \Pi(y) y dy \quad (9.41)$$

Everything stops! The left part does not match the right part.

Here is what we are missing: the contact terms. The correlations of vorticity were obtained, assuming the points do not coincide. In general, we can expect extra contact term:

$$\left\langle \omega_1 \omega_2 \delta \left(\Gamma - \oint_C \vec{v} d\vec{r} \right) \right\rangle = n_1 n_2 A_C^{-\frac{3}{2}} \Omega_2 \left(\Gamma A_C^{-\frac{1}{2}} \right) + X \delta_{12} \delta^2(1-2) \quad (9.42)$$

where X is to be determined, δ_{12} is Kronecker delta for vector indexes, and $\delta^2(1-2)$ is an invariant delta function on the surface. These contact terms display themselves only in the integral relations we have here and do not change correlations at far away points (which was assumed in¹²). With this term present, we get a perfect match if

$$X = \int_{\gamma}^{\pm\infty} \Pi(y) y dy \quad (9.43)$$

What could be the origin of such a term? Let us consider the second derivative of (9.42) by Γ . On the left, we find

$$\begin{aligned} \left\langle \omega_1 \omega_2 \delta'' \left(\Gamma - \oint_C \vec{v} d\vec{r} \right) \right\rangle &= \frac{\delta^2}{\delta\sigma(1)\delta\sigma(2)} \left\langle \delta \left(\Gamma - \oint_C \vec{v} d\vec{r} \right) \right\rangle = \\ &= \frac{\delta^2}{\delta\sigma(1)\delta\sigma(2)} A_C^{-\frac{1}{2}} \Pi \left(\frac{\Gamma}{A_C^{\frac{1}{2}}} \right) \end{aligned} \quad (9.44)$$

The contact term precisely of the form we need comes from the second functional derivative of A_C

$$\frac{\delta^2 A_C}{\delta\sigma(1)\delta\sigma(2)} \partial_A A^{-\frac{1}{2}} \Pi \left(\Gamma A^{-\frac{1}{2}} \right) = 2\delta_{12} \delta^2(1-2) \partial_A A^{-\frac{1}{2}} \Pi \left(\Gamma A^{-\frac{1}{2}} \right) \quad (9.45)$$

The rest of the terms were accounted for in recurrent equations for vorticity expectation values in,¹² but this one was missed (or, better to say,

ignored as we assumed all points were separate). The derivative of the X term matches this one as

$$\partial_\gamma^2 \int_\gamma^{\pm\infty} \Pi(y) y dy = -(\Pi(\gamma) + \gamma \Pi'(\gamma)) \quad (9.46)$$

and

$$2\partial_A A^{-\frac{1}{2}} \Pi \left(\Gamma A^{-\frac{1}{2}} \right) \propto -(\Pi(\gamma) + \gamma \Pi'(\gamma)) \quad (9.47)$$

Here we dropped factors of A_C as they are known to match by dimensional counting. So, the contact terms from the second functional derivative precisely match the missing terms in the self-consistency relation for the two-point function.

Let us present the result for the next correlation functions with corrected coefficients at $\alpha = \frac{1}{2}$, which were created in *Mathematica*[®] using symbolic integration by parts:

$$\Omega_1(\gamma) = \gamma \Pi(\gamma) \quad (9.48)$$

$$\Omega_2(\gamma) = \gamma^2 \Pi(\gamma) - \int_\gamma^{\pm\infty} y \Pi(y) dy \quad (9.49)$$

$$\Omega_3(\gamma) = \gamma^3 \Pi(\gamma) - 3 \int_\gamma^{\pm\infty} \gamma y \Pi(y) dy \quad (9.50)$$

$$\Omega_4(\gamma) = \gamma^4 \Pi(\gamma) + \frac{3}{2} \int_\gamma^{\pm\infty} y (y^2 - 5\gamma^2) \Pi(y) dy \quad (9.51)$$

$$\Omega_5(\gamma) = \gamma^5 \Pi(\gamma) + \frac{5}{2} \int_\gamma^{\pm\infty} \gamma y (3y^2 - 7\gamma^2) \Pi(y) dy \quad (9.52)$$

$$\Omega_6(\gamma) = \gamma^6 \Pi(\gamma) - \frac{15}{8} \int_\gamma^{\pm\infty} y (21\gamma^4 + y^4 - 14\gamma^2 y^2) \Pi(y) dy \quad (9.53)$$

$$\Omega_7(\gamma) = \gamma^7 \Pi(\gamma) - \frac{21}{8} \int_\gamma^{\pm\infty} \gamma y (33\gamma^4 + 5y^4 - 30\gamma^2 y^2) \Pi(y) dy \quad (9.54)$$

$$\dots \quad (9.55)$$

9.4. Discussion

The main result of this work is an exact computation of the critical index from self-consistency of the Minimal Area solution of the Loop Equations. With correct recurrent equations (9.32), the contact terms needed

for consistency of surface integrals of the vorticity correlation functions naturally arise from second functional derivatives of the regularized area ((9.9)).

The ends start meeting in this exotic solution, which initially raised so much confusion 26 years ago. However, does it meet the numerical experiment?

Initially, the authors of that experiment¹⁰ interpreted their results for the log-log derivative

$$\lambda(p) = \frac{d \log \langle |\Gamma|^p \rangle}{d \log \sqrt{A_C}} \quad (9.56)$$

as some bi-fractal model, switching from K41 value $\lambda(p) = \frac{4p}{3}$ at $p < 4$ to another slope $\lambda(p) \approx 1.16p$ at $4 \leq p \leq 10$. The linear fit of their data is not perfect; one can see that the slope $\frac{\lambda(p)}{p}$ is never a constant – it is greater than $\frac{4}{3}$ at small p and steadily decreases.

According to our theory, it should reach $\lambda(p) \rightarrow p$. The finite moments are not expected to obey the Area law – this is an opposite limit of large Γ , which corresponds to the saddle point Γ_0 in the moments integral after switching to $\ln \Gamma$ as integration variable

$$\begin{aligned} \langle |\Gamma|^p \rangle &= \int_0^\infty d\Gamma \Gamma^p P(\Gamma, C) \propto \\ \Gamma_0^{p+1} P(\Gamma_0, C) &\left(-(\Gamma_0 \partial_{\Gamma_0})^2 \ln P(\Gamma_0, C) \right)^{-\frac{1}{2}} (1 + \dots); \end{aligned} \quad (9.57)$$

$$p + 1 + \Gamma_0 \partial_{\Gamma_0} \ln (P(\Gamma_0, C)) = 0 \quad (9.58)$$

Here ... stand for higher corrections to the saddle point integration, related to higher derivatives $(\Gamma_0 \partial_{\Gamma_0})^n \ln P(\Gamma_0, C)$, $n > 2$ in Taylor expansion near the saddle point. For power-like $\ln P(\Gamma, C)$, these corrections go in inverse powers of p .

The largest of two possible saddle points at positive and negative Γ determines the asymptotic behavior of the moments. Another saddle point provides exponential corrections at large p . We expect the positive saddle point to dominate, as it decreases slower in numerical experiments,¹⁰ so we only use the $\Gamma > 0$ integral.

This saddle point at large p would approach the region of large Γ where we expect Area law to hold. Technically it is simpler to treat Γ_0

as a large independent variable and the saddle point equation (9.58) as a parametric equation for $p(\Gamma_0)$. In that case, one can explicitly compute all the terms to any order in the WKB expansion around the saddle point.

In practice, such saddle point approximations may be very accurate even for small p , as the Stirling formula for the Gamma function shows. This numerical luck explains the validity of the Area Law in a whole inertial range and even small moments.

Let us assume the following correction

$$\lambda(p) \rightarrow 2\alpha p + \beta \ln p \quad (9.59)$$

where the coefficient β is not universal and can depend on the shape of the loop and the area.¹⁷

The p dependence can be compared with experimental data¹⁸ at maximal available Reynolds number 1300. The following parameters fit the data at $p = 3, \dots, 10$ with adjusted $R_2 = 0.999991$ which means extremely well:

$$\alpha = 0.49 \pm 0.02 \quad (9.60)$$

$$\beta = 0.92 \pm 0.01 \quad (9.61)$$

We performed statistical analysis with *Mathematica*®. Let us compare with the experiment our asymptotic formula for the ratio $\frac{\lambda(p)}{p}$. (see Fig. 40). As we can see, the green curve passes within error bars through all the data points at $p = 3, \dots, 10$.

For those who do not believe in fitting, here is the plot of pure experimental data with error bars for $\frac{\lambda(p)-p}{\ln p}$ in a wider range of p including small p where we do not expect it to be constant.

It is consistent with the assumption of a constant limit, take a piece of paper and place its edge across the data points.

We take it as another validation of the Area Law. However, more experiments at higher Reynolds numbers would be needed to verify asymptotic index $\alpha = \frac{1}{2}$ with two or more significant digits. The ratio $\frac{\lambda(p)}{p}$

¹⁷This β term corresponds to some pre-exponential power of p^ξ in the moment $\langle \Gamma^p \rangle$ with the index ξ depending on $\ln A_C$ so that $\beta = 2\partial_{\ln A} \xi$.

¹⁸This data was shared with me by Kartik P. Iyer.

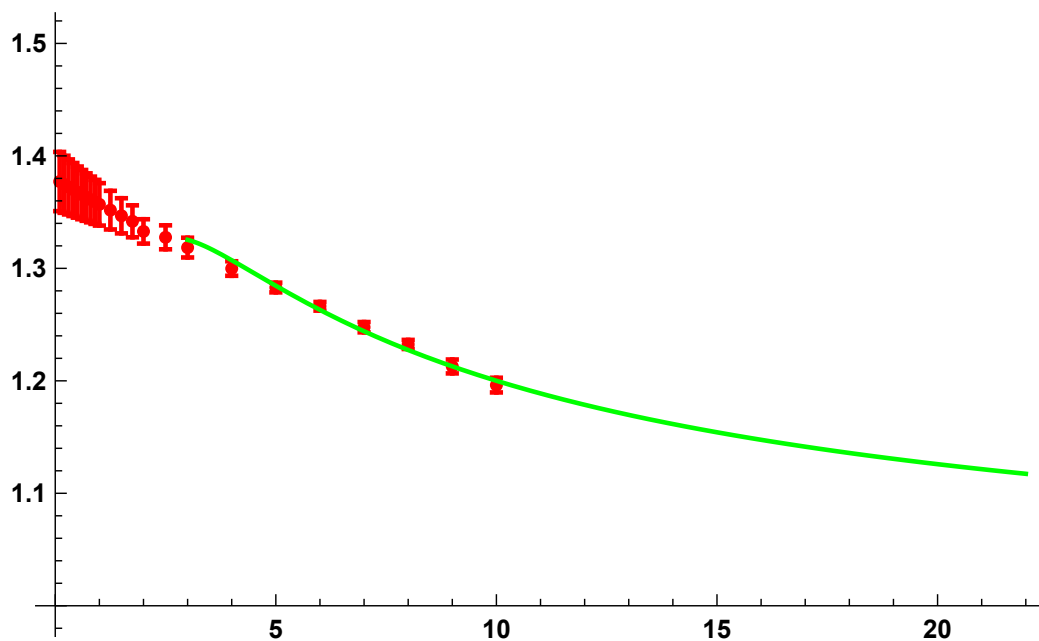


Figure 40: Effective index $\frac{\lambda(p)}{p}$ from 10^0 with our asymptotic fit (green): $\frac{\lambda(p)}{p} \approx 0.987832 + 0.921675 \frac{\log p}{p}$

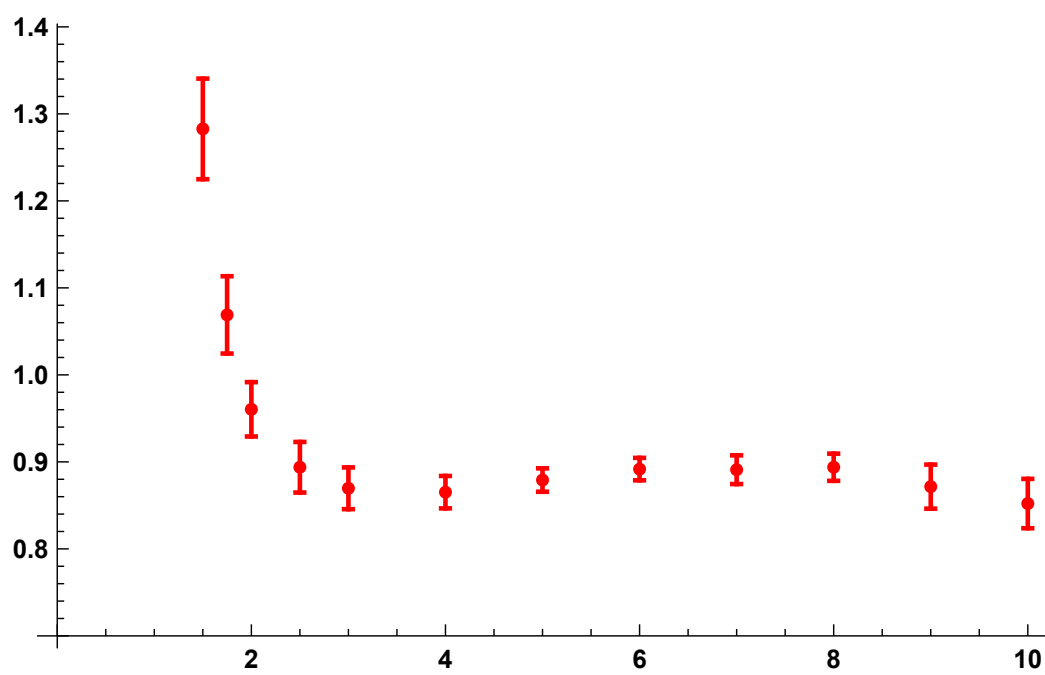


Figure 41: Experimental data for the ratio $\frac{\lambda(p)-p}{\ln p}$ from.¹⁰

is falling up to $p = 10$ and would keep falling after that as $\frac{\ln p}{p}$ according to our current fit. So, what happens with the experiment for $p = 11, \dots, 20$?

If we start believing the Minimal Surface, we have to try and see how the correlation between two circulations Γ_1, Γ_2 around planar loops in the xy plane depends upon the separation between these loops in the orthogonal direction z . (see Fig.42).

When the small loop starts inside the big one and moves in the z direction, the minimal surface will grow like a tower between these two loops. In the limit of a small loop much less than the big one (see Fig.39), we must approach the vorticity correlation as a function of the normal distance to the minimal surface for the large square (see Fig. 39). How does that correlation depend on z ?

Also, the "soccer gate" loop (made of two perpendicular squares touching one side) makes an even more interesting test than we suggested before. One could verify that mean vorticity is directed along the normal to the minimal surface anywhere at this surface, not just at the edge. Here is the minimal Surface for Soccer Gates loop, created with *Mathematica*[®] package⁵⁹(see Fig. 43).

10. Area Law

This section is based on a recent paper published in the '20-ties, after the DNS¹⁰ confirmed area law.

10.1. Introduction

In the previous two papers,^{12, 13} we reviewed and advanced the Minimal Area Solution⁷ for the Loop Equation in turbulence, which was recently verified experimentally.¹⁰ Let us repeat this theory's latest revision before advancing it further.

The basic variable in the Loop Equations is circulation around a closed loop in coordinate space $\oint_C v_\alpha dr_\alpha$.

The PDF for velocity circulation as a functional of the loop

$$P(C, \Gamma) = \left\langle \delta \left(\Gamma - \oint_C \vec{v} d\vec{r} \right) \right\rangle \quad (10.1)$$

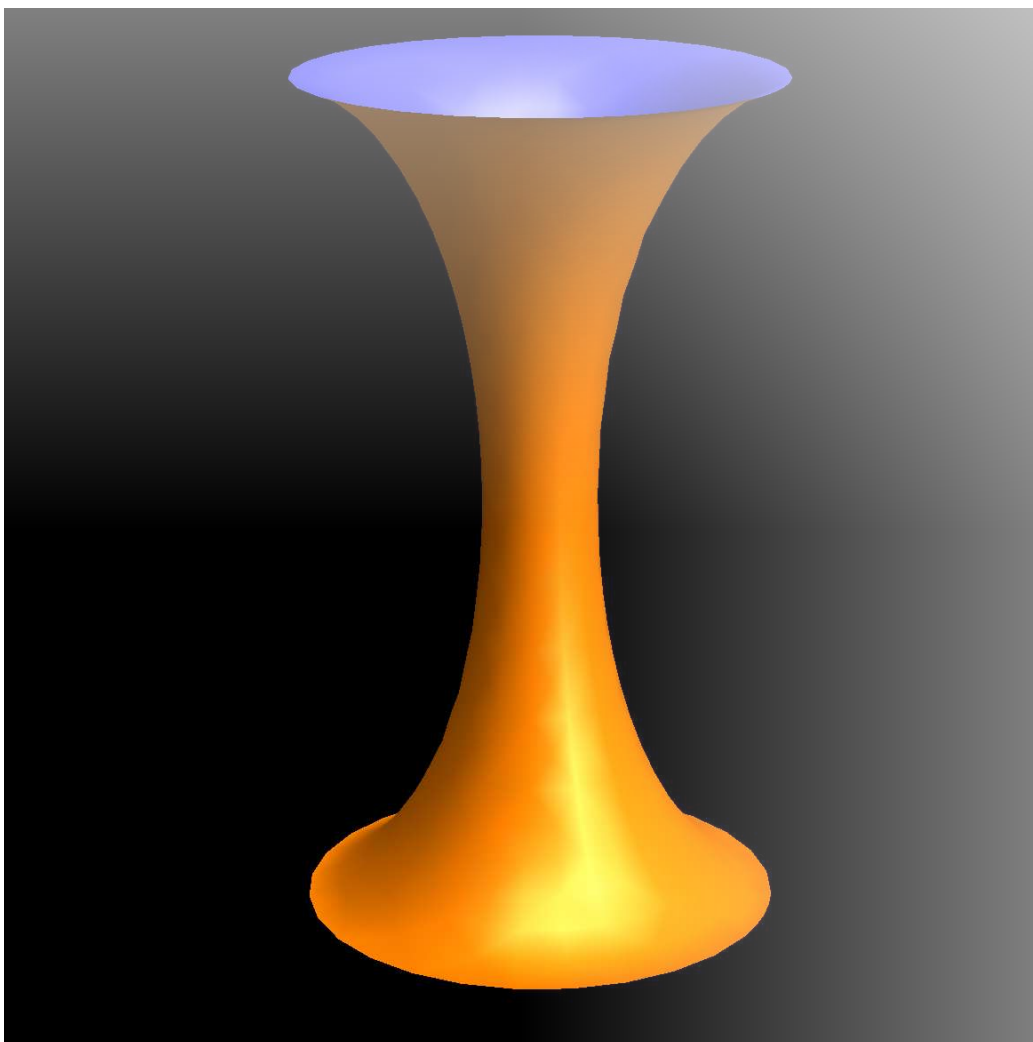


Figure 42: Tube-like minimal surface connecting two separated loops.

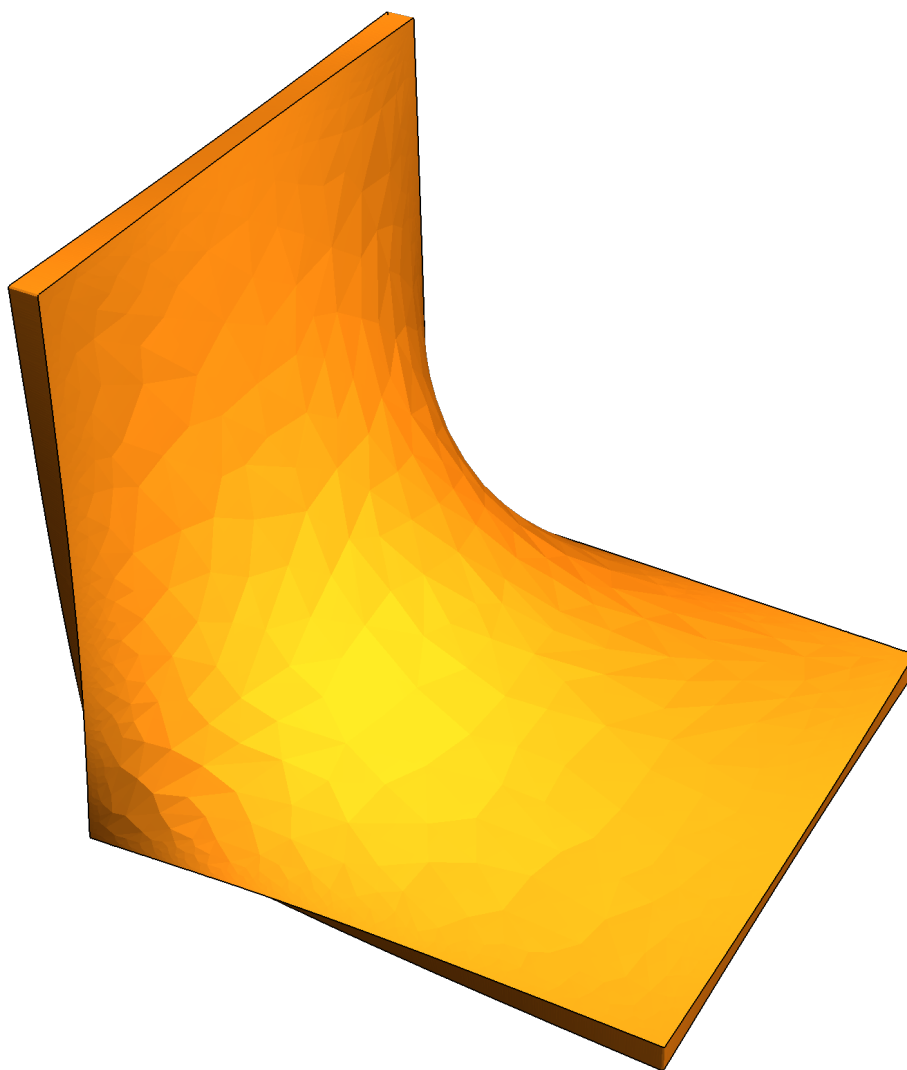


Figure 43: Minimal Surface bounded by soccer gates. Artificial thickness imitates viscosity effects.

with brackets $\langle \rangle$ corresponding to time average or average over random forces, was shown to satisfy certain functional equation (loop equation).

$$\frac{\partial}{\partial \Gamma} \frac{\partial}{\partial t} P(C, \Gamma) = \oint_C dr_i \int d^3 \rho \frac{\rho_j}{4\pi|\vec{\rho}|^3} \frac{\delta^2 P(C, \Gamma)}{\delta \sigma_k(r) \delta \sigma_l(r + \rho)} \left(\delta_{ij} \delta_{kl} - \delta_{jk} \delta_{il} \right) \quad (10.2)$$

The area derivative is defined using the difference between $P(C + \delta C, \Gamma) - P(C, \Gamma)$ where an infinitesimal loop δC around the 3d point r is added as an extra connected component of C . In other words, let us assume that the loop C consists of an arbitrary number of connected components $C = \sum C_k$. We add one more infinitesimal loop at some point away from all C_k . In virtue of the Stokes theorem, the difference comes from the circulation $\oint_{\delta C} \vec{v} d\vec{r}$, which reduces to vorticity at r

$$P(C + \delta C, \Gamma) - P(C, \Gamma) = d\sigma_i(r) \left\langle \omega_i(r) \delta' \left(\Gamma - \oint_C \vec{v} d\vec{r} \right) \right\rangle \quad (10.3)$$

where

$$d\sigma_k(r) = \frac{1}{2} \oint_{\delta C} e_{ijk} r_i dr_j \quad (10.4)$$

is an infinitesimal vector area element inside δC . In general, for the Stokes type functional, by definition:

$$U[C + \delta C] - U[C] = d\sigma_i(r) \frac{\delta U[C]}{\delta \sigma_i(r)} \quad (10.5)$$

The Stokes condition $\partial_i \omega_i(r) = 0$ translates into

$$\partial_i \frac{\delta U[C]}{\delta \sigma_i(r)} = 0 \quad (10.6)$$

where $\partial_i = \frac{\partial}{\partial r_i}$ is an ordinary spatial derivative rather than a singular loop derivative introduced in the Non-Abelian Loop Equations.

The fixed point of the chain of the loop equations (10.2) was shown to have a solution which is an arbitrary function of minimal area A_C bounded by C .

$$P(C, \Gamma) = F(A_C, \Gamma) \quad (10.7)$$

The Minimal Area can be reduced to the Stokes functional by the regularization (9.9).

In real world this r_0 would be the viscous scale $\left(\frac{\nu^3}{\varepsilon}\right)^{1/4}$. This is a positive definite functional of the surface, as one can easily verify using spectral representation:

$$\int_{S_C} d\sigma_i(r_1) \int_{S_C} d\sigma_j(r_2) \delta_{ij} \Delta(r_1 - r_2) \propto \int d^3k \exp\left(-\frac{k^2 r_0^2}{4\pi}\right) \left| \int_{S_C} d\sigma_i(r) e^{ikr} \right|^2 \quad (10.8)$$

In the limit $r_0 \rightarrow 0$, this definition reduces to the ordinary area:

$$A_C \rightarrow \min_{S_C} \int_{S_C} d^2\zeta \sqrt{g} \quad (10.9)$$

10.2. Stokes Condition and Mean Curvature

Let us study this amazing duality of Minimal Surface to turbulent flow. First of all, why a minimal surface? No string theory would require this minimal surface to arise as a classical solution (or at least we do not know any well-defined string theory equivalent to turbulence despite some interesting observations⁵⁵).

The Stokes condition ((10.6)) is satisfied by the minimum condition. When the surface changes into S' , the linear variation reduces by volume Stokes theorem to

$$\oint_{S'-S} d\sigma_i(r) \frac{\delta U[C]}{\delta \sigma_i(r)} = \int_{\delta V} d^3r \partial_i \frac{\delta U[C]}{\delta \sigma_i(r)} \quad (10.10)$$

with δV being infinitesimal volume between S' and S . This linear variation must vanish by the definition of the minimal surface for the regularized area and its local limit.

The area derivative of the Minimal Area in regularized form, then, as before, reduces to the elimination of one integration

$$\frac{\delta A_C}{\delta \sigma_i(r)} = 2 \int_{S_C} d\sigma_i(\rho) \Delta(r - \rho) \rightarrow 2n_i(\tilde{r}) \exp\left(-\pi \frac{r_\perp^2}{r_0^2}\right) \quad (10.11)$$

Where $n_i(\tilde{r})$ is the local normal vector to the minimal surface at the nearest surface point \tilde{r} to the 3d point r , and r_\perp is the component normal to the surface at \tilde{r} . With this regularization, the area derivative is defined everywhere in space but exponentially decreases away from the surface. Exactly at the surface, it reduces to twice the normal unit vector.

Let us investigate this issue in more detail.

Let us choose x, y coordinates in a local tangent plane to the minimal surface at some point which we set as an origin. In the quadratic approximation (which will be enough for our purpose), the equation of the surface reads:

$$z = \frac{1}{2} (K_1 x^2 + K_2 y^2) \quad (10.12)$$

$$n = \frac{[-K_1 x, -K_2 y, 1]}{\sqrt{1 + K_1^2 x^2 + K_2^2 y^2}} \quad (10.13)$$

where K_1, K_2 are main curvatures in planes $y = 0, x = 0$.

Now, at $r_0 \rightarrow 0$, the Stokes condition reduces to :

$$\int_{-\infty}^{\infty} dx \int_{-\infty}^{\infty} dy \partial_z \Delta(\vec{r}) \quad (10.14)$$

$$\propto \int_{-\infty}^{\infty} dx \int_{-\infty}^{\infty} dy \frac{z}{r_0^4} \exp\left(-\pi \frac{x^2 + y^2}{r_0^2}\right) \quad (10.15)$$

$$\propto \int_{-\infty}^{\infty} dx \int_{-\infty}^{\infty} dy \frac{K_1 x^2 + K_2 y^2}{r_0^4} \exp\left(-\pi \frac{x^2 + y^2}{r_0^2}\right) \quad (10.16)$$

$$\propto K_1 + K_2 = 0 \quad (10.17)$$

This sum is the mean curvature. So, the Stokes condition is **equivalent** to the equation for the minimal surface. It is nice to know!

10.3. Loop Equation Beyond Logarithmic Approximation

An important unanswered question in our recent papers^{12,13} is whether the loop equation was satisfied beyond the leading logarithmic approximation.

Within the Area law Ansatz, the steady solution of the loop equation (10.2) reduces in the limit $r_0 \rightarrow 0$ to:

$$r_0 \oint_C dr_i \int_{S_C} d\sigma(r') \frac{(r'_i - r_i) n_k(r) n_k(r') - n_i(r') (r'_k - r_k) n_k(r)}{|\vec{r}' - \vec{r}|^3} = 0 \quad (10.18)$$

Here $d\sigma(r') = |d\vec{\sigma}(r')|$ is the scalar area element for the point \vec{r}' at the surface. The distance $r_i - r'_i$ is measured in Euclidean space rather than along the surface. The factor of r_0 implies that the time derivative of our PDF is very small in the limit when viscosity goes to zero. In the d -dimensional problem, the factor would be r_0^{d-2} , and in particular, in two dimensions, there would be no factor. By renormalizing time:

$$t = \tau T_0; T_0 = \frac{A_C}{|\Gamma|} \left(\frac{A_C}{r_0^2} \right)^{\frac{d-2}{2}} \quad (10.19)$$

we eliminate this factor from the loop equation altogether. However, remember that reaching the equilibrium PDF we are investigating would take a large time T_0 at $d > 2$. (we reinserted here missing dimensional factors).

After dropping the factor r_0 in 3 dimensions:

$$\oint_C dr_i \int_{S_C} d\sigma(r') \frac{(r'_i - r_i)n_k(r)n_k(r') - n_i(r')(r'_k - r_k)n_k(r)}{|\vec{r}' - \vec{r}|^3} = 0 \quad (10.20)$$

This formula is the final form of the Loop Equation for steady PDF, depending on the minimal area.

10.4. Exact Solution for Flat Loop

Here is the biggest news of this paper: the minimal surface **exactly** solves the loop equation for a flat loop.

The thing is that at a flat loop (in the x, y plane) the minimal surface is flat as well so that both $\vec{n}(r) = \vec{n}(r') = (0, 0, 1)$ which makes the second term in (10.20) zero. As for the first term, it reduces to the gradient and vanishes after integration over a closed loop:

$$\oint_C dr_i \int_{S_C} d\sigma(r') \frac{(r'_i - r_i)}{|\vec{r}' - \vec{r}|^3} \propto \int_{S_C} d\sigma(r') \oint_C dr_i \partial_{r_i} \frac{1}{|\vec{r}' - \vec{r}|} = 0 \quad (10.21)$$

So, we claim that this is not just an asymptotic solution for the tails of the PDF; this is the exact solution.

In the case of 2D turbulence, where all loops are planar, vorticity is pseudoscalar, and the normal vector is $n = \pm 1$ depending on the

orientation of the loop, the loop equation for the minimal surface Ansatz reads

$$\oint_C dr_i \int_{S_C} d\sigma(r') \frac{(r'_i - r_i)}{|\vec{r}' - \vec{r}|^2} \propto \int_{S_C} d\sigma(r') \oint_C dr_i \partial_{r_i} \ln |\vec{r}' - \vec{r}| = 0 \quad (10.22)$$

Let us return to the loop equation's exact solution in three dimensions for a planar loop. In that case, it must apply to the moments of the circulation, in particular, to the second moment

$$\langle \Gamma^2 \rangle = A_C \int_{-\infty}^{\infty} d\gamma \gamma^2 \Pi(\gamma) \quad (10.23)$$

This formula raised objections¹⁹: one can explicitly compute this double integral

$$\langle \Gamma^2 \rangle = \oint_C dr_i \oint_C dr'_j \langle v_i(r) v_j(r') \rangle \quad (10.24)$$

taking the scaling law $\langle v_i(r) v_j(r') \rangle \propto \delta_{ij} |r - r'|^{2\alpha-1}$ where α is the scaling index of circulation in terms of the area. Integral looks nothing like an area, and, say, for the rectangle, it shows manifest dependence upon the aspect ratio at a fixed area.

Our answer is very simple: this is so for Kolmogorov index $\alpha = \frac{2}{3}$ as well as any other index except our prediction²⁰ $\alpha = \frac{1}{2}$. In this exceptional case, the second moment can be directly proven equal to the area.

Namely, in case $2\alpha = 1$, the velocity has zero dimension, so its correlator is proportional to $\ln |\vec{r} - \vec{r}'|$. The double loop integral by Stokes

¹⁹Sasha Polyakov, private communication.

²⁰Note that the argument of¹³ applies to an arbitrary dimension of space, as long as the vorticity surface was 2-dimensional.

theorem reduces to a double area integral

$$\langle \Gamma^2 \rangle = \oint_C dr_i \oint_C dr'_j \langle v_i(r) v_j(r') \rangle = \quad (10.25)$$

$$\int_{S_C} d\sigma(r) \int_{S_C} d\sigma(r') \langle \omega_3(r) \omega_3(r') \rangle \propto \quad (10.26)$$

$$\int_{S_C} d\sigma(r) \int_{S_C} d\sigma(r') \nabla^2 \ln |\vec{r} - \vec{r}'| \propto \quad (10.27)$$

$$\int_{S_C} d\sigma(r) \int_{S_C} d\sigma(r') \delta(\vec{r} - \vec{r}') = A_C \quad (10.28)$$

Q.E.D.

We also claim that for our solution, all higher moments are proportional to the powers of the area for the flat loop. However, this is hard to verify directly, as we have yet to determine the exact form of higher-order velocity correlations.

Note, however, that the same logarithmic velocity correlator in 3D space, as required to compute the second moment for a non-planar loop, will no longer produce δ functions for vorticity correlations. We may use the Stokes theorem and integrate it over some curved surface, but the vorticity correlator

$$\langle \omega_i(r) \omega_j(r') \rangle \propto (\delta_{ij} \partial^2 - \partial_i \partial_j) \ln |\vec{r} - \vec{r}'| \quad (10.29)$$

will have long term tails $\propto \frac{1}{(\vec{r} - \vec{r}')^2}$ unless taken on a flat surface. Therefore, our solution does not imply a short-range correlation of vorticity, just that it has a scaling dimension -1 .

An interesting property of our solution is that it leaves the scaling function arbitrary as long as it depends upon the minimal area. The dependence of higher vorticity correlations in a circulation background is uniquely expressed in the basic PDF scaling function, but this function remains arbitrary.

We shall accept the solution for the planar loop and try to generalize it for the non-planar one.

10.5. Loop Equation in Quadratic approximation

Let us introduce a local quadratic approximation to a surface, as before (with $K_1 = K, K_2 = -K$), and $n(r')$ given by (10.13), with z direction

being the local normal vector at the contour. The curvature K refers to the integration point r .

As we found the minimal surface in Appendix H in,⁷ the conformal coordinates at the boundary are consistent with these x, y in quadratic approximation: x goes along the local tangent direction of the loop, and y goes inside the surface. As for z it goes along the normal to the surface $n(r)$. We take r as an origin. The loop C expands as a piece of parabola in xy plane:

$$C_1 = x \quad (10.30)$$

$$C_2 = bx^2 \quad (10.31)$$

$$C_3 = 0 \quad (10.32)$$

Therefore the surface integral in the quadratic approximation of the integrand in $\oint_C dr_i$ becomes:

$$\int_{-\infty}^{\infty} dy \int_{-\infty}^{\infty} x dx \theta(y - bx^2) \frac{1 + \frac{K^2}{2} (x^2 - y^2)}{\sqrt{(x^2 + y^2)^3 (1 + K^2 (x^2 + y^2))}} \quad (10.33)$$

This integral vanishes by reflection symmetry $x \rightarrow -x$.

However, there is no reason to expect this reflection symmetry to hold beyond quadratic approximation. Cubic terms in the contour equation alone would destroy this reflection symmetry.

10.6. Minimal Area In Conformal Metric Field

The computations in the previous Section 10.5 suggest the following "conformal" Ansatz

$$A_C[\phi] = \min_{S_C} \int_{S_C} d\sigma_i(r_1) \int_{S_C} d\sigma_j(r_2) \delta_{ij} \Delta(r_1 - r_2) \exp \left(\frac{1}{2} (\phi(r_1) + \phi(r_2)) \right) \quad (10.34)$$

where conformal metric $\phi(r)$ is some external field defined in all R_3 , not just on the surface.

The local limit of this functional $A_C[\phi]$ tends to be the area in the external conformal metric

$$A_C[\phi] \xrightarrow{r_0 \rightarrow 0} \int_{S_C} d\sigma(r) \exp \left(\phi(R(x)) \right) \quad (10.35)$$

$$d\sigma(r) = \sqrt{(d\sigma_i(r))^2} = d^2x \sqrt{\det G} \quad (10.36)$$

with induced metric tensor, corresponding to parametric equation $\vec{r} = \vec{R}(x)$, $x = (u, v)$ of the surface S_C

$$G_{ab}(x) = \partial_a R_\mu(x) \partial_b R_\mu(x) \quad (10.37)$$

We derive an equation for ϕ later but now consider this area in the external field $A_C[\phi]$ as a functional of the surface at fixed external field $\phi(r)$. First of all, one can verify that this is a positive definite functional, just as before

$$\int_{S_C} d\sigma_i(r_1) \int_{S_C} d\sigma_j(r_2) \delta_{ij} \Delta(r_1 - r_2) \exp\left(\frac{1}{2}(\phi(r_1) + \phi(r_2))\right) \quad (10.38)$$

$$\propto \int d^3k \exp\left(-\frac{k^2 r_0^2}{4\pi}\right) \left| \int_{S_C} d\sigma_i(r) \exp\left(ikr + \frac{1}{2}\phi(r)\right) \right|^2 \quad (10.39)$$

Now, the Stokes condition will, as before, be satisfied by minimality. Still, it will be interesting to derive a replacement of the mean curvature equation for the ordinary minimal surface. Repeating the above computations in the local tangent plane, we find here:

$$K_1 + K_2 = n_i(x) \partial_i \phi(r)_{\vec{r}=\vec{R}(x)} \quad (10.40)$$

On the left, we have mean curvature at the surface, and on the right, we have the normal derivative of the conformal metric field projected at the surface.

This property means that we can keep the ordinary minimal surface, with $K_1 + K_2 = 0$, and ensure that the conformal metric varies only along the surface but not in the normal direction. In the local tangent plane, this means that $\phi(x, y, z) = \phi(x, y, 0)$, so it changes only in a local tangent plane but not in the normal direction.

Remember, this is just the Stokes condition, not yet the loop equation, but the net result is that we keep the minimal surface in the sense of being the surface of the minimal area in ordinary induced metric. However, the Extended Area $A_C[\phi]$ has an extra factor $\exp(\phi(r))$, which varies along the surface.

For the loop equation to hold, the following condition must be valid:

$$\frac{\oint_C dr_i \exp(\phi(r)) \int_{S_C} d\sigma(r') \exp(\phi(r'))}{|\vec{r}' - \vec{r}|^3} \frac{(r'_i - r_i) n_k(r) n_k(r') - n_i(r') (r'_k - r_k) n_k(r)}{|\vec{r}' - \vec{r}|^3} = 0 \quad (10.41)$$

We shall call it the self-consistency relation for the metric field. At a given surface S_C , this is an equation for the metric field on the surface. Thus we get a closed set of integrodifferential equations for the parametric equation of surface $r_i = R_i(u, v)$ and the external conformal metric $\phi(u, v)$, which is a two-dimensional vector field. So, we have a two-dimensional surface embedded in four-dimensional space x, y, z, ϕ .

Note also that there would now extra terms in the loop equation of the structure

$$\int d^3\rho \frac{\rho_j}{|\vec{\rho}|^3} \Delta(\vec{\rho}) \exp\left(\frac{1}{2}\phi(\vec{r} + \vec{\rho}) + \frac{1}{2}\phi(\vec{r})\right) \quad (10.42)$$

coming from the second area derivative of generalized area $A_{S_C}[\phi]$. These terms no longer vanish by space symmetry in the presence of a conformal metric field, but the leading term at $r_0 \rightarrow 0$ will be a gradient which vanishes after loop integration²¹

$$\begin{aligned} \oint_C dr_i \int d^3\rho \frac{\rho_i}{|\vec{\rho}|^3} \Delta(\vec{\rho}) \exp\left(\frac{1}{2}\phi(\vec{r} + \vec{\rho}) + \frac{1}{2}\phi(\vec{r})\right) &\propto_{r_0 \rightarrow 0} \\ \oint_C dr_i \partial_i \phi(\vec{r}) \exp(\phi(\vec{r})) &= 0 \end{aligned} \quad (10.43)$$

The next terms with $\partial^3\phi$, $(\partial^2\phi)\partial\phi$, $(\partial\phi)^3$ will already have r_0^2 in front of them, so they will be negligible compared to the leading $O(1)$ term in the loop equation.

Let us integrate the first term in (10.41) by parts

$$\begin{aligned} \oint_C dr_i \exp(\phi(r)) \int_{S_C} d\sigma(r') \exp(\phi(r')) \frac{n_i(r')(r'_k - r_k) n_k(r)}{|\vec{r}' - \vec{r}|^3} = \\ \oint_C dr_i \exp(\phi(r)) \int_{S_C} d\sigma(r') \exp(\phi(r')) n_k(r) n_k(r') \partial_{r_i} \frac{1}{|\vec{r}' - \vec{r}|} = \\ - \oint_C dr_i \exp(\phi(r)) (\partial_i n_k(r) + n_k(r) \partial_i \phi(r)) \\ \int_{S_C} d\sigma(r') \exp(\phi(r')) \frac{n_k(r')}{|\vec{r}' - \vec{r}|} \end{aligned} \quad (10.44)$$

²¹note also that extra condition $n_k \partial_k n(r) = 0$ was not used here, as $n_k(r) dr_k = 0$.

Moving term with $\partial_i \phi(r)$ to the left and all remaining terms to the right, we get

$$\begin{aligned} & \oint_C dr_i \exp(\phi(r)) \partial_i \phi(r) \int_{S_C} d\sigma(r') \exp(\phi(r')) \frac{n_k(r) n_k(r')}{|\vec{r}' - \vec{r}|} = \\ & - \oint_C dr_i \exp(\phi(r)) \int_{S_C} d\sigma(r') \exp(\phi(r')) \\ & \left(\frac{(n_i(r') - n_i(r)) (r'_k - r_k) n_k(r)}{|\vec{r}' - \vec{r}|^3} + \frac{\partial_i n_k(r) n_k(r')}{|\vec{r}' - \vec{r}|} \right) \end{aligned} \quad (10.45)$$

We used the fact $dr_i n_i(r) = 0$ to subtract $n_i(r)$ from $n_i(r')$ and remove spurious singularity in the surface integral. At this point exact solution seems impossible - even the mean curvature equation is a problem that can only be tackled by numerical minimization.

But we never know.

10.7. Vorticity Correlations and Equation for Scaling Index

Let us now repeat the computation of vorticity correlations. The area derivatives are modified trivially (because the regularized area is quadratic functional of $d\sigma_i$, we get a factor of 2):

$$\frac{\delta A_C[\phi]}{\delta \sigma_i(r)} = 2n_i(r) \exp(\phi(r)) \quad (10.46)$$

$$\int_{S_C} d\sigma_i(r) \frac{\delta A_C[\phi]}{\delta \sigma_i(r)} = 2 \int_{S_C} d\sigma_i(r) n_i(r) \exp(\phi(r)) \quad (10.47)$$

$$= 2A_C[\phi] \quad (10.48)$$

So, we get the same equations for vorticity correlations, including the self-consistency equation for α :

$$\alpha = \frac{1}{2} \quad (10.49)$$

All the vorticity correlations will acquire extra factors of $\exp(\phi)$:

$$\begin{aligned} & \left\langle \vec{\omega}_1 \dots \vec{\omega}_k \delta \left(\Gamma - \oint_C \vec{v} d\vec{r} \right) \right\rangle = \\ & |A_C[\phi]|^{-\frac{1}{2}} \vec{n}_1 \exp(\phi_1) \dots \vec{n}_k \exp(\phi_k) \\ & A_C[\phi]^{-\frac{k}{2}} \Omega_k \left(\Gamma A_C[\phi]^{-\frac{1}{2}} \right) \end{aligned} \quad (10.50)$$

So, the formulas look the same, and the scaling functions $\Omega_k \left(\Gamma A_C[\phi]^{-\frac{1}{2}} \right)$ satisfy the same recurrent equations and results expressing them in terms of integrals of $\Omega_0(\gamma) = \Pi(\gamma)$ stay the same as in.¹³ The only thing which changed is the extra dependence of the coordinates provided by conformal metric factor e^ϕ . So, we cannot predict the spatial dependence of vorticity correlations until we solve these heavy equations for ϕ and $\vec{R}(u, v)$.

10.8. Conclusion

The main result of this section is the exact solution of the loop equation for an arbitrary flat loop, which includes a 2D loop equation. With scaling index $\alpha = \frac{1}{2}$ as derived in the previous work, the minimal area solves the loop equations and passes the known tests for the circulation moments. For the general, non-planar loop, the equation for the minimal surface stays the same (mean curvature equals zero), and we derive an integral equation ((10.45)) for the self-consistent conformal metric. The correlation scaling functions stay the same, and local vorticity in expectation values is still directed along the normal to the minimal surface. The coordinate dependence of vorticity correlations gets modified by extra factors of conformal metric $\exp(\phi)$. In other words, we have a 2d-surface in 4-dimensional space x, y, z, ϕ with the dependence of the x, y, z coordinates given by the ordinary minimal surface, and the last coordinate changing along this minimal surface in case this surface is curved.

11. Recent progress of the Kelvinon Solution and Circulation PDF

11.1. Time evolution of the Kelvinon

We have recently clarified the meaning and the basic features of the domain wall solution of the loop equation and its relation to the Kelvin theorem and GBF.

The Kelvinon velocity field with some Clebsch winding numbers n, m , which we studied in the section 7, represents a class of time-dependent solutions \vec{v}_{nm} of the Euler equation. The external force \vec{f} is assumed fixed in this solution, to be averaged later.

The loop equation also has a particular solution in the WKB limit

$$\Psi_{nm}[C, \gamma] = \left\langle \left\langle \exp \left(i \gamma \oint_C \vec{v}_{nm} \cdot d\vec{r} \right) \right\rangle \right\rangle_t \Big|_f = \left\langle \exp (4\pi m i \gamma Z) \right\rangle_f \quad (11.1)$$

where $\langle \rangle_f$ is the averaging over the Gaussian distribution of constant vector \vec{f} with variance σ and $\langle \rangle_t$ is the time averaging for the evolution according to Clebsch Flow Equation.

The Kelvinon normalization constant Z depends upon \vec{f} through the energy balance equation (7.36). It is time-independent in the Clebsch Flow Equation, which is why we have removed the time averaging in (11.1).

The exponential of circulation of any stationary solution of the Euler equation would satisfy the WKB limit of the loop equation by construction. We have seen it in the example of the tensor area law solution of the loop equation, corresponding to the uniform global vorticity solution of the Navier-Stokes equation (inadequate to the turbulence problem).

We, however, are looking for something else in the loop equation. We need time independence of the velocity circulation over a **particular** stationary loop C .

For this conservation of circulation, it suffices to have a time-dependent solution of the Clebsch Flow Equation (3.39), such that the velocity field at the bounding loop C is aligned with its local direction. This alignment would make this loop stationary (the longitudinal motion re-parameterise the loop and does not count as a displacement).

The loop functional will be time independent in virtue of these boundary conditions, in agreement with the Kelvin theorem, as we have seen in the section 7.

As we have seen, these boundary conditions follow from the balance of most singular terms in the Clebsch Flow Equation. In addition, we saw that the velocity field was tangent to the discontinuity surface.

The Clebsch Flow Equation resolves the ambiguity of the Euler equations for the Clebsch field.

There are topological winding numbers (7.25),(7.29). These winding numbers are properties of the solution rather than extra conditions.

These winding numbers are conserved by the time evolution by the

Clebsch Flow Equation, as this continuous evolution preserves the topology.

We have to start this evolution from the Clebsch field with a particular topology and then let it evolve according to the Clebsch Flow Equation.

The explicit example of the Clebsch field with the required topology was presented in (7.8).

The time average of any loop functional made of a solution of the Clebsch Flow Equation with this example as initial conditions will provide the desired solution of the steady loop equation.

Thus, our Kelvinon does not belong to GBF. It is adjusted to the loop C by the requirement that C bounds its discontinuity surface.

Without this requirement, our circulation would not satisfy the loop equation, nor will it be time-independent.

In general case $C' \neq C$, this circulation would reduce to the area inside some loop at the Clebsch sphere S_2

$$\oint_{C'} \vec{v}_{nm} \cdot d\vec{r} = Z \oint_{\gamma} \phi_1 d\phi_2 = Z \text{Area}(\gamma) \quad (11.2)$$

where $\text{Area}(\gamma)$ is the area on S_2 outside the loop $\gamma = \vec{S}(C')$ mapped by the Clebsch field on this sphere.

By the Kelvin theorem, this area is always conserved in Euler dynamics for the **liquid** loop, moving with the flow. For a static loop, it is not conserved in general.

Our flow for Clebsch field is not steady; it evolves according to Clebsch Flow Equation. However, as long as the edge C of the singularity surface stays steady, as we assume, the circulation is conserved, which is all we need to satisfy the steady loop equation.

The curve $\gamma_C = \vec{S}(C)$ as we have seen, in virtue of our boundary conditions for the Clebsch field $S(C) = (0, 0, 1)$, reduced to an infinitesimal circle around the North pole of S_2 , which led to the external area being the whole area 4π of the sphere times the winding number m .

The constant Z is determined as a function of the force \vec{f} from the energy balance condition (7.36). Again, this is not the extra condition but rather a consequence of the full Navier-Stokes equation for steady state. Later, we take the limit of $\nu \rightarrow 0$ and leave the main terms.

Other than this approximation, this Ψ_{nm} represents an exact solution in the limit of $\nu \rightarrow 0$.

11.2. Kelvinon loop functionals and Gaussian forces

As we have found in the previous section 7 (see also Appendix E), there is the topologically stable Kelvinon solution $\vec{v}^K(\vec{r})$ of the Euler equations in Clebsch variables a the sphere S_2 (KLS domain wall bounded by the Alice string).

The loop functional $\Psi(C)$ for this solution represents the Gaussian average over the random force \vec{f} of the phase factor $\exp(i\Gamma_C/\nu)$ for the circulation $\Gamma_C = \int_C \vec{v}^K \cdot d\vec{r}$ (see (7.48), (7.41)):

$$\Psi(C) = \frac{\int_{R_3} d^3\vec{f} \exp\left(-\frac{\vec{f}^2}{2\sigma}\right) \exp(i\Gamma_C/\nu)}{\int_{R_3} d^3\vec{f} \exp\left(-\frac{\vec{f}^2}{2\sigma}\right)}; \quad (11.3a)$$

$$\Gamma_C = \oint_C \vec{v}^K \cdot d\vec{r} = 4\pi m Z; \quad (11.3b)$$

$$Z|_{\nu \rightarrow 0} \rightarrow \frac{\vec{f} \cdot \hat{S}^{-1} \cdot \vec{f}}{n^2 \Sigma[C]}; \quad (11.3c)$$

$$\Sigma[C] = \rho \frac{\pi^2 \sqrt{\nu}}{2} \left\langle \int_{\mathcal{S}_{disc}(C)} |d\vec{\sigma}| \left(\vec{\nabla}_t S_3 \right)^2 \sqrt{(-\hat{S}_{nn})} \right\rangle_t; \quad (11.3d)$$

$$\hat{S}_{\alpha\beta} = \left\langle \partial_\alpha (\phi \partial_\beta S_3 + \partial_\beta \Phi) \right\rangle_t \quad (11.3e)$$

with $\vec{\nabla}_t$ being the tangent gradient, $\mathcal{S}_{disc}(C)$ is the discontinuity surface for the Kelvinon, and \hat{S}_{nn} is the local normal strain. $\langle \rangle_t$ stands for averaging over the time evolution of the Clebsch field according to Clebsch Flow Equation.

The shape of discontinuity surface $\mathcal{S} : \partial\mathcal{S} = C$ is so far arbitrary. The vorticity at the surface is normal to it, just as required by the loop equation.

The velocity circulation around the loop C is $\Gamma_C = 4\pi Z m$ (see (7.25)).

In its initial form, Γ_C is a Stokes type functional of the loop C , which can be varied by area at any point \vec{r} in space, producing vorticity $\vec{\nabla} \times \vec{v}^K(\vec{r})$. The continuation from the surface to the whole space R_3 is provided by the Kelvinon solution $S_a(\vec{r})$.

The positive definite functional $\Sigma[C]$ represents the surface enstrophy coming from vorticity $\vec{\omega} = e_{abc} S_a \vec{\nabla} S_b \times \vec{\nabla} S_c$ (without the Z factor).

This vorticity is concentrated within the local width h ($\vec{r} \in \mathcal{S}_{disc}$) on the discontinuity surface $\mathcal{S}_{disc}(C)$ bounded by C .

The fact that Γ_C represents a velocity circulation over a steady edge of a steady discontinuity surface of the solution of the Euler equation (with fixed external force \vec{f}) automatically makes it a solution of the loop equation in the turbulent limit, as we discussed in the previous section.

The averaging over the Gaussian force can be interchanged with the loop operators.

Therefore, this $\Psi(C)$ satisfies the Euler loop equation. The same is true about any superposition of exponents of circulation of Euler solution, but the Kelvinon has a physical meaning we need.

The energy balance relation between Z and \vec{f} follows from the steady solution of the Navier-Stokes equation in the turbulent limit, which we discussed above, in section 6.

This relation is not an external constraint; it was derived by taking the time derivative of the fluid energy $\frac{1}{2} \int_{R_3} d^3r \vec{v}^2$, integrating by parts and taking boundary conditions at infinity, where the constant force \vec{f} is pumping in the energy, to be dissipated at the vortex sheet of our Kelvinon.

We used the energy balance relation from the full Navier-Stokes equation in the limit of $\nu \rightarrow 0$ (anomalous energy dissipation). We applied it to the normalization parameter Z of the non-stationary Euler solution for Clebsch field.

This modification of the Euler dynamics corresponds to the principle we suggested in the previous section 4.2: to consider the Euler dynamics as a limit $\nu \rightarrow 0$ of the Navier-Stokes dynamics.

This principle leads to stability conditions, selecting the solutions of the Euler equation. It also leads to anomalous dissipation 4.67, which normalizes the arbitrary area $4\pi Z$ of the sphere for the compactified Clebsch field in the weak steady Euler solution.

We took advantage of the superposition principle for the linear loop equation (Schrödinger equation in loop space in our quantum interpretation).

In the next section, we shall use this superposition principle to sum over topological classes.

11.3. Kelvinon and the Minimal Surface

With arbitrary discontinuity surface, this Γ is a functional of the loop **and the shape of discontinuity surface**. This surface defines the solution for the Clebsch Flow Equations given angular discontinuities $2\pi n, 2\pi m$ at this surface, around the loop C , and vanishing normal derivative of the velocity field.

Therefore, the circulation implicitly depends on the discontinuity surface through the Kelvinon field.

The analysis of the WKB limit of the loop equation in the previous section 10.6 showed that the solution could depend on the following functional of the loop and some scalar field $\rho(\vec{r})$ (conformal external metric)

$$A_C[\rho] = \int_{\vec{r} \in \mathcal{S}_{disc}} |d\vec{\sigma}| \exp(\rho(\vec{r})); \quad (11.4)$$

$$\partial_n \rho(\vec{r} \in \mathcal{S}_{disc}) = K_1 + K_2 \quad (11.5)$$

where K_1, K_2 are the main local curvatures of the surface.

Suppose we express this conformal metric locally through the tangent gradients of the Clebsch field S_3 . Its normal derivative will vanish due to the Neumann boundary condition for S_3 at the minimal surface.

This relation will lead to the extremum condition of the area of our surface, independently of the external conformal metric, as long as it obeys the same Neumann boundary conditions as S_3 .

Now we compare this form of the functional $A_C[\rho]$ with our Kelvinon solution, and we find the correspondence

$$\rho = 2 \log |\vec{\nabla}_t S_3| + \frac{1}{2} \log(-\hat{S}_{nn}) + \text{const} \quad (11.6)$$

11.4. The algebraic solution for the loop functional

Thus we have found an explicit analytic solution for the circulation PDF, solving the loop equation and corresponding to the KLS domain wall shaped as the minimal surface bounded by the loop C .

$$P_{nm}[\Gamma, C] = \int_{-\infty}^{\infty} \frac{d\gamma}{2\pi} \exp(-\imath \gamma \Gamma) \Psi_{nm}[\gamma|C] \quad (11.7)$$

Here $\Psi_{nm}[\gamma, C]$ is defined at (7.57).

The only unknown phenomenological parameter is the 3×3 symmetric matrix \hat{S}^{-1} .

We have fitted the distribution of $|\Gamma|$ for this solution to the DNS data from¹⁰ in the previous section 7.8. The fit was as good as it gets, which strongly supported the existence of these Kelvinons.

We can go one step further and study the effects of the time reversal breaking in the Kelvinon solution.

The Fourier transform of the circulation PDF

$$\Psi_{nm}[C, \gamma] = \frac{\left\langle \exp \left(i \gamma \oint_C v_\alpha dr_\alpha \right) \right\rangle_f}{\sqrt{\det \left(1 - i \gamma \frac{2m\sigma \hat{S}^{-1}}{n^2 \Sigma[C]} \right)}}; \quad (11.8)$$

depends from the loop C through the matrix $\hat{S}^{-1}/\Sigma[C]$.

In particular, the mean circulation

$$\left\langle \oint_C v_\alpha dr_\alpha \right\rangle = -i \frac{\partial}{\partial \gamma} \Psi_{nm}[C, \gamma] \Big|_{\gamma=0} = \frac{m\sigma \text{tr} \hat{S}^{-1}}{n^2 \Sigma[C]} \quad (11.9)$$

The mean strain \hat{S} must be traceless.

$$\text{tr} \hat{S} = 0; \quad (11.10)$$

$$(-1/a, 1/(a-b), 1/b) = \frac{2m\sigma}{n^2 \Sigma[C]} (1/q_0, 1/q_1, 1/q_2); \quad (11.11)$$

$$b > a > 0; \quad (11.12)$$

where (q_0, q_1, q_2) are eigenvalues of \hat{S} , adding up to zero. However, the eigenvalues of \hat{S}^{-1} do not add up to zero.

Therefore, the mean circulation of our solution is not zero. The low moments of our theory disagree with DNS, which means that the asymptotic laws of extreme turbulence require a rather large order of moments or the far tails of PDF.

11.5. PDF tails and time symmetry breaking

The asymptotic tails of the PDF can be easiest to compute from the integral representation

$$\Pi(\Gamma) = \int_{-\infty}^{\infty} dt \int_{-\infty}^{\infty} dx \frac{1}{2\pi\sqrt{\pi}} \exp\left(-\Gamma x - t^2(1+x/a)(1+x/(b-a))(1-x/b)\right) \quad (11.13)$$

The saddle point computation chooses one of the six saddle points in the complex plane.

Let us first consider the case of positive Γ . The relevant point in this case is

$$\left\{ t \rightarrow \frac{\sqrt{\Gamma}\sqrt{ab(b-a)}}{\sqrt{((2b-a)(a+b))}}, x \rightarrow b \right\}; \quad (11.14a)$$

$$\Pi(\Gamma \rightarrow +\infty) \rightarrow \frac{\exp(-b\Gamma)}{4\pi^{3/2}\sqrt{\Gamma}} \sqrt{\frac{ab(b-a)}{(a+b)(2b-a)}} \quad (11.14b)$$

Likewise, in the case of negative Γ

$$\left\{ t \rightarrow i \frac{\sqrt{-\Gamma}\sqrt{ab(b-a)}}{\sqrt{(a+b)(2a-b)}}, x \rightarrow -a \right\}; \quad (11.15a)$$

$$\Pi(\Gamma \rightarrow -\infty) \rightarrow \frac{\exp(a\Gamma)}{4\pi^{3/2}\sqrt{-\Gamma}} \sqrt{\frac{ab(b-a)}{(a+b)(2a-b)}} \quad (11.15b)$$

We observe the explicit breaking of the time-reversal symmetry in the turbulent region $|\Gamma| \gg \nu$. This breaking comes from the time-odd winding number m of the Kelvinon. With the anti-Kelvinon, we would have the PDF reflected $\Gamma \Rightarrow -\Gamma$.

We have the Stokes phenomenon from the point of view of the loop equation analysis. Two analytic functions give the asymptotic behavior at the positive and negative Γ .

This phenomenon resolves the paradox of Sasha Polyakov, who objected to the early version of the Area law on the following grounds. The Minimal area is invariant against the orientation reversal of the loop, as opposed to circulation, which changes its sign. The PDF must be an even function of the ratio of Γ to any function of the minimal area.

We now see two asymptotic solutions to the loop equation: one for positive and another for negative circulation.

The orientation reversal does not continue one asymptotic solution into another because of the Stokes phenomena in our integral representation (11.13).

We also see that for the non-planar loop C , the dependence of its shape is more complex than just the minimal area, though the discontinuity surface still coincides with the minimal surface.

Note that these asymptotic PDF tails are the missing piece of our theory 9.3, 10.7 of the vorticity correlations at the vortex surface. The recurrent equations (9.32) for these correlations relate them all to the PDF $\Pi(\Gamma)$ we have computed above.

The solutions of these equations for the PDF tails at large scaling argument $\gamma = \frac{\Gamma}{\sqrt{A_C[\rho]}}$ are elementary for our value of critical index $\alpha = \frac{1}{2}$:

$$\Omega_k(\gamma) \rightarrow \text{const} \frac{\gamma^k \exp(-B_{\pm}|\gamma|)}{\sqrt{|\gamma|}} \quad (11.16)$$

11.6. Matching the Kelvinon solution to the DNS

Let us compare these relations to DNS,¹⁰ courtesy of Kartik Iyer.

This raw data correspond to 8192³ DNS with $R_{\lambda} = 1300$. There are the first 8 moments of circulation for various Reynolds numbers.

The PDF data for velocity circulation corresponds to $r/\eta \approx 140$. The circulation is measured in viscosity ν (note that here we restored the correct normalization of circulation, which was lost in the previous analysis in section 7.8).

This data is the most extensive, with circulation $-1904.72 < \Gamma < 2048.47$. We discarded the extreme values, as the statistics were too small there.

The small absolute values of Γ were also discarded, as our theory only applies to large $|\Gamma|$. We selected the interval $610 < |\Gamma| < 1426$ corresponding to probabilities $10^{-7} > P > 10^{-14}$ and we fitted

$$\log \left(\Pi(\Gamma) \sqrt{|\Gamma|} \right) \approx A_{\pm} + B_{\pm} |\Gamma|; \quad (11.17)$$

$$(B_+, B_-) = (-b, -a); \quad (11.18)$$

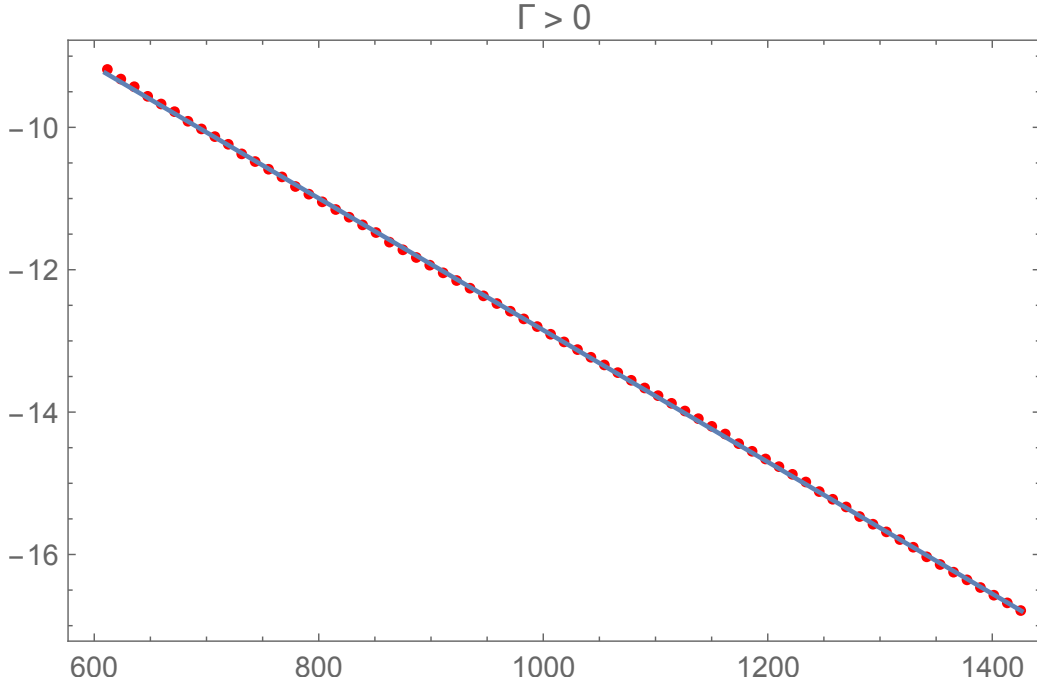


Figure 44: Fitting (11.6) for positive Γ

The positive tail has the following fit in the inertial regime

	Estimate	Standard Error	t-Statistic	P-Value	
A_+	-3.58916	0.0105971	-338.693	4.523×10^{-110}	(11.19)
B_+	-0.00925906	0.0000101328	-913.774	6.073×10^{-139}	

The negative tail has the following fit in the inertial regime

	Estimate	Standard Error	t-Statistic	P-Value	
A_-	-4.01871	0.0292907	-137.201	8.071×10^{-84}	(11.20)
B_-	-0.00877515	0.0000280073	-313.317	8.3194×10^{-108}	

There is about 5% breaking of time-reversal symmetry $\Gamma \Rightarrow -\Gamma$ which is well beyond the statistical errors $\sim 10^{-3}$.

The ratio $\beta = \frac{a}{b} = \frac{B_-}{B_+} = 0.947737$.

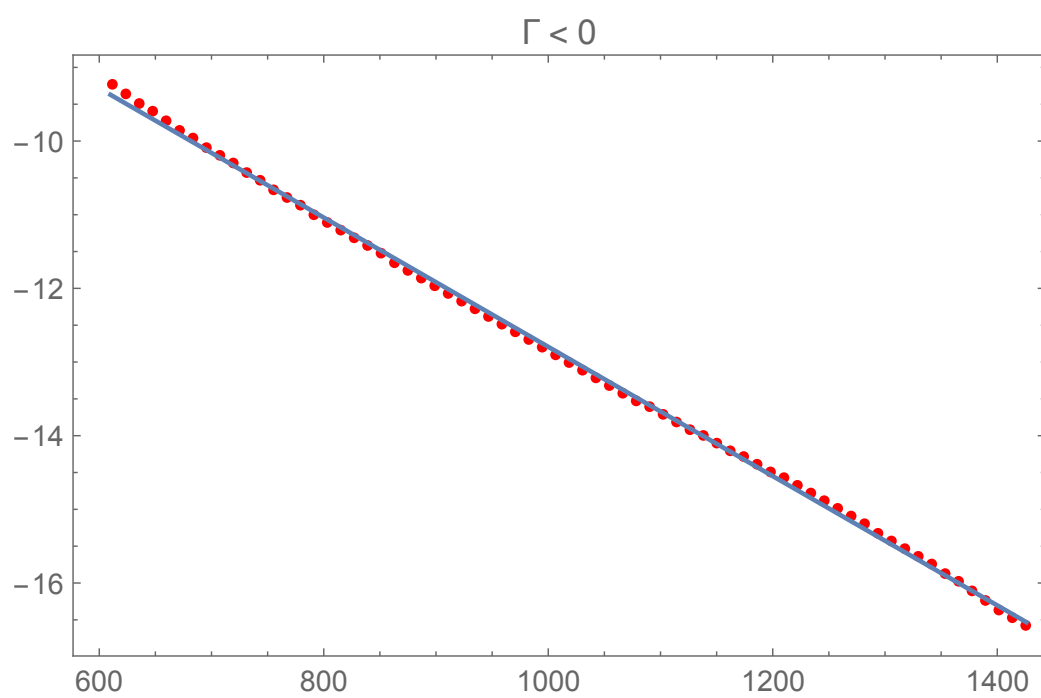


Figure 45: Fitting (11.6) for negative Γ

Remarkably, one simple algebraic formula (11.8) for the loop wave function describes all the probability tails for velocity circulation, including the asymmetry of the left and right tails.²²

It all follows from the Kelvinon solution of the Euler equation with a nontrivial winding number.

11.7. The circulation moments in Kelvinon solution

By construction, the Kelvinon solution only applies to high moments corresponding to the tails of the PDF. In particular, the first moment is finite in this solution, whereas in the DNS, it is subtracted.

Let us put together an explicit expression for the moments of circulation. We use the generating function

$$G_m(x) = \frac{1}{\sqrt{\det\left(1 - x \frac{2m\sigma\hat{S}^{-1}}{n^2\Sigma[C]}\right)}} = \quad (11.21)$$

$$\frac{1}{\sqrt{(1+x/a)(1-x/b)(1+x/(b-a))}}; \quad (11.22)$$

The first moment

$$\langle\Gamma\rangle = \frac{1}{2a} + \frac{a}{2b(b-a)} \quad (11.23)$$

²²As for the low moments, they are poorly matched in this solution. There is a regime change at some intermediate values of Reynolds number $\frac{\Gamma}{\nu}$. By construction, the Kelvinon solution only applies to intermittency phenomena. Our solution matched the Kelvinon asymptotic with DNS starting with $P < 10^{-7}$, $|\Gamma| > 610$. The same applies to the pre-exponential factor in PDF: such factors are modified by the next correction to the classical term of the WKB expansion. Thus, we cannot compare this factor yet.

The subsequent reduced moments $\langle (\Gamma - \langle \Gamma \rangle)^n \rangle$ are

$$0, \quad (11.24)$$

$$\frac{1}{a^2} + \frac{1}{(a-b)^2} + \frac{1}{b^2}, \quad (11.25)$$

$$6 \left(-\frac{1}{a^3} + \frac{1}{(a-b)^3} + \frac{1}{b^3} \right), \quad (11.26)$$

$$18 \left(\frac{5}{a^4} + \frac{4(a^2 - ab + b^2)}{a^2 b^2 (a-b)^2} + 5 \left(\frac{1}{(a-b)^4} + \frac{1}{b^4} \right) \right) \quad (11.27)$$

Recurrent equations for the moments are as follows:

$$\langle (\Gamma - \langle \Gamma \rangle)^n \rangle = n!^2 y_n; \quad (11.28a)$$

$$y_{-1} = 0; \quad (11.28b)$$

$$y_0 = 1; \quad (11.28c)$$

$$y_1 = 0; \quad (11.28d)$$

$$y_2 = 1/4(1/a^2 + 1/(a-b)^2 + 1/b^2); \quad (11.28e)$$

$$\begin{aligned} 2(4+n)a^2(a-b)^2b^2y_{n+4} = & \\ & -(a^2 - ab + b^2)y_n \\ & -(5+2n)a(a-b)by_{n+1} \\ & +(a^2 - ab + b^2)^2y_{n+2} \\ & +2(3+n)a(a-b)b(a^2 - ab + b^2)y_{n+3} \end{aligned} \quad (11.28f)$$

The asymptotic behavior of the moments at large order can be found from the saddle point in the integral representation

$$\begin{aligned} \langle (\Gamma - \langle \Gamma \rangle)^n \rangle = & \iint_{-\infty}^{\infty} \frac{dx dt}{2\pi i \sqrt{\pi} x^{n+1}} \\ & \exp \left(-t^2(1+ax)(1-bx)(1+(a-b)x) - x \langle \Gamma \rangle \right); \end{aligned} \quad (11.29)$$

We find the following saddle point contribution

$$\begin{aligned} \langle (\Gamma - \langle \Gamma \rangle)^n \rangle \rightarrow & \\ & \frac{ab(a-b)^{-n} \exp \left(\frac{1}{2} \left(-\frac{a}{b} - \frac{b}{a} + 1 \right) \right)}{2\sqrt{2}\pi^{3/2} \sqrt{(2b-a)(2a-b)(a^2 + a(2bn+b) + b^2)}} \end{aligned} \quad (11.30)$$

Note that with our $\beta = a/b < 1$ even moments are positive and odd ones are negative, which agrees with DNS¹⁰ (courtesy of Kartik Iyer).

Our scaling index relation $\alpha = \frac{1}{2}$ satisfied in DNS for the ratio of consecutive large even moments as a function of the size r of the square loop implies that

$$a \propto b \propto 1/r; \quad (11.31)$$

$$\log \langle (\Gamma - \langle \Gamma \rangle)^n \rangle \rightarrow n \log r - \frac{1}{2} \log n + \text{const}; \quad (11.32)$$

$$\eta(n) = r \frac{\partial}{\partial r} \log \langle (\Gamma - \langle \Gamma \rangle)^n \rangle \rightarrow n; \quad (11.33)$$

We conclude that there are no multi-fractal laws in the Kelvinon solution. Asymptotically, at large moments, we have linear trajectory $\eta(n) \rightarrow n$. At smaller n , and in particular, at $n = 3$, the moments are no longer determined by Kelvinon. The asymptotic line $\eta(n) = n$ does not cross the exact K41 value $\eta(3) = 4$. There is an intermediate regime at finite n , as it was suggested in.¹⁰

It becomes an important challenge to measure higher moments at large Reynolds numbers. Does the effective $\eta(n)/n$ get closer to 1? At the DNS in¹⁰ at $n \sim 10$ it was about 1.1 and falling.

We can only predict leading terms, as there are scale-dependent corrections from the higher order terms of the WKB expansion to logarithmic derivatives of the moments by the scale, which could be interpreted as scale-dependent logarithmic derivatives of the moments.

On the other hand, direct linear fit in the section 7.8 of the square root of the ratio of the eighth to the sixth moment as a function of the size in Fig.26 produced an ideal $R_2 > 0.999$ for the same data.¹⁰ This linear relation corresponds to $\eta(8) - \eta(6) = 2$.

This discrepancy between alternative fits means that one needs much more statistics and a much larger DNS to distinguish linear law from a power close to 1.

The intermediate moments could have a more complicated dependence on the loop size than the pure power law with any exponent.

11.8. Sum over topologies and quantum equivalence

Here is an important observation. The loop equation is a **linear** Schrödinger equation in loop space, even though the original Navier-Stokes and Euler equations are nonlinear.

There is no superposition principle in fluid dynamics, but there is such a principle in quantum mechanics in loop space.

We already used this superposition principle when we took the averaging over the random forces out of the loop functional. The average of the loop functionals, each satisfying the loop equation in virtue of the classical Euler equation with fixed force \vec{f} , also represented a solution to the loop equation.

Now we apply the same argument to the topological classes.

In virtue of the superposition principle for the linear equation, the general solution would be a superposition for the loop functional as well as for its Fourier transform, – the PDF

$$\begin{aligned} \Psi[C, \gamma] &= \sum_{n-\frac{1}{2} \in \mathbb{Z}, m \in \mathbb{Z}} A_{n,m} \Psi_{nm}[C, \gamma] = \\ &= \sum_{n-\frac{1}{2} \in \mathbb{Z}, m \in \mathbb{Z}} \frac{A_{nm}}{\sqrt{\det \left(1 - \imath \gamma \frac{2m\sigma \hat{S}^{-1}}{n^2 \Sigma[C]} \right)}}; \end{aligned} \quad (11.34)$$

$$\Pi[C, \Gamma] = \sum_{n-\frac{1}{2} \in \mathbb{Z}, m \in \mathbb{Z}} A_{n,m} \Pi_{nm}[C, \Gamma] \quad (11.35)$$

What are the weights A_{nm} ? At the moment, we cannot say, other than demand, that these weights must add up to 1. This problem remains for future research.

Here are some general considerations.

The solution of the Navier-Stokes equation is supposedly unique in the absence of forcing and at fixed initial data. There is even a Millennium Prize offered for proving or (for the sake of caution) disproving this widely accepted conjecture.

There is, though, an instability at a large enough Reynolds number (small enough viscosity compared to a typical velocity circulation).

In this case of infinitesimal viscosity, infinitesimal random forces at the boundary are known to lead to stochastic behavior, making the whole question of the uniqueness of the solution of the Navier-Stokes equation moot. The real turbulence problem is: what manifold is covered by this stochastic motion and what is the nature of spontaneous breaking of time reversal invariance in the Euler equation?

Coming back to the sum over topologies, let us consider the time evolution of the Navier-Stokes flow. There was a deterministic flow at the

initial moment, far from any fixed points. According to our scenario, it approaches one of the stable fixed points at some time, corresponding to certain topological charges of the Clebsch field.

By definition of the winding numbers, no continuous deformation can change them. However, in our system, we assumed some random external boundary forces \vec{f} , supplying the energy dissipated at large velocity gradients.

With a certain probability, these random forces can change topology as they violate the continuity of the solution. Moreover, an enhancement effect caused by large vorticity in vortex sheets leads to finite results of infinitesimal forcing at infinitesimal viscosity.

In that case, the flow will jump between topological classes, approach the fixed point in each class and cover the vicinity of this fixed point (which is, in fact, a fixed manifold).

In that picture, the coefficients A_{mn} are time frequencies (or probabilities) of Clebsch field getting into the corresponding topological class as a result of Gaussian random forcing.

Naturally, there is no sum over histories in our classical theory. The Navier-Stokes flow does not go over various alternatives with the weight $\exp\left(i \frac{S}{\nu}\right)$ at the same moment.

There are rather some dynamic instabilities triggered by external forcing, resulting in a weighted sum of contributions from various topological classes to the time average of the PDF over infinite time.

The turbulent flow spends some fraction of time in each of these classes, jumping from one to another, triggered by (unlikely) large fluctuations of the random force.

From that interpretation, it follows that all $A_{mn} > 0$, unlike quantum mechanics, where the eigenfunctions could add to wave function with complex or negative coefficients.

12. Conclusions and discussion

After 35 years of blind trials and errors, we are beginning to see the light.

12.1. Clebsch confinement and compactification phase transition

We have presented theoretical arguments and strong support from the DNS in favor of Kelvinons underlying the intermittency phenomena for

the velocity circulation in strong turbulence.

In the Introduction, we stated that the ultimate goal of turbulence studies was to find the solution of the Navier-Stokes equations in the limit of vanishing viscosity and explain why and how it covers some manifold instead of staying unique given Cauchy data.

We described our conjecture for this manifold and how it is covered in the present review paper, extending and debugging our recent research^{12,13,8,17,18,19,9,20,21}.

While trying to achieve this goal, we encountered ambiguity in the Euler equation, which is the limit of the Navier-Stokes we are studying. The Euler equation represents a Hamiltonian system in Clebsch variables. However, the topology of the target space for these variables remains arbitrary.

We adopted the sphere S_2 , which is one of the possibilities. Another would be R_2 , in which case there will be no topological numbers and no Kelvinons. We conclude that R_2 is appropriate for the weak turbulent flow and S_2 – for the strong turbulent one.

Thus, we conjecture that there is a compactification phase transition $R_2 \Rightarrow S_2$ for the Clebsch field, like that in a string theory.

The weak turbulence³⁹ has this Clebsch field propagating as plane waves and leading to the K41 energy spectrum in weak turbulence.

In strong turbulence, there are no Clebsch waves: this is a geometric phase, with Clebsch confined to a sphere in the target space.

The velocity circulation in our theory is proportional to the winding number of the Clebsch field satisfying the Clebsch Flow Equation (the Euler equation for Clebsch field with extra incompressible motion in target space S_2 in addition to passive flow in a self-parametrized velocity field).

The time evolution of the Clebsch field described by Clebsch Flow Equation is not steady, but it is compact, as the Clebsch field is confined to a sphere S_2 .

Here is our answer to the question posed in the Introduction: the Clebsch field covers S_2 driven by the Clebsch Flow Equation. This motion is more complex than a uniform covering of this sphere. Some nontrivial topology is involved, with two winding numbers $n \in \mathbb{Z} + \frac{1}{2}, m \in \mathbb{Z}$.

The circulation Γ_C is related to the integral of the Euler motion Z as $\Gamma_C = 4\pi mZ$. The infinitesimal tube around the loop C in physical space R_3 is mapped to the torus in Clebsch target space with the area $8\pi^2 nmZ$. ((7.29)).

12.2. Matching the DNS

The parameters depend upon the loop shape C through the time average of a surface integral (11.3) over the minimal surface \mathcal{S}_C of some function expressed in terms of the Kelvinon solution for the Clebsch field $\vec{S} \in S_2$.

This winding number is time-odd, which explains the asymmetry of the circulation PDF. The left and the right asymptotic behavior (11.14),(11.15) was perfectly fitted to the DNS.¹⁰

It is shown at (11.19),(11.20) and displayed at Fig.44, Fig. 45. The time-symmetry breaking is just 5%, but it is well beyond statistical error 0.1%. The ratio of fitted exponential decrements is $\beta \approx 0.95$.

The circulation moments for odd powers are negative, in agreement with DNS. The quantitative comparison must wait for the future DNS with larger order moments.

In principle, the higher moments add no information to the tails of the PDF, being related to these tails by the saddle point approximation of the one-dimensional integral for the moments at high order.

We need to compute the solution of the Clebsch Flow Equation for the Kelvinon field for the simplest loops. These solutions would allow computation of the dependence of the Kelvinon dissipation $\Sigma[C]$ and total momentum susceptibility $\hat{Q}[C] \approx \hat{S}^{-1}$ as functionals of the loop shape.

12.3. Extreme intermittency and its microscopic mechanism

The exponential decay of the velocity circulation distribution, discovered in the DNS in,¹⁰ and explained in this work, represents an extreme intermittency phenomenon.

The deviations of probability distributions in Statistical Physics from the Gaussian laws belong to the Critical Phenomena extensively studied in the previous century, culminating with the Renormalization Group and Conformal bootstrap.

These methods apply to **local** statistical systems, such as ferromagnetic near the Curie point or liquid Helium near the lambda point. The starting point of this Critical phenomena theory was a Gibbs distribution at a microscopic scale. The Renormalization group described the transformation of this distribution when the microscopic degrees of freedom are "integrated out" or averaged in the Gibbs partition function.

Using local operator algebra, the Conformal Bootstrap formalized the local conformal invariance of the microscopic Landau-Ginsburg Hamiltonian at the critical point. The operators' dimensions were renormalized compared to the initial local Hamiltonian. This conformal theory was also based on the locality property of the Gibbs distribution at a microscopic level.

Researchers have attempted to apply the same methods to the Turbulence problem for many years. Turbulence is not a usual statistical system with a given Gibbs distribution; the first problem is to find a substitute for this distribution in a dissipative system, where energy is not conserved.

Another complication is the lack of locality in incompressible fluid dynamics. Due to incompressibility conditions, pressure instantly redistributes the velocity field in the whole space. Long-range correlations and extended vortex structures explicitly violate the locality in turbulence.

Thus, some nonlocal physical mechanism is responsible for the intermittency of the velocity circulation. This circulation by the Stokes theorem equals the surface integral of the normal vorticity of a surface bounded by the loop. If the vorticity elements at this surface were random and independent, this circulation would become a Gaussian variable by the CLT.

It is decaying much slower, as an exponential, which manifests intermittency. It tells us that these strongly correlated elementary vorticities at the surface are part of a coherent structure with no or very little fluctuations. We argue that this structure is a vortex sheet with some normal vorticity at the surface.

12.4. Kelvinon as the substitute of Gibbs distribution

This vortex sheet and velocity field around it must satisfy some dynamical equation analogous to kinetic equations leading us to the Gibbs-Boltzmann distribution. Our theory says this equation is the loop equation, and its steady solution in extreme turbulent (i.e., WKB) limit is the Kelvinon.

There is no direct correspondence between the fixed point of the loop equation and the compact **stationary** solution of the Euler equation (if it even exists). The non-stationary Clebsch field of the Kelvinon corresponds to the stationary solution of the loop equation. Kelvin's theorem leads to the conservation of the circulation over a stationary spatial loop. Thus,

time-dependent Kelvinon represents a degenerate fixed point of the Loop Equation.

The time evolution by Clebsch Flow Equation covers this degenerate fixed point (or a manifold) while preserving the circulation. More precisely, the normalization factor Z in circulation is not changing in the course of evolution. It is a posteriori related to the ratio of two integrals over this evolution. This relation follows from the energy balance **outside** of the Euler dynamics, namely from the Navier-Stokes equation and the anomalous dissipation formula.

In the Boltzmann-Gibbs statistics, the Newton trajectory covers the energy surface due to the energy conservation, which leads to the ergodic hypothesis and the Gibbs distribution $\exp(-\beta E)$. In our theory, the conserved circulation of the Kelvinon plays the role of Gibbs's energy.

Conservation of the Gibbs distribution in phase space follows from the Liouville theorem. In our case, the conservation of our circulation distribution follows from the Kelvin theorem applied to the stagnant loop of the Kelvinon flow.

In some sense, our turbulence theory is simpler than the Critical phenomena, as it is described by a single classical Clebsch Flow Equation, leading to an algebraic solution for the loop functional.

Our distribution for velocity circulation has only three degrees of freedom f_x, f_y, f_z , which is infinitely less than a continuum of fluctuating field variables of the Gibbs distribution.

We explicitly constructed the initial data for the Clebsch field with specific winding numbers. Given these initial data and the usual boundary condition of vanishing normal derivatives to the discontinuity surface, the solution is specified up to arbitrary gauge function $h(\phi_1, \phi_2)$.

There could be a fixed point in the Clebsch Flow Equation, like the ergodic hypothesis for Newton's motion on the energy surface, but we no longer need this assumption. Our PDF for the velocity circulation only involves the time averages of certain space integrals depending on the time-dependent solution of this equation. We need to assume, of course, the existence of these averages over infinite time.

Using energy balance arguments, we computed the turbulent limit of the loop functional $\langle \exp(i\gamma\Gamma_C) \rangle$, averaged over Gaussian external forces. This functional turned out to be an algebraic function of γ (11.8).

Here is where we bypassed the ergodic hypothesis. The unique topology of the Kelvinon allowed us to relate the distribution of circulation to

certain time averages of this unknown compact motion on the Clebsch sphere.

On the other hand, there is an explicit loop equation for this PDF after averaging over random forces. We have studied this equation in 10.6. It contains unknown function $\Pi \left(\Gamma A_C[\rho]^{-\frac{1}{2}} \right)$ with $A_C[\rho]$ given by an integral over the minimal surface \mathcal{S}_C with external conformal metric field $\exp(\rho(\vec{r}))$. Now, we know this function from the Kelvinon solution

$$\Pi(x) = \text{const} \frac{e^{-B_\pm |x|}}{\sqrt{|x|}} \quad (12.1)$$

In principle, the loop equation in this Ansatz (10.45) can be used to compute unknown external metric $\exp(\rho(\vec{r}))$ at the minimal surface. This computation is a problem for future research.

12.5. Duality

The loop equation (beyond the strong turbulence WKB approximation) for the loop functional has the form of the Schrödinger equation in loop space with complex Hamiltonian.

This mysterious relation (8.61) between quantum wave function and the inverse Fourier integral of the classical probability needs to be fully understood. This relation leads to "quantum effects," such as sum over topologies, which are observable (in principle).

With recent advances in quantum computing, this relation opens an exciting possibility of **direct numerical solution of the loop equation on a quantum computer**.

Usually, it takes some artificial tricks to approximately map a nonlinear classical problem to a Schrödinger equation suitable for quantum computation. Here we have a Schrödinger equation in a loop space as a starting point!

The loop can be represented as a sequence of steps $\Delta_\alpha = \pm 1$ in each of three directions $\alpha = 1, 2, 3$ on an infinite cubic lattice. Closed loops we need correspond to each Δ_α entering together with the opposite step $-\Delta_\alpha$ somewhere in the sequence. This sequence of steps provides discrete parametrization of the quantum state in terms of ordinary spin variables $\Delta_\alpha = \pm 1$.

There is a technical problem with mapping these bits and the discrete version of a lattice Hamiltonian to the qubits, which we leave for future research.

Once this problem is solved, there will be a chance to go way beyond the existing DNS of the forced Navier-Stokes equation and simulate extreme turbulence.

Let us get back to the existing analytical methods.

The Kelvinon fixed point of the loop equation corresponds to the leading term of the WKB expansion, which goes in **positive** fractional powers of viscosity, which means asymptotic expansion in inverse powers of Reynolds number.

In terms of modern QFT, we have the **duality** between fluctuating velocity field and fluctuating geometry of the Clebsch field, mapping the physical space R_3 onto the sphere S_2 .

The strong turbulence corresponds to this dual geometric theory's weak (i.e., classical) phase. The complete theory would allow us to compute higher terms of this WKB expansion. This computation is a hard technical problem, but now it is within our reach once the loop equations are well-defined and the leading classical term is identified.

There are examples of such duality in low-dimensional flows. The Burgers equation describes 1D compressible flow. It is dual to the statistics of shocks,^{52,53,54} which are 1D versions of our vortex sheets.

Topology in the 1D case is much more primitive than in 3D, but this duality still holds. These shocks are responsible for the intermittency in the Burgers equation, which inspired us to look for topological defects in 3D Euler.

ADS/CFT duality in the conformal field theories is quite familiar to modern theoretical physicists specializing in QFT, String theory, and even Solid State Physics.

In turbulence, duality is something unknown, which sounds like a dangerous heresy. They say there could be only one physical picture, and this unique picture was given to us by the prophet Kolmogorov. We can only elaborate on this picture and build models.

This uniqueness of physical pictures is very common in Physics. However, on some rare lucky occasions, the universal physical phenomena can be described by more than one physical picture, more than one language, and more than one mathematical structure.

We mentioned velocity-shock duality in the Burgers equation and the

ADS/CFT duality in Quantum Field Theory.

There was a third story of unexpected duality, which we know from personal experience.⁵⁸ The 2D quantum gravity, as we now know it, can be described either by Liouville theory (continuum QFT) or by the random set of adjacent triangles, counted using random matrix theory and the theory of orthogonal polynomials.

It took us years of shouting from rooftops to convince the gravity community that the Liouville quantum field theory could be exactly solved by counting triangles with nineteenth-century mathematics.

In the case of the loop equations and vortex sheets, it took already 35 years to develop the idea of duality between fluctuating velocity and fluctuating geometry. Like it happened with Matrix Gravity models, nobody believed in these ideas while we were developing them by trial and error.

In the case of the Matrix Model of Quantum Gravity, the epiphany moment came when these two dual theories produced identical results for some critical indexes.

The perfect match of our predictions for the circulation PDF with the DNS,¹⁰ based on the conventional approach and compatible with Kolmogorov at intermediate Reynolds numbers, would, perhaps, have the same effect.

12.6. The local velocity and strain statistics

The statistics of the velocity field are another story.

In our theory, there is a significant difference between the potential and rotational parts of the velocity field.

In the Clebsch variables, vorticity is related to the Clebsch field by local expression. In contrast, potential velocity (including the strain tensor) involves the Biot-Savart integral, effectively accumulating vorticity distribution from the infinite volume and averaging over its fluctuations.

This non-locality and averaging make the statistics of the potential part very different from that of the rotational part.

As we argue in the section 5.8, the local velocity statistics are Gaussian due to the accumulation of tails from Biot-Savart integrals from uncorrelated vorticity structures far away from each other.

The Central Limit theorem, in this case, would work, unlike the case of the PDF of large circulations, which aggregate vorticity from a coherent vortex structure– the Kelvinon.

Moreover, the potential part of the local strain $W_{\alpha\beta} = \frac{1}{2}(\partial_\alpha v_\beta^{(pot)} + \partial_\beta v_\alpha^{(pot)})$ is expected to obey the distribution of a Gaussian random symmetric tensor, well known in the Random Matrix theory, with an obvious constraint of vanishing trace (5.99).

In order to select a potential part in DNS, one has to restrict $\vec{\omega}^2$ much lower than its mean square value $\langle \vec{\omega}^2 \rangle = \frac{\langle \mathcal{E} \rangle}{\nu V}$:

$$\langle \text{tr } \hat{W}^n \rangle_R = \frac{\int_R d^3r \text{tr } \hat{S}^n}{\int_R d^3r}; \quad (12.2)$$

$$\sigma^2 = \langle \text{tr } \hat{W}^2 \rangle_R; \quad (12.3)$$

$$R : \vec{\omega}^2 \ll \frac{\langle \mathcal{E} \rangle}{\nu V}; \quad (12.4)$$

This prediction can be verified in DNS, particularly the table of the moments, which we calculated analytically in (5.101), (5.102).

We used that distribution to compute the energy dissipation on a non-compact CVS vortex sheet in section 5.9.

The difference between potential and rotational velocity is manifest in the loop approach. The circulation PDF satisfies the closed equation, where the potential velocity part drops.

Moreover, the potential velocity correlations grow with distance, making us doubt the universality of the (potential part of) turbulent motion.

Why is the velocity fluctuation in the middle of the developed turbulent flow not influenced by the fluctuations near the boundary if their correlation function **grows** with separation?

These arguments do not apply to the vorticity fluctuations, which are at least decreasing.

The moments of the circulation (rotational part) are quite different from those of velocity differences (which mix both parts).

12.7. Heuristic model for the multi-fractal laws

We still need to quantitatively describe some phenomena observed in DNS, such as apparent multi-fractal scaling laws for moments of velocity differences, first suggested by Parisi and Frisch in⁶⁰ by (presumed) analogy with conformal field theory.

We do not see any theoretical grounds for conformal field theory here. Moreover, there are some obvious contradictions with conformal symmetry. For example, it would predict the scaling dimension of "conserved current" like velocity field $d - 1 = 2$ instead of observed $\approx -\frac{1}{3}$.

In terms of circulation moments scaling, this would correspond to $\eta(2) = -2$ instead of observed $\eta(2) \approx 2.7$. In terms of velocity moments, this would correspond to $\zeta(2) = -4$ instead of the observed value $\zeta(2) \approx 0.7$. Much further from the DNS than K41 scaling.

Still, the moments of velocity differences observed in DNS can be fitted well by the scaling laws with some positive nonlinear trajectory $\zeta(n)$, despite the lack of a microscopic theory.

Multi-fractal data representation could be related to other microscopic mechanisms, not just a local conformal symmetry of velocity correlation functions. Lacking such a microscopic mechanism, we still can work with phenomenological theories.

There is an impressive phenomenological approach by Sreenivasan and Yakhot,^{61,62,63} offering a model with a few parameters, accurately fitting the observed scaling indexes $\zeta(n)$.

These authors advocate the new phase transition to the "fourth state of turbulence," leading to saturation of the scaling index $\zeta(n)$.

In our picture, they observed the transition from weak to strong turbulence, originating in the compactification of the target space of the Clebsch variables.

These authors mostly considered the velocity differences rather than the velocity circulation we have studied, so there is no direct overlap between our theories.

Our compactification of the Clebsch variables influences the velocity differences they studied by an accumulation of tails of the Biot-Savart integrals from singular vortex structures. This accumulated effect is not as drastic as the one on vorticity but still would display itself as a regime change.

We can offer some heuristic explanations of the success of their model.

The turbulent flow is potential in most of the space, with vorticity collapsed into vortex sheets.

When two points measure velocity difference, with a certain small probability $\epsilon \ll 1$, a vortex sheet passes between them. With complementary probability $\alpha = 1 - \epsilon$, there will be a potential field where the Bernoulli law holds $p = -\frac{1}{2}\vec{v}^2$.

In this case, the velocity difference $\Delta\vec{v}(\vec{r}) = \vec{v}(\vec{r}) - \vec{v}(0)$ is a linear function for small \vec{r} . With probability ϵ , there will be a step function (velocity gap).

In,^{62,63} the infinite chain of the Hopf relations for expectation values of powers of velocity differences was closed by introducing the "turbulent viscosity." As a result of this approximation, the pressure was replaced by $p \Rightarrow -\frac{1}{2}\alpha\vec{v}^2$, with $\alpha \approx 0.95$.

Within our heuristics, this α is the probability of finding no vortex sheet between two points. After this closing, the relations for the velocity difference moments were nicely fitted⁶² to the DNS.

The microscopic theory of the potential part of turbulent velocity differences without any model approximations remains a problem for the future. In addition to fitting the DNS, this theory should give a space-time picture of relevant flow and explain the physical nature of the phase transition to the strong turbulence.

12.8. More predictions

We desperately need large-scale DNS to more accurately verify the Kelvinon theory's predictions (11.14),(11.15) and investigate vorticity's spatial distribution. We also need a confirmation of the Random Matrix predictions (12.2), (5.101), (5.102) for the potential strain moments. The next low-hanging fruit is vorticity correlation (11.16).

Acknowledgments

I am grateful to Theo Drivas, Dennis Sullivan, and other Stony Brook University Einstein seminar participants for stimulating discussions of this work, which helped me find errors in earlier versions.

Deep discussions at the seminars in IAS were both inspiring and elucidating; I would like to thank Peter Sarnak, Ed Witten, and other participants of the IAS seminars for their questions and comments.

I reported this work at various stages in the Tel Aviv University, New York University, Max Planck Institute, and Nankai symposium. I am grateful to the organizers of these talks and seminars, especially Grisha Falkovich, Marek Karliner, and Yang-Hui He, for their attention and help.

In the early stages of this long study, I greatly benefited from suggestions and criticism from my colleagues Sasha Polyakov, Pavel Wiegmann, Nikita Nekrasov, Sasha Zamolodchikov, Uriel Frisch, and Nigel Goldenfeld.

Grigory Volovik, Camillo De Lellis, and Elia Brué added significant pieces to my research and allowed me to publish these pieces here as Appendices. They should be credited for that, though they do not share responsibility for my conjectures.

Special thanks to Victor Yakhot and Katepalli Sreenivasan, who discussed, criticized, and supported my work all these years.

Arthur Migdal's help with *Mathematica*® is also greatly appreciated.

I also appreciate the thoughtful comments of my referee in IJMPA.

This research is supported by a Simons Foundation award ID 686282 at NYU Abu Dhabi. I am very grateful to Jim for his constant help and inspiration for my work, extending far beyond the financial support.

This project was completed while I was already working in ADIA. The atmosphere of creative freedom and academic research in the SPD department in ADIA, supported and encouraged by our Executive Director Majed Alromaithi, was essential in this final stage of my work. Thank you, Majed.

References

- [1] J. Burgers, A mathematical model illustrating the theory of turbulence, in: R. Von Mises, T. Von Kármán (Eds.), *Advances in Applied Mechanics*, Vol. 1, Elsevier, 1948, pp. 171 – 199. doi:[https://doi.org/10.1016/S0065-2156\(08\)70100-5](https://doi.org/10.1016/S0065-2156(08)70100-5).
URL <http://www.sciencedirect.com/science/article/pii/S0065215608701005>
- [2] A. A. Townsend, On the fine-scale structure of turbulence, *Proc. Roy. Soc. Lond. Ser. A* 208(1095) (1951) 534–542. doi:10.1098/rspa.1951.0179.
- [3] A. A. Migdal, Random surfaces and turbulence, in: V. G. Bar'yakhtar (Ed.), *Proceedings of the International Workshop on Plasma Theory and Nonlinear and Turbulent Processes in Physics*, Kiev, April 1987, World Scientific, 1988, p. 460.
- [4] M. E. Agishtein, A. A. Migdal, Dynamics of vortex surfaces in three dimensions: Theory and simulations, *Physica D: Nonlinear Phenomena* 40 (1) (1989) 91 – 118. doi:[https://doi.org/10.1016/0167-2789\(89\)90029-8](https://doi.org/10.1016/0167-2789(89)90029-8).
URL <http://www.sciencedirect.com/science/article/pii/0167278989900298>
- [5] Y. Kaneda, On the three-dimensional motion of an infinitely thin vortex sheet in an ideal fluid, *Physics of Fluids A* 2 (10) (1990) 1817–1826. doi:10.1063/1.857708.
- [6] P. Cvitanović, J. F. Gibson, Geometry of the turbulence in wall-bounded shear flows: periodic orbits, *Physica Scripta* T142 (2010) 014007. doi:10.1088/0031-8949/2010/t142/014007.
URL <https://doi.org/10.1088/0031-8949/2010/t142/014007>
- [7] A. Migdal, Loop equation and area law in turbulence, in: L. Baulieu, V. Dotsenko, V. Kazakov, P. Windey (Eds.), *Quantum Field Theory and String Theory*, Springer US, 1995, pp. 193–231. doi:10.1007/978-1-4615-1819-8.
URL <https://arxiv.org/abs/hep-th/9310088>

- [8] A. Migdal, Towards field theory of turbulence (2020).
URL <https://arxiv.org/abs/2005.01231>
- [9] A. Migdal, Vortex sheet turbulence as solvable string theory, *International Journal of Modern Physics A* 36 (05) (2021) 2150062.
doi:10.1142/S0217751X21500627.
URL <https://doi.org/10.1142/S0217751X21500627>
- [10] K. P. Iyer, K. R. Sreenivasan, P. K. Yeung, Circulation in high reynolds number isotropic turbulence is a bifractal, *Phys. Rev. X* 9 (2019) 041006.
doi:10.1103/PhysRevX.9.041006.
URL <https://link.aps.org/doi/10.1103/PhysRevX.9.041006>
- [11] K. P. Iyer, S. S. Bharadwaj, K. R. Sreenivasan, The area rule for circulation in three-dimensional turbulence, *Proceedings of the National Academy of Sciences of the United States of America* 118 (43) (2021) e2114679118. doi:10.1073/pnas.2114679118.
URL <https://europepmc.org/articles/PMC8639329>
- [12] A. Migdal, Universal area law in turbulence (2019).
URL <https://arxiv.org/abs/1903.08613>
- [13] A. Migdal, Scaling index $\alpha = \frac{1}{2}$ in turbulent area law (2019).
URL <https://arxiv.org/abs/1904.00900v2>
- [14] A. Migdal, Exact area law for planar loops in turbulence in two and three dimensions (2019).
URL <https://arxiv.org/abs/1904.05245v2>
- [15] A. Migdal, Analytic and numerical study of navier-stokes loop equation in turbulence (2019).
URL <https://arxiv.org/abs/1908.01422v1>
- [16] A. Migdal, Turbulence, string theory and ising model (2019).
URL <https://arxiv.org/abs/1912.00276v3>
- [17] A. Migdal, Probability distribution of velocity circulation in three dimensional turbulence (2020).
URL <https://arxiv.org/abs/2006.12008>

- [18] A. Migdal, Clebsch confinement and instantons in turbulence, *International Journal of Modern Physics A* 35 (31) (2020) 2030018. doi:10.1142/s0217751x20300185. URL <https://doi.org/10.1142/s0217751x20300185>
- [19] A. Migdal, Asymmetric vortex sheet, *Physics of Fluids* 33 (3) (2021) 035127. doi:10.1063/5.0044724. URL <https://doi.org/10.1063/5.0044724>
- [20] A. Migdal, Confined vortex surface and irreversibility. 1. properties of exact solution (2021). URL <https://doi.org/10.1142/S0217751X21500974>
- [21] A. Migdal, Confined vortex surface and irreversibility. 2. hyperbolic sheets and turbulent statistics (2021). arXiv:2105.12719. URL <https://arxiv.org/abs/2105.12719>
- [22] K. Shariff, G. E. Elsinga, Viscous vortex layers subject to more general strain and comparison to isotropic turbulence, *Physics of Fluids* 33 (3) (2021) 033611. doi:10.1063/5.0045243. URL <https://doi.org/10.1063/5.0045243>
- [23] G. E. Volovik, Superfluids in rotation: Landau–lifshitz vortex sheets vs onsager–feynman vortices, *UFN* 185 (2015) 970–979. doi:10.3367/UFNr.0185.201509h.0970.
- [24] K. Zhang, One-dimensional nexus objects, network of kibble-lazarides-shafi string walls, and their spin dynamic response in polar-distorted b -phase of ^3He , *Phys. Rev. Research* 2 (2020) 043356. doi:10.1103/PhysRevResearch.2.043356. URL <https://link.aps.org/doi/10.1103/PhysRevResearch.2.043356>
- [25] T. Ishihara, T. Gotoh, Y. Kaneda, Study of high–reynolds number isotropic turbulence by direct numerical simulation, *Annual Review of Fluid Mechanics* 41 (2008) 165–180. doi:10.1146/annurev.fluid.010908.165203.
- [26] D. Buaria, A. Pumir, E. Bodenschatz, P. K. Yeung, Extreme velocity gradients in turbulent flows, *New Journal of Physics* 21 (4) (2019)

043004. doi:10.1088/1367-2630/ab0756.
URL <https://doi.org/10.1088/1367-2630/ab0756>

- [27] K. R. Sreenivasan, On the scaling of the turbulence energy dissipation rate, *The Physics of Fluids* 27 (5) (1984) 1048–1051. arXiv:<https://aip.scitation.org/doi/pdf/10.1063/1.864731>, doi:10.1063/1.864731.
URL <https://aip.scitation.org/doi/abs/10.1063/1.864731>
- [28] G. Apolinario, L. Moriconi, R. Pereira, V. valadão, Vortex gas modeling of turbulent circulation statistics, *PHYSICAL REVIEW E* 102 (2020) 041102. doi:10.1103/PhysRevE.102.041102.
- [29] N. P. Müller, J. I. Polanco, G. Krstulovic, Intermittency of velocity circulation in quantum turbulence, *Phys. Rev. X* 11 (2021) 011053. doi:10.1103/PhysRevX.11.011053.
URL <https://link.aps.org/doi/10.1103/PhysRevX.11.011053>
- [30] W. T. Ashurst, A. R. Kerstein, R. M. Kerr, C. H. Gibson, Alignment of vorticity and scalar gradient with strain rate in simulated navier–stokes turbulence, *The Physics of Fluids* 30 (8) (1987) 2343–2353. arXiv:<https://aip.scitation.org/doi/pdf/10.1063/1.866513>, doi:10.1063/1.866513.
URL <https://aip.scitation.org/doi/abs/10.1063/1.866513>
- [31] A. Migdal, General vortex sheet, <https://www.wolframcloud.com/obj/sasha.migdal/Published/GeneralVortexSheet.nb> (August 2021).
- [32] G. K. Batchelor, *An Introduction to Fluid Dynamics*, Cambridge University Press, 2000. doi:10.1017/CB09780511800955.
- [33] A. Migdal, Burgers vortex sheet solution of the navier-stokes equation., <https://www.wolframcloud.com/obj/sasha.migdal/Published/BurgersSolutionNavierStol> (Feb 2021).
- [34] H. Lamb, *Hydrodynamics*, Dover publications, 1945.
URL <https://books.google.com/books?id=237xDg7T0RkC>

- [35] I. Khalatnikov, The hydrodynamics of solutions of impurities in helium ii, *Zh. Eksp. Teor. Fiz* 23 (1952) 169.
- [36] E. Kuznetsov, A. Mikhailov, On the topological meaning of canonical clebsch variables, *Physics Letters A* 77 (1) (1980) 37 – 38.
doi:[https://doi.org/10.1016/0375-9601\(80\)90627-1](https://doi.org/10.1016/0375-9601(80)90627-1).
URL <http://www.sciencedirect.com/science/article/pii/0375960180906271>
- [37] E. Levich, The hamiltonian formulation of the euler equation and subsequent constraints on the properties of randomly stirred fluids, *Physics Letters A* 86 (3) (1981) 165–168.
- [38] J. Marsden, A. Weinstein, Coadjoint orbits, vortices, and clebsch variables for incompressible fluids, *Physica D: Nonlinear Phenomena* 7 (1) (1983) 305 – 323. doi:[https://doi.org/10.1016/0167-2789\(83\)90134-3](https://doi.org/10.1016/0167-2789(83)90134-3).
URL <http://www.sciencedirect.com/science/article/pii/0167278983901343>
- [39] V. Yakhot, V. Zakharov, Hidden conservation laws in hydrodynamics; energy and dissipation rate fluctuation spectra in strong turbulence, *Physica D: Nonlinear Phenomena* 64 (4) (1993) 379 – 394. doi:[https://doi.org/10.1016/0167-2789\(93\)90050-B](https://doi.org/10.1016/0167-2789(93)90050-B).
URL <http://www.sciencedirect.com/science/article/pii/016727899390050B>
- [40] M. Brady, A. Leonard, D. Pullin, Regularized vortex sheet evolution in three dimensions, *Journal of Computational Physics* 146 (1998) 520–545.
- [41] Aayush Anand, Computing Enstrophy for the Stable Confined Vortex Surface. PHD thesis (January 2022).
- [42] A. Migdal, Algebraic cvs, <https://www.wolframcloud.com/obj/sasha.migdal/Published/A> (August 2021).
- [43] A. Migdal, Hyperbolic flow, <https://www.wolframcloud.com/obj/sasha.migdal/Published/A> (August 2021).

- [44] Wikipedia, Brouwer Fixed-point Theorem, https://en.wikipedia.org/wiki/Brouwer_fixed-point_theorem, [Online; accessed 11-June-2021] (2021).
- [45] Wikipedia, Random Matrix, https://en.wikipedia.org/wiki/Random_matrix, [Online; accessed 30-September-2021] (2021).
- [46] A. Migdal, Matrix integrals, <https://www.wolframcloud.com/obj/sasha.migdal/Published> (September 2022).
- [47] T. Matsuzawa, W. Irvine, Realization of confined turbulence through multiple vortex ring collisions, "Talk at the Flatiron Conference Universality Turbulence Across Vast Scales" (03/12/2019).
- [48] G. E. Volovik, K. Zhang, String monopoles, string walls, vortex skyrmions, and nexus objects in the polar distorted b phase of ^3He , *Phys. Rev. Research* 2 (2020) 023263. doi:10.1103/PhysRevResearch.2.023263.
URL <https://link.aps.org/doi/10.1103/PhysRevResearch.2.023263>
- [49] Wikipedia, Weierstrass–Enneper parameterization, https://en.wikipedia.org/wiki/Weierstrass%E2%80%93Enneper_parameterization, [Online; accessed 13-December-2019] (2019).
- [50] S. F. Shandarin, Y. B. Zeldovich, The large-scale structure of the universe: Turbulence, intermittency, structures in a self-gravitating medium, *Rev. Mod. Phys.* 61 (1989) 185–220. doi:10.1103/RevModPhys.61.185.
URL <https://link.aps.org/doi/10.1103/RevModPhys.61.185>
- [51] G. Falkovich, I. Kolokolov, V. Lebedev, A. Migdal, Instantons and intermittency, *Phys. Rev. E* 54 (1996) 4896–4907. doi:10.1103/PhysRevE.54.4896.
URL <https://link.aps.org/doi/10.1103/PhysRevE.54.4896>
- [52] A. M. Polyakov, Turbulence without pressure, *Physical Review E* 52 (6) (1995) 6183–6188. doi:10.1103/physreve.52.6183.
URL <https://doi.org/10.1103/physreve.52.6183>

- [53] V. Gurarie, A. Migdal, Instantons in the burgers equation, *Phys. Rev. E* 54 (1996) 4908–4914. doi:10.1103/PhysRevE.54.4908.
URL <https://link.aps.org/doi/10.1103/PhysRevE.54.4908>
- [54] J. BEC, K. KHANIN, Burgers turbulence, *Physics Reports* 447 (1-2) (2007) 1–66. doi:10.1016/j.physrep.2007.04.002.
URL <http://dx.doi.org/10.1016/j.physrep.2007.04.002>
- [55] A. A. Migdal, Turbulence as statistics of vortex cells, in: V. Mineev (Ed.), *The First Landau Institute Summer School, 1993: Selected Proceedings*, Gordon and Breach, 1993, pp. 178–204.
URL <https://arxiv.org/abs/hep-th/9306152v2>
- [56] A. Migdal, Loop equations and $\frac{1}{N}$ expansion, *Physics Reports* 201 (1983).
- [57] Makoto Umeki (July 1993). [link].
URL <https://arxiv.org/abs/hep-th/9307144>
- [58] D. Gross , A. Migdal, A nonperturbative treatment of two-dimensional quantum gravity, *Nuclear Physics B* 335 (1990).
- [59] R. Henrik Schumacher Beltukov, Can Mathematica solve Plateau’s problem (finding a minimal surface with specified boundary)? (2022).
URL <https://mathematica.stackexchange.com/questions/72203/can-mathematica-solve-plateaus-problem-finding-a-minimal-surface-with-specified-boundary>
- [60] G. Parisi, U. Frisch, On the singularity structure of fully developed turbulence turbulence and predictability, in: R. B. M Ghil, G. Parisi (Eds.), *Geophysical Fluid Dynamics: Proc. Intl School of Physics E. Fermi*, Amsterdam: North-Holland, 1985, pp. 84–88.
- [61] V. Yakhot, K. R. Sreenivasan, Anomalous scaling of structure functions and dynamic constraints on turbulence simulations, *Journal of Statistical Physics* 121 (5) (2005) 823–841. doi:10.1007/s10955-005-8666-6.
URL <https://doi.org/10.1007/s10955-005-8666-6>
- [62] K. R. Sreenivasan, V. Yakhot, Dynamics of three-dimensional turbulence from navier-stokes equations, *Phys. Rev. Fluids* 6 (2021) 104604. doi:10.1103/PhysRevFluids.6.104604.

URL <https://link.aps.org/doi/10.1103/PhysRevFluids.6.104604>

- [63] K. R. Sreenivasan, V. Yakhot, The saturation of exponents and the asymptotic fourth state of turbulence (2022). doi:10.48550/ARXIV.2208.09561.
URL <https://arxiv.org/abs/2208.09561>
- [64] A.P. Finne, T. Araki, R. Blaauwgeers, V.B. Eltsov , N.B. Kopnin , M. Krusius, L. Skrbek, M. Tsubota and G.E. Volovik, An intrinsic velocity-independent criterion for superfluid turbulence, *Nature* 424 (2003) 1022–1025.
- [65] G.E. Volovik, *The Universe in a Helium Droplet*, Clarendon Press, Oxford (2003).
- [66] T.D.C. Bevan , A.J. Manninen , J.B. Cook , J.R. Hook , H.E. Hall, T. Vachaspati and G.E. Volovik, Momentum creation by vortices in superfluid ^3He as a model of primordial baryogenesis, *Nature* 386 (1997) 689–692.
- [67] D. Vollhardt and P. Wölfle, *The Superfluid Phases of Helium 3*, Taylor & Francis, London, 1990.
- [68] G. Volovik, Linear momentum in ferromagnets, *J. Phys. C* 20 (1987) L83–L87.
- [69] D.S. Agafontsev, E.A. Kuznetsov and A.A. Mailybaev, "development of high vorticity structures and geometrical properties of the vortex line representation", *Phys. Fluids* 30 (2018).
- [70] G. Volovik, "wess-zumino action for the orbital dynamics of $^3\text{He-A}$ ", *JETP Lett.* 44 (1986) 185–189.
- [71] E.A. Kuznetsov and A.V. Mikhailov, "on the topological meaning of canonical clebsch variables", *Physics Letters A* 77 (1980) 37–38.
- [72] S. Blaha, Quantization rules for point singularities in superfluid ^3He and liquid crystals, *Phys. Rev. Lett.* 36 (1976).
- [73] G.E. Volovik, V.P. Mineev, Vortices with free ends in superfluid $^3\text{He-A}$, *JETP Lett.* 23 (1976).

- [74] G. Volovik, Monopoles and fractional vortices in chiral superconductors, Proc. Natl. Acad. Sc. USA 97 (2000) 2431–2436.
- [75] S. G. Chefranov, I. I. Mokhov, A. G. Chefranov, The hydrodynamic singular vortex on the sphere and the dirac monopole (2017). doi: 10.48550/ARXIV.1711.04124.
URL <https://arxiv.org/abs/1711.04124>
- [76] V.P. Mineyev, G.E. Volovik, Planar and linear solitons in superfluid ^3He , Phys. Rev. B 18 (1978) 3197–3203.
- [77] T. W. B. Kibble, G. Lazarides, and Q. Shafi, Walls bounded by strings, Phys. Rev. D 26 (1982) 435–439.
- [78] T. W. B. Kibble, G. Lazarides, and Q. Shafi, Strings in $SO(10)$, Phys. Lett. B 113 (1982) 237–239.
- [79] J.T. Mäkinen, V.V. Dmitriev, J. Nissinen, J. Rysti, G.E. Volovik, A.N. Yudin, K. Zhang, V.B. Eltsov, Half-quantum vortices and walls bounded by strings in the polar-distorted phases of topological superfluid ^3He , Nat. Comm. 10 (2019).
- [80] G. E. Volovik, K. Zhang, String monopoles, string walls, vortex-skyrmions and nexus objects in polar distorted B-phase of ^3He , Physical Review Research 2 (2020).

Appendix A. The Cylindrical CVS equations

Let us re-derive the cylindrical CVS equations of²⁰ without unnecessary assumption of real and equal functions $d\Gamma_{\pm}$ in (5.5).

The normal vector in complex notation

$$\sigma = \imath C'(\theta) \quad (\text{A.1})$$

The normal projection of velocity field

$$v_x\sigma_x + v_y\sigma_y = \mathbf{Re} (v_x - \imath v_y)\sigma = \frac{\mathbf{Im} \left((v_x - \imath v_y)C'(\theta) \right)}{|C'(\theta)|} \quad (\text{A.2})$$

The first CVS equation (vanishing normal velocity on each side) becomes

$$\mathbf{Im} (V_{\pm}(C(\theta))C'(\theta)) = 0; \forall \theta \quad (\text{A.3})$$

The second and third CVS equations require the computation of the strain related to the complex velocity $F_{\pm} = \phi'_{\pm}$. The strain on each side is a 3×3 matrix

$$\hat{S}_{\pm}(\eta) = \begin{pmatrix} \mathbf{Re} F'_{\pm}(\eta) + a & -\mathbf{Im} F'_{\pm}(\eta) & 0 \\ -\mathbf{Im} F'_{\pm}(\eta) & -\mathbf{Re} F'_{\pm}(\eta) + b & 0 \\ 0 & 0 & c \end{pmatrix} \quad (\text{A.4})$$

Let us introduce notations

$$F(\eta) = \frac{1}{2}(F_+(\eta) + F_-(\eta)); \quad (\text{A.5})$$

$$\Delta F(\eta) = F_+(\eta) - F_-(\eta); \quad (\text{A.6})$$

$$p = (a + b)/2; \quad (\text{A.7})$$

$$q = (a - b)/2 \quad (\text{A.8})$$

The null vector equation $(\hat{S}_+(\eta) + \hat{S}_-(\eta)) \cdot \Delta \vec{v} = 0$ provides the following complex equation

$$\Delta F^*(\eta)(F'(\eta) + q) + p\Delta F(\eta) = 0; \forall \eta \in C; \quad (\text{A.9})$$

The product

$$\Gamma(\theta) = C'(\theta)\Delta F(C(\theta)) \quad (\text{A.10})$$

is real, in virtue of the Neumann boundary conditions. The difference between the two Neumann equations (A.3) reduces to $\mathbf{Im} \Gamma = 0$.

Thus, multiplying (A.9) by $C'(\theta)C'^*(\theta)$ and using the fact that $\Gamma(\theta)$ is real we find

$$C'(\theta) (F'(C(\theta)) + q) + pC'^*(\theta) = 0; \forall \eta \in C; \quad (\text{A.11})$$

This equation is simpler than it looks: it is reduced to the total derivative.

$$\frac{d}{d\theta} (F(C(\theta)) + qC(\theta) + pC^*(\theta)) = 0 \quad (\text{A.12})$$

The generic solution is

$$F(C(\theta)) + qC(\theta) + pC^*(\theta) = A \quad (\text{A.13})$$

with some complex constant A .

Plugging it back to the (A.3) we have everything cancel except one term

$$\mathbf{Im} (AC'(\theta)) = 0; \forall \eta = C(\xi) \quad (\text{A.14})$$

The nontrivial solution for $C(\theta)$ would correspond to $A = 0$.

This solution is equivalent to the equation (5.13) we stated in the text.

Appendix B. Symmetric Traceless Random Matrices

Let us investigate the general properties of the Gaussian random matrix measure. First, the trace of the matrix is invariant against orthogonal transformations

$$W \Rightarrow O^T \cdot W \cdot O; \quad (\text{B.1})$$

$$O^T = O^{-1}; \quad (\text{B.2})$$

$$\text{tr } W \Rightarrow \text{tr } W \quad (\text{B.3})$$

therefore this measure stays $O(n)$ invariant after insertion of the delta function of the trace.

The mean value of $\text{tr } W^2$ can be computed by the following method. Consider the normalization integral

$$Z_n(\sigma) = \int dP_\sigma(W) \quad (\text{B.4})$$

By rescaling the matrix elements $W_{ij} = \sigma w_{ij}$ we find the property

$$Z_n(\sigma) = \sigma^{\frac{(n+2)(n-1)}{2}} Z_n(1) \quad (\text{B.5})$$

Taking the logarithmic derivative of the original integral, we get the identity

$$\frac{\sigma Z'_n(\sigma)}{Z_n(\sigma)} = \frac{\int dP_\sigma(W) \text{tr } W^2}{\sigma^2 Z_n(\sigma)} = \frac{\langle \text{tr } W^2 \rangle}{\sigma^2} \quad (\text{B.6})$$

On the other hand, taking the logarithmic derivative from (B.5), we find

$$\frac{\sigma Z'_n(\sigma)}{Z_n(\sigma)} = \frac{(n+2)(n-1)}{2} \quad (\text{B.7})$$

This formula produces the trace relation (5.98).

Higher moments of various products of matrix elements are also calculable analytically. We study these moments and the generation function in.⁴⁶

Appendix C. Spherical Gauge

The symmetric metric tensor g_{ij} in 2 dimensions has three independent components: two diagonal values g_{11}, g_{22} and one off-diagonal value $g_{12} = g_{21}$.

We take stereographic coordinates $z = z_1 + i z_2 = \tan \frac{\theta}{2} e^{i\varphi}$

$$g_{ij} = \delta_{ij} \rho; \quad (\text{C.1a})$$

$$\rho = \frac{1}{(1 + |z|^2)^2}; \quad (\text{C.1b})$$

$$z_a = \frac{S_a}{1 + S_3}; \quad (\text{C.1c})$$

$$S_a = \frac{2z_a}{1 + |z|^2}; \quad (\text{C.1d})$$

$$S_3 = \frac{1 - |z|^2}{1 + |z|^2}; \quad (\text{C.1e})$$

$$d^2 S = dz_1 dz_2 \rho \quad (\text{C.1f})$$

The $O(3)$ rotation in these coordinates reads (with $I, J, K = 1, 2, 3, a, b, c \dots = 1, 2$)

$$\delta S_I = e_{IJK} S_J \alpha_K; \quad (C.2a)$$

$$\delta z_a = \alpha_3 e_{ab} z_b - \frac{1}{2}(1 - |z|^2) \tilde{\alpha}_a - \tilde{\alpha}_b z_b z_a; \quad (C.2b)$$

$$\tilde{\alpha}_b = e_{bc} \alpha_c; \quad (C.2c)$$

The $O(3)$ transformation of the metric tensor involves the matrix $R_{ij} = \partial_j \delta z_i$

$$R_{ij} = \alpha_3 e_{ij} + \tilde{\alpha}_i z_j - \tilde{\alpha}_j z_i - \delta_{ij} \tilde{\alpha}_3; \quad (C.3)$$

$$\delta_{O(3)} g_{ij} = R_{ai} g_{aj} + R_{aj} g_{ai} \quad (C.4)$$

Computing the variation $\delta_{O(3)} g_{ij}$ of the conformal metric $g_{ij}^c = \rho \delta_{ij}$ we find

$$\delta_{O(3)} g_{12}^c = 0; \quad (C.5a)$$

$$\delta_{O(3)} g_{11}^c = -2\rho (z_1 \alpha_2 - z_2 \alpha_1); \quad (C.5b)$$

$$\delta_{O(3)} g_{22}^c = -2\rho (z_1 \alpha_2 - z_2 \alpha_1); \quad (C.5c)$$

The gauge transformation of conformal metrics produces

$$\delta_{gauge} g_{12}^c = (h_{22} - h_{11})\rho; \quad (C.6a)$$

$$\delta_{gauge} g_{11}^c = 2h_{12}\rho; \quad (C.6b)$$

$$\delta_{gauge} g_{22}^c = -2h_{12}\rho; \quad (C.6c)$$

$$h_{ij} = \partial_i \partial_j h(z_1, z_2) \quad (C.6d)$$

Now, we do not want to break the rotational invariance of the spherical metric. Therefore, any $h(z)$ satisfying the equations

$$h_{22} - h_{11} = 0; \quad (C.7)$$

$$h_{12} = -(z_1 \alpha_2 - z_2 \alpha_1); \quad (C.8)$$

$$-h_{12} = -(z_1 \alpha_2 - z_2 \alpha_1) \quad (C.9)$$

with some finite constant α_1, α_2 should not be restricted by our gauge conditions. Adding the last two equations, we immediately see that no such gauge functions could imitate the $O(3)$ rotations.

The independent conditions $h_{12} = 0, h_{11} = h_{22}$ combine into one complex equation

$$\hat{L}h = \rho \frac{\partial^2}{\partial \bar{z}^2} h = 0 \quad (\text{C.10})$$

These gauge conditions leave out arbitrary linear function $h = A + B_i z_i$, corresponding to constant shifts of Clebsch field. These constant shifts can be fixed by placing the origin at the South Pole, which we did.

For remaining nontrivial symplectomorphisms we have the gauge fixing Gaussian integral

$$\int D\lambda D\mu Dh \exp \left(i \int d^2 S \lambda \hat{L}_1 h + \mu \hat{L}_2 h \right); \quad (\text{C.11a})$$

$$\hat{L}_1 h = \rho \mathbf{Re} \hat{L} h; \quad (\text{C.11b})$$

$$\hat{L}_2 h = \rho \mathbf{Im} \hat{L} h; \quad (\text{C.11c})$$

The regularized determinant $\det \hat{L}$ is a universal number, which does not depend on our dynamical variables.

This operator being non-Hermitian, we are not sure how to regularize and compute this determinant, but this is immaterial, as it does not depend on dynamic variables and thus drops from the measure.

The symmetric metric tensor g_{ij} in 2 dimensions has three independent components: two diagonal values g_{11}, g_{22} and one off-diagonal value $g_{12} = g_{21}$.

We take stereographic coordinates $z = z_1 + i z_2 = \tan \frac{\theta}{2} e^{i \varphi}$

$$g_{ij} = \delta_{ij} \rho; \quad (\text{C.12a})$$

$$\rho = \frac{1}{(1 + |z|^2)^2}; \quad (\text{C.12b})$$

$$z_a = \frac{S_a}{1 + S_3}; \quad (\text{C.12c})$$

$$S_a = \frac{2z_a}{1 + |z|^2}; \quad (\text{C.12d})$$

$$S_3 = \frac{1 - |z|^2}{1 + |z|^2}; \quad (\text{C.12e})$$

$$d^2 S = dz_1 dz_2 \rho \quad (\text{C.12f})$$

The $O(3)$ rotation in these coordinates reads (with $I, J, K = 1, 2, 3, a, b, c \dots = 1, 2$)

$$\delta S_I = e_{IJK} S_J \alpha_K; \quad (\text{C.13a})$$

$$\delta z_a = \alpha_3 e_{ab} z_b - \frac{1}{2}(1 - |z|^2) \tilde{\alpha}_a - \tilde{\alpha}_b z_b z_a; \quad (\text{C.13b})$$

$$\tilde{\alpha}_b = e_{bc} \alpha_c; \quad (\text{C.13c})$$

The $O(3)$ transformation of the metric tensor involves the matrix $R_{ij} = \partial_j \delta z_i$

$$R_{ij} = \alpha_3 e_{ij} + \tilde{\alpha}_i z_j - \tilde{\alpha}_j z_i - \delta_{ij} \tilde{\alpha}_3; \quad (\text{C.14})$$

$$\delta_{O(3)} g_{ij} = R_{ai} g_{aj} + R_{aj} g_{ai} \quad (\text{C.15})$$

Computing the variation $\delta_{O(3)} g_{ij}$ of the conformal metric $g_{ij}^c = \rho \delta_{ij}$ we find

$$\delta_{O(3)} g_{12}^c = 0; \quad (\text{C.16a})$$

$$\delta_{O(3)} g_{11}^c = -2\rho (z_1 \alpha_2 - z_2 \alpha_1); \quad (\text{C.16b})$$

$$\delta_{O(3)} g_{22}^c = -2\rho (z_1 \alpha_2 - z_2 \alpha_1); \quad (\text{C.16c})$$

The gauge transformation of conformal metrics produces

$$\delta_{gauge} g_{12}^c = (h_{22} - h_{11})\rho; \quad (\text{C.17a})$$

$$\delta_{gauge} g_{11}^c = 2h_{12}\rho; \quad (\text{C.17b})$$

$$\delta_{gauge} g_{22}^c = -2h_{12}\rho; \quad (\text{C.17c})$$

$$h_{ij} = \partial_i \partial_j h(z_1, z_2) \quad (\text{C.17d})$$

Now, we do not want to break the rotational invariance of the spherical metric. Therefore, any $h(z)$ satisfying the equations

$$h_{22} - h_{11} = 0; \quad (\text{C.18})$$

$$h_{12} = -(z_1 \alpha_2 - z_2 \alpha_1); \quad (\text{C.19})$$

$$-h_{12} = -(z_1 \alpha_2 - z_2 \alpha_1) \quad (\text{C.20})$$

with some finite constant α_1, α_2 should not be restricted by our gauge conditions. Adding the last two equations, we immediately see that no such gauge functions could imitate the $O(3)$ rotations.

The independent conditions $h_{12} = 0, h_{11} = h_{22}$ combine into one complex equation

$$\hat{L}h = \rho \frac{\partial^2}{\partial \bar{z}^2} h = 0 \quad (\text{C.21})$$

These gauge conditions leave out arbitrary linear function $h = A + B_i z_i$, corresponding to constant shifts of Clebsch field. These constant shifts can be fixed by placing the origin at the South Pole, which we did.

For remaining nontrivial symplectomorphisms we have the gauge fixing Gaussian integral

$$\int D\lambda D\mu Dh \exp \left(i \int d^2 S \lambda \hat{L}_1 h + \mu \hat{L}_2 h \right); \quad (\text{C.22a})$$

$$\hat{L}_1 h = \rho \mathbf{Re} \hat{L} h; \quad (\text{C.22b})$$

$$\hat{L}_2 h = \rho \mathbf{Im} \hat{L} h; \quad (\text{C.22c})$$

The regularized determinant $\det \hat{L}$ is a universal number, which does not depend on our dynamical variables.

This operator being non-Hermitian, we are not sure how to regularize and compute this determinant, but this is immaterial, as it does not depend on dynamic variables and thus drops from the measure.

Appendix D. Geometric structure of constrained vortex surfaces (by Camillo De Lellis, Elia Bru )

This short note derives some geometric conditions that Migdal's constrained vortex surfaces have to satisfy.

Appendix D.1. CVS conditions: geometric interpretation and instability in the compact case

Let $\mathcal{S} \subset \mathbb{R}^3$ be a (sufficiently smooth) complete connected surface. We denote by \mathcal{S}_- the region enclosed by \mathcal{S} , and set $\mathcal{S}_+ := \mathbb{R}^3 \setminus (\mathcal{S} \cup \mathcal{S}_-)$.

According to Migdal's definition, a CVS (constrained vortex surface) solution to the Euler equations is a pair of (sufficiently smooth) velocity fields (v_-, v_+) defined on \mathcal{S}_- and \mathcal{S}_+ , respectively, such that

$$\operatorname{div} v_+ = \operatorname{div} v_- = 0 \quad (\text{D.1})$$

$$\operatorname{curl} v_+ = \operatorname{curl} v_- = 0 \quad (\text{D.2})$$

$$v_+, v_- \text{ are tangent to } \mathcal{S} \quad (\text{D.3})$$

$$(Dv_+ + Dv_-) \cdot (v_+ - v_-) = 0 \quad (\text{D.4})$$

$$|v_+|^2 - |v_-|^2 \text{ is locally constant on } \mathcal{S}. \quad (\text{D.5})$$

Moreover, the constrained vortex surface has to satisfy the following stability condition

$$\langle D(v_+ + v_-) \cdot n, n \rangle < 0, \quad (\text{D.6})$$

where n is the exterior normal to \mathcal{S} and $\langle a, b \rangle$ denotes the scalar product of the vectors a and b .

We have the following geometric characterization of (D.3), (D.4) and (D.5).

Theorem Appendix D.1. *Conditions (D.3), (D.4), (D.5) are satisfied iff*

$$\begin{cases} A(v_-, v_-) = A(v_+, v_+) \\ [v_+, v_-] = 0, \end{cases} \quad (\text{D.7})$$

where A is the second fundamental form of \mathcal{S} , and $[v_+, v_-]$ is the Lie bracket, i.e.

$$[v_+, v_-] = Dv_+ \cdot v_- - Dv_- \cdot v_+.$$

Remark Appendix D.2. *Recall that the Lie Bracket $[v_+, v_-] = (Dv_+ \cdot v_- - Dv_- \cdot v_+)|_{\mathcal{S}}$ is tangent to \mathcal{S} because v_+ and v_- are tangent to \mathcal{S} .*

Proof. Condition (D.5) is equivalent to

$$(Dv_+ \cdot v_+ - Dv_- \cdot v_-)|_{\mathcal{S}} \text{ is parallel to } n. \quad (\text{D.8})$$

We rewrite (D.4) as $I + II = 0$, where

$$\begin{aligned} I &= Dv_+ \cdot v_+ - Dv_- \cdot v_- \\ II &= -Dv_+ \cdot v_- + Dv_- \cdot v_+, \end{aligned}$$

and observe that I is normal to \mathcal{S} , as a consequence of (D.8), while II is tangent to \mathcal{S} . Indeed,

$$\langle II, n \rangle = A(v_+, v_-) - A(v_-, v_+) = 0.$$

In particular $I + II = 0$ iff $I = 0$ and $II = 0$. It is immediate to rewrite the two conditions as (D.7). □

Regarding the stability condition (D.6), we can prove the following rigidity result.

Theorem Appendix D.3. *If $\mathcal{S} \subset \mathbb{R}^3$ is a smooth compact closed surface and v_+, v_- a pair of vector fields that satisfy the conditions (D.1) and (D.3), then*

$$\int_{\mathcal{S}} \langle D(v_+ + v_-) \cdot n, n \rangle = 0. \quad (\text{D.9})$$

In particular, (D.6) cannot hold.

The same argument allows for a similar conclusion when \mathcal{S} is a smooth compact surface with boundary $\partial\mathcal{S}$ and $v^+ + v^-$ is tangent to the boundary.

Theorem Appendix D.4. *Assume $\mathcal{S} \subset \mathbb{R}^3$ is a smooth compact surface with smooth boundary $\partial\mathcal{S}$ and v_+, v_- a pair of vector fields that satisfy the conditions (D.1) and (D.3). If in addition $v^+ + v^-$ is tangent to $\partial\mathcal{S}$, then*

$$\int_{\mathcal{S}} \langle D(v_+ + v_-) \cdot n, n \rangle = 0. \quad (\text{D.10})$$

In particular, (D.6) cannot hold.

Remark Appendix D.5. Clearly Theorem Appendix D.3 can be thought as the particular case of Theorem Appendix D.4 has empty boundary. The smoothness needed by the proof given below is that the surface and its boundary are both C^1 (i.e. they have a tangent at every point, which in turn varies continuously), and that the vector fields are C^1 , i.e. continuously differentiable.

Proof of Theorem Appendix D.4. Fix a point $p \in \mathcal{S}$ and choose a local orthonormal frame around p consisting of e_1, e_2, n , where the vectors e_1 and e_2 are tangent to \mathcal{S} . Note that, since both v_+ and v_- are divergence free we have that $D(v_+ + v_-)$ is a trace-free matrix, and thus

$$\langle D(v_+ + v_-) \cdot n, n \rangle = -\langle D(v_+ + v_-) \cdot e_1, e_1 \rangle - \langle D(v_+ + v_-) \cdot e_2, e_2 \rangle. \quad (\text{D.11})$$

Let g be the Riemannian scalar product induced on \mathcal{S} by the Euclidean one, and denote by $\nabla^{\mathcal{S}}$ the corresponding Levi-Civita connection. Recall that the latter coincides with the connection induced by the Euclidean connection. This amounts to say that, if X, Y and Z are tangent vector fields to \mathcal{S} , then

$$g(\nabla_Y^{\mathcal{S}} X, Z) = \langle DX \cdot Y, Z \rangle.$$

If we apply this to $Y = Z = e_i$ and $X = v_+ + v_-$, (D.11) can be rewritten as

$$g(\nabla_{e_1}^{\mathcal{S}}(v_+ + v_-), e_1) + g(\nabla_{e_2}^{\mathcal{S}}(v_+ + v_-), e_2) = -\langle D(v_+ + v_-) \cdot n, n \rangle. \quad (\text{D.12})$$

Notice now that the left hand side of (D.12) is the divergence in \mathcal{S} of the tangent vector field $v_+ + v_-$, namely we have

$$\operatorname{div}_{\mathcal{S}}(v_+ + v_-) = -\langle D(v_+ + v_-) \cdot n, n \rangle. \quad (\text{D.13})$$

Next, by Gauss theorem, the fact that \mathcal{S} has a smooth boundary implies that

$$\int_{\mathcal{S}} \operatorname{div}_{\mathcal{S}}(v_+ + v_-) = - \int_{\partial \mathcal{S}} (v_+ + v_-) \cdot \nu, \quad (\text{D.14})$$

where we denote by ν the smooth unit vector field on $\partial \mathcal{S}$ which is tangent to \mathcal{S} , orthogonal to $\partial \mathcal{S}$ and points “inwards”, i.e. towards \mathcal{S} . Since $v_+ + v_-$ is parallel to $\partial \mathcal{S}$, the integrand in the right hand side of (D.14) vanishes identically, which allows us to conclude (D.10). \square

Appendix D.2. Rigidity of the CVS condition for closed surfaces

We prove rigidity results for closed connected CVS surfaces without imposing the stability condition (D.6). We prove that

- (A) there are no CVS solutions with \mathcal{S} homeomorphic to the sphere;
- (B) if \mathcal{S} has genus bigger than 1, then \mathcal{S} cannot be real analytic;
- (C) if \mathcal{S} has genus 1, then there are no axisymmetric solutions.

The precise formulation of (A) is the following:

Theorem Appendix D.6. *If (v_-, v_+) satisfies the CVS conditions (D.1), (D.2), (D.3), (D.4), (D.5), and \mathcal{S} is homeomorphic to the sphere, then $v_+ = 0$ and $v_- = 0$.*

Point (B) is a consequence of a more general fact which we state in the following theorem.

Theorem Appendix D.7. *The following holds:*

- (i) *If \mathcal{S} is a smooth closed connected CVS surface with genus different than 1, then $|v_+|^2 = |v_-|^2$.*
- (ii) *If \mathcal{S} is any smooth CVS surface and $|v_+|^2 = |v_-|^2$, then for any point $q \in \mathcal{S}$ one of the following conditions must necessarily hold:*
 - (a) *The Gauss curvature of \mathcal{S} is 0 at q ;*
 - (b) *$v_+(q) = v_-(q)$;*
 - (c) *$v_+(q) = -v_-(q)$.*

From the above theorem we draw the following simple

Corollary Appendix D.8. *Assume \mathcal{S} is a closed smooth connected CVS surface with genus strictly higher than 1. Then either $v_+ = v_-$ on some nontrivial open subset of \mathcal{S} , or $v_+ = -v_-$ on some nontrivial open subset of \mathcal{S} .*

Proof. In fact, if the sets $\{v_+ = v_-\}$ and $\{v_+ = -v_-\}$ contain no interior points, then the Gauss curvature would vanish on a dense set, and by continuity it must vanish anywhere. But it is well known that a surface with vanishing Gauss curvature cannot be closed. \square

The condition is even more stringent if \mathcal{S} is real analytic, i.e. it can be described as the graph of a function with a converging Taylor series around any point, up to rotation of the coordinates.

Corollary Appendix D.9. *Assume \mathcal{S} is a closed real analytic connected CVS surface with genus strictly higher than 1. Then either $v_+ = v_-$ on \mathcal{S} , or $v_+ = -v_-$ on \mathcal{S} .*

Proof. Since both v_+ and v_- are locally gradients of harmonic functions which satisfy the Neumann boundary condition, it turns out that their restrictions to \mathcal{S} are real analytic as well. But real analytic functions which vanish on a nontrivial open set, must vanish identically because \mathcal{S} is connected. \square

We finally detail the non existence result (C) for axisymmetric solutions of genus 1. Let us consider a closed simple curve $[0, 1] \ni t \rightarrow \gamma(t) = (\gamma_r(t), \gamma_z(t)) \in (0, \infty)^2$, and the associated torus of rotation $\mathcal{S} \subset \mathbb{R}^3$, parametrized by

$$(t, \theta) \rightarrow (\gamma_r(t) \cos \theta, \gamma_r(t) \sin \theta, \gamma_z(t)). \quad (\text{D.15})$$

We use polar coordinates $(x, y, z) = (r \cos \theta, r \sin \theta, z)$. Recall that $\frac{\partial}{\partial r}, \frac{1}{r} \frac{\partial}{\partial \theta}, \frac{\partial}{\partial z}$ is an orthonormal frame.

We look for CVS solutions with axisymmetry. The general Ansatz is the following.

$$\begin{aligned} v_- &:= \alpha \frac{1}{r^2} \frac{\partial}{\partial \theta} = \nabla \theta \\ v_+ &:= a(r, z) \frac{\partial}{\partial r} + b(r, z) \frac{1}{r} \frac{\partial}{\partial \theta} + c(r, z) \frac{\partial}{\partial z}, \end{aligned}$$

for some $\alpha \in \mathbb{R}$ and C^1 functions a, b and c .

Theorem Appendix D.10. *Let \mathcal{S} be given by (D.15), for some simple closed curve $\gamma = (\gamma_r, \gamma_z)$ of class C^2 . If (v_-, v_+) is an axisymmetric pair that satisfies the CVS conditions (D.1), (D.2), (D.3), (D.4), (D.5), then either $v_+ = v_-$ on \mathcal{S} , or $v_+ = -v_-$ on \mathcal{S} .*

Appendix D.3. Proof of Theorem Appendix D.6

Since \mathcal{S}_- is simply connected we can write $v_- = \nabla \Phi_-$ for some harmonic function Φ_- , whose gradient is tangent to \mathcal{S} . A simple integration by parts gives

$$\int_{\mathcal{S}_-} |v_-|^2 dx = \int_{\mathcal{S}_-} |\nabla \Phi_-|^2 dx = \int_{\mathcal{S}} \Phi_- \nabla \Phi_- \cdot n dx = 0, \quad (\text{D.16})$$

where n denotes the exterior normal to \mathcal{S} . We deduce that $v_- = 0$. Thanks to Theorem Appendix D.7(i) we deduce that $v_+ = 0$ on \mathcal{S} . Since v_+ is harmonic, the unique continuation principle implies that v_+ vanishes identically.

Appendix D.4. Proof of Theorem Appendix D.7

Let us begin by proving (i). A well-known theorem in topology implies that any tangent vector field to a closed surface \mathcal{S} with genus different than 1 must necessarily vanish at some point. This excludes that the constant in (D.5) is positive (because then v_+ would never vanish) or negative (because then v_- would never vanish).

Let us pass to the proof of (ii). The key ingredient is the following lemma, whose proof is postponed at the end of this section.

Lemma Appendix D.11. *Let $\Sigma \subset \mathbb{R}^3$ be a smooth surface and let $U \subset \Sigma$ be an open set. Assume the existence of smooth velocity fields u, w defined on U and tangent to Σ . If*

- (i) $u(p), w(p) \neq 0$ and $g_p(v, w) = 0$ for any $p \in U$, where g is the metric induced by the ambient space \mathbb{R}^3 ;
- (ii) $[u, w] = 0$ in U ;
- (iii) u and v are gradients in U , i.e. there exist $\alpha, \beta : U \rightarrow \mathbb{R}$ such that $g_p(u, \cdot) = d_p \alpha$ and $g_p(v, \cdot) = d_p \beta$ for any $p \in U$.

Then, the Gaussian curvature of Σ is zero in U .

Let us explain how to prove Theorem Appendix D.7(ii) given Lemma Appendix D.11. Fix q such that $v_+(q) \neq v_-(q)$ and $v_+(q) \neq v_-(q)$ and let U be a neighborhood of q where $v_+ - v_-$ and $v_+ + v_-$ never vanish. Since $|v_+|^2 = |v_-|^2$, we have $g_p(u, w) = 0$ for any $p \in U$. Theorem Appendix

D.1 implies that $[v_+, v_-] = 0$, hence $[u, w] = 0$ in U . Moreover, (D.2) imply that v_+ and v_- are irrotational in \mathcal{S}_+ and \mathcal{S}_- , respectively, and (D.3) says that v_+ and v_- are tangent to \mathcal{S} . This implies that, v_+ and v_- are locally gradients in \mathcal{S} . In particular u and w are locally gradients in U . We are in position to apply Lemma Appendix D.11 with $\Sigma = \mathcal{S}$, which implies that $K = 0$ in U , where K denotes the Gaussian curvature of \mathcal{S} . This implies in particular that the Gauss curvature of \mathcal{S} vanishes at q .

Appendix D.4.1. Proof of Lemma Appendix D.11

Fix $p \in U$. We claim that there exists local coordinates around p

$$X : W \subset \mathbb{R}^2 \rightarrow U, \quad (x, y) \rightarrow X(x, y) \in U,$$

such that

$$\frac{\partial}{\partial x} = u, \quad \frac{\partial}{\partial y} = w.$$

The claim follows from (ii), indeed we can define

$$X(x, y) = \phi_u^x \circ \phi_w^y(p) \in U,$$

where ϕ_u and ϕ_w are the flow maps associated to u and v , respectively. Observe that $X(0, 0) = p$. Condition (ii) implies that the flow maps commute, hence

$$\frac{\partial}{\partial x} X(x, y) = u \circ X(x, y), \quad \frac{\partial}{\partial y} X(x, y) = w \circ X(x, y), \quad (\text{D.17})$$

in particular (i), along with the implicit function theorem, says that X is a local parametrization in a neighborhood of p .

Let h be the metric in the new coordinates (x, y) . It turns out that

$$h_{x,y} = h_{y,x} = g \left(\frac{\partial}{\partial x}, \frac{\partial}{\partial y} \right) = g(u, w) = 0 \quad (\text{D.18})$$

as a consequence of the previous claim and condition (i). We claim that

$$\frac{\partial}{\partial y} h_{x,x} = \frac{\partial}{\partial x} h_{y,y} = 0. \quad (\text{D.19})$$

It immediately implies that Σ is flat in a neighborhood of p . Indeed, as a consequence of (D.19) we can write the metric as

$$h = a(x)dx^2 + b(y)dy^2,$$

which is clearly flat.

Let us prove (D.19). As a consequence of (iii) we get

$$\begin{aligned} \frac{\partial}{\partial y} h_{x,x} &= \frac{\partial}{\partial y} g \left(\frac{\partial}{\partial x}, \frac{\partial}{\partial x} \right) = 2g \left(\nabla_{\frac{\partial}{\partial y}} \frac{\partial}{\partial x}, \frac{\partial}{\partial x} \right) \\ &= 2\text{Hess } \alpha \left(\frac{\partial}{\partial y}, \frac{\partial}{\partial x} \right) \end{aligned} \quad (\text{D.20})$$

the symmetry of the Hessian implies

$$\text{Hess } \alpha \left(\frac{\partial}{\partial y}, \frac{\partial}{\partial x} \right) = \text{Hess } \alpha \left(\frac{\partial}{\partial x}, \frac{\partial}{\partial y} \right) = g \left(\nabla_{\frac{\partial}{\partial x}} \frac{\partial}{\partial x}, \frac{\partial}{\partial y} \right), \quad (\text{D.21})$$

on the other hand we know that $g \left(\frac{\partial}{\partial x}, \frac{\partial}{\partial y} \right) = 0$, hence

$$\begin{aligned} g \left(\nabla_{\frac{\partial}{\partial x}} \frac{\partial}{\partial x}, \frac{\partial}{\partial y} \right) &= \frac{\partial}{\partial x} g \left(\frac{\partial}{\partial x}, \frac{\partial}{\partial y} \right) - g \left(\frac{\partial}{\partial x}, \nabla_{\frac{\partial}{\partial x}} \frac{\partial}{\partial y} \right) \\ &= -g \left(\frac{\partial}{\partial x}, \nabla_{\frac{\partial}{\partial y}} \frac{\partial}{\partial x} \right), \end{aligned} \quad (\text{D.22})$$

where in the last step we used that $\left[\frac{\partial}{\partial x}, \frac{\partial}{\partial y} \right] = 0$. By collection (D.20), (D.21), and (D.22) we deduce

$$\frac{\partial}{\partial y} h_{x,x} = -\frac{\partial}{\partial y} h_{x,x},$$

which implies our claim. We argue in the same way to show that $\frac{\partial}{\partial x} h_{y,y} = 0$.

Appendix D.5. Proof of Theorem Appendix D.10

Without loss of generality we assume that $\gamma : [0, L] \rightarrow (0, \infty)^2$ is parametrized by arclength, where L is the length of γ . Recall that we look

for solutions of the form

$$\begin{aligned} v_- &:= \alpha \frac{1}{r^2} \frac{\partial}{\partial \theta} \\ v_+ &:= a(r, z) \frac{\partial}{\partial r} + b(r, z) \frac{1}{r} \frac{\partial}{\partial \theta} + c(r, z) \frac{\partial}{\partial z}, \end{aligned}$$

where $\alpha \in \mathbb{R}$ and a, b, c are C^1 functions.

Lemma Appendix D.12. *We have that $\text{curl } v_+ = 0$ if and only if $b(r, z)r$ is constant and*

$$\text{curl} \left(a(r, z) \frac{\partial}{\partial r} + c(r, z) \frac{\partial}{\partial z} \right) = 0. \quad (\text{D.23})$$

Proof. We compute

$$\text{curl } v_+ = \left(\frac{1}{r} \frac{\partial c}{\partial \theta} - \frac{\partial b}{\partial z} \right) \frac{\partial}{\partial r} + \left(\frac{\partial a}{\partial z} - \frac{\partial c}{\partial r} \right) \frac{1}{r} \frac{\partial}{\partial \theta} + \frac{1}{r} \left(\frac{\partial(rb)}{\partial r} - \frac{\partial a}{\partial \theta} \right) \frac{\partial}{\partial z}.$$

Since v_+ is axisymmetric, we have that $\text{curl } v_+ = 0$ if and only if

$$\begin{cases} \frac{\partial b}{\partial z} = 0 \\ \frac{\partial(rb)}{\partial r} = 0 \\ \text{curl} \left(a \frac{\partial}{\partial r} + c \frac{\partial}{\partial z} \right) = 0. \end{cases} \quad (\text{D.24})$$

The first two conditions amount to $br = C$, for some constant $C \in \mathbb{R}$. The latter amounts to (D.23). \square

Let us begin by considering the case $\alpha \neq 0$. Without loss of generality we can assume $\alpha = 1$. After imposing $\text{curl } v_+ = 0$, we can write

$$v_+ = a(r, z) \frac{\partial}{\partial r} + c(r, z) \frac{\partial}{\partial z} + C v_- =: w_+ + C v_-. \quad (\text{D.25})$$

To satisfy the CVS conditions we need to impose the following properties on w_+ :

- (1) $\text{div } w_+ = \text{curl } w_+ = 0$
- (2) w_+ is tangent to \mathcal{S}

$$(3) \quad |w_+|^2 + \frac{C^2-1}{r^2} = \ell \text{ in } \mathcal{S}, \text{ for some } \ell \in \mathbb{R}$$

$$(4) \quad [w_+, v_-] = 0 \text{ in } \mathcal{S}$$

$$(5) \quad A(w_+ + Cv_-, w_+ + Cv_-) = A(v_-, v_-)$$

We show that (2), (3) and (4) imply that γ_r is constant.

Condition (4). We compute

$$\begin{aligned} [w_+, v_-] &= \nabla_{w_+} v_- - \nabla_{v_-} w_+ \\ &= \nabla_{a \frac{\partial}{\partial r} + c \frac{\partial}{\partial z}} \left(\frac{1}{r^2} \frac{\partial}{\partial \theta} \right) - \frac{1}{r^2} \nabla_{\frac{\partial}{\partial \theta}} \left(a \frac{\partial}{\partial r} + c \frac{\partial}{\partial z} \right) = -\frac{2}{r^3} a \frac{\partial}{\partial \theta}. \end{aligned}$$

Hence, we have to impose

$$a(\gamma_r(t), \gamma_z(t)) = 0, \quad \text{for any } t \in [0, L]. \quad (\text{D.26})$$

Condition (2) and (3). Recall that

$$n = (\dot{\gamma}_z(t) \cos \theta, \dot{\gamma}_z(t) \sin \theta, -\dot{\gamma}_r(t)),$$

where n denotes the exterior normal to \mathcal{S} . By using (D.26), we deduce

$$w_+ = c(r, z) \frac{\partial}{\partial z}, \quad \text{on } \mathcal{S}, \quad (\text{D.27})$$

hence

$$0 = w_+ \cdot n = -c(\gamma_r(t), \gamma_z(t)) \dot{\gamma}_r(t).$$

In particular, by employing (D.27) and (3) we get

$$\begin{aligned} 0 &= |c(\gamma_r(t), \gamma_z(t))|^2 |\dot{\gamma}_r(t)|^2 = |w_+|^2 |\dot{\gamma}_r(t)|^2 \\ &= \left(\ell + \frac{1-C^2}{\gamma_r^2(t)} \right) |\dot{\gamma}_r(t)|^2. \end{aligned}$$

If either $C^2 \neq 1$ or $\ell \neq 0$, then $\gamma_r = \text{const}$. This is impossible because γ is a closed simple curved.

If $C^2 = 1$ and $\ell = 0$, then (3) implies that $|w_+|^2 = 0$ on \mathcal{S} . It amounts to $v_+ = v_-$ when $C = 1$ and $v_+ = -v_-$ when $C = -1$.

The case $\alpha = 0$. Let us now assume that $\alpha = 0$. By applying Lemma Appendix D.12 we deduce

$$v_+ = a(r, z) \frac{\partial}{\partial r} + c(r, z) \frac{\partial}{\partial z} + C \frac{1}{r^2} \frac{\partial}{\partial \theta} =: w_+ + C \frac{1}{r^2} \frac{\partial}{\partial \theta}.$$

In this case, to satisfy the CVS conditions we need to impose the following properties on w_+ :

$$(1') \quad \operatorname{div} w_+ = \operatorname{curl} w_+ = 0$$

$$(2') \quad w_+ \text{ is tangent to } \mathcal{S}$$

$$(3') \quad |w_+|^2 + \frac{C^2}{r^2} = \ell \text{ in } \mathcal{S}, \text{ for some } \ell \in \mathbb{R}$$

$$(4') \quad A(w_+ + C \frac{1}{r^2} \frac{\partial}{\partial \theta}, w_+ + C \frac{1}{r^2} \frac{\partial}{\partial \theta}) = 0.$$

We show that (4') forces $C = 0$. Since w_+ is tangent to \mathcal{S} , there exists $\lambda : \mathcal{S} \rightarrow \mathbb{R}$ such that

$$w_+(\gamma) = \lambda \left(\dot{\gamma}_r \frac{\partial}{\partial r} + \dot{\gamma}_z \frac{\partial}{\partial z} \right). \quad (\text{D.28})$$

We use the well-known identities

$$\begin{aligned} A \left(\dot{\gamma}_r \frac{\partial}{\partial r} + \dot{\gamma}_z \frac{\partial}{\partial z}, \dot{\gamma}_r \frac{\partial}{\partial r} + \dot{\gamma}_z \frac{\partial}{\partial z} \right) &= \kappa \\ A \left(\frac{\partial}{\partial \theta}, \frac{\partial}{\partial \theta} \right) &= \gamma_r \dot{\gamma}_z \\ A \left(\dot{\gamma}_r \frac{\partial}{\partial r} + \dot{\gamma}_z \frac{\partial}{\partial z}, \frac{\partial}{\partial \theta} \right) &= 0, \end{aligned}$$

where $\kappa = \ddot{\gamma}_z \dot{\gamma}_r - \ddot{\gamma}_r \dot{\gamma}_z$ is the curvature of γ . We deduce

$$0 = A \left(w_+ + C \frac{1}{r^2} \frac{\partial}{\partial \theta}, w_+ + C \frac{1}{r^2} \frac{\partial}{\partial \theta} \right) = \lambda^2 \kappa + \frac{C^2}{\gamma_r^3} \dot{\gamma}_z \quad (\text{D.29})$$

Let us consider $t_0 \in [0, L]$, a minimum point for γ_r . Since $\dot{\gamma}_r(t_0) = 0$ and γ is parametrized by arclength, we deduce that $\dot{\gamma}_z(t_0) \neq 0$. Hence, (D.29) implies that $\lambda(t_0) \neq 0$. So, in a small neighborhood of t_0 we can rewrite (D.29) as

$$\ddot{\gamma}_z \dot{\gamma}_r - \ddot{\gamma}_r \dot{\gamma}_z = \kappa = \frac{C^2}{\lambda^2 \gamma_r^3} \dot{\gamma}_z.$$

We multiply the latter by $\dot{\gamma}_z$, and use the identity $\ddot{\gamma}_z \dot{\gamma}_z = -\dot{\gamma}_r \dot{\gamma}_r$ (which is a consequence of $(\dot{\gamma}_r)^2 + (\dot{\gamma}_z)^2 = 1$), to get

$$\ddot{\gamma}_r = -\frac{C^2}{\lambda^2 \gamma_r^3} (1 - (\dot{\gamma}_r)^2). \quad (\text{D.30})$$

Using that $\dot{\gamma}_r(t_0) \geq 0$ and $\dot{\gamma}_r(t_0) = 0$ we conclude that $C = 0$.

We now use (3') to deduce that $v_+ = 0$. Indeed, $\lambda^2 = \ell$, since λ is continuous we deduce that λ is a constant. If $\lambda = 0$ then $v_+ = 0$. If $\lambda \neq 0$, then (D.30) gives $\kappa = 0$, which contradicts the fact that γ is closed.

Appendix D.6. Solutions with cylindrical symmetry

In²¹ Migdal finds stable solutions to the CVS equations with linear growth and vorticity concentrated on a cylinder $\mathcal{S} \subset \mathbb{R}^3$. It turns out that the cross section of \mathcal{S} is noncompact. Given the cylindrical symmetry and the linear growth at infinity, that is the best one can hope for. Below we show that there are *no* solutions to the CVS equations (irrespectively of the stability condition) with cylindrical symmetry, compact cross section and linear growth.

Consider:

- (i) a smooth simple closed curve $\sigma \subset \mathbb{R}^2$;
- (ii) the bounded simply connected domain Ω_- bounded by σ ;
- (iii) the unbounded domain $\Omega_+ := \mathbb{R}^2 \setminus (\sigma \cup \Omega_-)$;
- (iv) the surface $\mathcal{S} \subset \mathbb{R}^3$ given by $\sigma \times \mathbb{R}$;
- (v) the cylindrical domains $\mathcal{S}_\pm := \Omega_\pm \times \mathbb{R}$.

We are looking for two bounded vector fields $v_\pm : \Omega_\pm \rightarrow \mathbb{R}^2$ and a quadratic function $q : \mathbb{R}^3 \rightarrow \mathbb{R}$ with the following properties:

- (a) q is harmonic;
- (b) the maps $u_\pm := (v_\pm, 0) + \nabla q : \mathcal{S}_\pm \rightarrow \mathbb{R}^3$ are divergence free, curl-free and tangent to \mathcal{S} ;
- (c) for any point $p \in \mathcal{S}$, the vector $u_+(p) - u_-(p)$ belongs to the kernel of $Du_+(p) + Du_-(p)$.

We claim the following.

Theorem Appendix D.13. *v_{\pm} and q must vanish identically.*

We can in fact consider the following more general situation:

- (i') $\sigma_i, i \in \{1, \dots, N_0\}$, is an arbitrary finite collection of simple closed curves which are pairwise disjoint;
- (ii') $\{\Omega_j\}, j \in \{1, \dots, N_0 + 1\}$ are the connected components of $\mathbb{R}^2 \setminus \bigcup_i \sigma_i$;
- (iii') The surface $\mathcal{S} \subset \mathbb{R}^3$ is the union of the cylinders $\mathcal{S}_i := \sigma_i \times \mathbb{R}$;
- (iv') The cylindrical domains are given by $\Lambda_j := \Omega_j \times \mathbb{R}$.

Under these more general assumptions we are looking for $N_0 + 1$ bounded vector fields $v_j : \Omega_j \rightarrow \mathbb{R}^2$ and a quadratic function $q : \mathbb{R}^3 \rightarrow \mathbb{R}$ with the following properties:

- (a') q is harmonic;
- (b') The maps $u_j := (v_j, 0) + \nabla q : \Lambda_j \rightarrow \mathbb{R}^3$ are divergence-free, curl-free, and tangent to $\partial\Lambda_j \subset \mathcal{S}$;
- (c') If Λ_i and Λ_j have a common boundary \mathcal{S}_k , then for any point $p \in \mathcal{S}_k$ the vector $u_i(p) - u_j(p)$ belongs to the kernel of $Du_i(p) + Du_j(p)$.

Under these assumptions Theorem Appendix D.13 can be generalized to

Theorem Appendix D.14. *v_i and q must vanish identically.*

Proof of Theorem Appendix D.13. Consider the function $\varphi(x, y) = q(x, y, 0)$ and the vector field $\xi_{-}(x, y) = v_{-}(x, y) + \nabla \varphi(x, y)$. Observe that v_{-} is curl-free and, since Ω_{-} is simply connected, there is a potential $\zeta_{-} : \Omega_{-} \rightarrow \mathbb{R}$ for ξ_{-} . Now,

$$\frac{\partial \zeta_{-}}{\partial \nu} = 0 \quad \text{on } \sigma = \partial\Omega_{-}. \quad (\text{D.31})$$

On the other hand, since φ is quadratic, $\Delta \zeta_{-}$ is a constant. Observe that, therefore, from

$$\int_{\Omega_{-}} \Delta \zeta_{-} = \int_{\sigma} \frac{\partial \zeta_{-}}{\partial \nu} = 0, \quad (\text{D.32})$$

it turns out that

$$\Delta \zeta_- = \Delta \varphi = 0. \quad (\text{D.33})$$

But then we can integrate by parts to conclude

$$\int_{\Omega_-} |\nabla \zeta_-|^2 = \int_{\sigma} \zeta_- \frac{\partial \zeta_-}{\partial \nu} = 0. \quad (\text{D.34})$$

In particular ζ_- vanishes identically.

Define next $\zeta_+(x, y) = v_+(x, y) + \nabla \varphi(x, y)$. (c) implies that $\zeta_+(x, y)$ is in the kernel of $D\zeta_+(x, y)$ for every $(x, y) \in \sigma$. Assume ζ_+ is a potential for ζ_+ in some simply connected domain $U \cap \Omega_+$, where U is the neighborhood of some point $(x, y) \in \sigma$. Then the latter condition can be rewritten as

$$\frac{1}{2} \nabla |\nabla \zeta_+|^2 = 0 \quad \text{on } \sigma \cap U.$$

If $|\nabla \zeta_+| = 0$ on $\sigma \cap U$, then ζ_+ is a constant over $\sigma \cap U$ and if we extend ζ_+ to $\Omega_- \cap U$ by setting it equal to the latter constant, we immediately see that ζ_+ is C^1 on U and weakly harmonic, hence harmonic. So ζ_+ must vanish by unique continuation for harmonic functions. If $|\nabla \zeta_+| = c > 0$, we conclude that $D^2 \zeta_+(p)$ has a nontrivial kernel for every $p \in \sigma \cap U$, but since the trace of the two-dimensional matrix $D^2 \zeta_+(p)$ is zero, we must conclude that $D^2 \zeta_+$ vanishes identically on $\sigma \cap U$. But this means that $\frac{\partial \zeta_+}{\partial x}$ and $\frac{\partial \zeta_+}{\partial y}$ are both locally constant over $\sigma \cap U$. The assumption that $\frac{\partial \zeta_+}{\partial \nu} = 0$ on $\sigma \cap U$ implies therefore that $\nabla \zeta_+$ must vanish identically on $\sigma \cap U$.

Having concluded that both ζ_- and ζ_+ vanish identically, we immediately conclude that actually $u_+ = u_-$ on \mathcal{S} and that the corresponding function u given by defining $u = u_{\pm}$ on \mathcal{S}_{\pm} is the gradient of a quadratic harmonic function. Since u must be tangent to \mathcal{S} , we see right away that u must vanish identically. \square

Proof of Theorem Appendix D.14. The proof is by induction over the number N_0 of curves. The start of the the induction, namely $N_0 = 1$, is in fact Theorem Appendix D.13. Consider therefore an arbitrary $N_0 > 1$ and assume that the theorem is correct when N_0 is substituted by $N_0 - 1$. Fix a collection of curves σ_i as in (i') above. Each σ_i bounds a unique simply connected domain Ξ_i in \mathbb{R}^2 , and given that the curves are pairwise disjoint, each σ_j with $j \neq i$ is either contained in Ξ_i or in the interior of its complement. Since the curves are finitely many it is obvious that one of

them is an “innermost” curve, namely there is a Ξ_i which does not contain any curve σ_j . Without loss of generality we can assume $i = 1$ and observe that Ξ_1 must be one of the domains Ω_i : again without loss of generality we can assume it is Ω_1 . We then denote by Ω_2 the only other connected component of $\mathbb{R}^2 \setminus \bigcup_i \sigma_i$ whose boundary intersects σ_1 (in fact we must have $\sigma_1 \subset \partial\Omega_2$, but observe that the inclusion might be strict). If we set $v_- := v_1$ and $v_+ := v_2$, we can now repeat the argument of Theorem Appendix D.13. First of all the potential ζ_- exists in our case as well because Ω_1 is simply connected, and hence the conclusions (D.31)-(D.32) can all be drawn in our case as well. The subsequent argument leads to the conclusion that v^+ is in fact a smooth continuation of v^- across $\sigma_1 \cap U$ in any simply connected neighborhood U of $p \in \sigma = \sigma_1$: the argument can be taken verbatim in our case as long as U does not intersect any other curve σ_j with $j > 1$. In particular we conclude that σ_1 could actually be eliminated from the collection of curves because the function \tilde{v} defined to be v_1 in Ω_1 and v_2 in Ω_2 is in fact smooth across σ_1 . Having reduced the number of curves by 1 we can apply the inductive assumption and conclude the validity of the theorem. \square

Appendix E. Topological defects in Turbulent flows, (by Grigory Volovik)

Let us consider the Migdal view on classical turbulence (see Refs.^{18,9)} and look for the connections between the classical hydrodynamics and turbulence in liquids and quantum hydrodynamics and turbulence in fermionic superfluids.

Appendix E.1. Classical vs quantum turbulence

Of course, there are important differences between the turbulence in quantum and classical systems. In classical liquids, the viscous term has more derivatives than nonlinear Euler term. In fermionic superfluids both terms have the same number of derivatives, see Eq.(2) in Ref.⁶⁴ The corresponding Reynolds number is the ratio of two dimensionless parameters – the internal parameters of the liquid, reactive coefficient $1 - \alpha'$ and the dissipative one α . This Reynolds number does not depend on velocity: it depends only on such internal characteristic of the liquid as temperature T . By changing T , the transition to quantum turbulence is experimentally observed, when the ratio of the reactive and dissipative parameters crosses unity.

The possible relation of viscosity anomaly to chiral anomaly may follow from the observation that the parameters α and α' in Eq.(2) of Ref.⁶⁴ are related to the Adler-Bell-Jackiw (ABJ) chiral anomaly. The vortex has chirality, and its motion produces the spectral flow in the vortex cores, which is similar to that in ABJ anomaly and which in some limit case is described by the ABJ equation.⁶⁵ In that limit, which takes place for vorticity in chiral superfluid $^3\text{He-A}$, the ABJ equation with the proper prefactor has been experimentally confirmed.⁶⁶

Appendix E.2. Clebsch hydrodynamics vs Heisenberg ferromagnets

The velocity field in Clebsch variable (ϕ_1, ϕ_2, ϕ_3) is $v_i = -\phi_2 \nabla_i \phi_1 + \nabla_i \phi_3$. In the Migdal theory, velocity and vorticity are determined in the compact space S^2 , see Eq.(43) for vorticity in terms of the unit vector $\hat{\mathbf{S}}$:

$$\omega_{ik} = (\nabla \times \mathbf{v})_{ik} = Z(\hat{\mathbf{S}} \cdot (\nabla_i \hat{\mathbf{S}} \times \nabla_k \hat{\mathbf{S}})) . \quad (\text{E.1})$$

The polar and azimuthal components of the unit vector $\hat{\mathbf{S}}$ are $\phi_1/Z = \cos \theta$, $\phi_1 = \phi$, while Z is adiabatic invariant in the absence of viscosity.

Eq.(E.1) also takes place in chiral superfluid $^3\text{He-A}$, where vorticity is expressed in terms of the unit vector of the orbital angular momentum $\hat{\mathbf{l}} \equiv \hat{\mathbf{S}}$. In this superfluid the prefactor Z is fixed, $Z = \hbar/4m_3$, where m_3 is the mass of the ^3He atom,^{67,65} and this equation is known as the

Mermin-Ho relation. Since in the chiral superfluid $\kappa = \pi\hbar/m_3$ is the quantum of circulation, the prefactor Z in Migdal hydrodynamics plays the role of the circulation quantum, see Sec. Appendix E.4.

However, the Clebsch fields are not well determined, since ϕ_2 is not defined at $\theta = 0$. Actually these Clebsch variables are exactly the same as used in ferromagnets, where the magnetization is $\mathbf{M} = M\hat{\mathbf{m}} \equiv Z\hat{\mathbf{S}}$, $M - M_z = M(1 - \cos\beta) \equiv Z(1 - \cos\beta) = \phi_1$, and $\phi \equiv \phi_2$. Here β is the angle of deflection of magnetization from the z -axis, and ϕ is the azimuthal angle of magnetization. The role of vorticity is played by the effective gauge field $F_{ik} \equiv \omega_{ik}$ acting on electrons from magnetization.⁶⁸ The pseudoelectric field $F_{i0} \equiv \omega_{i0}$ gives rise to the so-called spin-motive force acting on electrons. These gauge fields are related to the Berry phase.

In ferromagnets, ϕ and M_z (or $M - M_z$, since M is the dynamical invariant) are canonically conjugate variables. But since $\phi \equiv \phi_2$ is not well determined, the $3 + 1$ action $\int dt dV M_z \dot{\phi}$ is substituted by the $4 + 1$ Wess-Zumino term, $\int dt d\tau dV F_{0\tau}$, see Eq.(19) in Ref.⁶⁸ Probably such approach is to be used in Migdal theory.

One may say that the big difference with ferromagnets is that there the magnetization is observable, while in hydrodynamics the Clebsch variables are not. However, if the spin-orbit interaction is neglected, the magnetization becomes unobservable. But the effective gauge invariant gauge field $F_{\mu\nu}$ acting on fermions in ferromagnets will be observable in the same way as its analog – gauge invariant vorticity $\omega_{\mu\nu}$, which is expressed in terms of the unit vector $\hat{\mathbf{S}}$ of the analog of magnetization.

Appendix E.3. Topological objects: hedgehog, instanton, domain wall, quantum of circulation

Since $M \equiv Z$ is the dynamical invariant in reversible dynamics, the reversible hydrodynamics is fully determined by the unit vector of magnetization $\hat{\mathbf{m}} \equiv \hat{\mathbf{S}}$. It has two topological invariants π_2 and π_3 .

The π_2 invariant is $N = \int dS_i \omega^i / Z$. It is proportional to the velocity circulation along the moving loop, which is conserved in moving liquid in the absence of dissipation. For the closed surface, the invariant N should be integer describing the topological defects – the hedgehogs or monopoles. In ferromagnets, where $\hat{\mathbf{m}}$ is the original variable and vorticity (gauge field ω_{ik}) is the secondary variable, the hedgehog in $\hat{\mathbf{m}}$ field looks as the Dirac monopole in the Berry phase, with the unobservable Dirac line, at which the Berry phase changes by 2π .

In hydrodynamics, where vorticity ω_{ik} is the original variable and $\hat{\mathbf{S}}$ is the secondary one, the hedgehogs in the $\hat{\mathbf{S}}$ field are impossible as separate objects. The Dirac line attached to such monopole is singular and is observable. The same is in the chiral superfluids, where the Dirac line is the singular doubly quantized vortex, $m = 2$ (or $m = 2N$ in general case, where N is the topological charge of the monopole). Nevertheless, in Migdal theory the integer m is important, because the circulation $\Gamma = Zm$, and thus the prefactor Z plays the role of circulation quantum, and m is the number of quanta.

The π_3 invariant is the Hopf invariant, which is proportional to the integral over helicity: $N_3 = \int d^3r \mathbf{v} \cdot \boldsymbol{\omega} / Z^2$. The corresponding topological defect is instanton, which describes the process of creation of helicity from the "vacuum".

In Heisenberg ferromagnets there are no domain walls, because $\pi_0 = 0$. In hydrodynamics the surfaces are possible at which the prefactor Z changes sign. Probably the vortex sheets in Migdal theory – the thin pancake-like regions of increasing vorticity⁶⁹ are the analogous objects.

Appendix E.4. Dynamic invariants in hydrodynamics (circulation and helicity) and their quantization in superfluids

In Migdal theory, the circulation $\Gamma = Zm$ is the dynamic invariant. In superfluids, the quantity m becomes the integer number, i.e. the circulation is quantized: $Z = 2\pi\hbar/m_4$ and $Z = \pi\hbar/m_3$ is the quantum of circulations in Bose superfluid ^4He with mass of atom m_4 and in Fermi superfluid ^3He with mass of atom m_3 correspondingly, and m is the number circulation quanta. Thus in Migdal theory, the prefactor Z plays the role of circulation quantum, and m plays the role of the number of quanta, which becomes integer in the quantum case.

In the same manner, in superfluids the integral of helicity is quantized, $H = Z^2 N_3$ with integer N_3 . The integer N_3 in superfluids is the topological invariant: it is the knot invariant in Bose superfluid ^4He and in Fermi superfluid $^3\text{He-B}$, and the Hopf invariant $\pi_3(S^2)$ in the chiral superfluid $^3\text{He-A}$. In both Fermi superfluids, the quantum of helicity is $Z^2 \propto (\hbar/m_3)^2$. In classical hydrodynamics, the prefactor $Z^2 \propto (\hbar/m_3)^2$ serves as the "quantum of helicity", and N_3 serves as the "number of quanta", which becomes the integer topological invariant in the quantum case of superfluids.

The quantization of helicity and of circulation in superfluids provide two examples, which illustrate the main property of the dynamical invariants in classical systems. The dynamic invariant in classical systems become quantized in integer numbers in the quantum systems, N_3 and N correspondingly.

Similar situation is in Heisenberg ferromagnets. In classical equations $M \equiv Z$ is the dynamic invariant, which is conserved in the Landau–Lifshitz equation without dissipation. In ferromagnets the total magnetic moment $\int d^3x M$ becomes quantized in terms of $\hbar/2$, i.e. $\int d^3x M = k\hbar/2$, where k is integer. This quantization follows from the Wess-Zumino term in action.⁷⁰

Appendix E.5. Hydrodynamics in terms of tetrads

Let us introduce the orthogonal triad of unit length:

$$\mathbf{e}_1, \mathbf{e}_2, \hat{\mathbf{S}} = \mathbf{e}_1 \times \mathbf{e}_2. \quad (\text{E.2})$$

The velocity field:

$$v_i = Z(\mathbf{e}_1 \cdot \nabla_i \mathbf{e}_2 - \mathbf{e}_2 \cdot \nabla_i \mathbf{e}_1), \quad (\text{E.3})$$

where Z is the dynamical invariant. The vorticity is expressed in terms $\hat{\mathbf{S}}$ field (according to the Mermin-Ho relation) in the same way as in Migdal theory in Eq.(43) of Ref.:¹⁸

$$\omega_{ik} = (\nabla \times \mathbf{v})_{ik} = Z(\hat{\mathbf{S}} \cdot (\nabla_i \hat{\mathbf{S}} \times \nabla_k \hat{\mathbf{S}})). \quad (\text{E.4})$$

The triad field variables correspond to three Clebsch fields, but as distinct from the Clebsch fields the triad is well determined everywhere, except for the real topological singularities.

The $SO(3)$ space of triad, and S^2 space of $\hat{\mathbf{S}}$ provide the geometry, including the effective metric, and topology. The topological invariants are well determined in terms of $\hat{\mathbf{S}}$, or in terms of rotation of the dyad about $\hat{\mathbf{S}}$ -axis. They are integer for special geometries, while the circulation and helicity are represented by these invariants multiplied by the dynamical invariants Z and Z^2 correspondingly.

Appendix E.6. Dirac monopole with observable Dirac strings

The hydrodynamics of incompressible fluid has been discussed in terms of the \mathbf{S} -vector in Ref.⁷¹ The unit vector description allows the topological objects $\pi_3(S^2) = \mathbb{Z}$, which describe the Hopf structure, and also the instantons. It also allows the defects of the group $\pi_2(S^2) = \mathbb{Z}$, the hedgehogs, or monopoles, in which the \mathbf{S} -vector wraps N times around a sphere. In tetrads, where the target space is $SO(3)$, the Hopf structures are allowed, since $\pi_3(SO(3)) = \mathbb{Z}$. But the hedgehogs do not exist as separate objects, since $\pi_2(SO(3)) = 0$. That is why the monopole in \mathbf{S} -field has singular Dirac string (the vortex singularity) attached to the monopole, which is observable.^{72,73,74}

The simplest monopole is the radial hedgehog in the $\hat{\mathbf{S}}$ field: $\hat{\mathbf{S}} = \hat{\mathbf{r}}$. Its topological π_2 charge is $N = 1$. Let us consider two configurations of $N = 1$ monopole: (i) with one Dirac string with winding number $m = 2N = 2$; and (ii) with two strings, each with winding number $m = 1$.

Appendix E.7. Dirac monopole with one Dirac string

(z, ρ, ϕ) are cylindrical coordinates and (r, θ, ϕ) are spherical coordinates. The velocity field is

$$\mathbf{v}(\mathbf{r}) = Z\hat{\phi}\frac{1 - \cos\theta}{r \sin\theta}, \quad \nabla \cdot \mathbf{v} = 0, \quad (\text{E.5})$$

and vorticity field:

$$\boldsymbol{\omega}(\mathbf{r}) = Z\frac{\hat{\mathbf{r}}}{r^2} + 2Z\theta(-z)\hat{\mathbf{z}}\delta_2(\boldsymbol{\rho}), \quad \nabla \cdot \boldsymbol{\omega} = 0. \quad (\text{E.6})$$

The vorticity is equivalent to magnetic field of Dirac monopole with charge Z , i.e. $\mathbf{B} \equiv \boldsymbol{\omega}(\mathbf{r})$. The magnetic flux is conserved, $\nabla \cdot \mathbf{B} = 0$. The $4\pi Z$ flux from the monopole is compensated by the magnetic flux along the singular flux tube (observable Dirac string) to the monopole. Here there is the single Dirac string on the lower half-axis, $z < 0$. It is the vortex line with circulation $2Z$, or winding number $m = 2$ in Migdal notations. The triads are

$$\hat{\mathbf{S}}(\mathbf{r}) = \hat{\mathbf{r}}, \quad \mathbf{e}_1 + i\mathbf{e}_2 = e^{i\phi}(\hat{\boldsymbol{\theta}} + i\hat{\boldsymbol{\phi}}). \quad (\text{E.7})$$

This topological structure with vortex terminated by monopole may have some connection to tornado, see Figs. E.46 and E.47. Here the funnel cloud moves towards the ground and when it reaches the ground it forms

tornado in Fig.E.48. Before the tornado is formed the funnel cloud is the vortex with the end point. The end point represents the monopole-hedgehog in the $\hat{\mathbf{S}}$ -field and the funnel cloud represents its Dirac string. Probably the monopole may exist also at the final stage of the tornado: when tornado is dying the end of the vortex leaves the ground.

Appendix E.8. Dirac monopole with two Dirac strings

In this case the velocity field is:

$$\mathbf{v}(\mathbf{r}) = -Z\hat{\phi}\frac{\cos\theta}{r\sin\theta}, \quad (\text{E.8})$$

and vorticity field:

$$\boldsymbol{\omega}(\mathbf{r}) = Z\frac{\hat{\mathbf{r}}}{r^2} + Z\text{sign}(z)\hat{\mathbf{z}}\delta_2(\boldsymbol{\rho}). \quad (\text{E.9})$$

Now the flux from the monopole is compensated by the magnetic fluxes which enter the monopole along two Dirac strings. Each string (vortex line) has circulation Z , or winding number $m = 1$ in Migdal notations. The triads are

$$\hat{\mathbf{S}}(\mathbf{r}) = \hat{\mathbf{r}}, \mathbf{e}_1 + i\mathbf{e}_2 = \hat{\boldsymbol{\theta}} + i\hat{\phi}. \quad (\text{E.10})$$

Appendix E.9. General case with two Dirac strings and monopole with charge N

The monopole in \mathbf{S} -field with topological charge N , has the Dirac strings with the total winding number $m = 2N$. The triads can be chosen as extension of $m = 1$ monopole in Eq.(E.10):

$$\mathbf{e}_1 + i\mathbf{e}_2 = (\hat{\boldsymbol{\theta}} + i\hat{\phi})^N. \quad (\text{E.11})$$

There are two Dirac strings, at $z < 0$ and at $z > 0$, each with winding number $m = N$ (the total winding number is $m = 2N$). It is not clear whether the monopoles with $|N| > 1$ could be realized.

Appendix E.10. Monopole in spherical layer

The monopole configuration with $N = 1$ with two strings, each with $m = 1$, is realized for hydrodynamics of ideal incompressible fluid in a thin spherical layer.⁷⁵ Here $\mathbf{S} = \hat{\mathbf{r}}$, and thus the topological charge of the monopole is $N = 1$. The first term in the RHS of Eq.(E.9) can be neglected



Figure E.46: Since the end point of the vortex is not seen, this is probably the funnel cloud, which is the vortex (Dirac string) terminated by the Dirac monopole.

in the limit of large radius of the sphere. Then the velocity field satisfies both stationary equations for incompressible fluid:

$$\nabla \cdot \mathbf{v} = 0, \quad \nabla \times (\mathbf{v} \times \boldsymbol{\omega}) = 0. \quad (\text{E.12})$$

This is the monopole, which core is represented by the inner sphere.

The simplest realization is tornado in Figs. E.48 and E.49, where the Earth represents the core of the monopole.

Viscosity resolves the singularity on Dirac line. This configuration can be also described in terms of $\hat{\mathbf{S}}$ -vector: $\hat{\mathbf{S}}(\mathbf{r})$ is vertical outside the tornado and becomes radial on the axis. The simplest model for that is the Rankine vortex, which has constant vorticity inside the tube, $\boldsymbol{\omega} = \text{const} \hat{\mathbf{z}}$, and zero vorticity outside the tube, $\boldsymbol{\omega} = 0$. The cylindrical surface of the tube experiences singularity, the jump in vorticity.



Figure E.47: One more monopole.

Appendix E.11. From monopole to pancake vortex sheet

Now we can adiabatically deform the inner sphere, so that the topological invariant $N = 1$ is conserved. Then the flow will be automatically adjusted to the new configuration of the core.

There are several interesting deformations with the conservation of axial symmetry.

One may adiabatically decrease the radius of the core. In the limit of small radius the configuration will represent the monopole with the singular core.

One may deform the inner sphere to the disk of small thickness without violating the axial symmetry and the discrete symmetry with respect to inversion: $\mathbf{S}(\mathbf{r}) = -\mathbf{S}(-\mathbf{r})$, $\mathbf{v}(\mathbf{r}) = \mathbf{v}(-\mathbf{r})$, $\boldsymbol{\omega}(\mathbf{r}) = -\boldsymbol{\omega}(-\mathbf{r})$. This would result in the Migdal vortex sheet.

So, let us consider the monopole structure obtained when the inner sphere in Sec. Appendix E.10 is adiabatically (i.e. with conservation of topological invariant $N = 1$) deformed to the thin disk. In the vicinity of the disk one has $S_z(z) = |S_z| \text{sign}(z)$, i.e. the disk represents the domain wall, where S_z changes sign, but $|S_z(\rho)|$ is continuous across the sheet. Velocity is $\mathbf{v} = Z S_z \nabla \phi_2(\mathbf{r})$. Let us first consider $\phi_2(\mathbf{r}) = \phi_2(\phi) = \phi$,



<https://upload.wikimedia.org/wikipedia/commons/4/4d/Trombe.jpg>

Page 1 of 1

Figure E.48: Tornado can be represented as Dirac string, while the spherical core of the Dirac monopole is represented by the Earth.



Figure E.49: One more Dirac string



Figure E.50: Dirac strings again

the azimuthal angle. In this case the flow is circulating in the opposite directions on two sides of the disk:

$$\mathbf{v} = Z S_z \nabla \phi = Z \frac{|S_z(\rho)|}{\rho} \text{sign}(z) \hat{\phi}. \quad (\text{E.13})$$

The vorticity has the $\delta(z)$ singularity at the disk and $\delta_2(\rho)$ singularity on the axis:

$$\boldsymbol{\omega} = \hat{\rho} \delta(z) \frac{Z |S_z(\rho)|}{\rho} + Z \hat{\mathbf{z}} \text{sign } z \left(\delta_2(\rho) + \frac{1}{\rho} \partial_\rho |S_z(\rho)| \right). \quad (\text{E.14})$$

This structure represents the monopole with $N = 1$ and two Dirac strings, each with winding number $m = 1$. The core of the monopole is represented by the disk. On two sides of the disk one has the flow circulating in opposite directions. The singular contribution $\delta_2(\rho)$ to vorticity along z axis represents two Dirac strings with opposite circulations. These Dirac strings enter the monopole (vortex sheet disk) from two sides.

Appendix E.12. Wall bounded by string

In the present scenario, the disk itself represents the Z_2 domain wall at which S_z changes sign. In the body of the disk, the vector $\hat{\mathbf{S}}_\perp$ has $2\pi n$ rotations across the disk. In the Migdal scenario the vector \vec{S}_\perp changes sign., and it makes half-integer number of rotations $(2n + 1)\pi$, or, a reflection in addition to $2\pi n$ rotations.^{18,9}

In both cases the edge of the disk represents the circular string (ring), which terminates the domain wall. This string has either the π_1 winding

number n , or the winding number $n + 1/2$. In the first case it is the analog of the soliton terminated by strings,⁷⁶ while in the second case it is the analog of Kibble-Lazarides-Shafi (KLS) wall^{77,78} bounded by Alice strings. The similar configuration, the domain wall bounded by Alice string (half-quantum vortex), has been experimentally studied in the polar phase of superfluid ^3He .⁷⁹ The general topology of the KLS walls bounded by string was discussed in Ref.⁸⁰ In both cases, solitons terminated by strings and domain walls terminated by strings, the classification is in terms of the relative homotopy groups. The winding number n or $n + 1/2$ is the element of topology of such combined objects.

These combined objects are described by the combination of topologies. This includes $\pi_2(S^2) = \mathbb{Z}$ (the topological charge $N = 2m$ of the hedgehog-monopole and the winding number of Dirac strings, which enter the monopole); $\pi_1(S^1) = \mathbb{Z}$ (the winding number n of the soliton and of the circular ring, which terminates the soliton); $\pi_0(\mathbb{Z}_2) = \mathbb{Z}_2$ (the domain wall).

Appendix E.13. $SO(3)$ hydrodynamics of incompressible liquid

Let us introduce instead of the triads with unit length \mathbf{e}_a , the more general triads \mathbf{E}_a :

$$\mathbf{E}_1 = A\mathbf{e}_1, \mathbf{E}_2 = A\mathbf{e}_2, \mathbf{L} = \mathbf{E}_3 = \mathbf{E}_1 \times \mathbf{E}_2 = Z\mathbf{e}_3 \equiv Z\mathbf{S}, \quad (\text{E.15})$$

$$\mathbf{E}_1^2 = \mathbf{E}_2^2 = A^2 = Z, \mathbf{E}_1 \cdot \mathbf{E}_2 = 0. \quad (\text{E.16})$$

The velocity field is:

$$v_i = \mathbf{E}_1 \cdot \nabla_i \mathbf{E}_2. \quad (\text{E.17})$$

Note that this is the general form of velocity, which is not violated by the condition of incompressibility. The latter condition is obtained by gauge transformation in Eq.(E.25).

We have the following PB for canonically conjugate variables:

$$\{E_1^i(\mathbf{r}_1), E_2^k(\mathbf{r}_2)\} = \delta^{ik} \delta(\mathbf{r}_2 - \mathbf{r}_1). \quad (\text{E.18})$$

Eq.(E.18) gives:

$$\{L^i(\mathbf{r}_1), E_a^k(\mathbf{r}_2)\} = e^{ikl} E_a^l \delta(\mathbf{r}_2 - \mathbf{r}_1), \quad (\text{E.19})$$

$$\{L^i(\mathbf{r}_1), L^k(\mathbf{r}_2)\} = e^{ikl} L^l \delta(\mathbf{r}_2 - \mathbf{r}_1), \quad (\text{E.20})$$

$$\{v_i(\mathbf{r}_1), E_k^a(\mathbf{r}_2)\} = \nabla_i E_k^a \delta(\mathbf{r}_2 - \mathbf{r}_1), a = 1, 2, 3. \quad (\text{E.21})$$

The Eq.(E.21) gives the following motion equations for the tetrad fields \mathbf{E}_a , with $a = 1, 2, 3$:

$$\dot{\mathbf{E}}_a + (\mathbf{v} \cdot \nabla) \mathbf{E}_a = 0, \quad (\text{E.22})$$

Multiplying each of 3 equations to the corresponding \mathbf{E}_a one obtains that each of three equation gives the equation for Z :

$$\dot{Z} + (\mathbf{v} \cdot \nabla) Z = 0. \quad (\text{E.23})$$

This demonstrates that Z can be chosen as constant in spacetime.

The PB for velocity field are:

$$\{v_i(\mathbf{r}_1), v_k(\mathbf{r}_2)\} = e_{ikl} \omega^l(\mathbf{r}_1) \delta(\mathbf{r}_2 - \mathbf{r}_1). \quad (\text{E.24})$$

Gauge transformation which does not change the distribution of vector \mathbf{L} (and the vorticity, which is expressed in terms of \mathbf{L}), is:

$$\mathbf{E}_1 + i\mathbf{E}_2 \rightarrow (\mathbf{E}_1 + i\mathbf{E}_2) e^{i\Phi}, \quad \mathbf{v} \rightarrow \mathbf{v} + \nabla \Phi. \quad (\text{E.25})$$

This is the rotation of the dyad \mathbf{E}_1 and \mathbf{E}_2 by angle Φ about the local direction of \mathbf{L} -vector. The gauge transformation is needed to satisfy the incompressibility condition $\nabla \cdot \mathbf{v} = 0$. It is analogous to transformation from 3 Clebsch variables to 2. But as distinct from Clebsch variables, triads correctly deal with such structures, where Clebsch variables have unphysical singularities (for example in the configuration with monopole and Dirac strings in Sec.Appendix E.6).

Appendix E.14. Spin connection and torsion

The metric, which follows from tetrads, is flat:

$$g^{ik} = \delta^{ab} E_a^i E_b^k. \quad (\text{E.26})$$

Spin connection and torsion are

$$C_i^{12} = -C_i^{21} = \mathbf{E}_1 \cdot \nabla_i \mathbf{E}_2 = -\mathbf{E}_2 \cdot \nabla_i \mathbf{E}_1 = v_i. \quad (\text{E.27})$$

$$T_{ik}^a = \partial_i E_k^a - \partial_k E_i^a. \quad (\text{E.28})$$

Appendix E.15. Conclusion

It looks that not only the relativistic quantum field theories, but also the quantum hydrodynamics of topological superfluids can be useful for study the important structures emerging in classical liquids.

Acknowledgements. This work has been supported by the European Research Council (ERC) under the European Union's Horizon 2020 research and innovation programme (Grant Agreement No. 694248).